UNIVERSITÉ DE MONTRÉAL

THE EFFECT OF FLUXES AND BINDERS ON THE BONDING MECHANISM AND PROPERTIES OF IRON ORE PELLETS

by

Birendra Chandra JENA

DEPARTMENT OF METALLURGICAL ENGINEERING

ÉCOLE POLYTECHNIQUE

THESIS SUBMITTED IN PARTIAL FULFILLMENT OF REQUIREMENTS
FOR THE DEGREE OF DOCTOR OF PHILOSOPHY (Ph.D.)

(Metallurgical Engineering)

April 1989

© Birendra Chandra JENA 1989

Permission has been granted to the National Library of Canada to microfilm this thesis and to lend or sell copies of the film.

The author (copyright owner) has reserved other publication rights, and neither the thesis nor extensive extracts from it may be printed or otherwise reproduced without his/her written permission.

L'autorisation a été accordée à la Bibliothèque nationale du Canada de microfilmer cette thèse et de prêter ou de vendre des exemplaires du film.

L'auteur (titulaire du droit d'auteur) se réserve les autres droits de publication; ni la thèse ni de longs extraits de celle-ci ne doivent être imprimés ou autrement reproduits sans son autorisation écrite.

ISBN 0-315-50217-7

UNIVERSITÉ DE MONTRÉAL

ÉCOLE POLYTECHNIQUE

This thesis entitled:

THE EFFECT OF FLUXES AND BINDERS ON THE BONDING MECHANISM AND PROPERTIES OF IRON ORE PELLETS

submitted by Birendra Chandra Jena
for obtaining the degree of
Doctor of Philosophy (Ph.D.)
is duly accepted by the jury of examiners consisting of

Mr. F. Ajersch, Ph.D., president

Mr. C.W. Bale, Ph.D.

Mr. H. Lien, Ph.D.

Mr. Michel Rigaud, D.Sc.A.

S U M M A R Y

The present work was undertaken with the objective of 1) studying the effect of type of binder and fluxes on the bonding mechanism and 2) evaluating peat moss as a binder for the production of self fluxed pellets.

Pellets were produced from high silica specularite concentrates of Mount Wright origin. Two sets of pellets were produced i) at the laboratory level, by producing green pellets in a small disc pelletiser and indurating them in a resistance furnace and ii) at a pilot plant level, by producing pellets in a standard disc pelletiser and indurating them in a pot grate. The first set of pellets were used exclusively for bonding mechanism studies and the second set was used for evaluating peat moss as a binder.

Laboratory pellets were produced in the basicity range of 0.2-1.6 for bonding mechanism studies. Bentonite and peat moss were used as binders. The specific basicity levels were obtained by using only limestone or a combination of dolomite and limestone as flux. In the pellets which were produced using dolomite as flux, the dolomite addition was maintained at 9% of the dry mix and the rest being limestone to achieve the specific basicity level. The bonding phases were characterised by using optical microscope, image analyser and SEM-EDS.

It was observed that the bonding in acid pellet (i.e.: 0.2 basicity) mainly consisted of iron oxide bridges. The bonding phase was predominantly a glassy silicate in the pellets produced in the basicity range of 0.8 to 1.6. The glass phase had solidified from a melt which was formed throughout the pellet during induration. The amount of glass phase increased with increasing basicity due to larger amount of melt formation. The glass phase contained varied amount of Fe, Ca, Si, Al and Mg as its composition was dependent on local chemistry of the melt. The iron content of this phase was found to decrease with increasing basicity.

It was noticed that characteristic change in the mineral structure and nature of the melt was brought about by the presence of MgO in the mix. In the pellets with dolomite addition presence of a zoned silicate structure was observed, which consisted of a pale gray magnesian ferrugenous phase and a dark phase with little Mg and lower Fe content. With increased basicity the quantity of magnesian ferrugenous phase decreased. Moreover, the formation of magnesioferrite in these pellets was observed, which did not conform to the stoichiometric composition ($MgO \cdot Fe_2O_3$) but a phase highly deficient in MgO. The quantity of magnesioferrite was found to increase with increasing basicity.

The presence of calcium ferrite was observed in the pellet with limestone and bentonite addition at basicity of 0.8, but no appreciable amount of calcium ferrite was observed in the pellets with limestone and bentonite addition at 1.6 basicity.

The type of binder had marginal effect on the nature of the bonding phase. Peat moss addition was found to decrease the amount of calcium ferrite formation and invariably resulted in a highly porous pellet matrix.

It was observed that melt formation through the addition of fluxes has a great influence on the metallurgical properties of the pellets as the strength properties and swelling characteristics are improved by increasing the basicity. Optimum pellet properties were obtained in the pellets of 1.3 basicity with peat moss and dolomite addition as pellet reducibility was enhanced due to peat moss addition and dolomite addition was beneficial in maintaining a balance between various pellet properties.

The reducibility of the pellet was found to increase with basicity, reach a maximum at 1.3 basicity and then decrease. The reducibility of the pellets at the low basicity of 0.8 remained low in spite of high porosity. Absence of fine intragranular pores in the reduced wustite grains was found to be the cause of low reducibility in these pellets. In pellets above 1.3 basicity, low reducibility was due to the decrease in the pellet porosity.

The pellets in the pilot scale were produced at 0.8, 1.1 and 1.3 basicity using peat moss, peat moss + bentonite and bentonite as binders. The pellet basicity was maintained by addition of dolomite and limestone, keeping dolomite level at 9%, similar to the laboratory scale pellets. The pellets with peat moss addition were found to possess adequate green and fired strength properties although they were

inferior to the pellets with bentonite additions. Superior metallurgical properties such as LTBT, reducibility and swelling were observed in the pellets with peat moss addition. This was attributed to the higher porosity in the pellets due to peat moss addition. The pilot tests demonstrate that peat moss can replace bentonite as binder for the production of self-fluxed pellets without compromising on pellet quality.

S O M M A I R E

Les objectifs du présent travail ont été, 1) d'étudier l'influence des agents liants et fluxants sur les mécanismes de liaison et 2) d'évaluer le rôle de la tourbe en tant qu'agent liant, lors de la production des boulettes d'oxydes de fer auto-fondantes.

Les boulettes ont toutes été produites à partir du minerai concentré d'hématite spéculaire du Mont-Wright. Deux séries distinctes de boulettes ont été produites 1) en laboratoire, les boulettes vertes étant formées dans un petit disque de boulettage puis cuites dans un four à résistances 2) à l'échelle pilote, les boulettes vertes étant formées dans un disque de boulettage standard et la cuisson effectuée dans un simulateur de cuisson. La première série de boulettes a servi exclusivement à l'étude des mécanismes de liaison et la deuxième série à l'évaluation de la tourbe comme liant.

Les boulettes de laboratoire ont été produites dans un intervalle de basicité variant de 0,2 à 1,6. La bentonite et la tourbe ont été les deux agents liants utilisés. La basicité visée a été obtenue en utilisant comme agent fluxant soit de la chaux soit un mélange de dolomie et de chaux. Pour les boulettes avec addition de dolomie, la quantité de dolomie utilisée était maintenue à 9% poids dans le mélange à sec, la chaux étant incorporée au mélange en quantité variable pour atteindre la basicité désirée. Les phases liantes entre les grains

d'hématite ont été identifiées en se servant de la microscopie optique de l'analyseur d'images et du microscope électronique à balayage (MEB-EDX).

Il a été observé que dans les boulettes acides (à 0,2 de basicité) la liaison est principalement assurée par des ponts ou cols entre grains d'oxyde de fer. À basicité plus élevée (0,8 à 1,6), la phase liante principale est une phase silicatée vitreuse. Cette phase vitreuse résulte de la solidification d'une phase liquide, qui elle, s'est formée durant la cuisson des boulettes. La quantité de cette phase vitreuse croît avec la basicité. Cette phase contient des quantités variables de Fe, Ca, Si, Ap et Mg, et sa composition varie selon la localisation du liquide formé dans la boulette lors de sa cuisson. Le contenu en fer dans la phase vitreuse liante décroît lorsque la basicité globale de la boulette croît.

Il a été démontré que des changements caractéristiques de la structure et de la nature de la phase liante sont liés à la présence de MgO dans le mélange initial. Ainsi dans les boulettes avec addition de dolomie la phase silicatée est formée de deux zones, l'une gris pâle, magnesio-ferrugineuse, l'autre très foncée, contenant peu de magnésium et un pourcentage en fer aussi réduit. À basicité croissante la quantité de phase magnésio-ferrugineuse décroît. La présence de magnésioferrite ($MgO \cdot Fe_2O_3$) dans ces boulettes avec dolomie a aussi été observée mais toujours avec une composition sous-stoechiométrique en MgO. Toutefois à basicité croissante la quantité de spinelle magnésio-ferrite, elle, croît.

La présence de ferrite de calcium a été aussi observée dans les boulettes avec chaux et bentonite, à une basicité de 0,8 mais aucune quantité de ferrite de calcium n'a pu être observée dans ces boulettes lorsque la basicité a été portée à 1,6.

La bentonite ou la tourbe en tant qu'agent liant n'ont qu'un effet marginal sur la nature des phases liantes. Une légère décroissance dans la quantité de ferrite de calcium a été observée dans les boulettes avec tourbe. L'effet principal de la tourbe s'est manifesté invariablement par une porosité accrue.

Il a été observé que l'addition d'agents fluxants exerce une très grande influence sur les propriétés métallurgiques des boulettes notamment leurs propriétés reliées à la cohésion et au gonflement qui croissent en fonction directe de la basicité. Les propriétés optimales ont été obtenues avec des boulettes, de 1,3 de basicité, avec addition de dolomie et de tourbe lorsqu'on prend en considération la réductibilité des boulettes. Celle-ci est améliorée grâce à l'addition de tourbe, alors que la dolomie permet de maintenir un bon compromis entre toutes les propriétés physiques et chimiques désirées.

La réductibilité des boulettes croît de façon générale lorsque la basicité croît jusqu'à 1,3 mais décroît au-delà. Dans notre étude la réductibilité relative des boulettes à 0,8 de basicité était déjà faible en dépit d'une porosité élevée. Ceci serait dû au fait que les grains de wustite une fois réduits ne présenteront pas la porosité intergranulaire que l'on a observé dans les autres cas. Toutefois à 1,3 de basicité et au-delà la baisse de réductibilité dépend directement de

la décroissance de la porosité globale initiale de la boulette. Il apparaît donc qu'il faille distinguer entre porosité initiale et porosité en cours de réduction.

Pour les boulettes produites à l'échelle pilote on a choisi trois basicités seulement: 0,8, 1,1 et 1,3, avec addition de tourbe, seulement, tourbe et bentonite et bentonite seulement comme référence. Toutes les boulettes contenaient 9% de dolomie, la basicité étant ajustée en réglant le pourcentage de chaux ajouté. Pour les boulettes avec addition de tourbe les propriétés mécaniques atteintes, à vert et après cuisson, étaient adéquates quoique inférieures aux boulettes avec addition de bentonite. Toutefois, pour ces mêmes boulettes additionnées de tourbe, des propriétés métallurgiques supérieures ont été obtenues (LTBT, réductibilité et gonflement). Ces améliorations notables ont été attribuées à la formation de boulettes de plus grande porosité lorsqu'il y a ajout de tourbe. Ces essais à l'échelle pilote ont donc confirmé qu'il était possible de remplacer la bentonite par de la tourbe pour la production de boulettes auto-fondantes sans compromis inhibitoire sur la qualité des boulettes, à condition de bien contrôler la nature et la morphologie des phases liantes, donc de bien comprendre les mécanismes de liaison dans ces boulettes.

A C K N O W L E D G E M E N T S

I wish to express my sincere gratitude to Prof. Michel Rigaud for having suggested the problem, his valuable guidance and constructive critisism throughout this work.

I also extend my heart felt gratitude to Dr. S.C. Panigrahy for his valuable advice, active interest and constant encouragement during this work.

My sincere thanks are due to the Centre de Recherches Minérales in Quebec City, for providing financial assistance for the work and pilot plant facilities to carry out part of the investigation. I am thankful to Mr. Guy Paquet and Mr. André Lemay of CRM for their valuable help in conducting pot grate trials.

I am also thankful to Messrs. André Désilets, Lucien Gosselin, Jean Claudinon and André Riel; technicians of the Metallurgical Engineering Department for their continued assistance during the investigation.

Thanks are also due to the Director, Regional Research Laboratory, Bhubaneswar, India for granting me leave of absence to pursue my Ph.D. program.

I am also thankful to Ms. Céline Labelle for her help in the preparation of the thesis.

I express my sincere appreciation to my friends for their help and encouragements throughout the work and last but not the least to my wife Kalyani and daughters Namrata and Ananya for their endured patience.

T A B L E O F C O N T E N T S

PAGE

SUMMARY iv

SOMMAIRE viii

ACKNOWLEDGEMENTS xii

TABLE OF CONTENT xiv

LIST OF TABLES xviii

LIST OF FIGURES xxii

INTRODUCTION 1

CHAPTER 1 - BASIC ASPECTS OF PELLETISATION 7

1. Pelletisation process 7

2. Bonding mechanism during various stages of pellet formation .. 8

2.1 Bonding mechanism for green ball formation 8

2.2 Bonding mechanism during induration 13

3. Alternative binders to bentonite 18

4. Fluxed pellets 24

5. The porous pellets 28

PAGE

CHAPTER 2 - EXPERIMENTAL PROCEDURES 31

1. Production of pellets 31

2. Production of fluxed pellets in the laboraotry 32

2.1 Preparation of green pellets 33

2.1.1 Preparation of pellet mix 35

2.1.2 Green pellet formation 35

2.2 Pellet induration 36

3. Production of pellets in pilot plant scale to study pellet properties 37

3.1 Preparation of green pellets 38

3.1.1 Preparation of pellet mix 39

3.1.2 Green ball formation 40

3.1.3 Pellet induration 40

4. Procedure for bonding mechanism studies 42

4.1 Thermogravimetric and differential thermal analysis (TGA & DTA) 42

4.2 Pellet mineralogy and characterisation of bonding phases 43

4.2.1 Sample preparation 43

4.2.2 Pellet mineralogy 43

4.2.3 Phase area measurement using image analyser 44

4.2.4 Microanalysis 44

5. Pellet testing procedure 45

5.1 Green compression strength 45

PAGE

5.2 Drop number..... 45

5.3 Dry compression strength..... 46

5.4 Porosity measurements of fired pellets..... 46

5.5 Tumbler strength..... 47

5.6 Compression strength of fired pellets..... 48

5.7 Low temperature breakdown test (LTBT)..... 48

5.8 Reducibility test..... 49

5.9 Swelling test..... 51

CHAPTER 3 - RESULTS: LABORATORY PELLETS..... 54

1. TGA and DTA results..... 54

2. Phase area measurement by image analyser..... 60

3. Microanalysis results..... 61

4. Mineralogy of pellets at various basicity levels..... 69

4.1 Basicity 0.2..... 69

4.2 Basicity 0.8..... 72

4.3 Basicity 1.3..... 80

4.4 Basicity 1.6..... 86

5. Chemical analysis of fired pellets..... 94

6. Properties of the fired pellets..... 96

6.1 Porosity..... 96

6.2 Compression strength..... 99

6.3 Reducibility..... 101

6.4 Swelling..... 119

PAGE

CHAPTER 4 - RESULTS: PILOT SCALE PELLETS 122

1. Green stage properties 122

1.1 Green compression strength and drop number 122

1.2 Dry compression strength 123

2. Chemical analysis of fired pellets 124

3. Pellet mineralogy 124

4. Porosity 138

5. Compression strength 140

6. Tumbler strength 143

7. Low temperature break down test (LTBT) 143

8. Reducibility 146

9. Swelling 152

CHAPTER 5 - SYNTHESIS 156

1. Pellet mineralogy 156

1.2 Bonding mechanism of the pellets 162

1.3 Effect of peat moss on green stage properties 165

1.4 Effect of peat moss on fired pellet properties 166

2. Conclusions and recommendations 171

2.1 Recommendations 173

2.2 Claims of originality 175

REFERENCES 176

APPENDIX 1 - REDUCTION KINETICS OF IRON OXIDE PELLETS 193

APPENDIX 2 - PHASE EQUILIBRIA DURING PELLET INDURATION 218

LIST OF TABLES

TABLE		PAGE
1	Chemical composition of Mount Wright specularite concentrate	2
2	List of inorganic and organic substances which were tried as an alternative binder to bentonite	19
3	Performance of the alternative binders	19
4	Raw material size and chemical analysis	31
5	The proximate analysis of peat moss and coke breeze	32
6	Pellet designation and percent weight of binders and fluxes in green pellet mix (dry basis)	34
7	Weight percentages of additives for pellet production in pilot scale	39
8	Percentage area of different mineralogical phases as measured by image analysis	61
9	Average composition of glass phase in dolomite fluxed pellet (SEM-EDS)	62
10	Average composition of glass phase in limestone fluxed pellets (SEM-EDS)	63
11	Average composition of magnesioferrite in pellets fluxed with dolomite (SEM-EDS)	63
12	Average composition of major crystalline phases (SEM-EDS)	64

TABLE		PAGE
13	Microanalysis of two calcium ferrite phases as shown in Figure 18	68
14	Microanalysis of mineralogical phases as shown in Figure 21	71
15	Microanalysis of mineralogical phases as shown in Figure 26	75
16	Microanalysis of mineralogical phases as shown in Figure 27	76
17	Microanalysis of mineralogical phases as shown in Figure 28	77
18	Microanalysis of mineralogical phases as shown in Figure 29	78
19	Microanalysis of mineralogical phases as shown in Figure 34	83
20	Microanalysis of mineralogical phases as shown in Figure 35	84
21	Microanalysis of mineralogical phases as shown in Figure 36	85
22	Microanalysis of mineralogical phases as shown in Figure 41	89
23	Microanalysis of mineralogical phases as shown in Figure 42	90
24	Microanalysis of mineralogical phases as shown in Figure 43	91

TABLE		PAGE
25	Microanalysis of mineralogical phases as shown in Figure 44	92
26	A chemical composition of fired pellets	95
27	Physical and reduction properties of the fired pellets	97
28	Green pellet properties	123
29	Chemical composition of fired pellets	125
30	Percentage phase area of the mineralogical phases in pellets produced in pilot scale	130
31	Microanalysis of mineralogical phases as shown in Figure 73	131
32	Microanalysis of mineralogical phases as shown in Figure 74	132
33	Microanalysis of mineralogical phases as shown in Figure 75	133
34	Microanalysis of mineralogical phases as shown in Figure 76	134
35	Average composition of glass phase in pilot scale pellets (SEM-EDS)	136
36	Average composition of magnesioferrite in pellets produced in the pilot scale	137
37	Average composition of hematite and calcium ferrite in pellets produced in pilot scale	137
38	Porosity of the fired pellets	139
39	Compression strength of the fired pellets	141

TABLE		PAGE
40	Tumbler strength of the pellets.....	143
41	Low temperature breakdown test (LTBT) of the peat moss and bentonite added pellets.....	146
42	Reducibility of fired pellets.....	148
43	Maximum swelling of fired pellets.....	159

L I S T O F F I G U R E S

FIGURE		PAGE
1	Different stages of green ball formation.....	11
2	Alternative of green ball formation.....	13
3	The classic stages of liquid phase sintering involving mixed powders which form a liquid on heating.....	16
4	Laboratory disc pelletiser.....	36
5	Pattern of thermal treatment and relationship between time and temperature.....	37
6	Typical pellet induration cycle (pilot scale pellets)...	41
7	Scheme of a Beckman air pycnometer.....	47
8	Equipment for the determination of tumbler strength.....	48
9	Schematic diagram of reducibility apparatus.....	50
10	A typical reducibility curve.....	50
11	Schematic diagram of dilatometer.....	52
12	Typical curve obtained from the dilatometer.....	52
13	Set up for swelling test.....	53
14	Weight loss as a function of time and temperature of the raw materials used.....	55
15	DTA curves of pellet mix and concentrate.....	56
16	DTA and TGA curves of the pellet mixes showing occurence of weight loss during melting.....	58

FIGURE		PAGE
17	Fe-O-Ca phase diagram.....	59
18	Electron micrograph of two types of calcium ferrites observed in 5 LB pellets.....	68
19	Typical microphotograph of 2 DB pellets.....	70
20	Typical microphotograph of 2 DP pellets.....	70
21	Typical electron micrograph of 2 DB pellets.....	71
22	Typical photomicrograph of 3 LB pellets.....	73
23	Typical photomicrograph of 3 LP pellets.....	73
24	Typical photomicrograph of 3 DB pellets.....	74
25	Typical photomicrograph of 3 DP pellets.....	74
26	Electron micrograph of 3 LB pellets.....	75
27	Electron micrograph of 3 LP pellets.....	76
28	Electron micrograph of 3 DB pellets.....	77
29	Electron micrograph of 3 DP pellets.....	78
30	Typical photomicrograph of 5 LB pellets.....	81
31	Typical photomicrograph of 5 LP pellets.....	81
32	Typical photomicrograph of 5 DB pellets.....	82
33	Typical photomicrograph of 5 DP pellets.....	82
34	Typical electron micrograph of 5 LB pellets.....	83
35	Typical electron micrograph of 5 DB pellets.....	84
36	Typical electron micrograph of 5 LP pellets.....	85
37	Typical photomicrograph of 6 LB pellets.....	87
38	Typical photomicrograph of 6 LP pellets.....	87
39	Typical photomicrograph of 6 DB pellets.....	88

FIGURE		PAGE
40	Typical photomicrograph of 6 DP pellets.....	88
41	Typical electron micrograph of 6 LB pellets.....	89
42	Typical electron micrograph of 6 LP pellets.....	90
43	Typical electron micrograph of 6 DB pellets.....	91
44	Typical electron micrograph of 6 DP pellets.....	92
45	Effect of basicity on the porosity of the pellets.....	98
46	Effect of basicity on compression strength of the pellets.....	100
47	Relationship between compression strength and porosity..	100
48	Effect of basicity on reducibility of the pellets.....	102
49	Typical photomicrographs of reduced pellets (3 DB).....	103
50	Typical photomicrographs of reduced pellets (3 LB).....	104
51	Typical photomicrographs of reduced pellets (3 LP).....	105
52	Typical photomicrographs of reduced pellets (5 DB).....	106
53	Typical photomicrographs of reduced pellets (5 DP).....	107
54	Typical photomicrographs of reduced pellets (5 LB).....	108
55	Typical photomicrographs of reduced pellets (5 LP).....	109
56	Typical photomicrographs of reduced pellets (6 DB).....	110
57	Typical photomicrographs of reduced pellets (6 DP).....	111
58	Typical photomicrographs of reduced pellets after 15, 30, 45 and 60 minutes of reduction (pellet type 2 DP)...	114
59	Typical photomicrographs of reduced pellets after 15, 30, 45 and 60 minutes of reduction (pellet type 3 DP)...	115

FIGURE		PAGE
60	Typical photomicrographs of reduced pellets after 15, 30, 45 and 60 minutes of reduction (pellet type 5 DP)...	116
61	Typical photomicrographs of reduced pellets after 15, 30, 45 and 60 minutes of reduction (pellet type 6 DP)...	117
62	Effect of porosity on the reducibility of the pellets above 1.3 basicity.....	119
63	Effect of basicity on swelling of the pellets.....	120
64	Typical photomicrographs of the 1 B pellet.....	126
65	Typical photomicrographs of the 1 BP pellet.....	126
66	Typical photomicrographs of the 1 P_2 pellet.....	127
67	Typical photomicrographs of the 2 B pellet.....	127
68	Typical photomicrographs of the 2 BP pellet.....	128
69	Typical photomicrographs of the 2 P_1 pellet.....	128
70	Typical photomicrographs of the 2 P_2 pellet.....	129
71	Typical photomicrographs of the 3 B pellet.....	129
72	Typical photomicrographs of the 3 P_2 pellet.....	130
73	Electron micrograph of 1 B pellet.....	131
74	Electron micrograph of 2 P_2 pellet.....	132
75	Electron micrograph of 3 B pellet.....	133
76	Electron micrograph of 3 P_2 pellet.....	134
77	Effect of peat moss on the porosity of the pellets.....	139
78	Effect of peat moss and bentonite on the compression strength.....	142

FIGURE		PAGE
79	Effect of porosity on the compression strength of the pellets	142
80	Tumbler strength as a function of porosity	144
81	Effect of basicity on the reducibility of the pellets	149
82	Polished sections of reduced bentonite - and peat moss - added pellets basicity of 1.1	149
83	Typical photomicrographs of reduced pellets (1 P_2)	150
84	Typical photomicrographs of reduced pellets (2 P_2)	150
85	Typical photomicrographs of reduced pellets (3 P_2)	151
86	Typical swelling curves of peatmoss added pellets at different basicities	154
87	Effect of basicity on the swelling of CRM pellets	155
88	Mineralogical reactions taking place during induration of pellet	158
A-1	Representation of a grain model for the reaction of a porous solid with a gas	195
A-2	Schematic representation of the two stages of reduction of a porous pellet	195
A-3	Time-reduction relationship in the pellets of 0.8 basicity	209
A-4	Time-reduction relationship in the pellets of 1.3 basicity	210
A-5	Time-reduction relationship in the pellets of 1.6 basicity	211

FIGURE		PAGE
A-6	Time-reduction relationship in the pellets with dolomite and bentonite addition	213
A-7	Time-reduction relationship in the pellets with dolomite and peatmoss addition	214
A-8	Time-reduction relationship in the pellets with limestone and bentonite addition	215
A-9	Time-reduction relationship in the pellets with limestone and peatmoss addition	216
A-10	The system $FeO-SiO_2$ in air	219
A-11	The system $FeO-Fe_2O_3-SiO_2$ system in air	220
A-12	The system $2CaO\cdot Fe_2O_3-FeO\cdot Fe_2O_3-Fe_2O_3$	222
A-13	The system $2CaO\cdot Fe_2O_3-FeO\cdot Fe_2O_3-Fe_2O_3$ showing isothermal sections between 1135°C and 1230°C	223
A-14	The system magnesium oxide-iron oxide in air	225
A-15	Phase equilibria relations in the system $FeO-MgO-Fe_2O_3$ at 1300°C	226
A-16	System $CaO-Fe_2O_3-SiO_2$ (in equilibrium with air)	229
A-17	Chemical compositions of oxide mixtures and their microstructures after heating at 1400°C for 15 min. in air	230
A-18	System $CaO-MgO-Fe_2O_3$ at 1500°C in air	231
A-19	Pseudobinary system $Ca_2SiO_4-MgFe_2O_4$ in air	231
A-20	System $Ca_2Fe_2O_3-Ca_2SiO_4-MgFe_2O_4-Mg_2SiO_4$ melting isotherms	232

I N T R O D U C T I O N

Iron ore pellets are spherical shaped materials produced from concentrates having high iron content (more then 63% iron) with uniform mechanical strength and even porosity in the range of 25-30%. Iron ore pellets are mainly used as burden material in blast furnaces. Depending on the amount of flux addition the pellets are classified as acid or fluxed pellets. If the amount of flux in the pellet is sufficient to produce appropriate amount of slag for the amount of iron in the pellet, then it is known as self fluxed pellet. The self fluxed pellets possess superior pellet properties compared to acid pellets in terms of physical strength, reduction behaviour, swelling characteristics and high temperature properties. As these pellets meet progressively stringent quality requirements, more attention has been given to their use.

The properties of the pellets are largely governed by the form and degree of bonding achieved between ore particles and the stability of these bonding phases during reduction of iron oxides. Therefore studies on the bonding mechanism of the pellets are of prime importance in understanding the basis for the production of pellets of desired quality. The bonding in a pellet is affected by the type and nature of iron ore or concentrate, gangue and other additives and the pelletizing process conditions.

A limited number of investigations have been carried out on the bonding in fluxed hematite pellets in the basicity range of 0.5-1.0 [1,2,3,4,5,6,7]. Moreover since the pelletizing conditions are charactieristic of a particular ore/concentrate, it is essential to investigate the bonding mechanism for each particular concentrate.

Mount Wright specular hematite deposit, which is situated in the north of Quebec is one of the largest in Canada. Therefore, in this study pellets produced from high silica specular hematite were used to examine the effect of various parameters such as basicity, type of flux and binder on the bonding mechanism. The chemical composition of the concentrate is given in Table 1.

TABLE 1 - Chemical composition of Mount Wright specularite concentrate.

% Fe	% SiO_2	% Al_3O_3	% CaO	% MgO	% TiO_2	% Others
66	4.9	0.5	0.04	0.04	0.20	0.03

Bentonite is commonly used as binder in pelletizing industry. Due to short supply of good quality bentonite, the price of bentonite has increased. Moreover, use of bentonite is also associated with disadvantages such as chemical contamination and additional flux requirement.

Use of porous pellets has been found to be beneficial as reduction and high temperature properties are improved due to increased

porosity. This has resulted in higher productivity and lower coke rate in the blast furnace [8,9,10].

In order to obviate the disadvantages of using bentonite as binder and increase the porosity in the pellets, several alternative combustible binders have been investigated [11,12,13,14,15]. One of the combustible binders which has aroused considerable interest as a substitute to bentonite is peat moss. Use of peat moss in the production of acid pellets has resulted in increased porosity, improved reducibility and lower swelling [14]. Other advantages of peat moss addition are: marginal heat saving during firing through realisation of heat content of peat moss and non toxicity.

As peat moss is abundantly available in the north of Quebec and in the vicinity of iron ore mines, a study was undertaken to evaluate peat moss as binder for production of self fluxed pellets.

So, in summary, the objectives of the present study are:

1. To study the effect of type of binder and flux on the bonding mechanism of self fluxed pellets.
2. To evaluate peat moss as a binder for the production of fluxed pellets.

To achieve the objectives, two sets of pellets were produced using high silica specular hematite concentrate. One set of pellets was

produced in the laboratory to study the bonding mechanism and the other set was produced in pilot plant scale to evaluate peat moss as binder. The pellets produced were of blast furnace grade. The basicity index B used in the study is defined as

$$B = \frac{\text{Wt\% } CaO + \text{Wt\% } MgO}{\text{Wt\% } SiO_2 + \text{Wt\% } Al_2O_3}$$

The pellets used for bonding mechanism studies were prepared in a small disc pelletiser and indurated in a resistance furnace. Pellets were produced at the basicity indices of 0.2, 0.8, 1.3 and 1.6. At each basicity level, basicity index was maintained by addition of only limestone or dolomite and limestone as flux. The dolomite addition was restricted to 9% in order to maintain the MgO level in the pellet to 1.8 to 2%, which is the normal industrial practice. To investigate the effect of binders the pellets were produced using 1% bentonite and 3% peat moss as binders. The peat moss addition had to be limited to 3% as the concentrate contained 1-1.4% coke breeze and any further addition of peat moss would lower the mechanical properties of the pellets to unacceptable levels. The coke breeze addition is now considered as a standard energy saving practice in the pelletizing plants in Quebec. The bonding mechanism studies were carried out by characterizing the bonding phases using optical microscope, scanning electron microscope and energy dispersive spectrometer. Some physical and reduction properties of the pellets such as porosity, compression strength, reducibility and swelling were also determined using standard test procedures.

The pellets used to evaluate peat moss as binder were produced in a standard disc pelletiser and indurated in a pot grate. The pellets were produced at 3 basicity levels of 0.8, 1.1 and 1.3. The basicity index was maintained by addition of 9% dolomite and limestone. Peat moss addition was made at two levels i.e.: 1.5 and 3%. Pellets were produced with 1% bentonite addition which served as reference pellets for the assessment of pellet properties of peat moss added pellets. To study the combined effect of peat moss and bentonite, pellets were also produced with 0.5% bentonite and 1.5% peat moss additions. The green stage and fired properties along with pellet mineralogy were evaluated.

The thesis has been divided into five chapters.

The first chapter deals with basic aspects of pelletisation. In this chapter the pelletisation process is briefly described which is followed by a discussion on the bonding mechanism at various stages of pelletisation. The current issues which are of concern to pelletisation process are: alternative binder to bentonite, production of fluxed and porous pellets. A literature review on these three issues has been made. In the second chapter the experimental procedures for production and testing of each set of pellets is described. The results of laboratory scale pellets and pilot scale pellets are presented in chapters 3 and 4 respectively. In chapter 3, results of the bonding mechanism studies are presented first which is followed by the presentation of fired pellet properties. In chapter 4, green and fired stage properties of the pilot scale pellets are presented. Chapter 5 contains discus-

sions on the bonding mechanism of fluxed pellets, the role of peat moss on green stage properties and fired pellet properties, conclusion and recommendations. The discussion on bonding mechanism is preceded by a literature review on pellet mineralogy.

C H A P T E R 1

BASIC ASPECTS OF PELLETISATION

1. PELLETISATION PROCESS

The pelletisation process essentially consists of three steps: 1. raw material preparation, 2. green ball formation and 3. induration. Each process step is very important for good pellet production and is influenced by the preceeding process step. A defect which is introduced at one process step cannot be totally eliminated in subsequent steps.

In the first process step raw materials such as iron ore concentrate, binders, fluxes and other additives are ground to finer sizes and mixed thoroughly. Thorough mixing is very essential to obtain uniform distribution of binder and additives in the mix and to compensate for the differences in the chemical composition of different constituents. In the second process step the mix is rolled in a pelletising drum or disc with addition of small amount of water. Wet balls in the required size range are formed which are known as green pellets. These green pellets are indurated at a temperature just below the softening point of the ore under oxidising atmosphere following an induration cycle consisting of drying, preheating, firing and cooling. Under these conditions suitable pellet properties such as good compression strength, abrasion resistance, etc., are achieved. Different types of

kilns such as shaft furnace, travelling grate and grate kiln are used to indurate green pellets.

For details on pelletising process, various publications [1, 16, 17, 18, 19, 20] can be consulted.

2. THE BONDING MECHANISMS DURING VARIOUS STAGES OF PELLET FORMATION

A pellet should have adequate mechanical strength right from the green ball formation stage so that it preserves its integrity during subsequent process steps.

2.1 Bonding mechanism during green ball formation

Forces which contribute to the formation of green pellets are of two kinds [23]:

1. Physical;
2. Applied or mechanical.

Physical forces responsible for formation of agglomerates originate from following sources [21]:

1. Vaan der Waals, magnetic, electrostatic forces, etc. which cause attraction between solid particles.
2. Surface dependant factors such as particle size, particle size distribution, particle shape and crystal structure.

3. Material dependent factors such as wettability, absorption capacity due to porous structure, availability of swelling component, chemical properties of primary ores.
4. Interfacial and capillary forces due to the presence of a liquid phase.

Mechanical forces are required to bring individual wetted particles within the pelletising charge into contact with one another so that physical forces can facilitate their growth [22]. The mechanical action of moving the material is provided by means of rolling, tumbling, agitation and compressing in a suitable apparatus.

Forces such as Vaanderwaals', magnetic etc., have very insignificant contribution to green ball formation. Raw material dependent factors affect the ballability to a great extent. Therefore optimization of process conditions for green pellet formation is attained by adjusting factors such as amount of wetting agent, particle size and shape, balling equipment, etc.

A liquid which completely wets the particle surface is required for the formation of green balls out of solid particles. The liquid acts like a binder. Capillary forces developing between the particles due to air-liquid interfacial tension are the major force which contribute to hold the particles together. Under the action of such forces a certain tensile strength develops. The capillary forces are dependant on the relative distribution of the liquid and air phases in the porous agglomerate [22,23].

In the pelletising equipment such as drums or discs the solid particles are subjected to rolling along with the liquid. The rolling action of the solid particles have a high compression effect on the green balls, in the order of several MN/m^2 [24]. This high pressure is generated on the surface of the balls where a few particles take the load of the entire ball.

The formation of green ball takes place in several stages [1] which is shown in Figure 1. The solid particles are wetted when they come in contact with the liquid. The liquid coats the particle with a thin film (phase A). Liquid bridges are formed when different wetted particles contact each other due to surface tension (phase B). Due to movement of the particles inside the balling unit and water droplets the first agglomerates are formed (phase C). At this stage the ratio of liquid to the void volume of agglomerate is quite low. The liquid is held in discrete lens like rings at the point of contact between particles and the air phase forms a continuous phase. The liquid is said to be in a pendular state. With increasing liquid content densification of the agglomerates take place as the liquid rings coalesce to form a continuous phase (phase D) and the air phase is trapped. The agglomerate is said to be in a funicular stage. At this stage capillary forces of the liquid bridges are fully active. When the void volume of the agglomerate is completely filled with liquid the optimum of ball formation is said to have been achieved. At this stage the liquid has not coated the outer surface of the agglomerate (phase E). Concave liquid surfaces form on the outer pores and capillary suction is holding the

ore particles together. The agglomerate is said to be in capillary state. When the agglomerate is fully coated with liquid film the final stage of ball formation is exceeded. The surface tension of the water droppet become fully active.

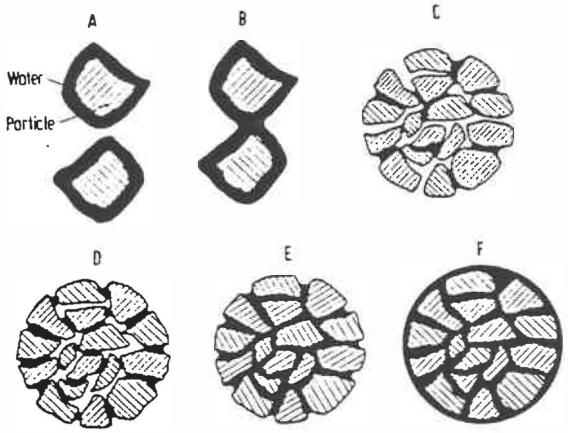


FIGURE 1 - Different stages of green ball formation [1].

Apart from compacting the agglomerates due to pressure and movement, the rolling movement of the particles in the pelletising equipment also damages mechanically weak granules which have not attained sufficient strength. The weak balls may desintigrate to minor fragments or even finer particles. During green ball formation these fractions are layered into moist stable green balls.

Sastry and Fuerstenau [25] have suggested that the ball formation takes place following a different method as shown in Figure 2.

1. Layering of fine particles to each other and formation of an agglomerate.
2. Conglomeration of smaller balls already existing resulting from relative motion and certain pressure.
3. Layering on and incorporation of minor fragments from damaged green balls into existing sound ones.
4. Incorporation of fine grained abraded material from weak pellets into the surface of stronger pellets.

During green ball production the formation and disintigration takes place simultaneously. Only strong balls survive and weakballs are destroyed. Finally only uniform, dense and stable balls are produced. Figure 2 describes alternative mechanism for green pellet formation.

According to the visco-capillary bonding model developed by Wada and Tsuchiya [26] viscosity of interstial liquid also contributes to the green pellet strength in addition to the capillary forces.

Since major bonding in the green pellets is provided by the interstitial moisture, the binder plays a role in the bonding mechanism. It is responsible for uniform distribution and control of moisture inside the pellet structure [27]. According to Roorda et al. [11], the binder improves green pellet bonding by increasing the viscosity of the moisture.

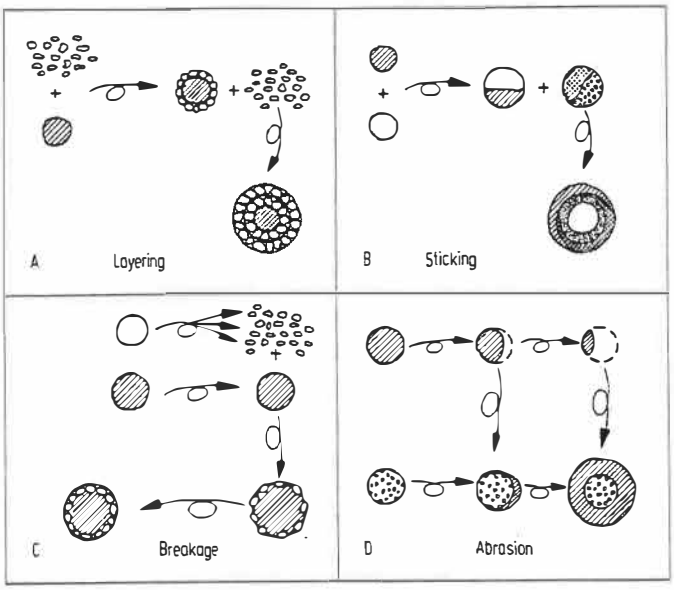


FIGURE 2 - Alternative of green ball formation [25].

2.2 Bonding mechanism during induration

During the initial stage of induration, i.e. drying, the moisture inside the pellet begins to evaporate . As a result, the bonding due to capillary forces and surface tension gradually diminishes. Although physical forces such as molecular, adhesive, Vaander Waal's and electrostatic may be active at this stage their contribution to bonding is negligible. The binder which is dispersed through out the pellet structure provides bonding between the ore particles by formation of contact bridges designated as "mortar bridges" by Rumpf [21]. These bonds are active until the formation of other types of bonds during later part of induration.

During the later part of induration several factors such as recrystallisation and grain growth of the hematite, formation of compounds due to reaction of flux with gangue and iron oxide are responsible for the bonding in the pellets. Bonding occurs both in the solid and liquid stage. However, in fluxed pellets major bonding occurs due to presence of a liquid phase.

Solid state bonding in iron ore pellets occurs in following two stages [7,28]:

1. Activation of the movement of the crystal lattice which causes molecular rearrangements, the closing together of particles (neck growth) with slight amount of densification.
2. Formation of a coherent network of ore particles and connected pores with recrystallisation and rapid densification.

Solid state bonding in hematite pellets is mainly influenced by temperature and particle size. The formation of hematite network is reported to occur above 1100°C [1]. Higher extent of bonding is achieved in pellets with increasing proportion of fine particles as these particles recrystallise and form "bridges" between coarser particles [2, 3, 28, 29, 30, 31].

Fine hematite particles also react with lime to form ferrite which also contribute to solid state bonding [6, 31, 32, 33, 34] in the temperature range of 1000-1200°C. However, this bonding is of little importance as the ferrites disappear at the advent of liquid formation.

With increase in temperature a liquid phase appears in the pellet due to melting of calcium ferrites [31, 32] or low melting gangue minerals [2]. Presence of melt during induration radically changes the strenghening mechanism which essentially follows three classic steps of liquid phase sintering as described in ceramics and powder metallurgy literature [35,36], i.e.:

1. Particle rearrangement;
2. Solution reprecipitation;
3. Solid state particle coalescence.

The above three stages overlap each other and are shown schematically in Figure 3. The particle rearrangement step appears to be an important bonding mechanism. There is rapid initial densification as the wetting liquid exerts capillary force on the solid particles. As the particles are drawn together due to surface tension forces, changes occur in the shape of pores and the character of porosity. The extent of densification attained by rearrangement is dependent on amount of melt, particle size and solubility of the solid in the melt.

As the melt spreads through the space between the solid particles, dissolution of hematite and gangue particles takes place [31, 37, 38]. The non metallic mineral components of the mix dissolve completely and the ore components dissolve to a limited extent. The fine particles are fully dissolved and the larger ones are only attacked at the surface [38]. Due to difference in the solubility of fine and large

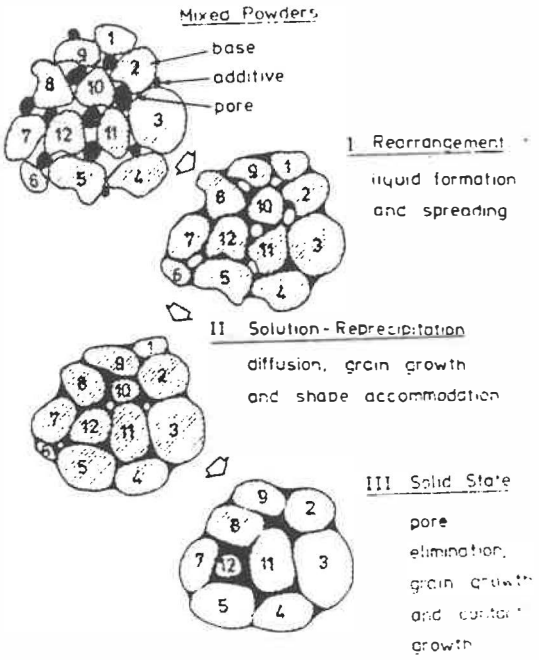


FIGURE 3 - The classic stages of liquid phase sintering involving mixed powders which form a liquid on heating [36].

grains a concentration gradient is established in the melt. This causes diffusion of material from small grains to larger grains resulting in coarsening of larger grains [36]. This is the second stage i.e. the solution reprecipitation.

The reaction of dissolved silica with ferrites leads to the appearance of a silicate melt and reprecipitation of iron oxide [39].

The solid state particle coalescence which is the third stage of liquid phase sintering, is not considered significant in bonding of fluxed iron ore pellets. On the other hand the strengthening of the pellets is influenced to a great extent by the binding phase which solidifies from the melt. The silicate is the major binding phase in

the fluxed pellet. The silicate slag phase is vitreous or crystalline depending on the basicity, cooling rate and additives [38, 40, 41, 42]. At low basicity of 0.8 vitreous silicate is formed [38, 43, 44]. As the basicity is increased with the addition of CaO, crystalline silicate formation takes place along with crystallization of calcium ferrites. At the basicities of 1.8 and above the binding phase mainly consists of calcium diferrite and dicalcium silicate [45]. In the intermediate basicity range the binding phase contains varied amount of vitreous and crystalline silicates and calcium ferrites [44,46]. The pellets having only vitreous or crystalline binding phase are reported to have good strength properties where as the pellets with mixed phases have inferior strength properties. The lower strength is attributed to the heterogeneity of the binder phase [44, 46].

Nekrasov et al. [38] has observed the change in the nature of silicate from glassy to crystalline by lowering the cooling rate and addition of MgO.

Although bentonite is known to promote melt formation in the presence of gangue and flux, its individual contribution to bonding is not known. While Lu et al [39] have suggested that bentonite promotes solid state bonding, Ranade et al [10] have suggested formation of alumino-silicate due to bentonite addition. However, they have not found any conclusive evidence of the presence of such a phase from the microscopic studies.

In summary, in the green pellets the bonding is provided by water bridges between the ore particles. The slag phase solidifying out of the melt provides the bonding in the fired pellets.

3. ALTERNATIVE BINDERS TO BENTONITE

Binders have been found to be indispesable for iron ore pelletisation as they influence each step of the process. The binders affect green ball formation by controlling the movement of water within the rolling ore mass by maintaining uniform water distribution. They also control the pellet growth due to their good moisture absorption capacity. They finally provide a stable bond during early stages of induration.

Due to its inherent properties bentonite is the most commonly used binder in pelletising industry. However, the drawbacks associated with its use such as short supply of binder grade bentonite, increasing cost and chemical contamination of the ore with silica and alumina had led to the search of an alternative binder to bentonite. Several inorganic and organic substances which are listed in Table 2 were tried as binder. Their performance as binder is listed in Table 3.All the inorganic substances were found to contaminate the ore concentrate, influence metallurgical properties or cause environmental concern. On the other hand as the organic binders burnt off or volatilised during pelletisation no contamination in the pellet occurred. But these substances were not claimed as a suitable replacement to bentonite since

they did not satisfy other requirements such as moisture controlling ability [51, 54].

TABLE 2 - List of inorganic and organic substances which were tried as an alternative binder to bentonite.

SUBSTANCES		REFERENCES
Inorganic substances	NaCl, NaB_2, KCl, NH_4Cl, CaO, CaOH, $CaCl_2$, borax, Na_2CO_3	1, 47, 48, 49, 50
Organic substances	Starch, dextrin, glucose, humic acid derivatives, sulphate, lye, lignins, paper and sugar plant waste, liqours etc., jaguar, peridur	11, 12, 15, 47, 50, 51, 52

TABLE 3 - Performance of the alternative binders.

BINDER	GREEN STAGE PROPERTIES	DRY PELLET STRENGTH	BALLABILITY	WATER ABSORPTION CAPACITY	OTHERS	REFERENCES
Alkali salts $NaCO_3$, NaO, etc.	good	good	NA	NA	Contamination swelling	47, 50
Hydrated lime	good	good	poor	poor	-	1, 48, 49
Starch, sulphite lye, etc.	good	good	NA	NA	Poor strength during induration	50
Humic acid derivatives	good	good	poor	poor	-	52
Peridur	good	good	good	good	-	11, 12, 54
Peat moss	good	good	poor	good	good metallurgical properties	13, 14, 15

Redgion et al. [50] used organic substances such as starch, dextrin, sulphite lye and alginate as binders. The green impact strength was reported to improve with 3% sulphite lye addition. However, these substances burnt off during initial stages of firing, i.e. before the commencement of recrystallisation bonding. Hence they do not improve the strength during firing. Redgion et al. [50] also observed that inorganic salts such as NaOH, Na_2CO_3, K_2CO_3 and $CaCl_2$ are more effective than organic substances for the green, dry and fired strength of the pellets. The favourable effect on the green strength is attributed to the increased surface tension of water due to salt addition [50]. This appears to be an acceptable explanation since surface tension of water is a major force which contributes to green pellet strength.

Tigerschold [48] found that good pellets were obtained by using lime as a binder as green and dry strength properties of these pellets were comparable with those of the pellets with bentonite addition. Hydration of the lime is the reason for good pellet strength. Lime hydrate acts like a hydrogel due to formation of high surface area and adherence of high amount of water to the surface. The colloidal properties of the hydrogel improved the plasticity of ore mix and strengthened the bonding mechanism or dried pellets [1]. In a latter investigation [49] the combined effect of lime hydrate and increased surface area was found to be beneficial in improving pellet properties. Although hydrated lime is being used as a binder in several off shore pelletising operations due to its lower cost, it is not considered as a

good binder as it does not possess the water absorption and thixotropic properties of bentonite [56].

Humate derivatives developed from various substances such as animal manures to acrylamide polymers were claimed to be a suitable substitute to bentonite [52]. However, they showed a poorer ballability and moisture controlling ability to bentonite.

Ball et al. [47] studied the role of additives on the strength of dry pellets by using water soluble electrolytes (NaCl, NaBr, NH_4Cl, etc.), non electrolyte (glucose, fructose) and non soluble substances. They observed that the dry compression strength is a function of solubility and cell volume of the water soluble additives. They argued that pellets formed with an additive of high solubility and cell volume will have good dry compression strength due to formation of dense thin crust which closes the inter particle voids during drying. They further observed that in the pellets with bentonite addition dry stage bonding is provided by the random dispersion of bentonite in the pellet structure. Their observation that dry pellet strength is a function of $(Na_2, K_2)O$ content of the bentonite is in confirmity with the observations made by Stone [63] and Fuerstenau and Clark [64] who correlated the improved dry strength to the high negative zeta potential resulting from sodium salt addition.

Only two substances; peridur, a cellulose derivative and peat moss a carbonaceous material appear to be most promising alternative to bentonite (10, 11, 12, 13, 14; 54, 55).

A cellulose based binder, peridur has been claimed as a substitute to bentonite [11, 12, 54]. The pellets produced with peridur are reported to have good green stage properties, dry strength and good moisture retention capacity. The pellets have high drop number which is attributed to the high viscosity of the interstitial moisture resulting from peridur addition [11]. Improved reduction properties in the pellets has been claimed due to increased porosity as the binder burnt off during induration [10]. However, high cost of peridur may be a deterrent for replacing bentonite although very low peridure addition has been claimed to give good pellet properties. Moreover, due to low level of binder addition, high porosity in the pellets may not be achieved in fluxed pellets (a requirement for high reducibility); the difference between the porosities of peridur and bentonite added acid pellets is found to be small [10, 11]. What is not clear is; how the pellet strength is retained during preheating period as the cellulose bond would burn off at preheating temperature. Since trials with peridur were carried out with magnetite in most of the cases, the strength retention problem might not have been acute as strength development due to magnetite to hematite oxidation starts around 375°C. In case of hematite the strengthening mechanism is slow during preheating as appreciable strength is not obtained below 1100°C [1].

Peat moss has been periodically investigated as a binder since initial industrial application of pelletisation in 1954 [57, 58]. The investigations were discontinued as the process was considered economically unviable compared to the use of bentonite [13]. Increase in the

price and inconsistency in quality of bentonite have renewed interest to pursue further research on peat moss. Encouraging results were obtained by Appleby, Lemay and Morimoto [59] by using peat moss as a binder at Sidbec pelletising plant. On further investigation at Centre de Recherches minérales, Quebec city it was observed that the binder quality of the peat moss is not dependent on the humic acid content [13]. Statistical analyses have also shown that there is no correlation between the physical and chemical properties of the binder with green-stage properties of the pellets [61,62]. It was observed that the binder properties of peat moss are influenced by the addition of water soluble bases at a particular pH which changed the surface of peat moss from hydrophobic to hydrophilic. Small addition of KOH, Na_2CO_3, NaOH is found to be effective whereas slightly soluble CaOH produced opposite results. The binding characteristics of peat moss is improved by increasing peat moss concentration of the feed, increasing pH of the feed with water soluble base and fine grinding of peat moss. However, from all these studies [13, 60, 61], the influence of peat moss on the fired pellet properties is not clear [13, 64] since low reducibility and high swelling in the pellets are reported. It is possible that other additives such as calcite and dolomite might have influenced these properties. Investigations by Panigrahy et al. [14] have shown that acid pellets produced from low and high specularite concentrate using 1-3% peat moss as binder possess adequate green, dry and fired strength and have superior reducibility and swelling properties than the pellets with bentonite addition. They [14] claim that high porosity

in the pellets obtained, due to peat moss addition, was responsible for the good reduction and swelling properties. Godin et al. [55] also obtained good quality pellets using 1% peat moss as binder. They reported low swelling in these pellets.

From the review of previous work it is seen that while the binding properties of peat moss has been established from these studies, adequate information on the effect of peat moss on the fired pellet properties are not available since the study was limited to acid pellets.

4. FLUXED PELLETS

Several investigators, Edstrom [65], Tigerschold [48], and Ilmoni and Uggla [66] have observed that addition of lime to the iron ore pellet mix improves cold compression and reduction strengths of the pellets. Merklin and Devaney [67] observed poor reducibility of the lime fluxed pellets which they attributed to the slag sealing. Chang and Malcolm [4] investigated quality of fired pellets using several iron bearing raw materials and concluded that superior pellet property requirements such as high strength, high reducibility and low swelling could be met by producing lime fluxed pellets. They [4] attributed high reducibility to the presence of calcium ferrites and superior strength properties due to slag bond. Kortmann and Burghardt [68] studied the influence of silica and lime on the quality or iron ore pellets. They observed that the compression and tumbling strength of the fired pel-

lets are improved with increasing CaO/SiO_2 ratio of 1.0. Above that ratio the strength values decreased. The reducibility initially decreased with lime addition reaching a minimum at the CaO/SiO_2 ratio of 0.7 and then increased with increasing CaO/SiO_2 ratio. The low reducibility was attributed to insufficient strength and heavy shrinkage which adversely affect the passage of reducing gas inside the pellet. The swelling was also reported to reach a maximum at low CaO/SiO_2 ratio of 0.4 and then decrease with increasing CaO/SiO_2 ratio. Silica addition was effective in decreasing the swelling. However, they reported heavy disintingration during low temperature disintigration test in fluxed pellets. Similar observations were also made by Swedish researchers [42, 69], who found that lime pellets above the CaO/SiO_2 ratio of 1.8 showed very poor low temperature breakdown strength (LTB). They inferred that calcium diferrite which is the major bonding phase in these pellets is weakened during low temperature reduction and is incapable of absorbing the strains generated during iron oxide reduction. But this is not a satisfactory explanation since calcium ferrite is not reduced below 650°C [70,71]. Shigaki et al. [70] suggested that the fragility of calcium ferrite is the reason for low LTB strength of the pellet. On the other hand Mitra et al. [72] and Friel and Erickson [73] have shown that calcium ferrite bonds are strong enough to withstand low temprature disintigration. Moreover, the high basicity pellets show low swelling [42], indicative of high degree of structural integrety in the binding phase which is unaffected by the reducing atmosphere [6, 74]. Therefore, it is unlikely that calcium ferrites is

the possible cause of low temperature disintigration. Matsuno et al. [89] also have found no correlation between LTB and calcium ferrite.

Because of superior pellet properties lime fluxed pellets became a high quality burden in Japan and Russia [39, 75]. However, lime fluxed pellets were found to have poor high temperature properties such as low softening and melting down temperature, high degree of contraction and retarded rate of reduction at high temperature [76, 77]. The lime fluxed pellets form a metallic shell on the surface and an iron oxide slag with a lower melting point (below 1250°C) at the core during reduction in the blast furnace. The molten slag migrates to the surface from the inside of the pellet and seals off the pores. This prevents the diffusion of reducing gas into the core thus resulting in retarded rate of reduction. Efforts on improving high temperature reduction properties of lime fluxed pellets led to the development of dolomite fluxed pellets [69, 76, 77, 78]. These pellets were found to have a lower contraction ratio, higher softening and melting down temperatures and less retardation of reduction as compared to lime fluxed pellets [76]. This improvement in high temperature properties was attributed to presence of MgO which raises the melting points of slag and iron oxide [80]. The optimum MgO content of dolomite fluxed pellets in the basicity range (CaO/SiO_2) of 1.2 to 1.8 is found to lie between 1.2 to 2.0% [76, 90].

Another laboratory study [45] showed dolomite addition to be more effective than lime or magnesia addition on improving pellet properties. Other MgO bearing fluxes such as olivine, magnesia, etc.

also have been used for the production of fluxed pellets (80, 81, 82, 83, 84]. These studies were carried out in order to understand the effect of MgO on the pellet properties. Sugiyama et al. [80] have shown that thermal decomposition of magnesite increases the porosity of fired pellet and this serves to improve the reducibility. They have concluded that the properties of MgO containing pellets are characterised by magnesioferrite. The amount of magnesioferrite in the pellet is a function of CaO/SiO_2 ratio. Hasanek and Keddeman [81] studied the effect of MgO addition the strength properties of fired pellets by adding magnesite dolomite and olivine as flux. They [81] observed that cold compression strength and low temperature breakdown (LTB) are adversely affected by MgO addition. Similar observation has also been made by Kong Ling Tan et al. [84] who have identified the presence of complex spinel as the cause of poor LTB. On the contrary, completely opposite observation has been made by Thanning [42], who has stated that the spinel is responsible for improving low temperature breakdown strength.

Summarising, the fluxed pellets have better strength and reduction properties compared to acid pellets. However, lime fluxed pellets have poor high temperature properties which could be improvised by the addition of MgO. Addition of MgO raises the melting points of the slag and iron oxides. There are conflicting views on the effect of magnesio-ferrite and calcium diferrites on the LTB property of the pellets.

5. THE POROUS PELLETS

The beneficial effect of the porosity on the reducibility of the pellets has been known for a long time. The reactive gases reach the interior of the pellet through the interconnected pores. With increasing porosity the passage of reacting gas in the interior of the pellet is facilitated and this results in higher reducibility.

The increase in porosity has also been found to decrease LTBT [91] and swelling in pellets [69, 85]. Apart from the having beneficial effect on the medium temperature properties of the pellet, the porosity also has salutary effect on the high temperature properties of the pellet. By increasing the degree of pre-reduction at lower temperature, a smaller amount of wustite is made available for formation of liquid slag at high temperature [39]. Further, the pores enhance high temperature reducibility and are able to contain the liquid slag thus preventing leakage [86].

Several methods have been adopted to increase porosity in the pellets such as incorporation of MgO bearing compounds [83, 84, 85, 86, 87, 88], coarser feed [90], carbonaceous materials [8, 9, 91] and combustible binders [10, 11, 12, 13, 14] in the pellet. Most notable improvement in porosity has been reported due to addition of carbonaceous materials.

An increase in pellet porosity has been reported due to addition of magnesite and dolomite [80, 85]. Increase in porosity is attributed to the decomposition of carbonates and is stated to be the cause of increased reducibility and decreased swelling [80]. The poro-

sity is also reported to increase due to olivine addition [83]. Due to stabilisation of magnesioferrite a smaller degree of sintering takes place in the pellet which is stated to be the cause of increase in porosity. The reducibility of the pellet is favourably affected by MgO addition [96].

Sugiyama et al. [90] have increased open porosity of the pellets and thereby improved the reduction properties of the pellets by incorporating coarser feed of upto 40% without affecting mechanical properties of the pellets.

A new type of fluxed pellet has been developed by Fujita et al. [92] to improve reducibility of the pellets. In this pellet a slag phase containing rankinite and tridymite precipitates among iron oxide grains. This precipitated slag phase initiates cracks, when heated during reduction. The fragmentation of pellets is reported to have improved the reducibility substantially.

Japanese researchers at Kobe Steel [8, 9] further improved the quality of the dolomite fluxed pellets by enhancing the porosity in the pellets. By using 2.5% saw dust the porosity was reported to increase from 26.3 to 34.7%. This resulted in the increase in the degree of reduction by 8-12%. A decrease in the fuel rate by 13% was also reported.

Elmquist et al. [91] had studied the effect of porosity on pellet properties by using various carbonaceous additives such as saw dust, peat and lignite. They observed that porosity and ferrous iron content increased with increasing amounts of carbonaceous additives.

The increase in porosity has a favourable effect on pellet reducibility and adverse effect on compression and tumbler strength. Similar observation was also made by Stegmiller et al. [93] who used 0.5 to 2.0% charcoal fines in the pellets. They concluded that high porosity pellets having overall good quality characteristics can be produced with 1-5% charcoal addition.

Bentell [87] has reported an 8-10% increase in porosity in the pellets by addition of 2% peat moss of 50% moisture content. This resulted in the increase in reducibility.

At Dofasco, marginal increase in reducibility in acid pellets has been reported by Stewart [94] inspite of significant increase in porosity by addition of carbonaceous substances such as peat moss saw dust and tree bark. Similar observation is also made by Gariépy [64]. While Stewart [94] has stated the absence of fine interconnected pore structure to be the reason for marginal improvement in reducibility, pellet chemistry may have more contribution as he has also reported improvement in reducibility by increasing MgO/SiO_2 ratio.

Producing porous pellets by using combustible binder has already been discussed in a preceding section dealing with alternative binders to bentonite. As stated earlier, two combustible binders peridur and peat moss have shown promising results.

Summarising, highly porous pellets can be produced by using carbonaceous additives which have improved metallurgical properties at low and high temperatures.

CHAPTER 2

EXPERIMENTAL PROCEDURES

1. PRODUCTION OF PELLETS

In the present work two sets of pellets were produced. One set of pellets was produced in the laboratory to study the effect of fluxes and binder on the bonding mechanism of pellets. The second set of pellets was produced in the pilot plant scale to assess the effect of peat moss on pellet properties. High silica specular hematite of Mount Wright was used for the present study. the size and chemical analysis of the raw materials are given in Tables 1 and 4. The proximate analysis and heat content of peat moss and coke breeze is shown in Table 5.

TABLE 4 - Raw material size and chemical analysis.

RAW MATERIAL	SIZE	% Fe	% SiO_2	% Al_2O_3	% CaO	% MgO	% Na_2O	% K_2O
Dolomite	65% (- 44 μ)	0.22	1.0	0.4	30.30	20.75	-	-
Limestone	65% (- 44 μ)	-	2.0	0.6	53.00	0.50	-	-
Bentonite	69% (- 44 μ)	2.41	64.43	18.42	1.5	2.00	2.22	0.60

TABLE 5 - The proximate analysis of peat moss and coke breeze.

	PEAT MOSS (moisture free) (%)	COKE BREEZE (%)
Fixed carbon	29.2	80
Volatile matter	59.1	5.5
Ash content	11.7	13.0
Specific heat content	20.580 kJ/kg	26.350 kJ/kg

2. PRODUCTION OF FLUXED PELLETS IN LABORATORY

For this part of the study pellets were produced in a wide range of basicities; from 0.2 to 1.6. Bentonite and peat moss were used as binders to assess their effect on bonding. Addition of 1% bentonite was made in pursuance with the present industrial practice. Peat moss addition was restricted to 3% in veiw of the fact that the concentrate contained about 1.4% coke breeze and further addition of peat moss may weaken the pellet. To study the effect of fluxes on bonding, limestone and dolomite were used as fluxes to obtain a specific basicity. In dolomite fluxed pellets MgO content was maintained at about 2% at all basicities. Therefore, in dolomite fluxed pellets some amount of limestone addition was made to attain specific basicity.

Initially a few numbers of pellets were prepared by hand [95]; first making cyclindrical compacts and subsequently shaping those compacts to spheres by abrasion technique. The pellets were indurated in a

horizontal furnace having three different temperature zones. However, the compression strength of these pellets was very low. Moreover, only a small number of pellets could be prepared by this technique, which was not adequate for carrying out tests to assess overall pellet properties. Therefore, this method of pellet preparation had to be discontinued. Green pellets were produced in a small disc pelletiser and indurated in a Lindberg furnace. The compression strength of pellets produced by the latter method improved considerably.

2.1 Preparation of green pellets

The pellets were prepared at four basicity levels, i.e., 0.2, 0.8, 1.3 and 1.6. At each basicity level, pellets were prepared with the addition of either 1% bentonite or 3% peat moss to assess the effect of binder. At 0.2 basicity the pellets were produced with the addition of 1.8% dolomite in confirmity with the practice adopted for the production of acid pellets at some of Quebec's pelletising plants. All other basicity levels were achieved by addition of i) limestone and ii) combination of 9% dolomite and balance limestone. Addition of 9% dolomite corresponded to a MgO content of approximately 2% in the fired pellets. The iron ore concentrates contained 1.4% of coke breeze which is a standard energy saving practice at majority of pelletising plants in Quebec. The pellet designations and amounts of different additives in the raw mix are shown in Table 6. The numbers 2, 3, 5 and 6 referred to basicity levels 0.2, 0.8, 1.3 and 1.6 respectively. The letter L referred to the pellets using limestone as flux and the letter D

referred to pellets produced with dolomite or dolomite and limestone as flux. The letters B and P referred to pellets using bentonite peat moss as binders respectively.

TABLE 6 - Pellet designation and percent weight of binders and fluxes in green pellet mix (dry basis).

BASICITY $\left(\frac{CaO + MgO}{SiO_2 + Al_2O_3}\right)$	PELLET TYPE	WEIGHT %. BINDER/ADDITIVE			
		Bentonite	Peat moss (55% H_2O)	Dolomite	limestone
0.2	2DB	1.0		1.8	
	2DP		3.0	1.8	
0.8	3DB	1.0		9.0	0.1
	3DP		3.0	9.0	
	3LB	1.0			8.9
	3LP		3.0		7.4
1.3	5DB	1.0		9.0	6.4
	5DP		3.0	9.0	3.7
	5LB	1.0			14.9
	5LP		3.0		12.8
1.6	6DB	1.0		9.0	10.5
	6DP		3.0	9.0	6.8
	6LB	1.0			18.7
	6LP		3.0		16.1

2.1.1 Preparation of pellet mix

About 1 kilogram of concentrate was mixed thoroughly by an impeller type agitator after adding required amounts of binder and flux. A small amount of NaOH addition was made to improve surface properties of peat moss before mixing with the concentrate. NaOH was dissolved in water and mixed with peat moss. The pH of the solution was adjusted to 10.5-11.

2.1.2 Green pellet formation

Green pellets were prepared in a small disc pelletiser of 29 cm dia. at an inclination of 42° rotating at 20 rpm. The pellet feed was charged to the disc through a vibratory feeder. The feed rate was controlled through a variac. The water was added through a burette drop by drop. The disc pelletiser is shown in Figure 4. After initial seed formation the pellets grew with further addition of pellet mix. Pellets fell off the disc after attaining a certain size and were collected on a 10 mm screen. Pellets of + 10 mm -15 mm size were taken for drying.

By optimising pelletising conditions about 90% of the pellets in the size range of + 10 mm - 15 mm were produced. The time for producing peat moss added pellets were longer than that of bentonite added pellets. NaOH addition to the peat moss was found to affect the ballability of the pellets. With very low NaOH addition (0.01%) the ballability was poor. With increasing NaOH addition to 0.1% the ballability was improved. this confirmed that NaOH does change the surface characteristics of peat moss and enhances its capacity for binding [13].

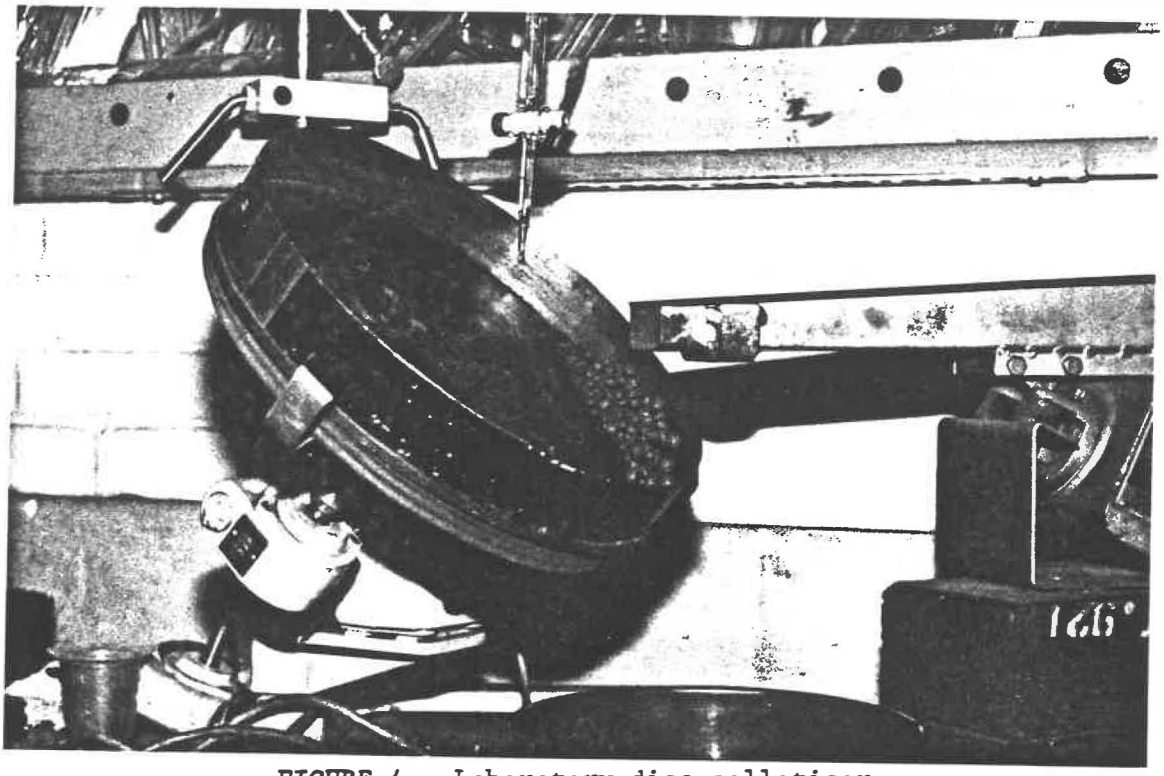


FIGURE 4 - Laboratory disc pelletiser.

2.2 Pellet induration

The green pellets were dried in an electric oven for 24 hours at 110°C. The dried pellets were indurated in a Lindberg furnace. The furnace was heated to the firing temperature and held at that temperature for 15 minutes. After that the furnace was shut off and the fired pellets were allowed to cool inside the furnace. The induration cycle of the pellets is shown in Figure 5. All the pellets were fired at 1300°C except the pellets produced with limestone and bentonite addition at 1.3 and 1.6 basicities. When fired at 1300°C, these pellets partially melted and formed a semifused aggregate. To avoid pellet sticking, these pellets were fired at 1275°C. On the other hand no such

sticking was observed in the pellets produced with peat moss as binder. This was also not observed in any dolomite fluxed pellets using either bentonite or peat moss as binder.

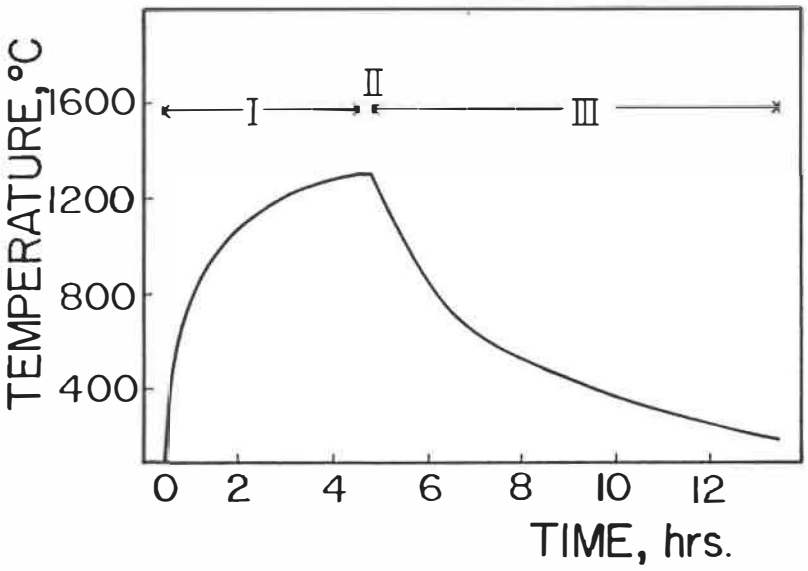


FIGURE 5 - Pattern of thermal treatment and relationship between time and temperature.

3.0 Production of pellets in pilot plant scale to study pellet properties

To evaluate the performance of peat moss as a binder for the production of self fluxed pellets and its effect on the fired pellet properties, pellets were then prepared in pilot plant scale. The green pellets were produced in a standard disc pelletiser and fired in a pot grate. The reason for conducting trials at this scale was to optimise the process conditions for commercial scale operation. Pellets at 3 basicities; 0.8, 1.1 and 1.3 were produced by adjusting the basicities

by the addition of dolomite and addition. The MgO content in the pellet was maintained at approx. 1.8% conforming to industrial practice. Therefore the dolomite addition had to be restricted to 9% and balance of the flux requirement was met by limestone addition. Pellets were made by adding 1.5% and 3% peat moss at each basicity level. For comparison of pellet properties pellets were made with 1% bentonite addition. In order to observe the combined effects of bentonite and peat-moss pellets were also produced with 0.5% bentonite and 1.5% peat moss addition.

3.1 Preparation of green pellets

Mount Wright specularite concentrates from Quebec's north shore were used for this study. The chemical composition of the raw materials are given in Tables 1 and 4. The pellet designation and weight percent of different additives are given in Table 7. The pellets were designated according to the basicity and type of binder addition. The numbers 1, 2 and 3 corresponded to basicities 0.8, 1.1 and 1.3 respectively. The letter B corresponded to pellets with 1% bentonite addition, P_1 and P_2 to pellets with 1.5% and 3% peat moss respectively. The pellets with 0.5% bentonite and 1.5% peat moss were designated BP.

TABLE 7 - Weight percentages of additives for pellet production in pilot scale.

BASICITY	PELLET TYPE	% ADDITIVES		
		Bentonite	Peat moss	limestone
0.8	1 B	1.0	-	0.8
	1 BP	0.5	1.5	0.2
	1 P_2	-	3.0	-
1.1	2 B	1.0	-	4.2
	2 BP	0.5	1.5	3.5
	2 P_1	-	1.5	2.8
	2 P_2	-	3.0	2.8
1.3	3 B	1.0	-	7.0
	3 BP	0.5	1.5	6.1
	3 P_2	-	3.0	5.0

1% coke breeze and 9% dolomite were added to the raw mixes for pellet production.

3.1.1 Preparation of pellet mix

Ore concentrates and other additives were thoroughly mixed in a strutevent's mixer. NaOH was added to the pellet mix having peat moss as binder similar to the laboratory scale pellets. This was added to peat moss in a peekay mixer prior to mixing with other raw materials. The pH was also maintained in the range of 10.5-11.

3.1.2 Green ball formation

Green pellets were made in a standard disc pelletiser of 1 meter dia. at an inclination of 45° and 20 rpm. Water was added through three different jets to maintain ball stability. Moisture content of the pellets varied from 8-9.5%. With optimised green balling conditions a narrow size distribution of the pellets was obtained. More than 90% of the pellets fell in the range of 10-15 mm. For the peat moss added pellets this was achieved with a slightly longer pelletising time. The pellet size was slightly smaller than bentonite added pellets. Good pellets could not be obtained with 1.5% peat moss addition due to poor ballability other than pellets at 1.1 basicity. Therefore production of pellets with 1.5% peat moss addition was abandoned.

3.2 Pellet induration

Green pellets were fired in a pot grate furnace following a firing cycle of 41 minutes consisting of drying, preheating, firing and cooling. The optimum firing cycle was decided on the basis of the trial firing of the pellets with bentonite addition at 1.1 basicity. Temperatures at the top, middle and bottom layers of the bed were 1315, 1260 and 1235°C respectively. Figure 6 shows a typical pellet induration cycle. No difficulties were encountered during firing of pellets with peat moss addition.

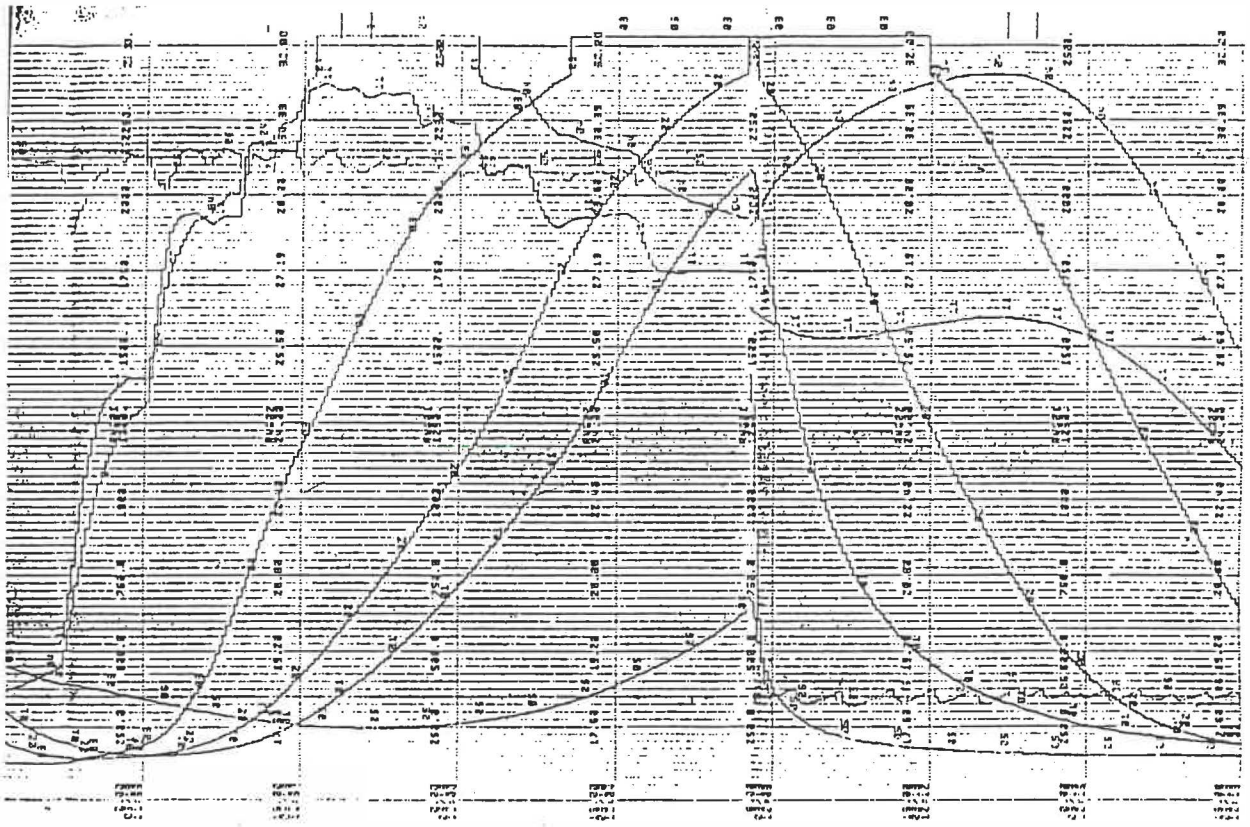


FIGURE 6 - Typical pellet induration cycle (pilot scale pellets).

4. PROCEDURE FOR BONDING MECHANISM STUDIES

Bonding mechanism in the laboratory pellets was studied by carrying out thermal analysis of the raw materials and pellet mixes and characterising the bonding phases in the fired pellets. Information on the interaction of the raw material constituents such as one concentrate, gangue, flux and binders was obtained from the thermal analysis studies.

4.1 Thermogravimetric and differential thermal analysis (TGA & DTA)

A Mettler thermoanalyser was used for carrying out thermogravimetric analysis (TGA) and differential thermal analysis (DTA), studies. Alumina powder was used as reference material. The thermal analysis was done for the raw materials such as iron ore concentrate, limestone, dolomite, peat moss and coke breeze. This was also carried out for the pellet mixes of 1.3 and 1.6 basicity pellets. Approximately 200 miligrams of the weighed sample was placed on a thermobalance and heated following the simulated pellet firing cycle. Changes in the weight (TGA) and heat content (DTA) of the material with temperature was recorded in a chart recorder. From the thermal analysis results the nature of the reaction, i.e. decomposition, oxidation, exothermic, etc. was determined. By correlating the results of the individual raw material components and pellet mix, information on bonding mechanism was obtained.

4.2 Pellet mineralogy and characterisation of bonding phases

The mineralogy and the bonding phases of the pellets were analysed by using optical microscope, image analyser and SEM-EDS. Mineralogical examination was made using a metallurgical microscope. The mineralogical phases were quantified by using image analyser. SEM-EDS system was used to determine the chemical composition of the bonding phases.

4.2.1 Sample preparation

The pellets were sectioned and mounted in sample holders by using a mixture of epoxy and hardener as embedding material. The samples were polished by using standard polishing procedure and final polishing was done by using diamond paste. The polished surfaces were cleaned with carbon tetrachloride. A minimum of three samples were prepared for each pellet type.

4.2.2 Pellet mineralogy

Pellet microstructure was analysed under reflected light by using a metallurgical microscope. Various mineralogical phases were identified and their distribution in the pellet microstructure was noted.

4.2.3 Phase area meausrement using image analyser

Information on the distribution of various mineralogical phases were obtained by measuring the area of the phases. A Kontron IBAS interactive image analysis system was used for this purpose. Images of the pellet microstructure were entered into a special image processing unit by video camera from the optical microscope. Area of the phases were measured by using an IBAS measuring program which estimated the phase area by discriminating the gray level of each phase. A minimum of 50 fields were randomly scanned for phase area measurement. The IBAS measuring program estimated the percentage area the mineralogical phases in each field. The average percentage phase area was calculated on the basis of 50 fields.

4.2.4 Microanalysis

Distribution of elements in the crystalline and bonding phases was determined from the semi-quantitative microanalysis by using scanning electron microscope and energy dispersive spectrophotometer. A JEOL JSM 820 scanning electron microscope with Tracor Northern TN2000 analysis system was used for the above purpose. The non conducting epoxy surface of the specimen was coated with colloidal graphite to make it electrically conducting. A filament voltage of 25 kV was used throughout this work. Spot analysis in various phases was carried out by accumulating X-ray spectra for 30 seconds. A minimum of 50 spots in each phase were analysed for each pellet type.

5. PELLET TESTING PROCEDURE

Pellets are intermediate products which are subsequently processed for iron making in the blast furnace or in a direct reduction plant. Pellet property requirements are different in both cases. In the present case pellets were produced for blast furnace use. The testing methods used for evaluation of various pellet properties were by following standard procedures set by International Standards Organisation (ISO) except for swelling. For swelling, a dilatometric method was used.

5.1 Green compression strength

Compression strength of the green pellets was determined by compressing the pellets between two parallel plates up to breaking. The test was carried out on a platform balance with weight indication by means of a pointer. The pellet was placed on the lower steel plate and was gradually compressed with the upper still plate and the pointer position was observed. The pellet breakage was indicated by the jumping back of the pointer. The maximum weight load observed was taken as the compression strength. Ten pellets were tested to obtain the average compression strength of the pellet.

5.2 Drop number

The drop number of a pellet indicates the capability of the pellet to withstand deformation during the drops it undergoes in the course of its transportation. The green pellet was dropped on to a

steel plate from a height of 46 cms and the number of drops each ball could withstand without cracking or crumbling was noted. This was the drop number of the pellet. Average drop number was determined by dropping ten pellets.

5.3 Dry compression strength

The dry compression strength of the pellet was measured by putting the dry pellet between two parallel plates similar to determining green compression strength. The average strength was determined by measuring ten pellets.

5.4 Porosity measurements of fired pellets

The porosity of fired pellets was determined by the air pycnometer and wax coating method [85]. The volume of the weighed pellets was measured by a Beckman air comparison pycnometer shown in Figure 7. Then the pellets were coated with molten wax at 60°C. The volume of the wax coated pellet was measured and the porosity of the pellet was determined by the following formula

$$P_o = \left(1 - \frac{\rho_t}{\rho_a} \right) \times 100$$

where P_o = open porosity,

ρ_t = apparent density of the sample,

ρ_a = corresponding apparent density (before wax coating).

Fifty pellets were taken for porosity measurement.

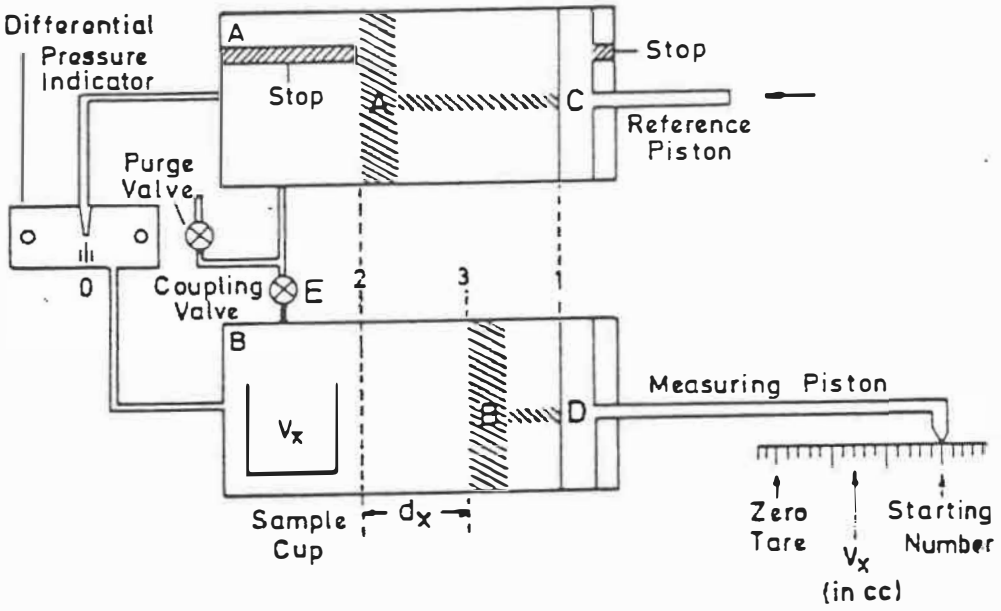


FIGURE 7 - Scheme of a Beckman air pycnometer.

5.5 Tumbler strength

According to ISO standard [96], a representative pellet sample of 15 kilograms was tumbled in a horizontal drum of 1 meter dia. and 0.5 meter length. Two lifters of each 5 cm high were located inside the drum. The drum was rotated for eight minutes at 8 rpm. The pellets were screened and factions + 6.3 mm and - 0.5 mm were determined. T index or tumbler index was reported as the weight fraction of + 6.3 mm fraction. The equipment used for tumbling test is shown in Figure 8.

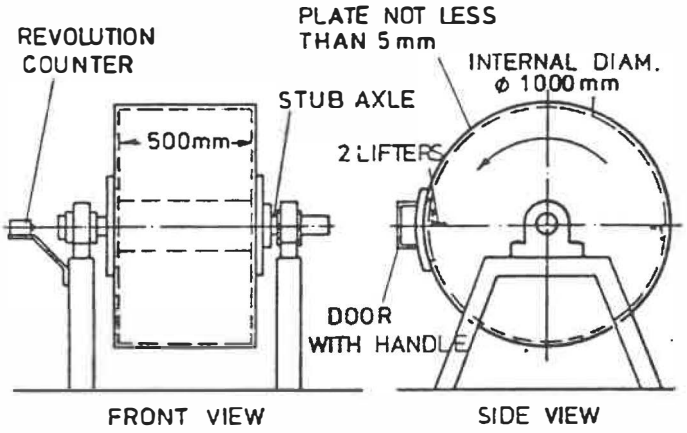


FIGURE 8 - Equipment for the determination of tumbler strength (ISO 3271-1975).

5.6 Compression strength of fired pellets

According to ISO procedure [97], pellets of uniform roundness having 12 ± 1 mm diameter were selected to ensure an even point load. One individual pellet was placed between two parallel steel plates and the compression load was applied according to a specified time schedule till breaking of the pellet. Twenty five pellets were used for determining compression strength.

5.7 Low temperature breakdown test (LTBT)

Low temperature breakdown test (LTBT) indicates the behaviour of the pellets near the top of the blast furnace where they encounter a weak reducing gas at a low temperature of 500°C.

According to ISO procedure [98], reduction of 500 g of pellets was carried out at 500°C for 60 minutes. A reducing gas containing 2% H_2, 20% CO, 20% CO_2 and balance N_2 was used. After cooling to room temperature under nitrogen atmosphere the pellets were tumbled in a drum and then screened. The LTBT value is expressed in percentage of + 6.3 mm fraction.

5.8 Reducibility test

Reducibility of the pellets was determined by a modified ISO reducibility test procedure [14]. Approximately 100 grams of pellets were heated to 950°C in nitrogen atmosphere. On attaining the temperature, the pellets were reduced by using a gas mixture of 40% CO and 60% N_2. The reduction was carried out up to 70% after which the reduced pellets were cooled to room temperature in nitrogen gas. From a plotting of percentage reduction and time the parameter reducibility $(dR/dt)_{40}$ was determined by using the following relation ship:

$$\left(\frac{dR}{dt} \right)_{40} = \frac{33.6}{t_{60} - t_{30}}$$

where t_{30} and t_{60} are times to attain 30 and 60 percent reduction respectively. A schematic diagram of the reducibility apparatus is shown in Figure 9 and in Figure 10, a typical reducibility curve for the pellets is shown.

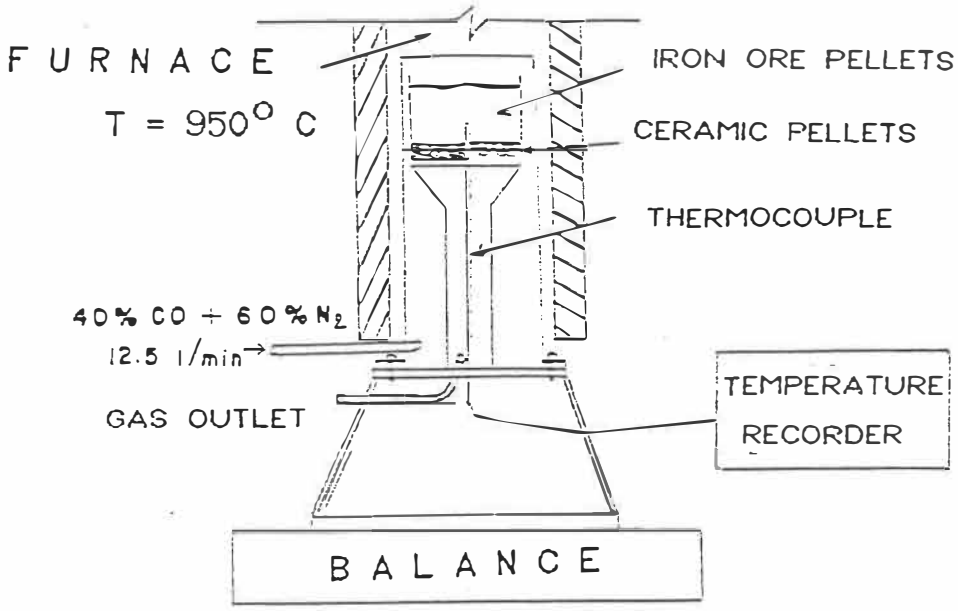


FIGURE 9 - Schematic diagram of reducibility apparatus.

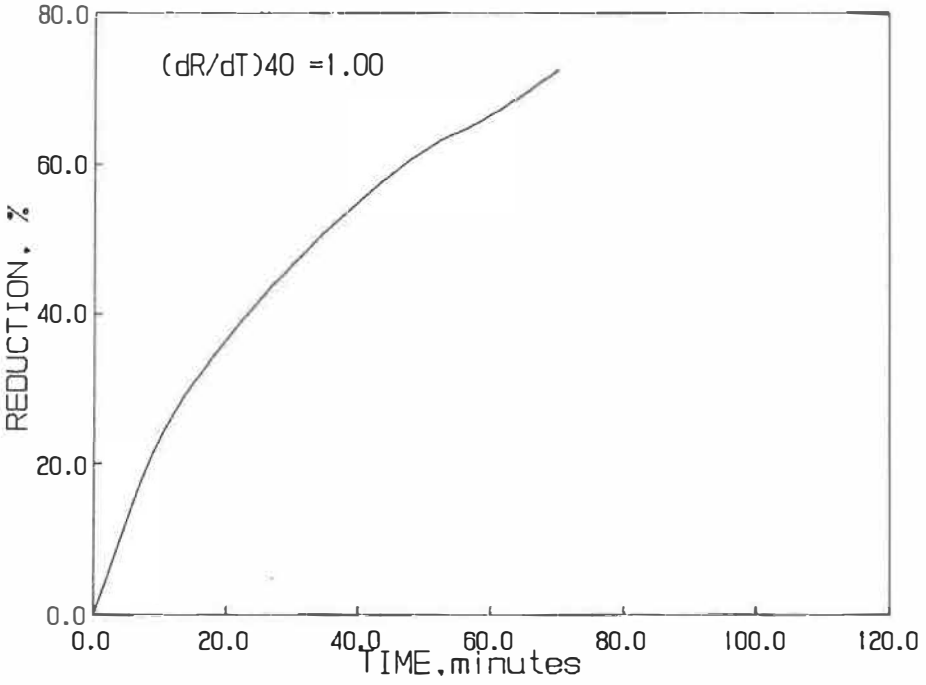


FIGURE 10 - A typical reducibility curve.

5.9 Swelling test

Swelling test indicates the swelling behaviour of the pellets. The swelling is caused by the expansion of volume due to the conversion of hematite to magnetite. This results in development of stress in pellet structure. Extent of damage caused to the pellet structure is dependent on the condition prevailing to counteract such damage.

Swelling behaviour of the pellets was determined in a dilatometer adapted to operate in a reducing chamber [99]. A schematic diagram of the dilatometer is shown in Figure 11. A single pellet of 12 ± 0.5 mm diameter was placed in the centre of the reaction tube on a perforated stainless steel support held in place by an alumina tube for easy circulation of reducing gas. The pellet was heated upto 950°C under nitrogen gas flowing at the rate of 0.5 litre/minute. After the system had reached steady state condition the reducing gas of composition 40% CO + 60% N_2 was introduced. The increase in the diameter of the pellet was continuously recorded which was transmitted by a quartz sensor tube touching the top of the pellet. A typical normal swelling curve is shown in Figure 12. Maximum swelling in the pellet was followed by contraction. At that point nitrogen gas was reintroduced and pellet was allowed to cool. Maximum swelling was the percentage change in the pellet volume. Five pellets of each pellet type were used for the swelling test. The set up for swelling test is shown in Figure 13.

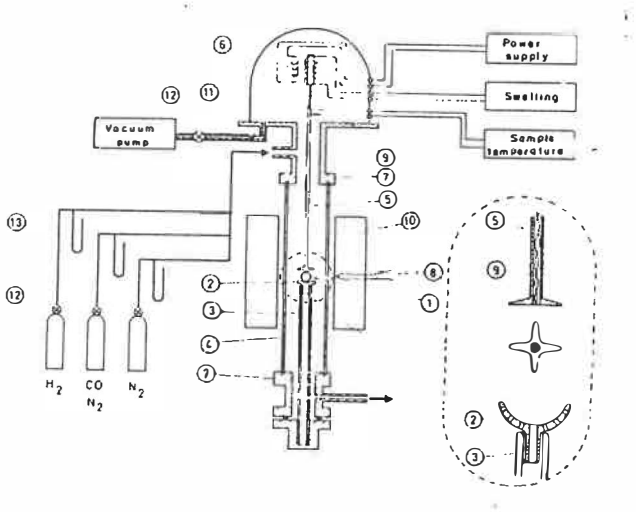


FIGURE 11 - Schematic diagram of dilatometer [99].

1) Iron oxide pellet, 2) stainless steel sample holder, 3) alumina support tube, 4) alumina furnace tube, 5) quartz sensor tube, 6) transducer, 7) watercooled O-ring seals, 8) control thermocouple, 9) measuring thermocouple, 10) furnace, 11) glass bell, 12) valve, 13) flow meters.

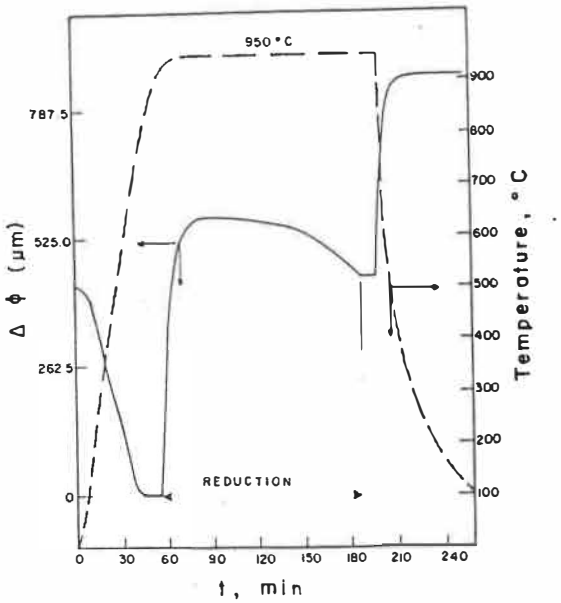


FIGURE 12 - Typical curve obtained from the dilatometer [99].

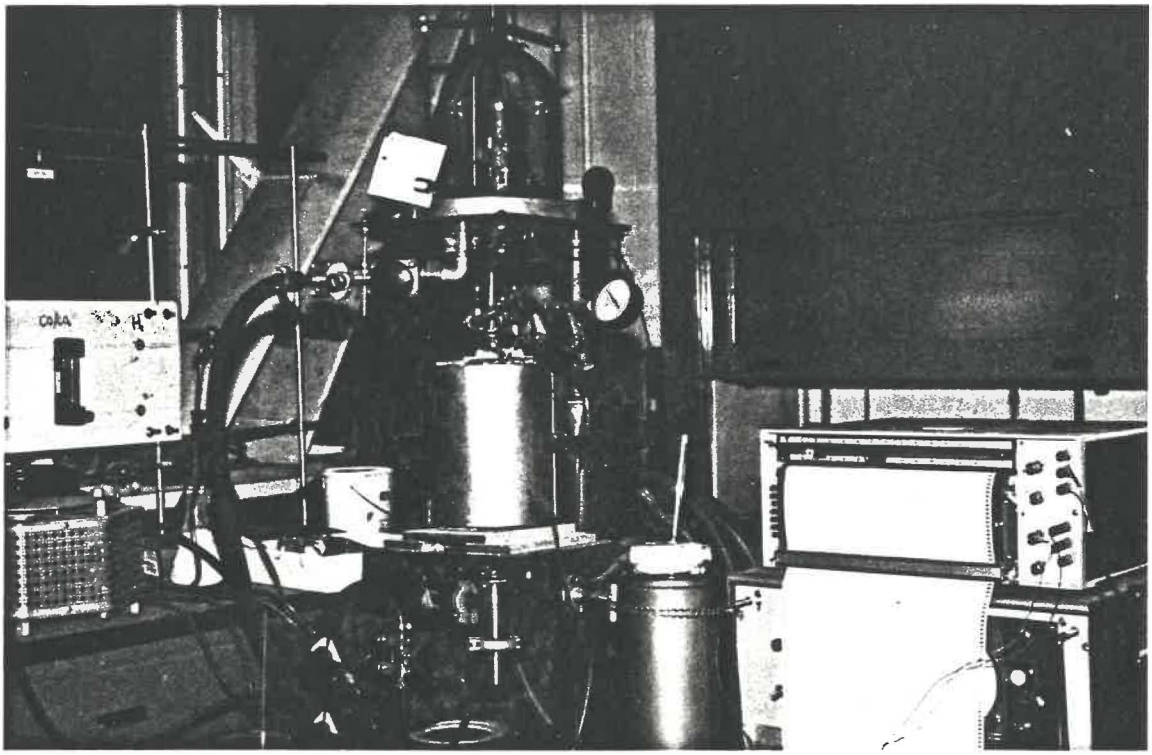


FIGURE 13 - Set up for swelling test.

CHAPTER 3

RESULTS: LABORATOBY PELLETS

1. TGA AND DTA RESULTS

The weight loss as a function of time and temperature of various raw materials such as ore concentrale, peat moss, coke breeze etc. is shown in Figure 14. It is noticed that ore concentrate undergoes virtually no weight loss during firing. Peat moss has almost entirely burnt off before reaching preheating temperature of 950°C. The fluxes limestone and dolomite were observed to undergo some weight loss in the temperature range of 700-900°C indicating the dissociation of carbonates. At 1200°C some amount of coke breeze still remained unburnt and combustion of coke breeze was continuing.

From the above observations it was apparent that during induration of a fluxed pellet containing peat moss, the combustion of peat moss and dissociation of flux is complete before the pellet has reached 950°C. These reactions cause formation of additional pores in the pellet.

Differential thermal analysis of some pellet mixes corresponding to the composition of pellets at 1.3 and 1.6 basicity was done along with the ore concentrates. The DTA curves in the temperature range of 700, 1200°C are shown in Figure 15. In all the samples endoth-

ermic peaks are observed at ~ 800°C and ~ 1200°C. In the pellet mix of 1.6 basicity two endothermic peaks are observed at 1205°C and 1225°C respectively. These peaks are not observed in ore concentrate. The endothermic peak around 800°C indicates the dissociation of fluxes, and the peaks in the vicinity of 1200°C denote formation of liquid phase. The peaks are observed to be more prominent with increasing limestone addition. Absence of endothermic peak in the ore concentrate at this temperature range indicates that melt formation does not take place

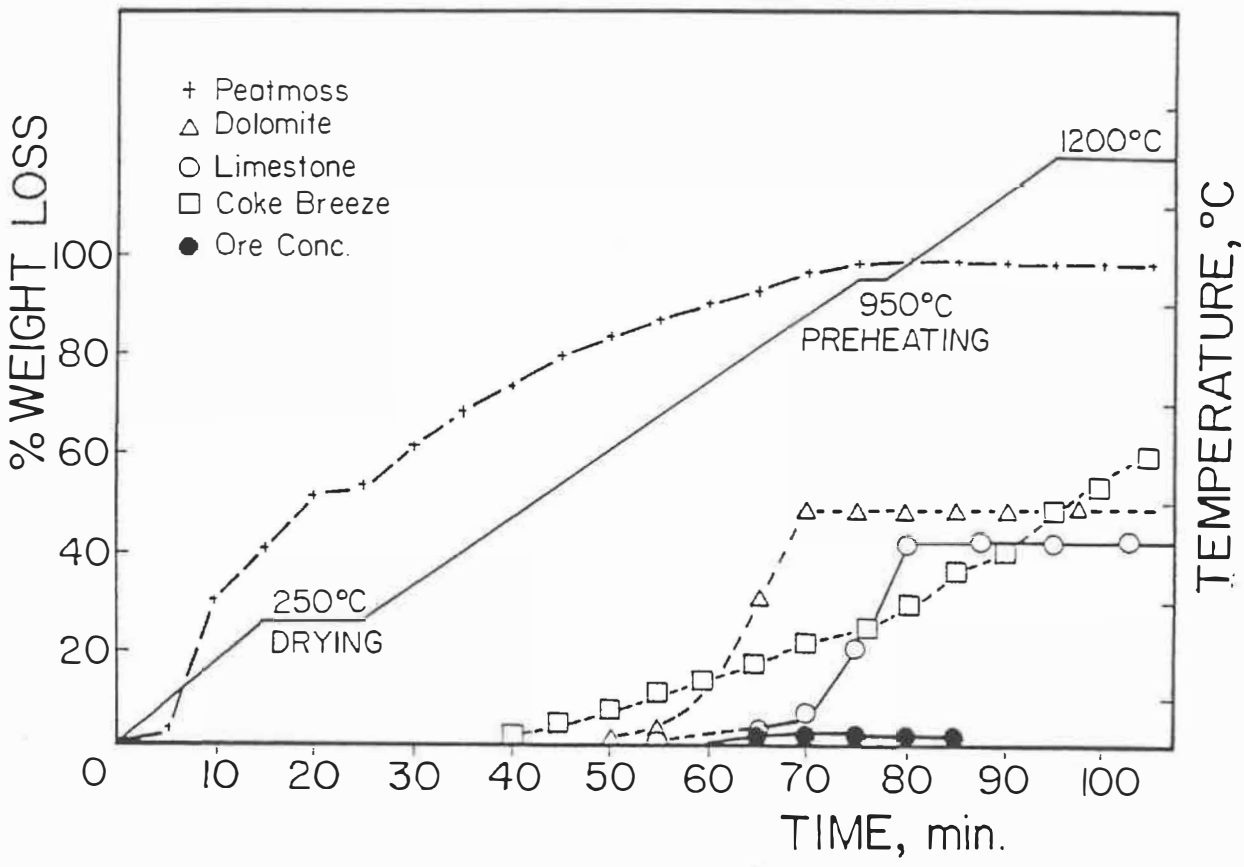


FIGURE 14 - Weight loss as a function of time and temperature of the raw materials used.

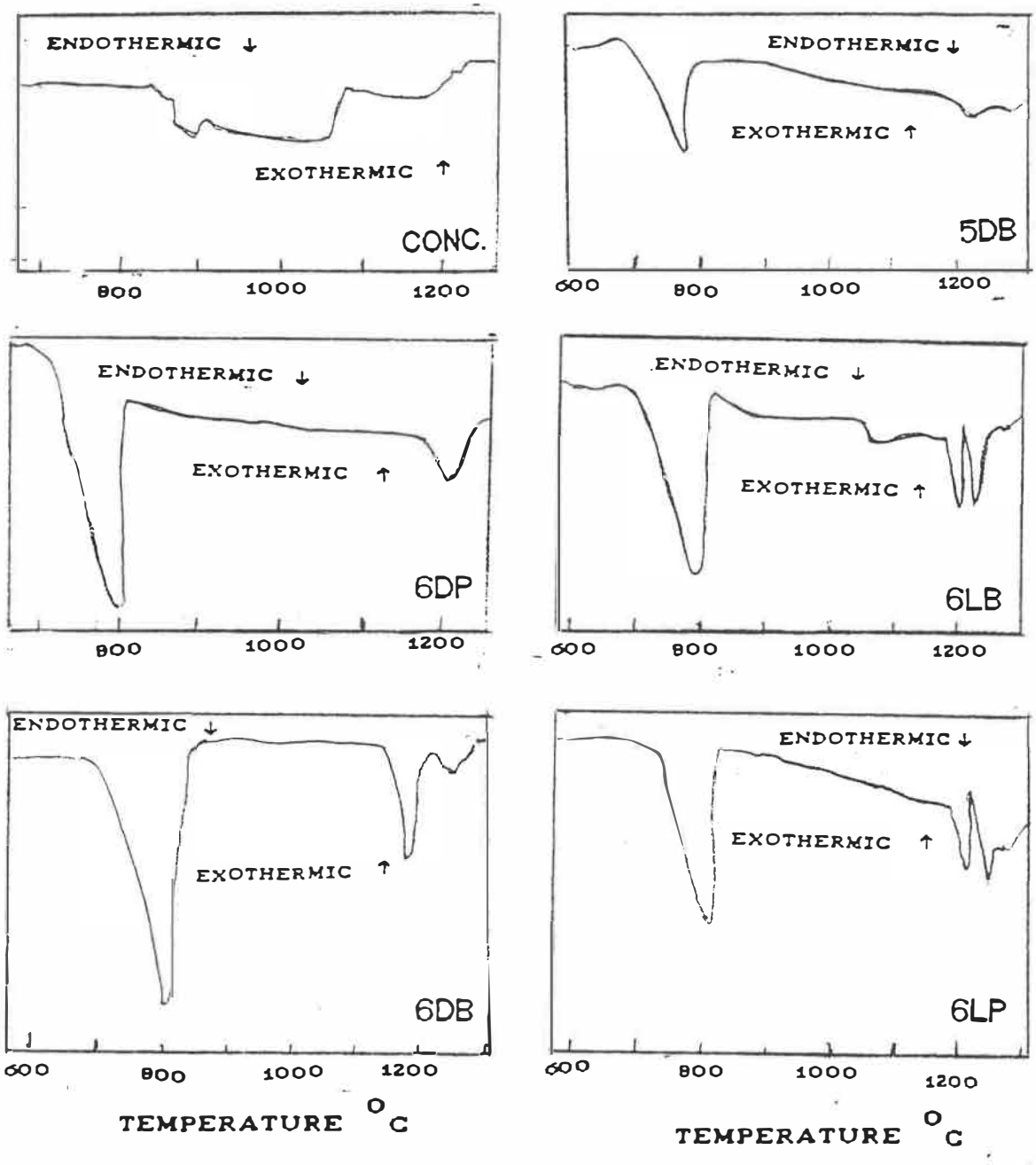


FIGURE 15 - DTA curves of pellet mix and concentrate.

without flux addition. This also rules out the possibility of reaction of silica with iron oxide which could form a melt. Since reaction between silica and lime is not favoured due to kinetic considerations, it is inferred that formation of calcium ferrites takes place due to reaction of hematite with calcium oxide in the solid state. These ferrites have formed a melt as their melting points are between 1205-1225°C [100]. It is further noticed that a slight but significant weight loss takes place with the commencement of the endothermic reaction (see Figure 16). Regain of the weight is observed during cooling period. This suggests that reduction of iron oxide is accompanied by the formation of liquid phase which is reoxidised on cooling. According to the CaO-Fe_2O_3 equilibrium phase diagram of Philip and Muan [101] (see Figure 14) a small amount of magnetite is present at the melting temperatures of calcium ferrites. Therefore, we conclude that some magnetite formation takes place during incongruent melting of the calcium ferrites which reoxidise to hematite upon cooling.

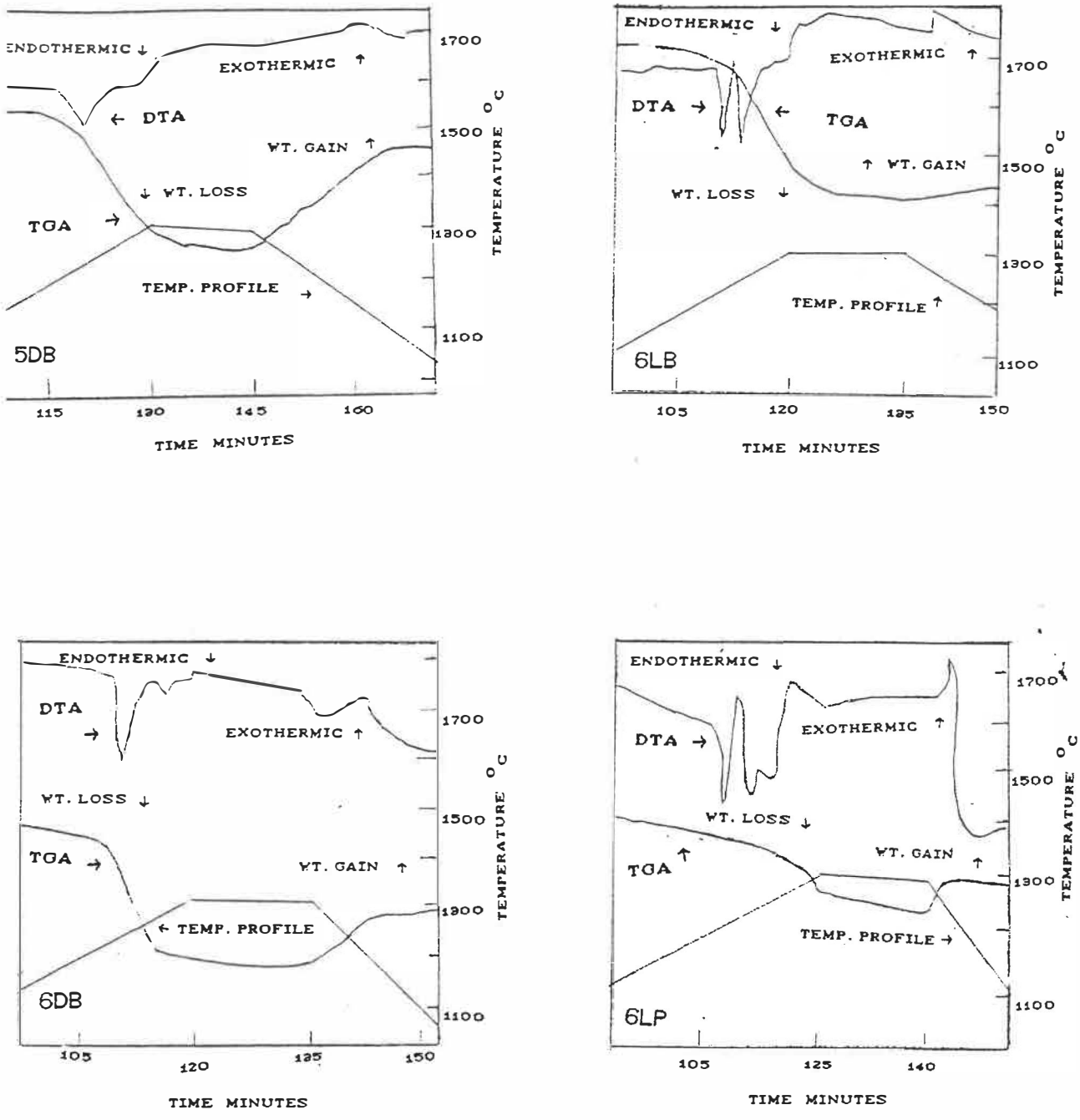


FIGURE 16 - DTA and TGA curves of the pellet mixes showing occurence of weight loss during melting.

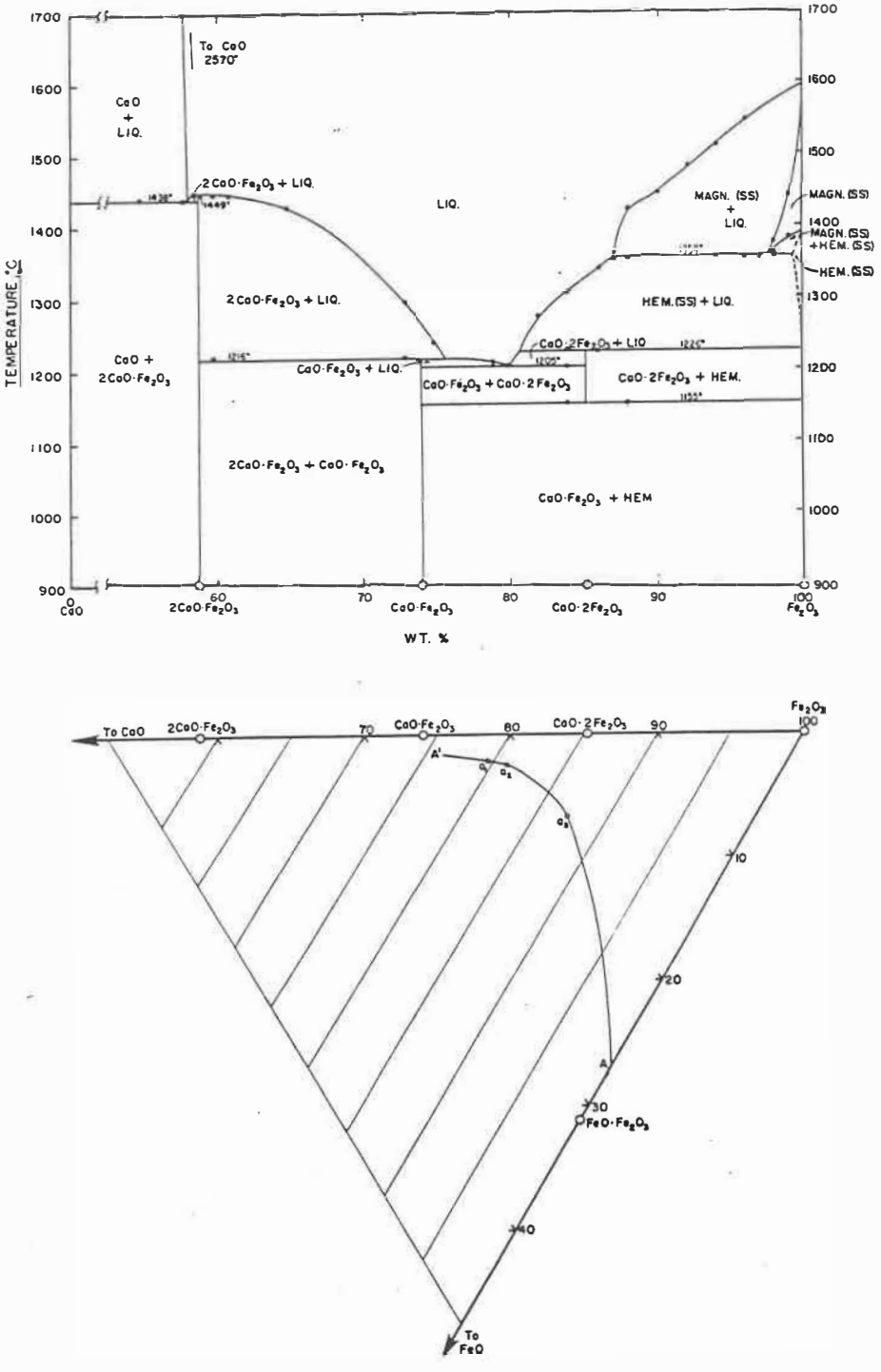


FIGURE 17 - Fe-O-Ca phase diagram [100].

2. PHASE AREA MEASUREMENT BY IMAGE ANALYSER

The amounts of different mineralogical phases present at various basicity levels are shown in Table 8. The percentage phase area was measured by using image analyser as described in Chapter 2. No data on 0.2 basicity pellets are shown in Table 8 as negligible amounts of a slag and magnesioferrites were observed in the pellets at this basicity which was difficult to quantify in the image analyser. From the image analysis results it is observed that hematite is the predominent phase in all types of pellets. The amount of magnesioferrite which is observed in dolomite fluxed pellets increases with increasing basicity. It is generally observed that there is higher amount of slag formation in limestone fluxed pellets than the pellets with dolomite addition. The presence of MgO in dolomite fluxed pellets raises the liquidus temperature of the slag phase so that less amount of liquid slag is formed. The pellets produced with peat moss addition have less amount of slag than pellets with the pellets produced with bentonite addition at the same basicity level. This is attributed to the higher amount of gangue content in bentonite added pellets which require higher amount of flux to maintain the basicity level. This resulted in higher amount of slag formation.

TABLE 8 - Percentage area of different mineralogical phases, as measured by image analysis.

BASICITY	PELLET	SLAG	CALCIUM FERRITE	MAGNETITE/ MAGNESIOFERRITE	HEMATITE
0.8 B	3 DB	12.7	-	8.5	78.8
	3 DP	11.4	-	9.3	79.3
	3 LB	16.8	-	6.2 (magnetite)	77.0
	3 LP	15.9	-	-	84.1
1.3	5 DB	16.2	-	11.4	72.3
	5 DP	15.4	-	10.2	74.4
1.6	6 DB	19.4	-	8.5	78.8
	6 DP	17.2	-	9.3	79.3
	6 LB	15.5	16.8	-	67.8
	6 LP	19.6	0.9	-	79.4

* Pellet designation has been described on page 33.

3. MICROANALYSIS RESULTS

The results of microanalysis as estimated by SEM-EDS are given in Tables 9 to 12. The average chemical composition of the glass phases in dolomite and limestone fluxed pellets are given in Tables 9 and 10 respectively. The average composition of magnesioferrite is shown in Table 11 and the average compositions of the major crystalline phases are given in Table 12.

TABLE 9 - Average composition of glass phase in dolomite fluxed pellet (SEM-EDS).

BASICITY	PELLET DESIGNATION	GLASS PHASE (ZONED/SINGLE)	Fe_2O_3	SiO_2	CaO	MgO	Al_2O_3	RELATIVE PROPORTION IN GLASS PHASE
0.2	2 DB	Zoned { Pale gray	34.1	46.1	15.1	3.3	1.4	80%
		Zoned { Dark	28.5	57.4	11.7	1.3	1.1	20%
0.8	3 DB	Zoned { Pale gray	38.2	36.2	22.2	2.8	0.6	70%
		Zoned { Dark	21.5	49.5	28.3	-	0.7	30%
	3 DP	Zoned { Pale gray	42.2	33.8	20.7	2.7	0.6	70%
		Zoned { Dark	27.8	46.7	24.8	-	0.7	30%
1.3	5 DB	Zoned { Pale gray	40.3	25.1	32.2	1.6	0.8	50%
		Zoned { Dark	17.6	38.6	43.8	-	-	20%
		Single	15.3	29.7	53.3	1.0	0.7	30%
	5 DP	Zoned { Pale gray	41.4	27.8	29.2	1.2	0.4	50%
		Zoned { Dark	13.4	40.6	44.7	0.4	0.9	20%
		Single	14.4	35.5	50.1	-	-	30%
1.6	6 DB	Zoned { Pale gray	33.6	26.4	38.1	1.0	0.8	25%
		Zoned { Dark	21.5	32.0	45.4	0.4	0.7	15%
		Single	10.2	29.8	58.0	1.5	0.5	60%
	6 DP	Zoned { Pale gray	34.2	22.0	42.6	1.1	0.1	-
		Zoned { Dark	18.4	27.1	54.2	-	0.3	-
		Single	9.7	27.2	63.1	-	-	-

TABLE 10 - Average composition of glass phase in limestone fluxed pellets (SEM-EDS).

BASICITY	PELLET DESIGNATION	Fe_2O_3	SiO_2	CaO	MgO	Al_2O_3
0.8	3 LB	11.6 27.6	41.3 34.7	46.7 36.6	- 0.1	0.4 1.0
	3 LP	17.7 39.0	36.9 33.4	45.4 24.5	- 1.7	- 1.4
1.3	5 LB	13.4 26.2	32.5 26.2	53.7 44.1	- 0.6	- 2.0
	5 LP	9.5 36.0	33.5 27.5	57.0 36.1	- 0.2	- 0.2
1.6	6 LB	10.1 29.9	28.0 23.1	61.3 46.7	- 0.6	- 2.0
	6 LP	13.6 33.2	29.8 22.8	56.3 43.8	0.2 -	0.1 0.2

TABLE 11 - Average composition of magnesioferrite in pellets fluxed with dolomite (SEM-EDS).

BASICITY	PELLET DESIGNATION	Fe_2O_3	SiO_2	CaO	MgO	Al_2O_3
0.2	2 DB	96.1	-	0.2	3.6	0.1
	2 DP	-	-	-	-	-
0.8	3 DB	90.0	1.3	0.5	8.3	-
	3 DP	91.3	0.8	0.4	7.4	0.1
1.3	5 DB	91.0	0.9	1.6	6.3	0.2
	5 DP	91.9	0.3	1.3	6.4	0.1
1.6	6 DB	91.7	0.4	1.6	5.9	0.4
	6 DP	93.7	0.1	1.3	4.8	0.1

TABLE 12 - Average composition of major crystalline phases (SEM-EDS).

MINERALOGICAL PHASE	Fe_2O_3	SiO_2	CaO	MgO	Al_2O_3	REMARKS
Hematite (H)	99.5	0.4	0.1	-	-	All types of pellets
Hematite (H) (crystallized in slag)	95.7	1.7	2.5	-	0.1	All types of pellets
Magnetite (M)	97.1 (Fe_3O_4)	0.5	1.5	0.7	0.2	Only limestone fluxed pellets
Calcium ferrites (CF)	80.3	5.9	12.7	0.1	1.0	Observed only at B = 1.3 and 1.6
Calcium ferrites (CF) (crystallized in slag)	70.5	13.7	14.8	0.4	0.6	Observed in pellets B = 0.8

The analysed elements are presented in their respective oxide form in which they actually exist. Fe exists in both ferric and ferrous states. But determination of its respective state by SEM-EDS is rather difficult and time consuming, it is assumed that all Fe existed in ferric state unless otherwise specified.

From the analyses of micro constituents in the pellets it is observed that the chemical composition of the glass phase is heterogeneous at each basicity level. The glass phase varied in its Fe, Si, Ca, Mg and Al contents. The composition of the glass phase appeared to be divided into 2-3 groups with different iron contents. The average composition of the glass phases are shown in Tables 9 and 10 respectively for dolomite and limestone fluxed pellets.

In the pellets two different types of glass phases were observed under the reflected light. One of the glass phases contained a

zoned glass phase which consisted of pale gray and dark phase. The other type of glass phase consisted of single dark phase. The pale gray zone is rich in Fe and Mg. The zoned glass phase is observed in dolomite fluxed pellets whose proportion to single silicate phase decreases with increasing basicity from 0.8 to 1.6. The chemical composition of the silicate phase does not vary much with type of binder.

It is seen from the Table 9 that zoned glass phase has relatively high iron content. In the zoned glass phase, higher amounts of magnesium oxide and iron oxide are present in the pale gray zone than the dark zone. Since the zoned phase is observed in dolomite fluxed pellet, its formation is attributed to the presence of MgO in the melt. As the basicity of the pellet is increased to 1.3 and 1.6, the amount of zoned glass phase decreases with the decrease in Mg content in the pale gray zone.

The silicate phase in the limestone fluxed pellets consisted of a single dark phase. As seen from the Table 10 the chemical composition of the glass fall into two separate groups with significantly different iron content. The iron content in the silicate varied inversely with the Si and Ca content. The variation with respect to Ca is more pronounced. This indicates that a melt containing high calcium oxide dissolves less amount of iron oxide.

In the dolomite fluxed pellets a phase was observed under optical microscope which resembled magnetite. From microanalysis presence of some amount of magnesium is noticed in this phase. Therefore, this phase is identified as magnesioferrite. The average composition of

magnesioferrite at various basicities is shown in Table 11. It can be seen from the Table that the magnesioferrite phase does not conform to stoichiometric composition of ($MgO\ Fe_2O_3$) as it contains less amount of MgO. It is believed that magnetite which is formed during incongruent melting of calcium ferrites reacts with MgO to form the complex spinel of the type ((1 - x) Mg•x Fe)O during firing. This complex spinel dissociates into magnesioferrite deficient in MgO during cooling as FeO reoxidises to Fe_2O_3. The reoxidation during cooling is confirmed from thermogravimetric analysis. With increasing basicity more amount of magnesioferrite formation takes place with decreasing MgO content. This is due to the dilution effect as the same level of dolomite addition was maintained for all the pellets. The magnesioferrite phase contains some amount of CaO and SiO_2 depending on the local chemistry (see Table 11).

Formation of magnesioferrite also affected the distribution of magnesium in the glass phase. With increasing amount of magnesioferrite formation at higher basicities, less magnesium was available for the glass phase. Therefore the magnesium content in the glass phase decreased. The proportion of zoned phase also decreased.

The average chemical composition of calcium ferrites is shown in Table 12. Presence of calcium ferrite was observed at 0.8 basicity, in the pellets with bentonite and limestone addition. In pellets with peat moss and limestone addition it was observed at 1.3 basicity. In dolomite fluxed pellet calcium ferrite was observed at the basicities of 1.3 and 1.6 irrespective of binder addition. However, appreciable

amounts of calcium ferrite was formed only in pellets produced with limestone and bentonite addition at 1.6 basicity.

Some amount of silicon and aluminium is present in the calcium ferrite. Therefore, the ferrites may be termed as silicoferrite of calcium and aluminium (SFCA). Two types of SFCA are observed which differ in chemical composition and appearance. These two types of ferrites are shown in Figure 18 as both types are present in the pellet with bentonite and dolomite addition at 1.3 basicity. The point analyses of the ferrites in Figure 18 are shown in Table 13. As it can be seen from the Figure 18 and Table 13, smaller size SFCA crystals contain comparatively higher amounts of silicon, calcium and aluminium and lower amount of iron than larger size crystals. The occurrence of small size crystals is observed in pellets up to 1.3 basicity and the larger size crystals are observed in the pellets above 1.3 basicity. It is apparent that while SFCA crystallizes from a melt containing high calcium, its growth is related to the solubility of iron in silicate glass phase. At lower basicity high amount of iron oxide is dissolved in the glass phase. As a result less amount of iron is available for SFCA formation and this restricts the growth of the crystal. As the basicity increases, solubility of iron oxide in the glass phase decreases. The excess iron oxide from the melt precipitates in the ferrite phase and increases the crystal size. Since crystal growth takes place due to iron oxide precipitation, the concentrations of other elements in the phase such as silicon, calcium, etc. are diluted. Therefore, the big ferrite crystals are observed to contain lower amounts of these elements.

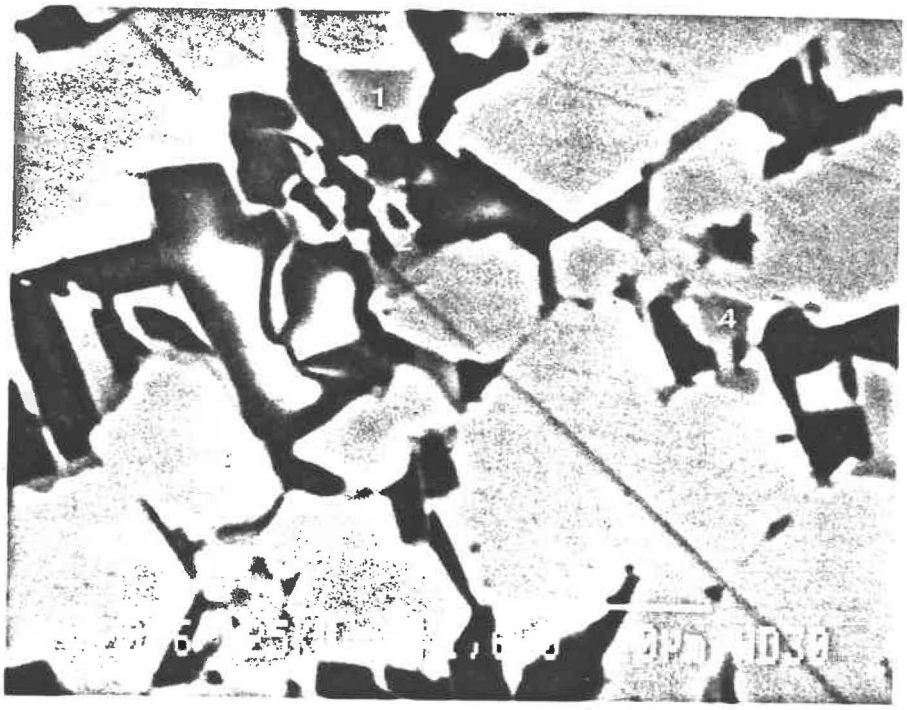


FIGURE 18 - Electron micrograph of two types of calcium ferrites observed in 5 LB pellets.

TABLE 13 - Microanalysis of two calcium ferrite phases as shown in Figure 18.

POINT	Fe_2O_3	SiO_2	CaO	MgO	Al_2O_3
1	77.8	7.2	13.9	-	1.1
2	69.4	10.4	18.5	-	1.7
3	66.4	12.3	19.5	-	1.8
4	79.7	6.2	13.4	-	0.7

4. MINERALOGY OF PELLETS AT VARIOUS BASICITY LEVELS

4.1 Basicity 0.2

Typical photomicrographs of the pellets at the basicity of 0.2 with bentonite and peat moss are shown in Figures 19 and 20 respectively. The scanning electron microphotograph of bentonite added pellet is shown in Figure 21 with point analysis in Table 14. In these pellets bonding is provided mainly by consolidation of crystal bridges formed by recrystallised hematite grain. The recrystallisation process took place in solid state involving small and ultrafine particles. Since a very small amount of flux (1.8% dolomite) addition was made to the pellet little amount of slag is formed due to incipient fusion of ultrafine ore particles gangue and flux during pellet firing. The slag formed thin films between comparatively large hematite grains thus providing bonding between them. A part of the ultrafine hematite crystallised from the melt. The presence of free silica was often observed (Figure 16) in the pellet as most of the silica did not react at this basicity. This indicates that no reaction between silica and hematite had taken place. The pellet structure is dominated by pores. In peat moss added pellets more pores are formed and the pellet structure is open textured. A small amount of magnesioferrite is present in the pellet with low MgO content. The composition of the slag does not differ very much with the type of binder. Zoned silicate phases are noticed in which pale gray phase is predominant. The slag phase contained high amount of SiO_2, Fe_2O_3 with some amount of CaO, MgO and Al_2O_3. The CaO content in the slag phases varied between 14-19%. The zoned slag phases

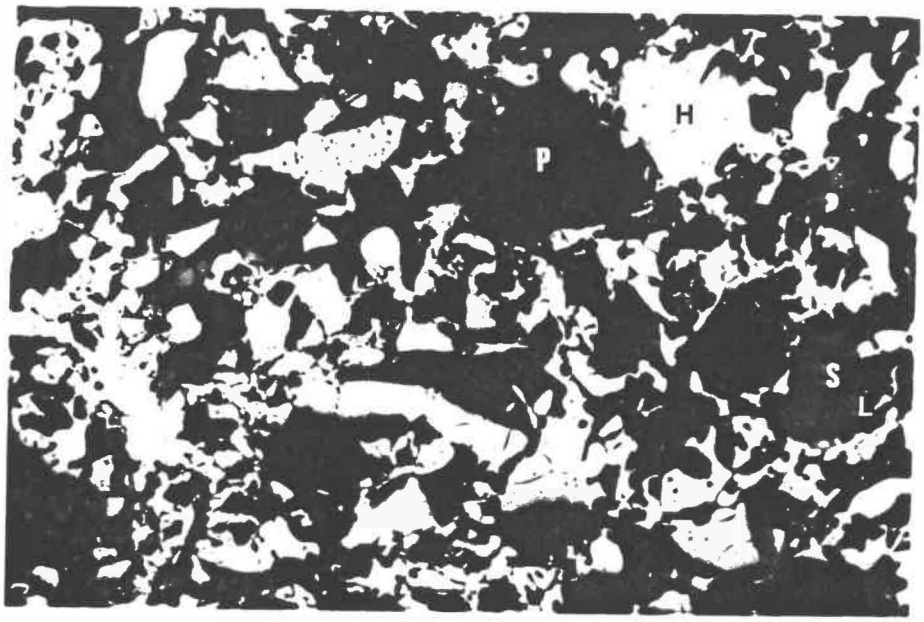


FIGURE 19 - Typical microphotograph of 2 DB pellets. (0.2 basicity, flux: dolomite; binder: bentonite).
H: hematite; S: free silica; G: glass; P: pore.

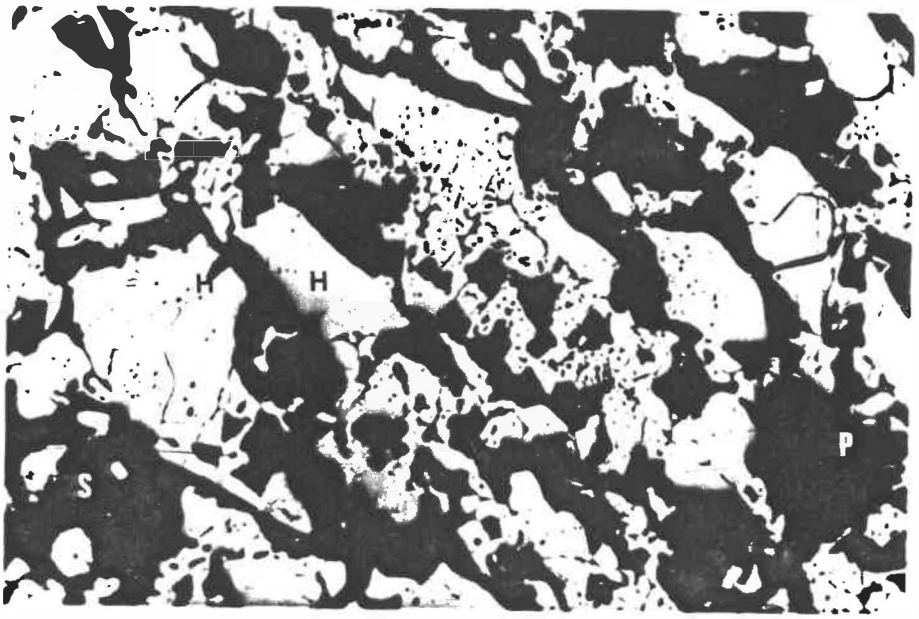


FIGURE 20 - Typical microphotograph of 2 DP pellets. (0.2 basicity, flux: dolomite; binder: peat moss).
H: hematite; S: free silica; G: glass; P: pore.

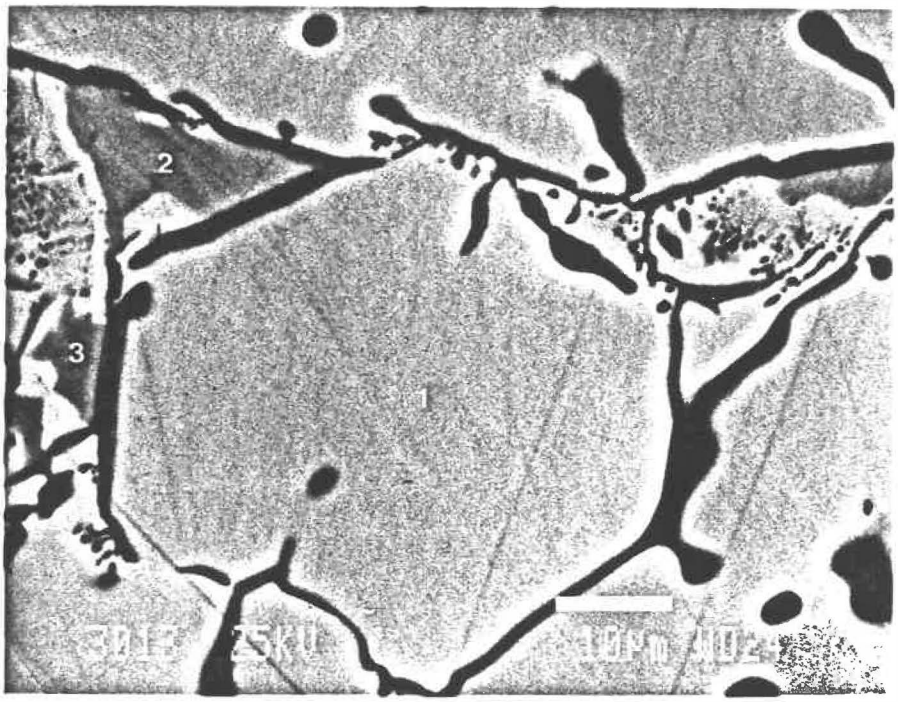


FIGURE 21 - Typical electron micrograph of 2 DB pellets.

TABLE 14 - Microanalysis of mineralogical phases shown in Figure 21.

POINT	Fe_2O_3	SiO_2	CaO	MgO	Al_2O_3	PHASE
1	98.0	1.2	0.8	-	-	Hematite
2	96.7	-	-	3.3	-	Magnesioferrite
3	95.2	-	0.4	4.3	0.1	Magnesioferrite

differred in chemical composition as the pale gray phase contained higher amount of MgO and Fe_2O_3 than the dark phase. The dark phase contained higher amount of SiO_2.

4.2 Basicity 0.8

Typical photomicrographs of pellets with bentonite and peat moss addition for both limestone and dolomite fluxed pellets are shown in Figures 22 to 25. The electron microphotographs are shown in Figures 26-29 with microanalysis of phases in Tables 15-18. Due to a higher amount of flux addition, there increased glass formation at this basicity results in the bonding of the pellets via glass phase. The pellet structure is somewhat consolidated due to the surface tension forces of the liquid phase which was formed during induration and brought the ore particles closer. The liquid has filled the pores and on cooling has bonded the ore particles as can be seen from the pellet microstructure (Figures 22-25). However, only a marginal decrease in the porosity was observed. This shows that the melt which was formed locally is insufficient to close all the pores and enough pores are left behind in the pellet structure.

Silicates formed from the melt are the major bonding phases in limestone fluxed pellets with bentonite and peat moss addition. The glass phase is somewhat evenly distributed between the hematite grains. The liquid phase has attacked the big hematite grains on the faces thus causing some amount of surface smoothening as seen in Figure 22. The slag bond is heterogeneous in its mineral composition and structure. A

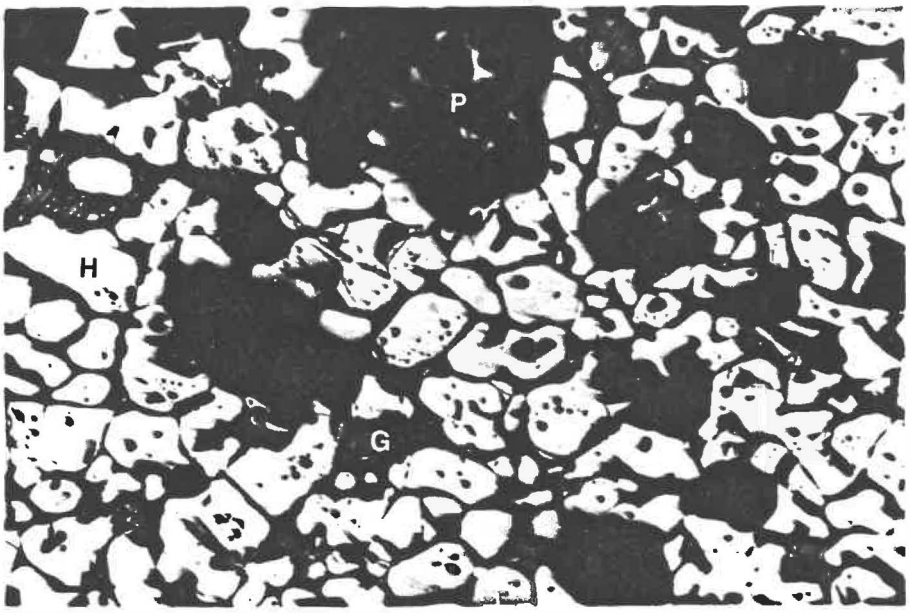


FIGURE 22 - Typical photomicrograph of 3 LB pellets. (Basicity: 0,8, flux: limestone; binder: bentonite).
H: hematite; G: glass; P: pore.

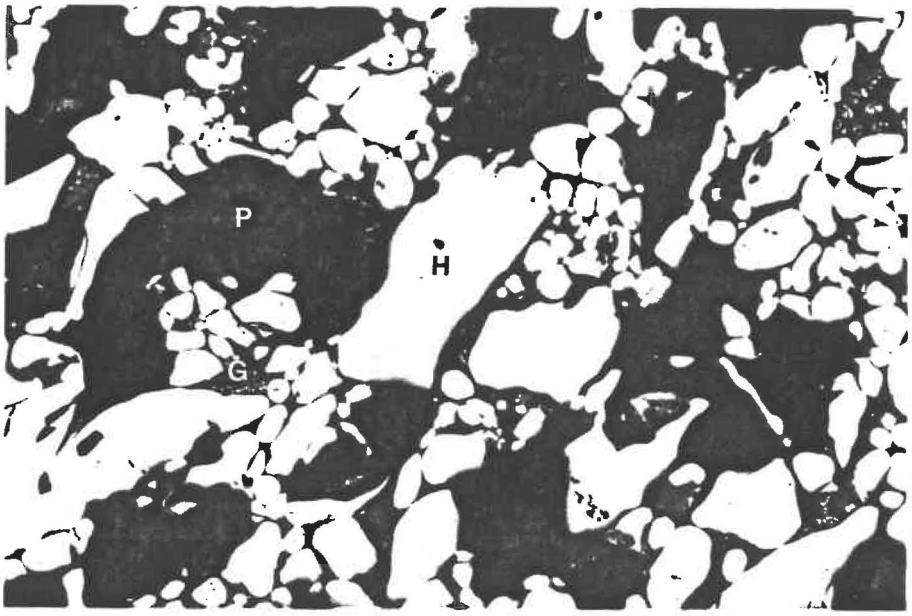


FIGURE 23 - Typical photomicrograph of 3 LP pellets. (Basicity: 0.8, flux: limestone; binder: peat moss).
H: hematite; G: glass; P: pore.

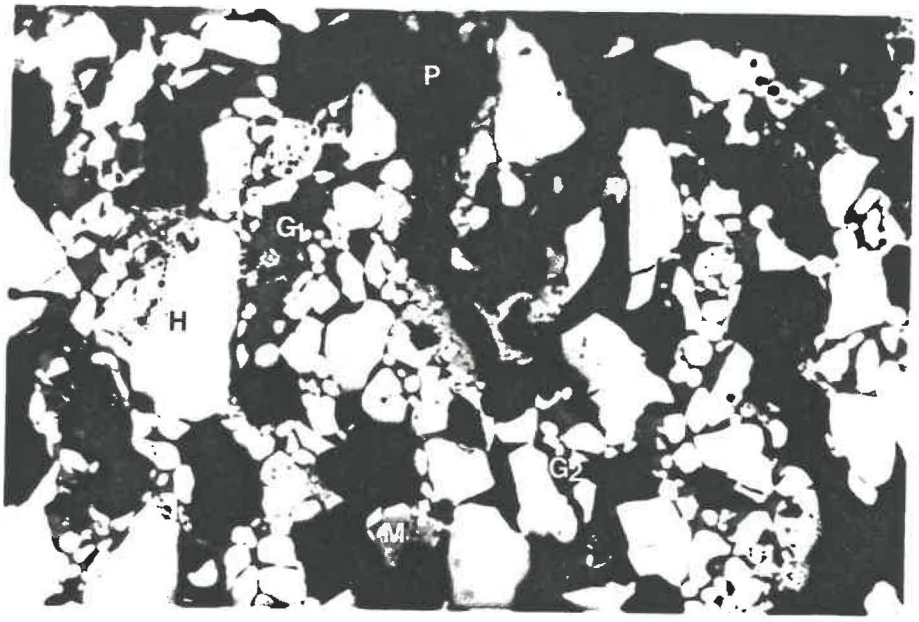


FIGURE 24 - Typical photomicrograph of 3 DB pellets. (Basicity: 0.8, flux: dolomite; binder: bentonite).
H: hematite; M: magnesioferrite; G_1: glass (pale grey); G_2: glass (dark); P: pore.

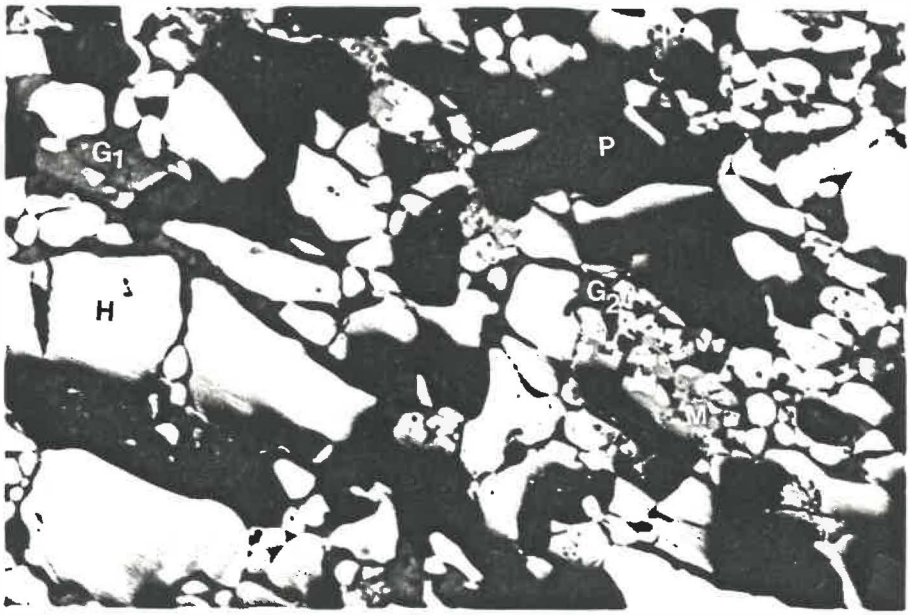


FIGURE 25 - Typical photomicrographs of 3 DP pellets. (Basicity: 0.8, flux: dolomite; binder: peat moss).
H: hematite; M: magnesioferrite; G_1: glass (pale grey); G_2: glass (dark); P: pore.

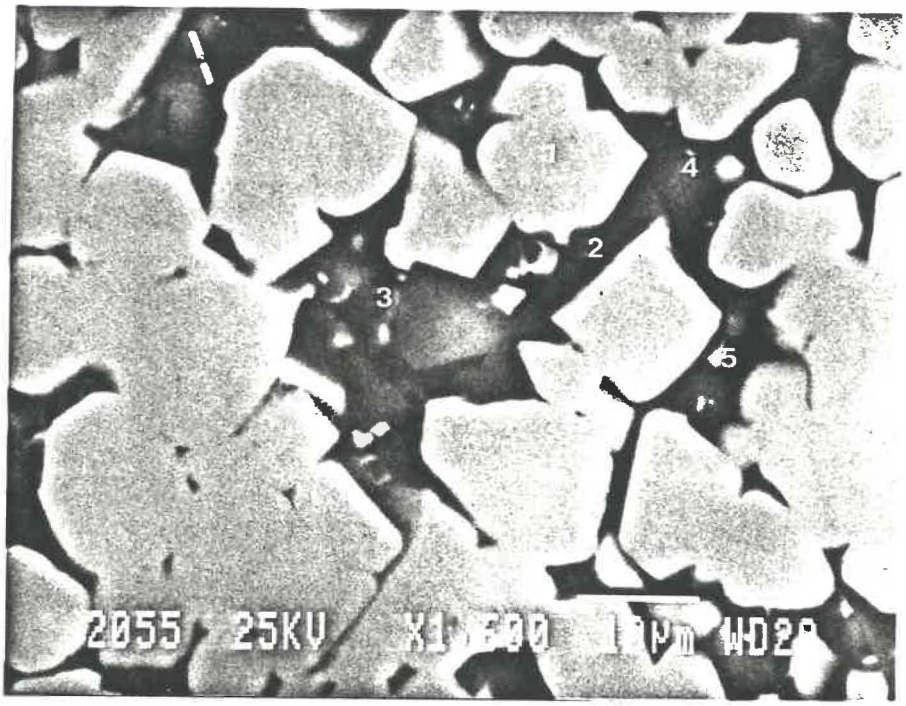


FIGURE 26 - Electron micrograph of 3 LB pellet.

TABLE 15 - Microanalysis of mineralogical phases shown in Figure 26.

POINT	Fe_2O_3	SiO_2	CaO	MgO	Al_2O_3	PHASE
1	99.3	0.5	0.2	-	-	Hematite
2	24.2	40.1	35.5	-	0.2	Glass
3	26.9	35.8	37.3	-	-	Glass
4	10.4	41.7	47.9	-	-	Glass
5	9.6	42.4	48.0	-	-	Glass

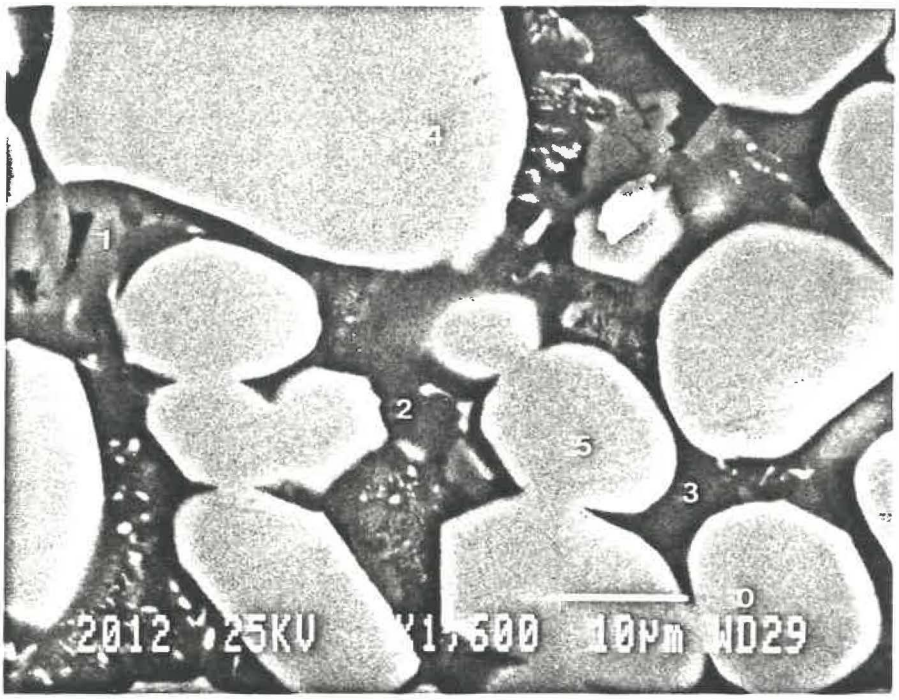


FIGURE 27 - Electron micrograph of 3 LP pellet.

TABLE 16 - Microanalysis of mineralogical phases shown in Figure 27.

POINT	Fe_2O_3	SiO_2	CaO	MgO	Al_2O_3	PHASE
1	33.2	35.4	27.2	2.4	1.9	Glass
2	18.7	34.4	46.9	-	-	Glass
3	30.8	45.4	19.2	0.9	3.7	Glass
4	99.4	0.1	0.5	-	-	Hematite
5	98.3	1.2	0.5	-	-	Hematite

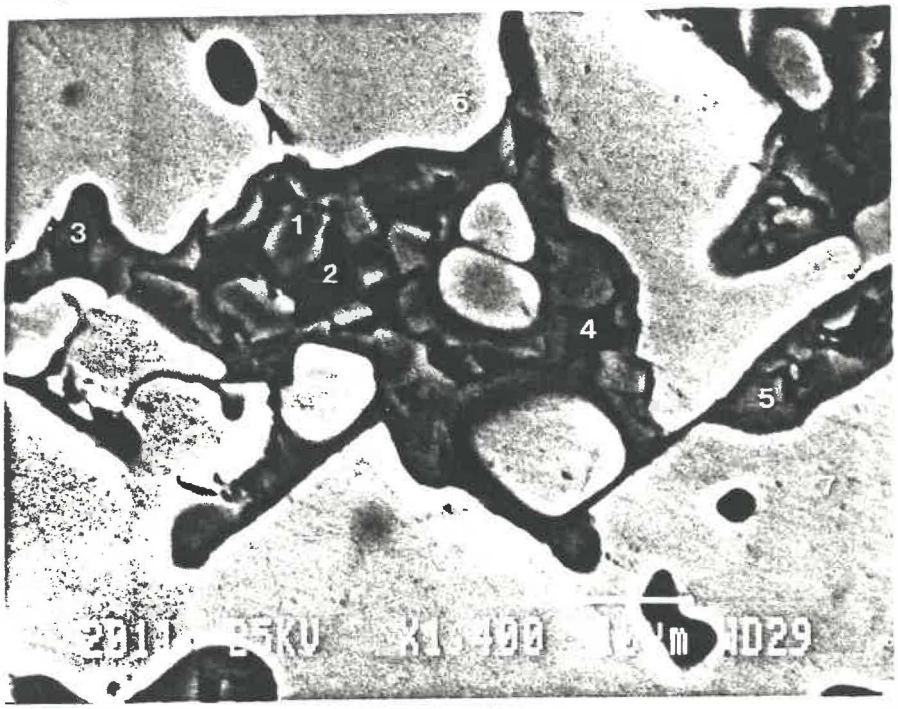


FIGURE 28 - Electron micrograph of 3 DB pellet.

TABLE 17 - Microanalysis of mineralogical phases shown in Figure 28.

POINT	Fe_2O_3	SiO_2	CaO	MgO	Al_2O_3	PHASE
1	33.3	38.0	21.8	4.6	2.3	Glass (pale gray)
2	25.2	56.4	17.2	-	1.2	Glass (dark)
3	39.2	35.3	21.4	3.9	0.2	Glass (pale gray)
4	22.9	43.6	33.5	-	-	Glass (dark)
5	35.4	37.4	22.4	4.8	-	Glass (pale gray)
6	99.1	0.8	0.1	-	-	Hematite
7	98.5	1.0	0.5	-	-	Hematite

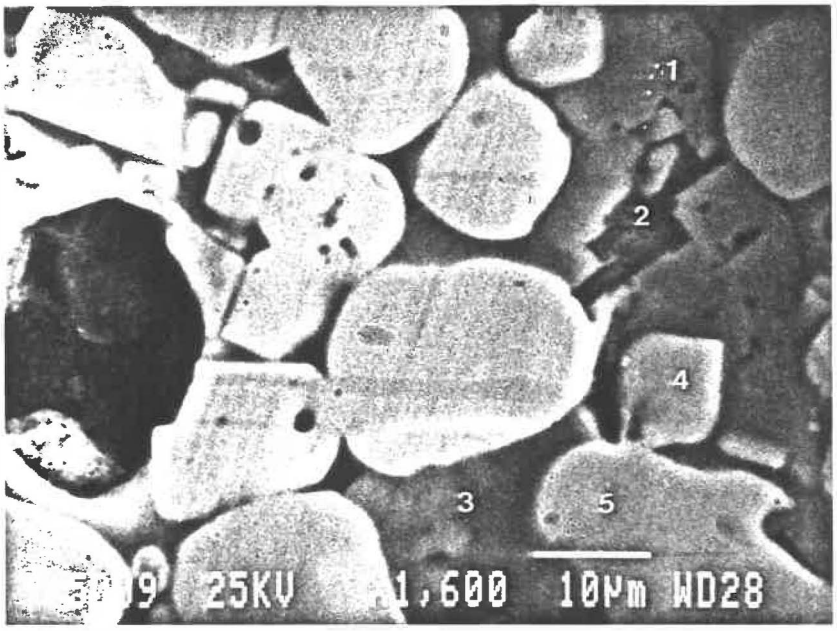


FIGURE 29 - Electron micrograph of 3 DP pellet.

TABLE 18 - Microanalysis of mineralogical phases shown in Figure 29.

POINT	Fe_2O_3	SiO_2	CaO	MgO	Al_2O_3	PHASE
1	37.2	35.8	22.5	3.8	0.7	Glass (pale gray)
2	29.3	46.6	23.3	-	0.8	Glass (dark)
3	35.1	36.8	22.6	4.7	0.8	Glass (pale gray)
4	91.4	-	0.1	8.5	-	Magnesioferrite
5	98.6	1.2	0.2	-	-	Hematite

small amount of bonding phase was found to be calcium ferrite aproaching the range of compositions of silicoferrites of calcium and aluminium (SFCA). There is a large difference in the degree of porosity of the bentonite and peat moss added pellets. The latter pellets have higher porosity. The pore structure is also different. In pellets with bentonite addition the pores approached spherical shape as the ore particles were pulled together due to the presence of melt. In peat moss added pellets this is less prominent due to higher porosity.

In pellets produced with dolomite addition, zoning of glass phase was quite evident (see Figures 28 and 29). The major proportion of glass phase was of pale gray phase. The pale gray phase is high in MgO and Fe_2O_3. It contained less amount of SiO_2. The dark phase is high in SiO_2 and CaO with low Fe_2O_3 and virtually no MgO. Relatively less amount of slag was formed in these pellets due to the presence of MgO which increased the liquidus temperature of the slag phase. The distribution of Fe, Ca, Mg, Si and Al in the bonding phase varied widely. This indicates that only localised melting has taken place. Some amount of unreacted silica was also observed in the pellets. In peat moss added pellets more pores were distributed in the pellet matrix. However, the elemental distribution in the bonding phase did not show any significant change. Some amount of magnesioferrite was formed as described earlier. The microanalysis of this phase showed that MgO content varied between 7-9%.

4.3 Basicity 1.3

The typical photomicrographs of the pellets are shown in Figures 30-33. The typical SEM photomicrographs are shown in Figures 34-36 with the microanalyses, in Tables 19-21. With higher amount of slag bonding the pellet structure has further consolidated and the big ore particles are brought to closer contact and agglomerate. The pores have tended to become spherical and their size has become bigger. This is more visible in limestone fluxed pellets in which lower porosity was observed. In dolomite fluxed pellets the decrease in porosity is marginal. The network of slag bond has spread to more areas in the pellet. Due to increased flux addition the CaO content in the slag has increased compared to that at 0.8 basicity. The SiO_2 and Fe_2O_3 content was observed to decrease. At this basicity free silica was absent in the pellets indicating assimilation of silica in the slag.

In the pellets with limestone and bentonite addition, the formation of calcium ferrites, particularly around pores, was noted (Fig. 30). The pore denotes the former location of the flux which was formed upon the calcination of the latter. The calcined flux has reacted with adjacent hematite and gangue particles to form a melt from which calcium ferrite has precipitated (see Fig. 30). Hematite is the predominant crystalline phase. Magnetite amounted to approximately 10%, correlating well with the relatively high FeO content noted for these pellets. The bonding phase consisted of silicates with varied Fe, Ca, Si, Al and Mg content and a small amount of calcium ferrite. Typical

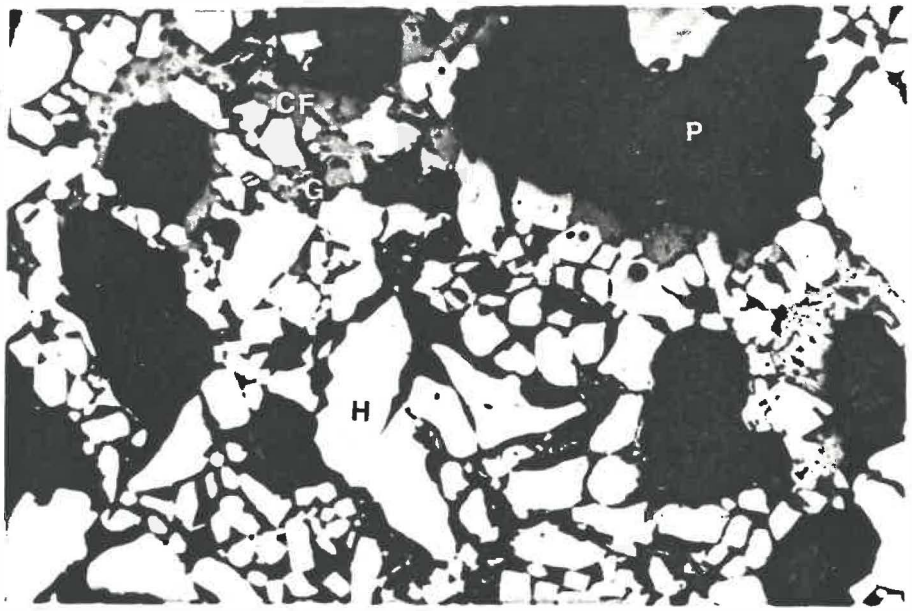


FIGURE 30 - Typical photomicrograph of 5 LB pellets (Basicity: 1.3, flux: limestone; binder: bentonite).
H: hematite; CF: SFCA; G: glass; P: pore.

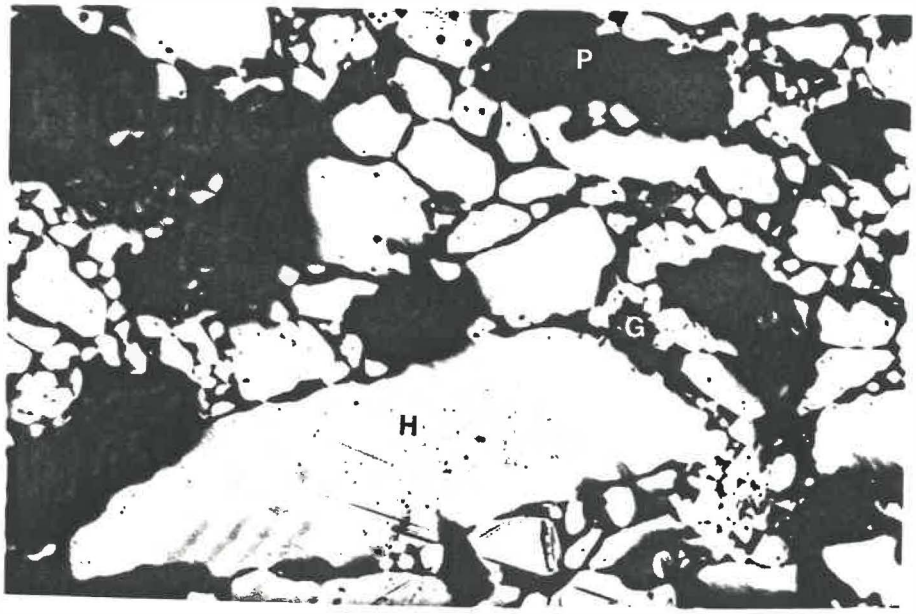


FIGURE 31 - Typical photomicrograph of 5 LP pellets (Basicity: 1.3, flux: limestone; binder: peat moss).
H: hematite; CF: SFCA; G: glass; P: pore.

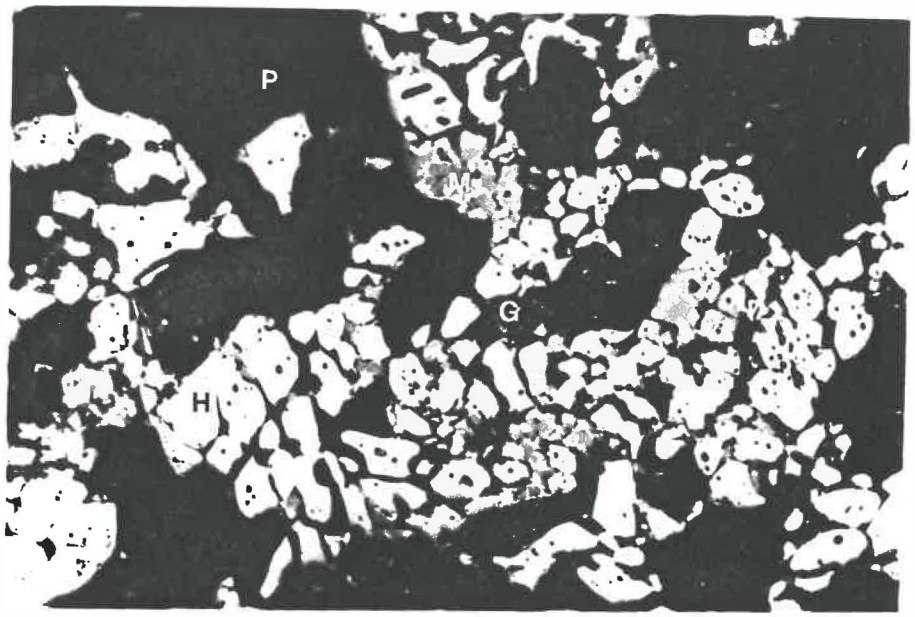


FIGURE 32 - Typical photomicrograph of 5 DB pellets (Basicity: 1.3, flux: dolomite; binder: bentonite).
H: hematite; M: magnesioferrite; G: glass; P: pore.

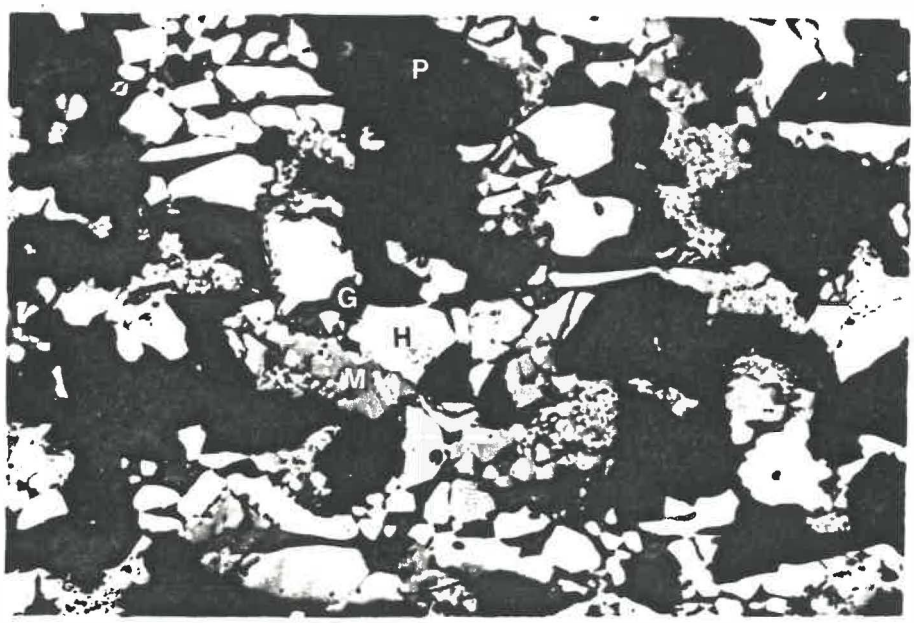


FIGURE 33 - Typical photomicrograph of 5 DP pellets. (Basicity: 1.3, flux: dolomite; binder: peat moss.
H: hematite; M: magnesioferrite; G: glass; P: pore.

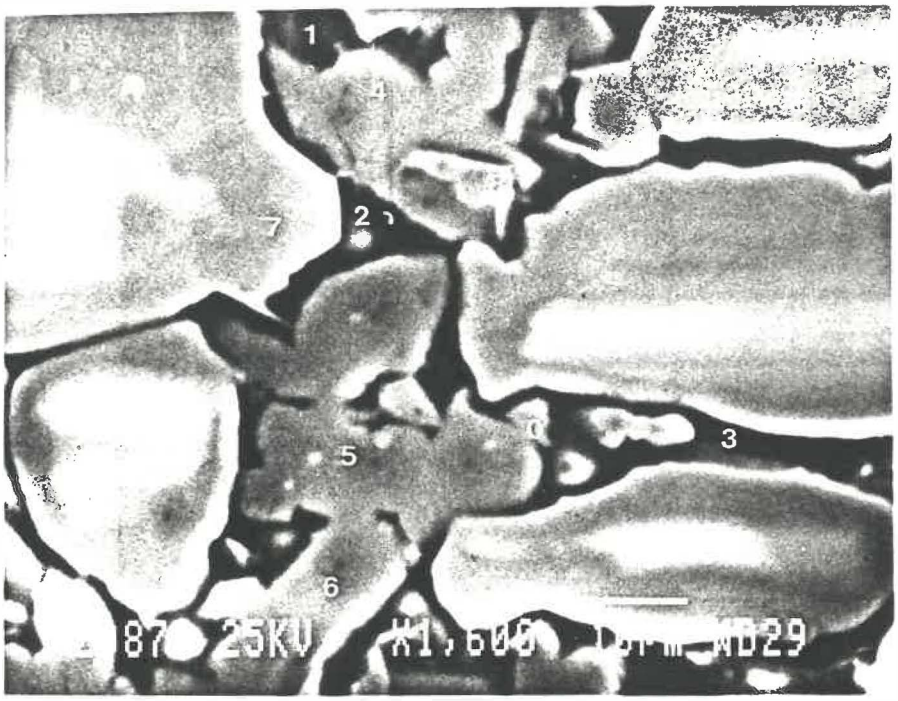


FIGURE 34 - Typical electron micrograph of 5 LB pellets.

TABLE 19 - Microanalysis of mineralogical phases shown in Figure 34.

POINT	Fe_2O_3	SiO_2	CaO	MgO	Al_2O_3	PHASE
1	24.6	30.2	45.2	-	-	Glass
2	16.8	30.4	52.8	-	-	Glass
3	9.9	34.1	56.0	-	-	Glass
4	81.5	4.9	13.3	-	0.3	SFCA
5	81.3	5.2	13.2	-	0.3	SFCA
6	79.6	5.8	13.3	0.5	0.8	SFCA
7	99.1	0.4	0.5	-	-	Hematite
8	97.7	1.2	1.1	-	-	Hematite

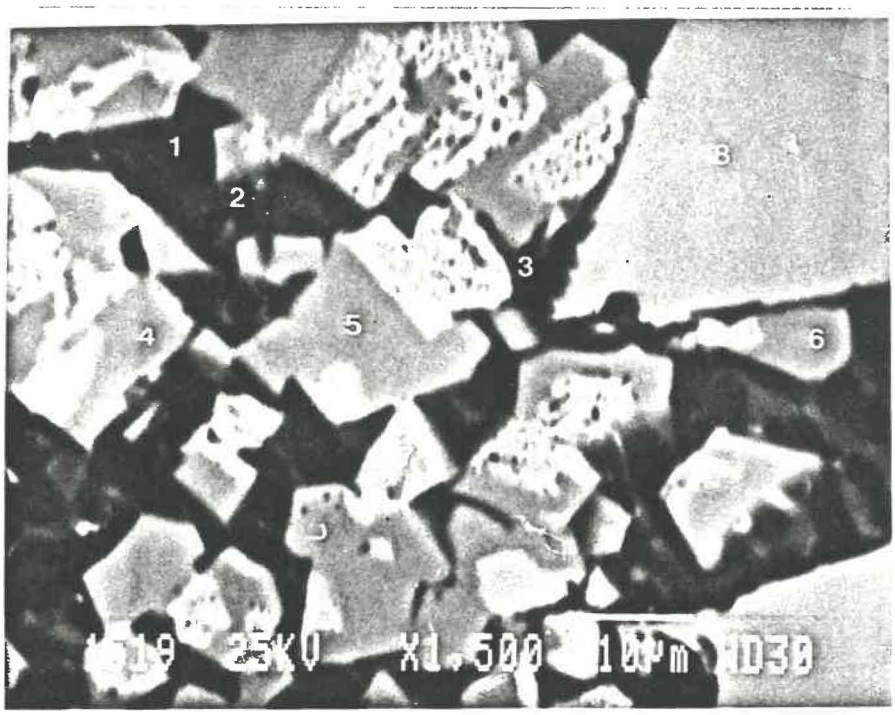


FIGURE 35 - Typical electron micrograph of 5 DB pellets.

TABLE 20 - Microanalysis of mineralogical phases shown in Figure 35.

POINT	Fe_2O_3	SiO_2	CaO	MgO	Al_2O_3	PHASE
1	35.2	26.2	35.4	3.2	-	Glass
2	21.0	35.8	42.9	-	0.2	Glass
3	11.1	29.8	54.6	1.8	2.7	Glass
4	90.6	0.8	1.7	6.9	-	Magnesioferrite
5	93.6	-	1.1	5.3	-	Magnesioferrite
6	91.4	-	1.4	7.2	-	Magnesioferrite
7	97.4	1.2	1.4	-	-	Hematite
8	99.5	0.3	0.1	-	-	Hematite

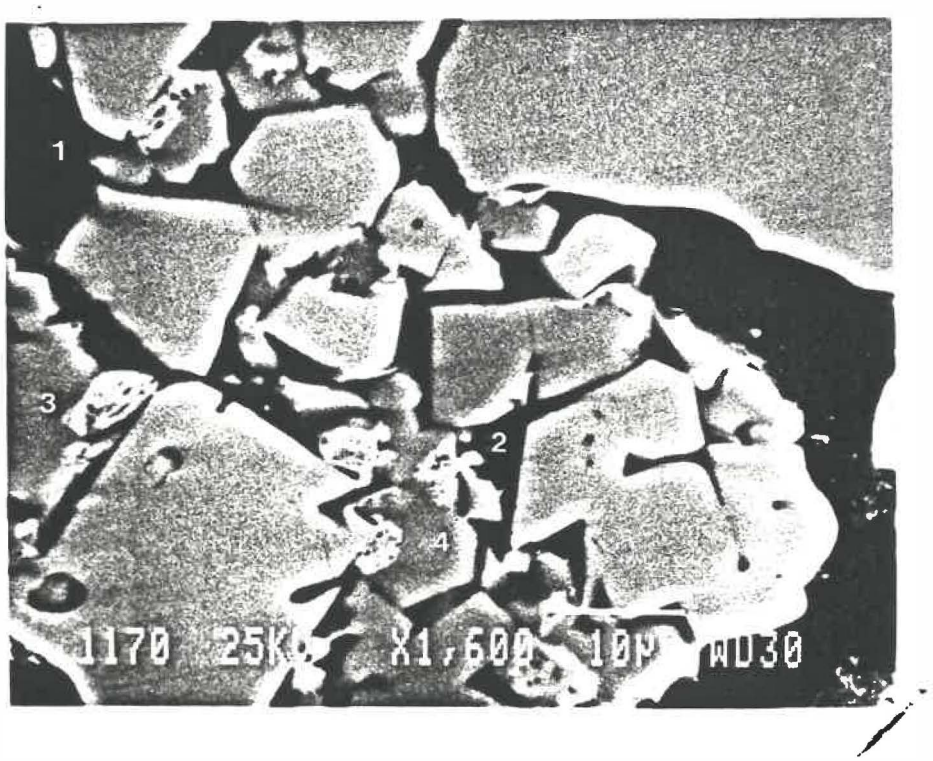


FIGURE 36 - Typical electron micrograph of 5 DP pellets.

TABLE 21 - Microanalysis of mineralogical phases shown in Figure 36.

POINT	Fe_2O_3	SiO_2	CaO	MgO	Al_2O_3	PHASE
1	43.7	27.8	26.1	2.4	-	Glass
2	22.5	30.8	46.7	-	-	Glass
3	92.5	-	0.8	6.7	-	Magnesioferrite
4	91.4	-	0.9	7.3	0.4	Magnesioferrite
5	99.3	-	0.7	-	-	Hematite

compositions of different mineralogical phases in a pellet with limestone and bentonite addition is shown in Figure 34 and Table 19.

In pellets with dolomite addition, little formation of calcium ferrites was observed. The amount of magnesioferrite in the pellet was higher than that of 0.8 basicity with less MgO content. Zoning was observed in the bonding silicate phase although the amount had some what diminished. The pale gray phase contained higher amount of Mg and Fe and the dark phase was relatively low in Mg and Fe and high in silicon and calcium. The pale gray phase contained less MgO than the pellet of 0.8 basicity. Another silicate phase was observed which did not have any zoned structure and its chemical composition was similar to the composition of glass phase in the pellets with limestone addition. It is believed that formation of this glass phase was facilitated due to depletion of Mg from the melt as most of the Mg was concentrated in magnesioferrite phase.

The pellets with peatmoss addition had similar mineral assemblage but a highly porous structure.

4.4 Basicity 1.6

Typical photomicrographs of the pellets of 1.6 basicity are shown in Figures 37 to 40 and typical SEM photomicrographs are shown in Figures 41 to 44 with microanalysis in Tables 22-26. As high amount of flux was added to attain this basicity, large amount of melt was formed which influenced the pellet structure significantly. Pore channels were closed due to flow of the melt. A compact structure was formed due to

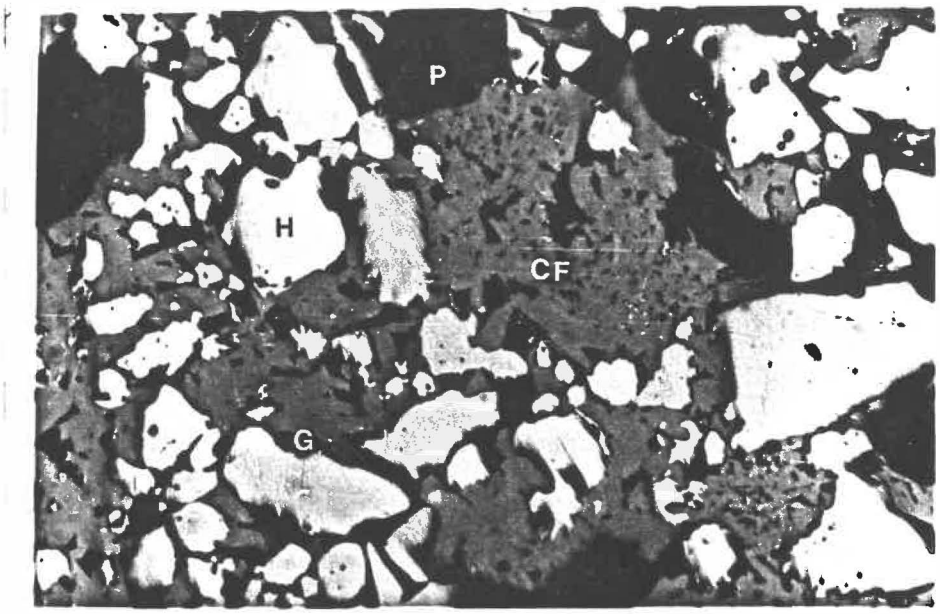


FIGURE 37 - Typical photomicrograph of 6 LB pellets (Basicity: 1.6, flux: limestone; binder: bentonite).
H: hematite; CF: SFCA; G: glass; P: pore.

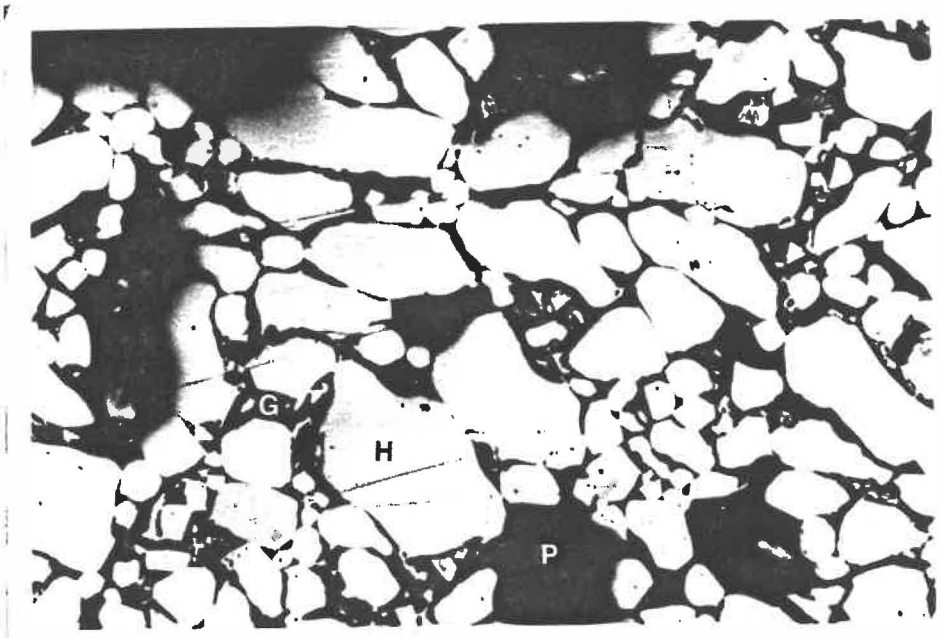


FIGURE 38 - Typical photomicrograph of 6 LP pellets. (Basicity: 1.6, flux: limestone; binder: peat moss).
H: hematite; CF: SFCA; G: glass; P: pore.



FIGURE 39 - Typical photomicrograph of 6 DB pellets. (Basicity: 1.6, flux: dolomite; binder: bentonite).
H: hematite; M: magnesioferrite; G: glass; P: pore.

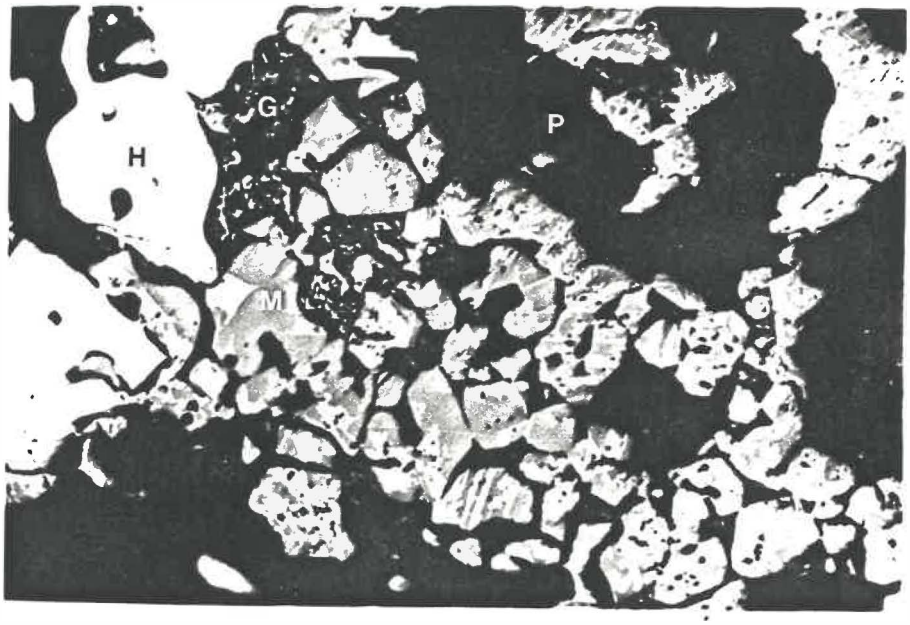


FIGURE 40 - Typical photomicrograph of 6 DP pellets. (Basicity: 1.6, flux: dolomite; binder: peat moss).
H: hematite; M: magnesioferrite; G: glass; P: pore.



FIGURE 41 - Typical electron micrograph of 6 LB pellets.

TABLE 22 - Microanalysis of mineralogical phases shown in Figure 41.

POINT	Fe_2O_3	SiO_2	CaO	MgO	Al_2O_3	PHASE
1	30.1	22.7	47.0	-	0.2	Glass
2	83.9	3.5	11.7	0.3	0.6	SFCA
3	84.0	3.6	11.8	-	0.6	SFCA
4	84.9	3.1	11.8	-	0.2	SFCA
5	99.9	-	0.1	-	-	Hematite
6	99.6	-	0.2	-	0.2	Hematite
7	99.9	-	0.1	-	-	Hematite

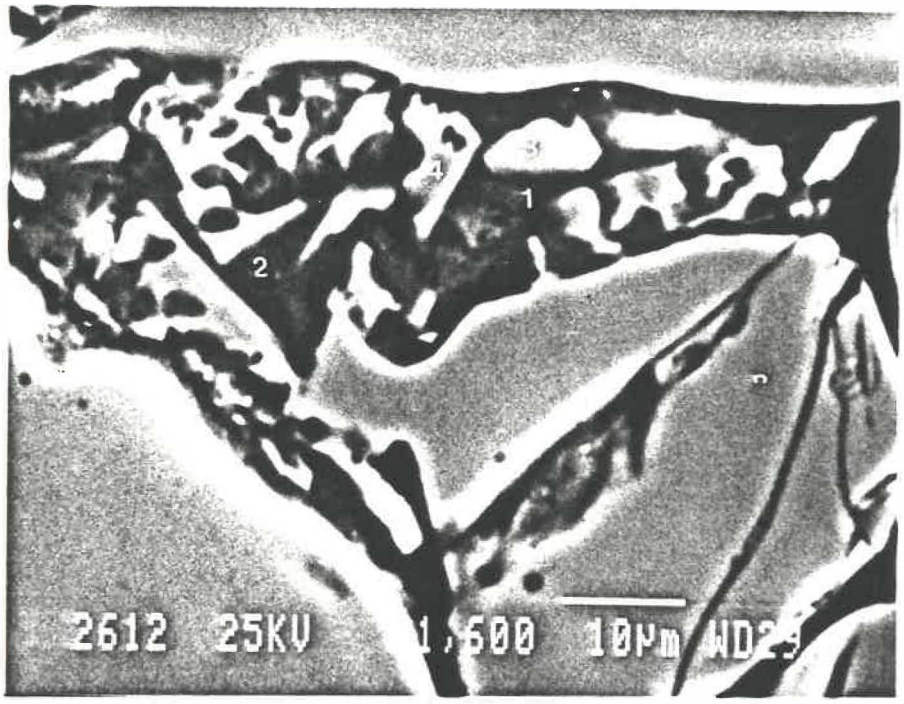


FIGURE 42 - Typical electron micrograph of 6 LP pellets.

TABLE 23 - Microanalysis of mineralogical phase shown in Figure 42.

POINT	Fe_2O_3	SiO_2	CaO	MgO	Al_2O_3	PHASE
1	17.9	32.1	49.6	-	0.4	Glass
2	29.2	15.3	55.5	-	-	Glass
3	96.9	0.7	2.4	-	-	Hematite
4	96.0	0.9	3.1	-	-	Hematite

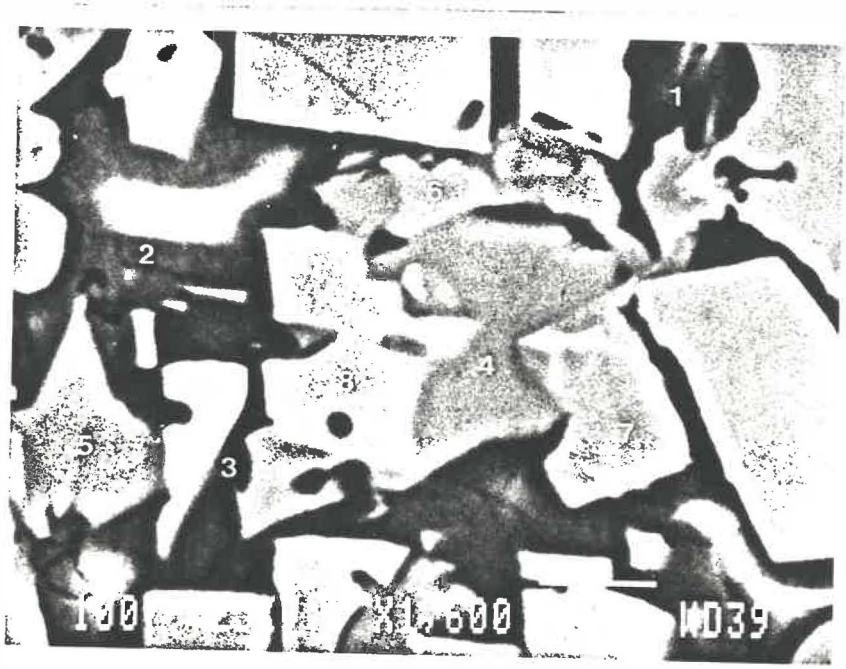


FIGURE 43 - Typical electron micrograph of 6 DB pellets.

TABLE 24 - Microanalysis of mineralogical phases shown in Figure 43.

POINT	Fe_2O_3	SiO_2	CaO	MgO	Al_2O_3	PHASE
1	21.5	32.0	45.5	0.3	0.7	Glass
2	29.0	25.1	44.0	1.3	0.6	Glass
3	10.0	58.5	29.6	1.0	0.9	Glass
4	79.7	4.9	13.4	0.7	1.3	SFCA
5	77.5	7.0	12.3	1.4	1.8	SFCA
6	88.9	1.3	3.3	5.6	0.9	Magnesioferrite
7	92.5	-	1.1	6.0	0.4	Magnesioferrite
8	99.9	-	0.1	-	-	Hematite
9	99.5	0.1	0.4	-	-	Hematite

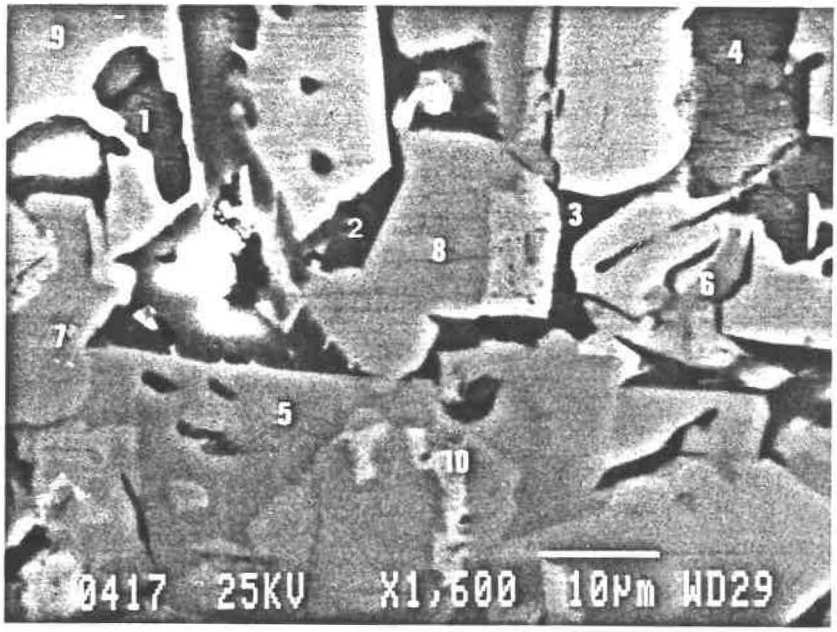


FIGURE 44 - Typical electron micrograph of 6 DP pellets.

TABLE 25 - Microanalysis of mineralogical phases shown in Figure 44.

POINT	Fe_2O_3	SiO_2	CaO	MgO	Al_2O_3	PHASE
1	12.4	24.2	63.4	-	-	Glass
2	16.1	30.2	53.7	-	-	Glass
3	35.2	20.9	43.9	-	-	Glass
4	37.1	23.9	38.1	0.2	0.7	Glass
5	80.2	5.8	12.2	1.1	0.7	SFCA
6	84.5	4.3	10.5	0.7	-	SFCA
7	92.2	-	1.3	6.5	-	Magnesioferrite
8	95.1	-	0.7	4.2	-	Magnesioferrite
9	99.9	-	0.1	-	-	Hematite
10	99.7	-	0.3	-	-	Hematite

flow of the melt. A compact structure was formed due to surface tension of the melt. As a result of shrinkage the coarse hematite particles aproached each other and agglomerated as seen in pellets with limestone and peat moss addition (see Fig. 38). This also causes the pores to become spherical. A good amount of ore particles dissolve in the melt during induration. On cooling various crystalline phases precipitate out depending on the nature of the melt.

In pellets produced with limestone and bentonite an appreciable amount of calcium ferrite is as formed (Fig. 37). The hematite still dominated the pellet structure. But unlike the basicities of 0.8 and 1.3, the magnetite formation has significantly reduced. The bonding phase primarily consisted of calcium ferrites and to a lesser extent of silicate glass phase.

Peat moss addition resulted in significant decrease in calcium ferrite formation. The bonding was primarily by silicate glass phase with small hematite crystals. The glass phase retained significant amounts of hematite which contained some amount of Si and Ca. The pellet structure at this basicity appeared more consolidated in comparison to the peat moss added pellets at other basicities.

In pellets with dolomite and bentonite much less zoning in the silicate bonding phase was observed. The mineralogical assemblage is similar to the pellet of 1.3 basicity. Higher amount of magnesioferrite was formed. A typical pellet structure showing the presence of magnesioferrite with formation of lamellar hematite is shown in Figure 39.

The pellets with peat moss addition had the similar pellet mineralogy as the pellet with bentonite but the pellet structure showed a high degree of pore formation (Figure 40). However, the amount of pores was less than the amount observed in pellet of 1.3 basicity and the pellet structure appeared to be more consolidated.

5. CHEMICAL ANALYSIS OF FIRED PELLETS

The chemical composition of the fired pellets are shown in Table 26. It is observed that pellets produced with only limestone and bentonite contain relatively high FeO. Since these pellets have comparatively low porosity and the intergranular slag phase envelopes the magnetite phase, it is believed that magnetite phase could not undergo sufficient reoxidation. This apparently is the reason for high FeO content of these pellets. Moreover, some amount of FeO may have been retained in the slag phase as the slag forming conditions are better with addition of limestone and bentonite. It is also noted that pellets produced with peat moss addition have slightly higher Fe content due to negligible contamination.

TABLE 26 - Chemical composition of fired pellets.

PELLET DESIGNATION	Fe_2O_3	FeO	SiO_2	Al_2O_3	CaO	MgO	K_2O	N_2O	TiO_2
2 DB	92.00	0.13	5.75	0.35	1.55	0.49	0.01	0.07	0.10
3 DB	89.94	< 0.05	5.50	0.32	1.95	2.10	0.007	0.08	0.08
5 DB	84.37	< 0.05	6.05	0.50	6.30	2.48	0.007	0.05	0.13
6 DB	82.94	0.13	5.55	0.45	8.25	2.16	0.005	0.05	0.17
3 LB	85.61	2.89	5.70	0.45	5.15	0.13	0.004	0.06	0.09
5 LB	80.16	4.84	6.45	0.65	7.85	0.14	0.003	0.04	0.09
6 LB	84.65	0.20	5.05	0.40	9.05	0.18	0.003	0.03	0.18
2 DP	92.25	0.30	4.95	0.42	1.25	0.47	0.01	0.10	0.10
3 DP	89.34	0.05	4.95	0.40	2.80	2.15	0.011	0.09	0.09
5 DP	87.26	0.27	4.92	0.40	4.65	2.03	0.009	0.07	0.09
6 DP	84.66	0.13	4.72	0.33	7.70	2.11	0.006	0.05	0.09
3 LP	87.16	1.92	5.45	0.45	4.55	0.37	0.006	0.08	0.19
5 LP	86.71	0.13	4.95	0.35	7.00	0.12	0.006	0.15	0.08
6 LP	86.90	< 0.05	4.50	0.25	7.65	0.13	0.005	0.07	0.09

6. PROPERTIES OF THE FIRED PELLETS

As a small amount of pellets were produced, a limited number of tests were conducted to characterise the physical properties of the pellets. The tests conducted were: porosity, compression strength, reducibility and swelling, test results are shown in Table 27.

6.1 Porosity

The variation of porosity as a function of basicity and pellet type is shown in Figure 45, up to 1.3 basicity the porosities of the pellets were observed to be high irrespective of flux and binder type. The porosity of the pellets drastically dropped with increase in basicity to 1.6. Pellets with peat moss addition have very high porosity. The high porosity is caused by the burning of peat moss. The liquid phase which is formed during induration is insufficient to close these extra pores.

A marginal decrease in the porosity of the pellets with dolomite is observed as the basicity is increased from 0.2 to 1.3. Less amount of liquid is formed in these pellets during induration due to presence of MgO, which is not adequate to fill the pores. Good amount of liquid formation at the basicity of 1.6 causes a substantial decrease in porosity. The porosity of the pellets with peat moss addition is 7-10% higher than the porosity of pellets with bentonite addition.

TABLE 27 - Physical and reduction properties of the fired pellets.

BASICITY	PELLET DESIGNATION	POROSITY %	COMPRESSION STRENGTH kg/PELLET	REDUCIBILITY $(dR/dt)_{40}$	MAXIMUM SWELLING %
0.2	DB	32.50	186.4	0.49	25.4
	DP	40.09	115.9	0.60	23.35
0.8	DB	32.72	195.64	0.62	28.46
	DP	41.14	120.45	0.82	24.35
	LB	31.71	204.5	0.64	31.23
	LP	37.04	210.64	0.76	24.79
1.3	DB	30.25	190.91	1.34	11.47
	DP	40.91	127.27	1.75	21.99
	LB	28.44	200.00	1.24	26.64
	LP	30.92	222.73	1.27	16.34
1.6	DB	23.55	268.73	0.83	12.66
	DP	30.34	200.00	1.40	10.52
	LB	22.65	279.54	0.73	12.33
	LP	23.65	281.82	0.75	12.66

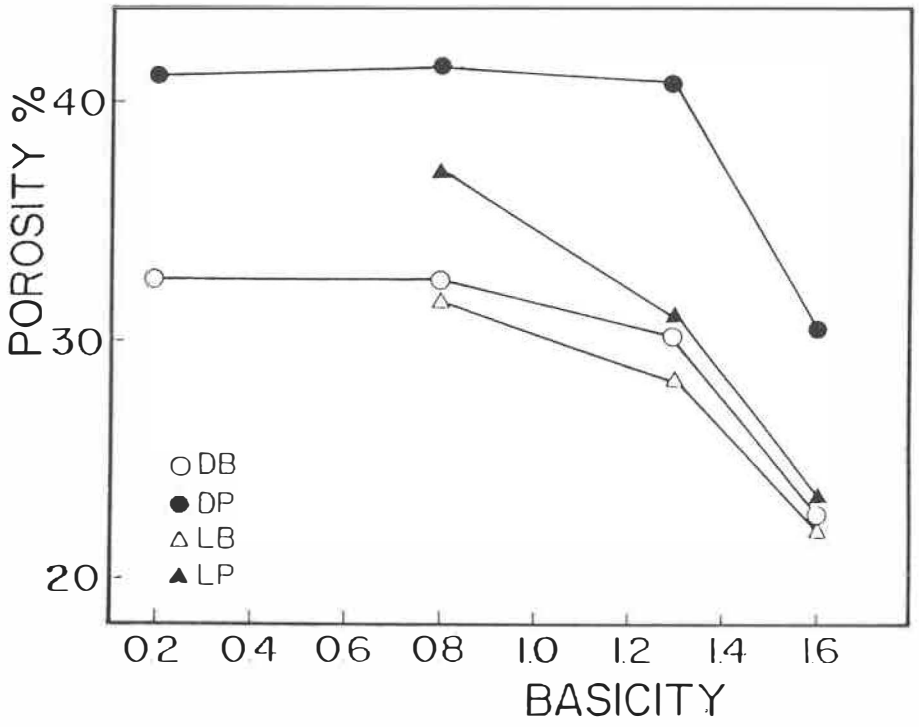


FIGURE 45 - Effect of basicity on the porosity of the pellets.

The porosities of the pellets with limestone addition are lower compared to the pellets with dolomite addition. This is more pronounced in the pellets with peat moss addition. Larger amount melt formation during induration due to the presence of lime filled some of the extra pores created by the burning of peat moss. At higher basicities the difference between the porosities in the pellets with peat moss and bentonite narrowed down as more number of pores were closed due to higher availability of CaO.

6.2 Compression strength

The variation of compression strength as a function of basicity and type of pellet is shown in Figure 46. It is noticed that there is insignificant change in the compression strength of the pellets as the basicity is increased upto 1.3. On futher increase in pellet basicity to 1.6 a considerable improvement in the compression strength is observed. The porosity of the pellets is considered to be the major factor influencing the compression strength as a linear correlation is observed in Figure 47. The compression strength is noted to decrease with increase in porosity.

The pellets with dolomite addition have low compression strength up to 1.3 basicity which are below the accepted compression strength of 200 kg/pellet [1]. The compression strengths of pellets with peat moss addition are also very low. The porosity values of these pellets are very high. As the porosity of these pellets decrease at 1.6 basicity due to increasing amount melt at the induration temperature the compression strength increases considerably and the pellets possess acceptable compression strength.

The compression strength of pellets with limestone addition are higher compared to pellets with dolomite addition. Even the pellets with peat moss addition have compression strength above the minimum accepted value. Increased amount of slag bonding in these pellets has resulted in improved compression strength along with decrease in porosity.

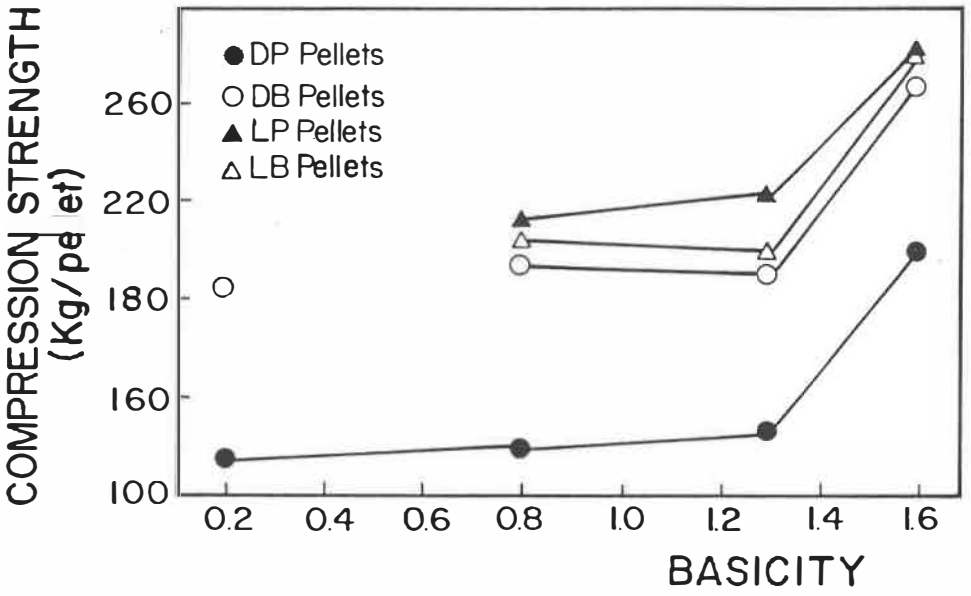


FIGURE 46 - Effect of basicity on compression strength of the pellets.

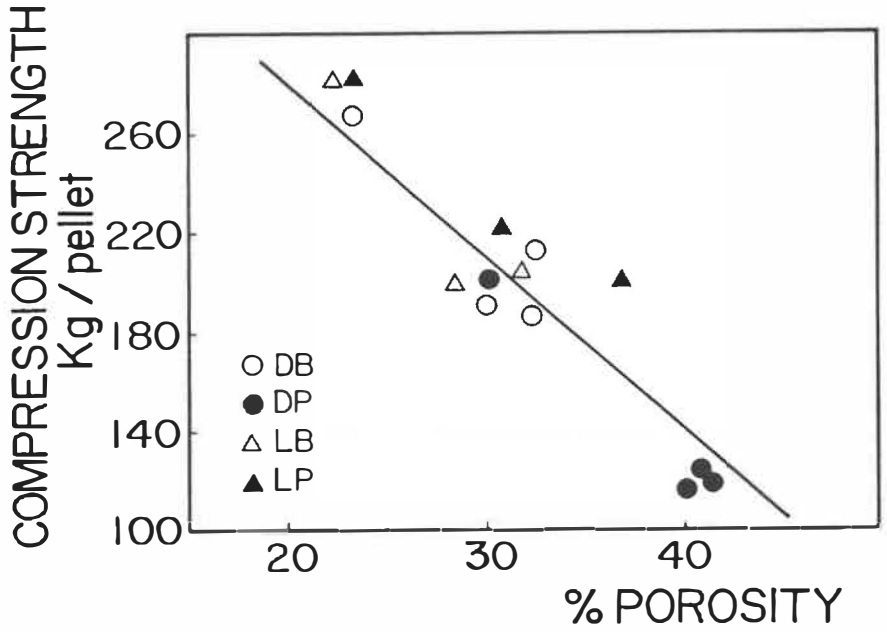


FIGURE 47 - Relationship between compression strength and porosity.

6.3 Reducibility

The variation in pellet reducibility as a function of pellet basicity and pellet types are shown in Figure 48. The reducibility of the pellet is seen to increase with increasing basicity which reaches a maximum at 1.3 basicity and decreases with further increase in basicity. This phenomenon is observed in all types of pellets. The addition of peat moss and dolomite has the most favourable effect on the reducibility as maximum reducibility is acheived in the pellets produced with these additives. The typical microstructures of the reduced pellets are shown in Figures 49 to 57. From the mineralogy of reduced pellets with peat moss addition the extent of reduction was found to be uniform through out the pellet i.e. the proportion of metallic iron to wustite was same at the periphery and the centre of the pellet (see Figures 51, 53, 55 and 57). This indicates that due to high porosity of these pellets the penetration of reducing gas is facilitated thus resulting in higher reducibility.

Lower reducibility in pellets with limestone addition is attributed to lower porosity in these pellets and partly to the enveloping of the iron oxide grains by the glass phase as seen in the pellet with 0.8 and 1.3 basicity (see Figs. 50 and 54). The mineralogy of reduced pellet shows that there is less extent of reduction in the centre than at the periphery of the pellet. The accessibility of reducing gas to the iron oxide is decreased due to lower porosity and enveloping of slag phase.

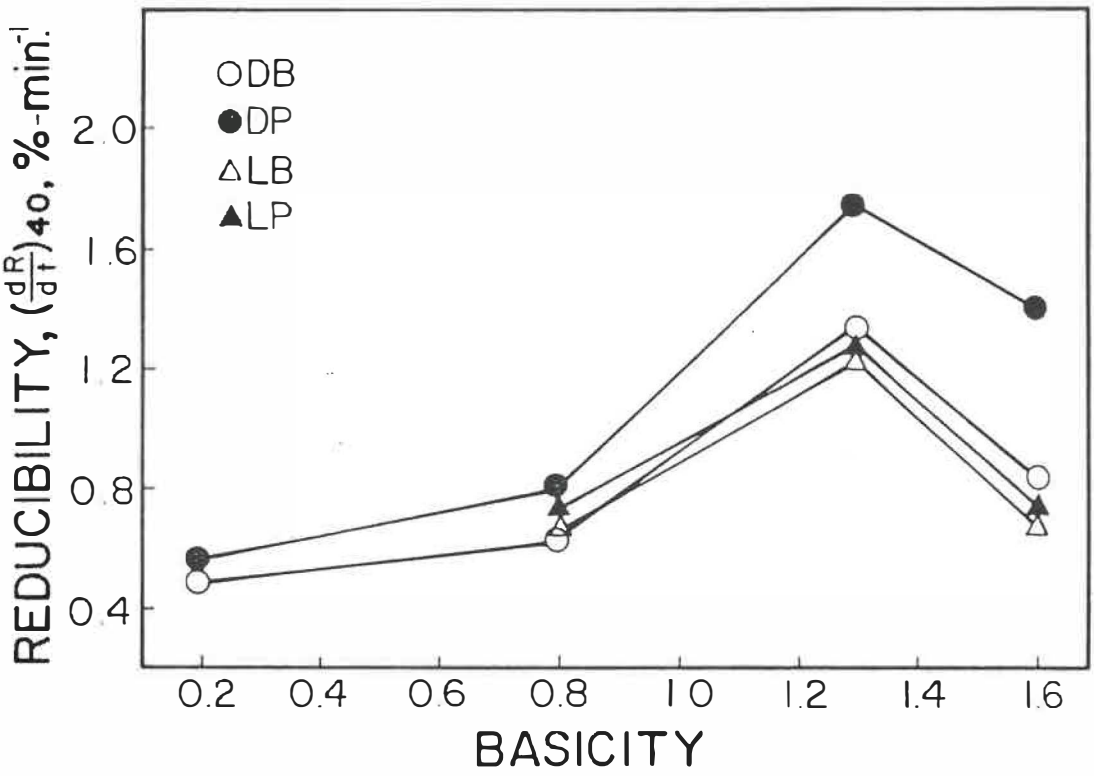
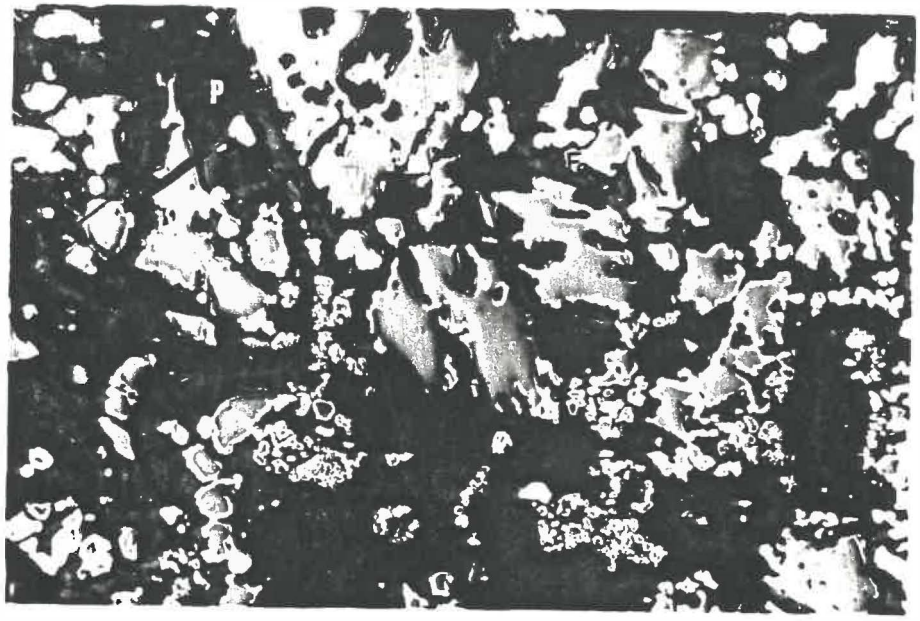
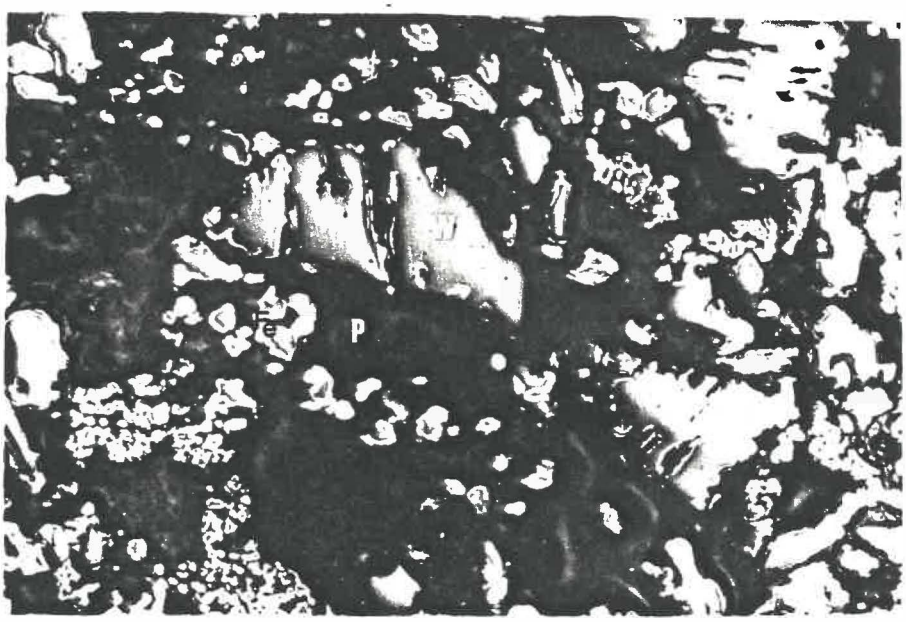


FIGURE 48 - Effect of basicity on reducibility of the pellets.

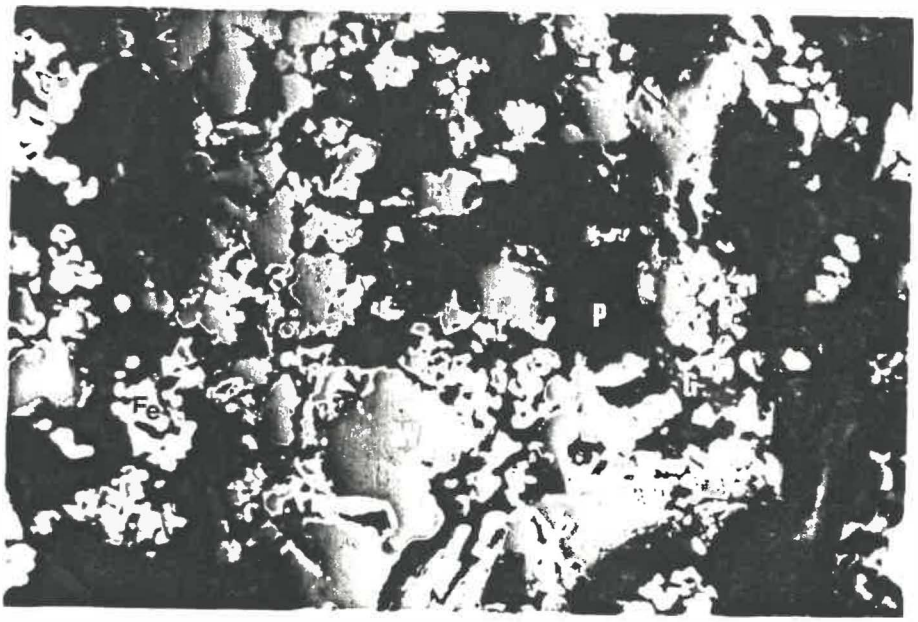


a) periphery

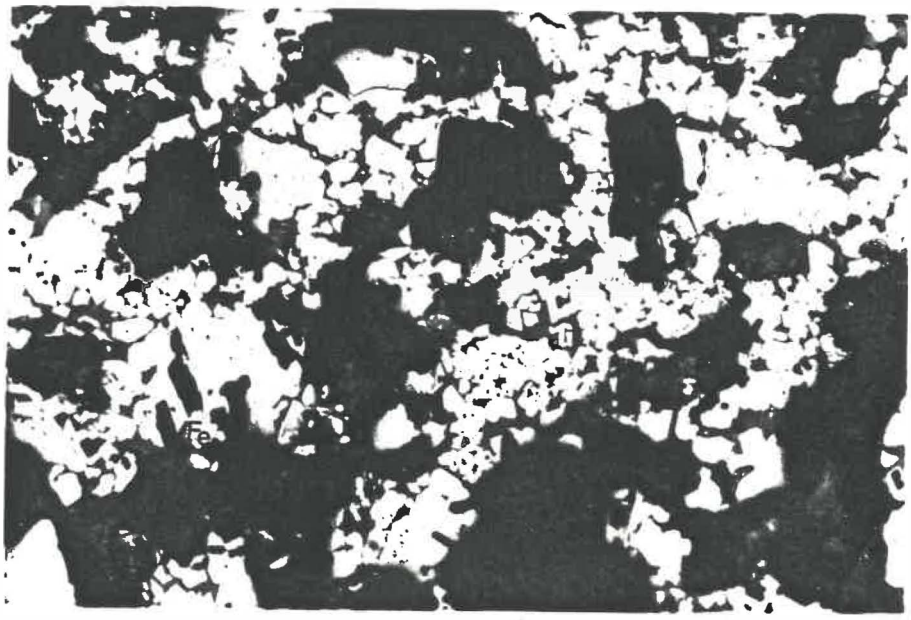


b) centre

FIGURE 49 - Typical photomicrographs of reduced pellets (3 DB). W: wustite; Fe: metallic iron; G: glass; P: pore.

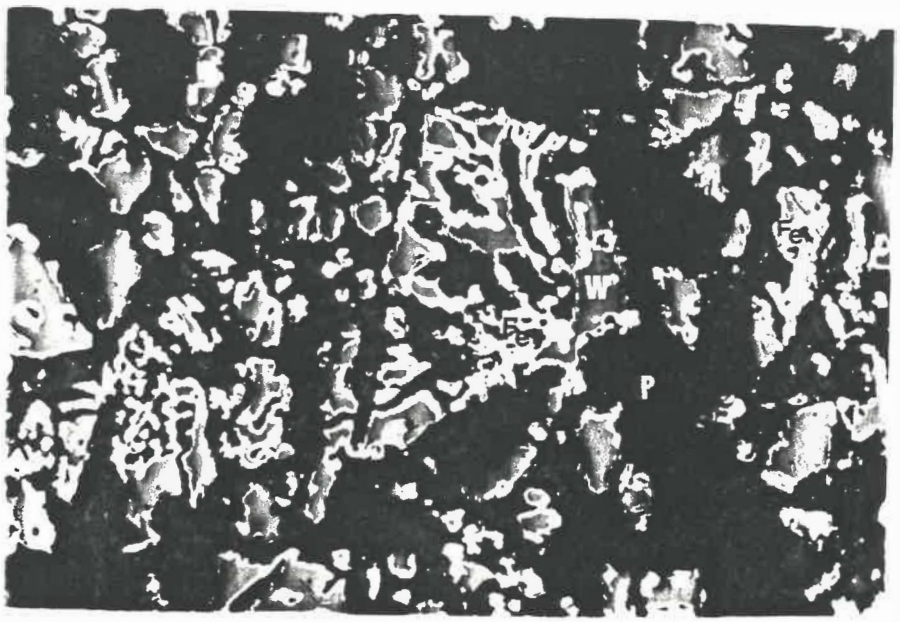


a) periphery



b) centre

FIGURE 50 - Typical photomicrographs of reduced pellets (3 LB).
W: wustite; Fe: metallic iron; G: glass; P: pore.

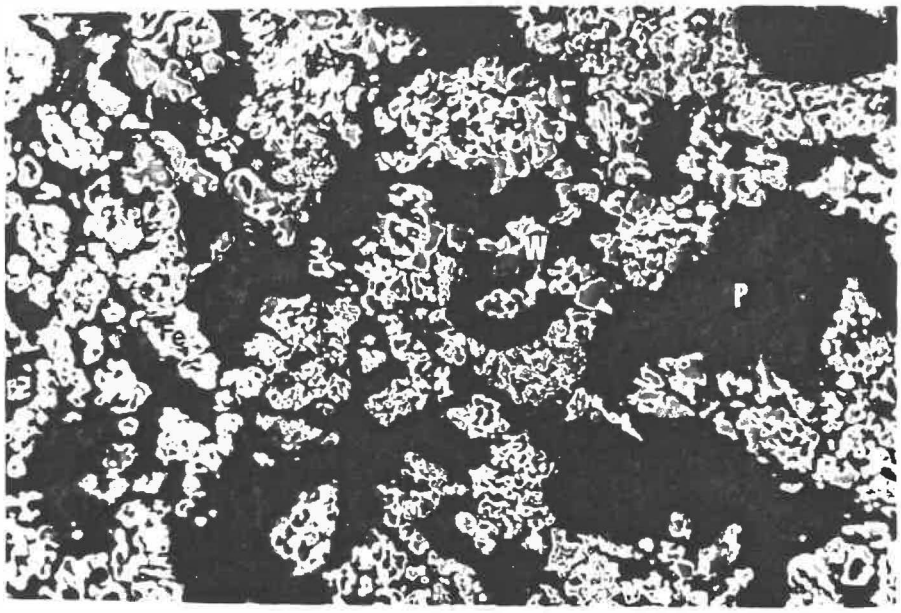


a) periphery

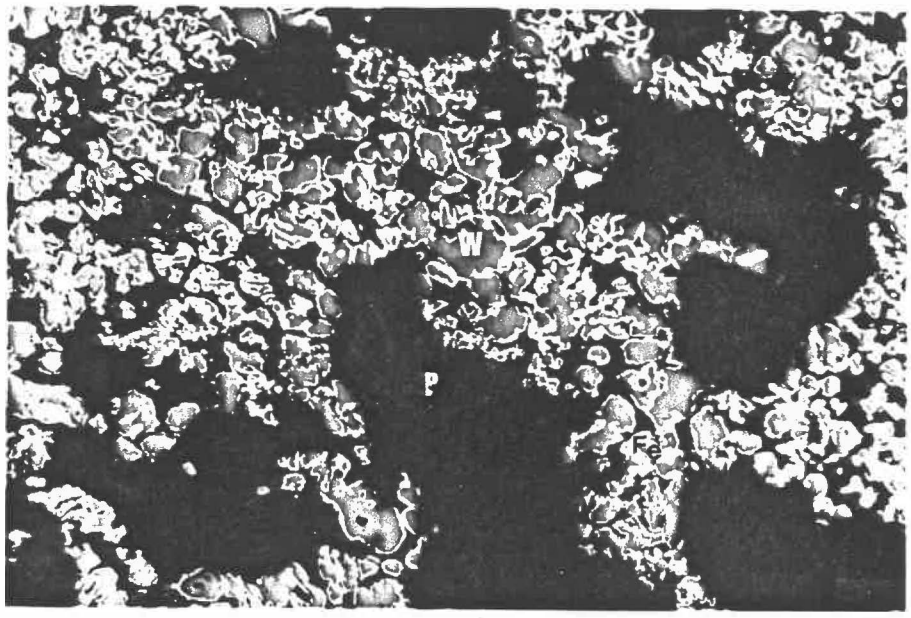


b) centre

FIGURE 51 - Typical photomicrographs of reduced pellets (3 LP).
W: wustite; Fe: metallic iron; G: glass; P: pore.

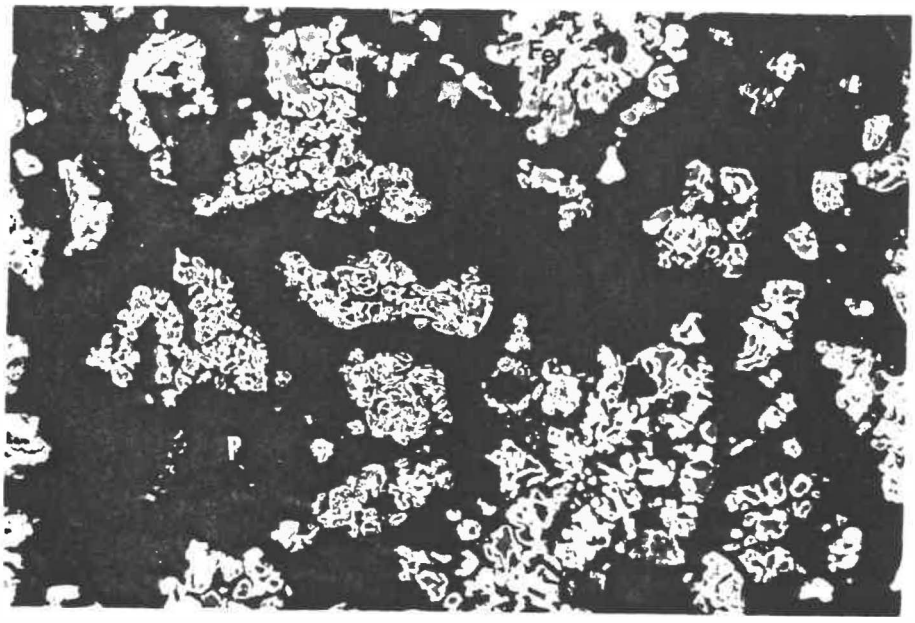


a) periphery

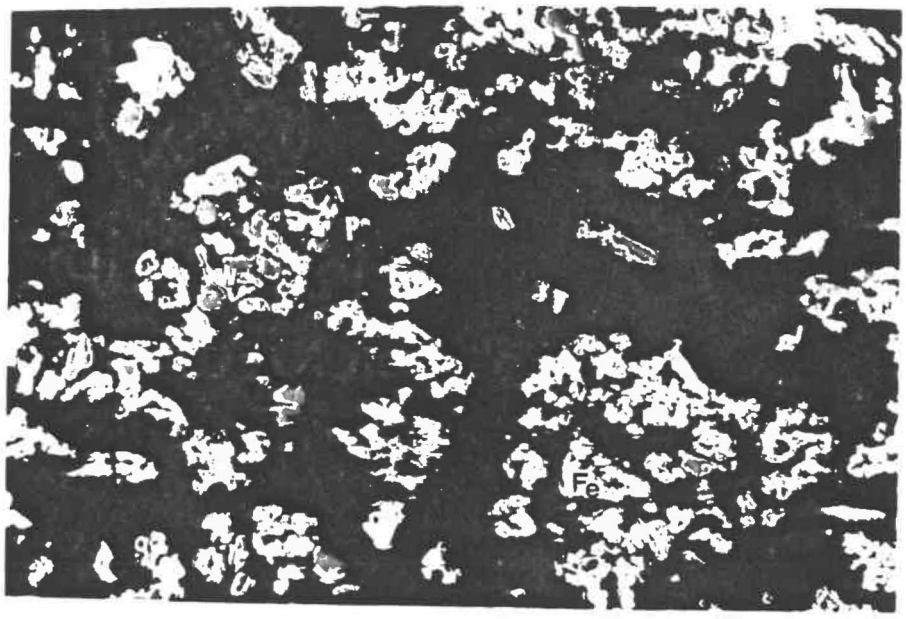


b) centre

FIGURE 52 - Typical photomicrographs of reduced pellets (5 DB).
W: wustite; Fe: metallic iron; G: glass; P: pore.

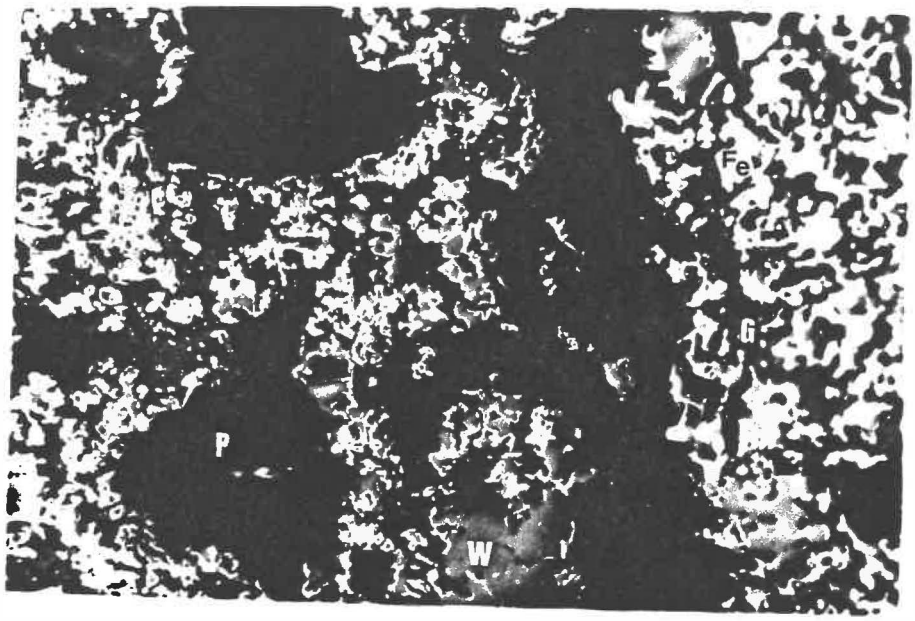


a) periphery

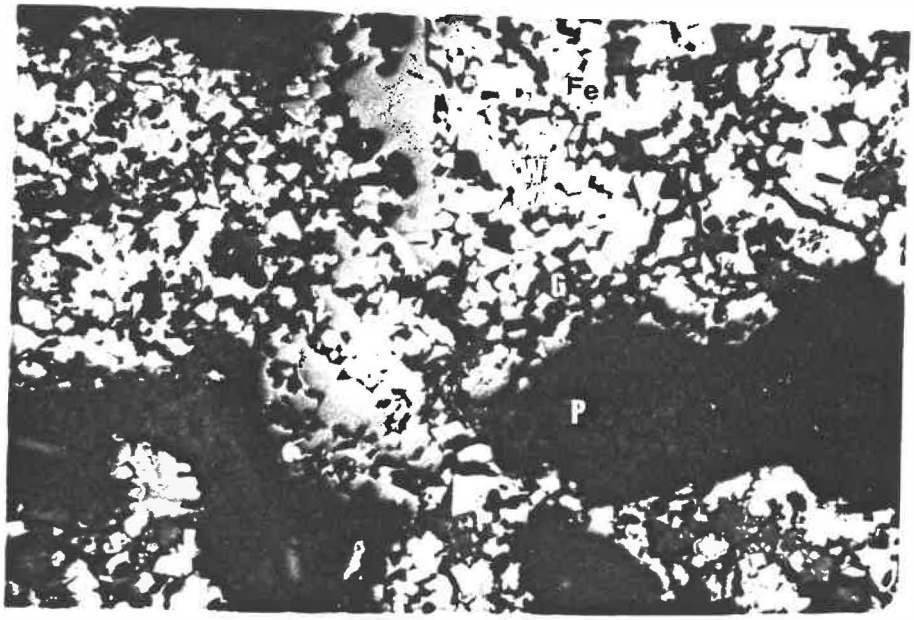


b) centre

FIGURE 53 - Typical photomicrographs of reduced pellets (5 DP).
W: wustite; Fe: metallic iron; G: glass; P: pore.

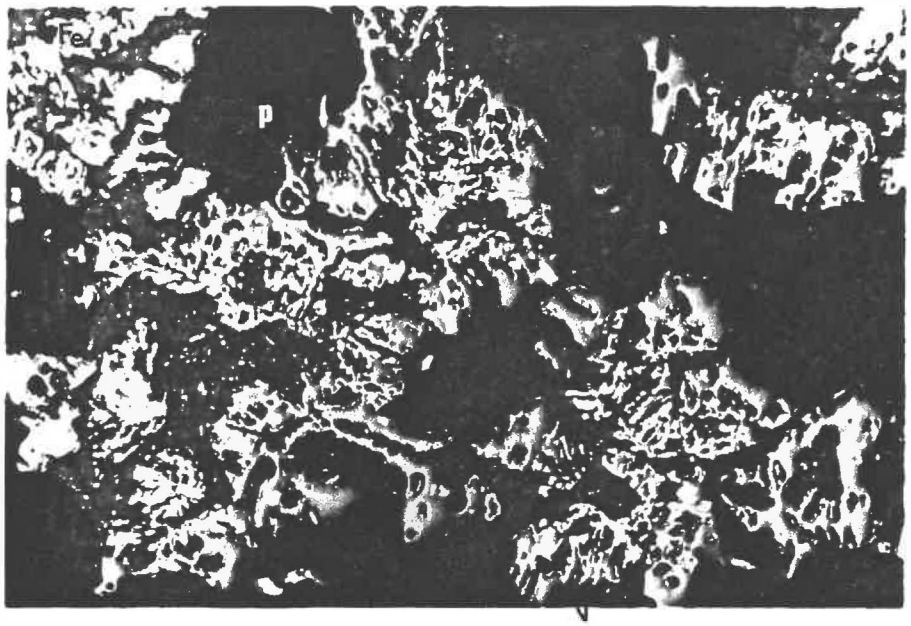


a) periphery

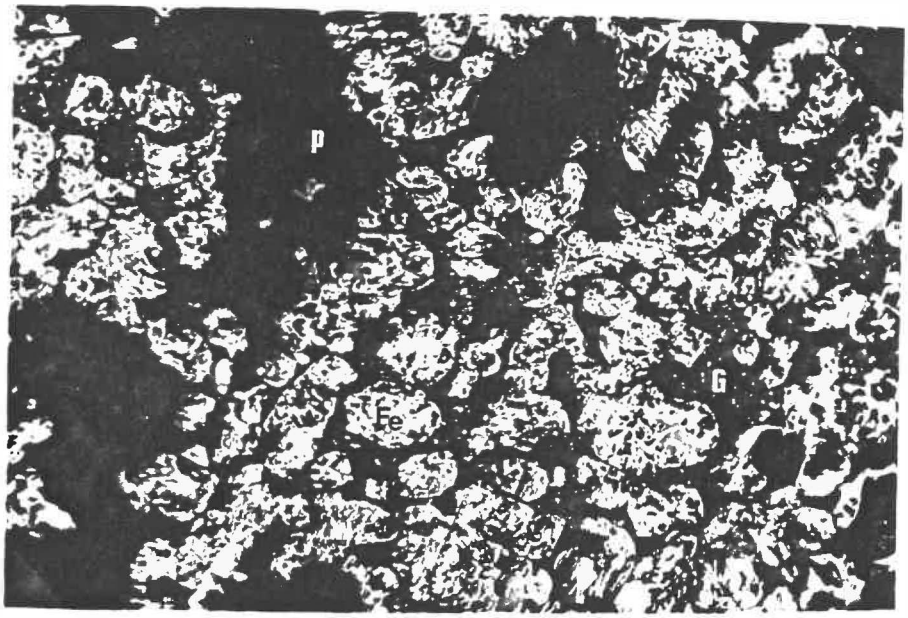


b) centre

FIGURE 54 - Typical photomicrographs of reduced pellets (5 LB).
W: wustite; Fe: metallic iron; G: glass; P: pore.

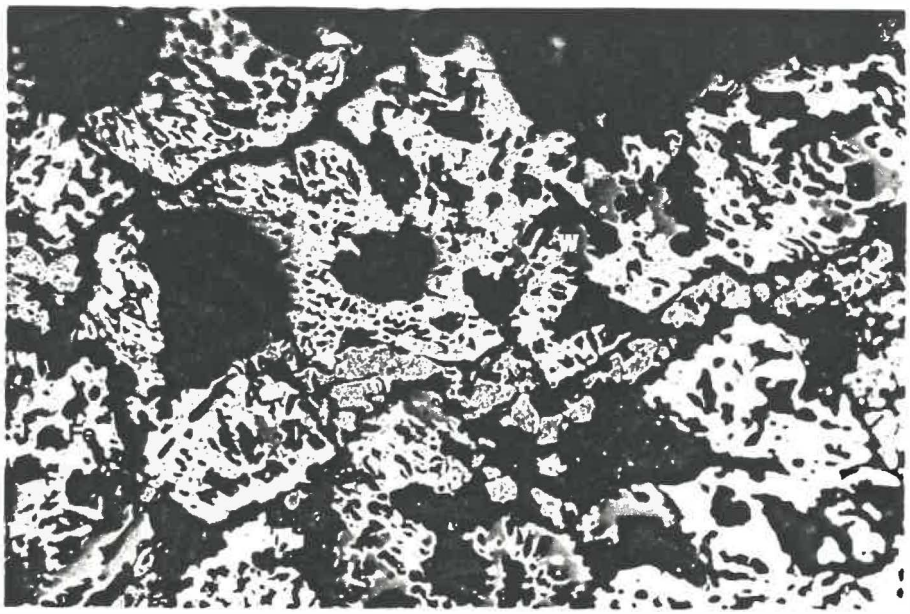


a) periphery

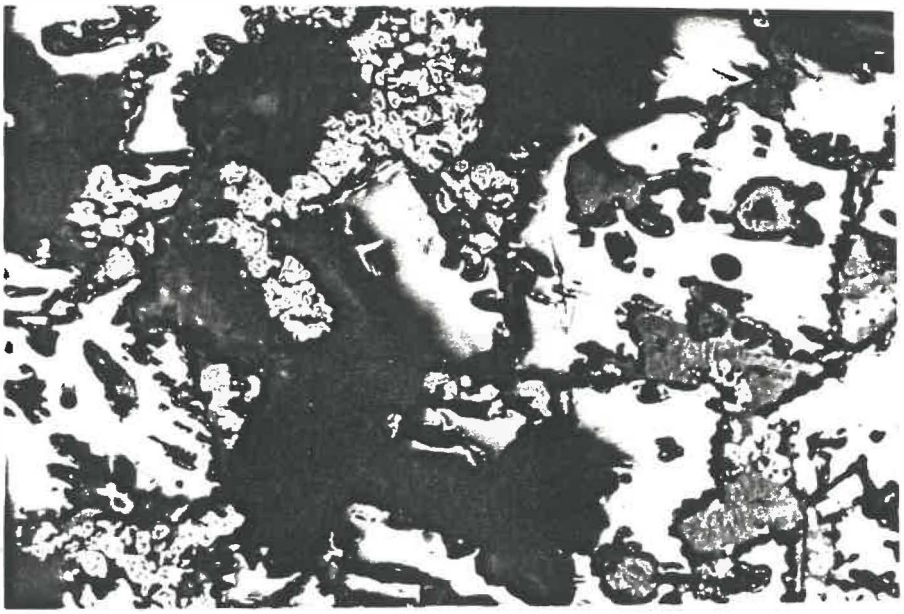


b) centre

FIGURE 55 - Typical photomicrographs of reduced pellets (5 LP).
W: wustite; Fe: metallic iron; G: glass; P: pore.

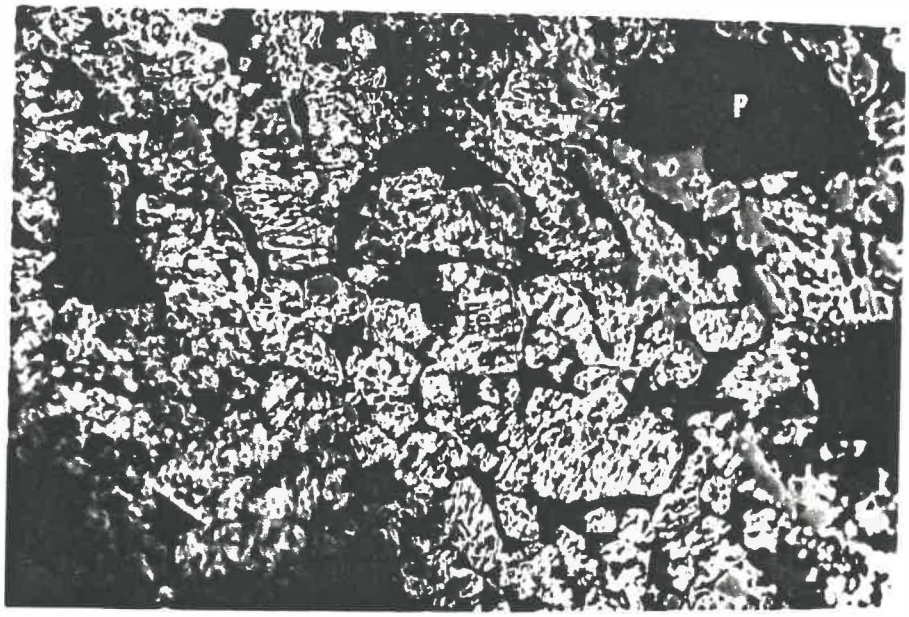


a) periphery

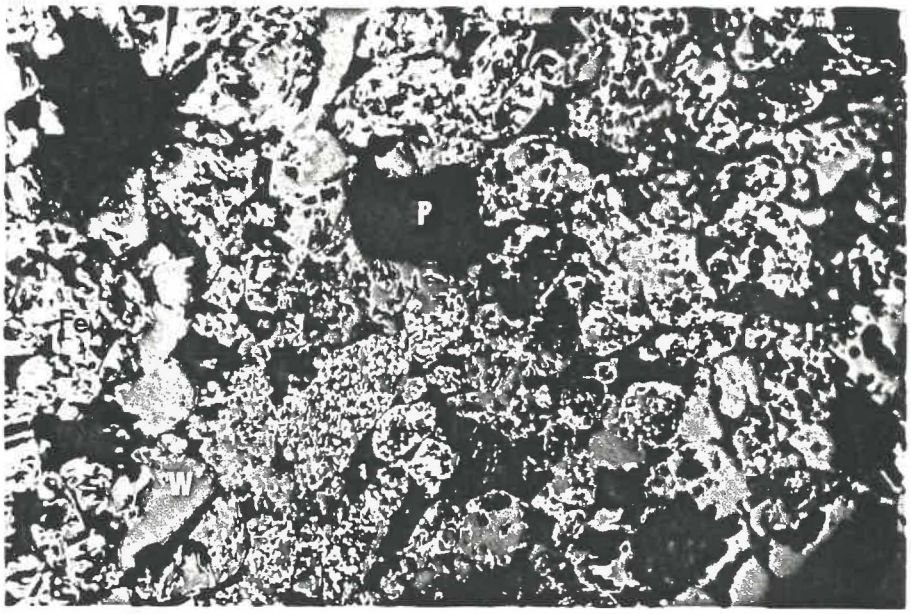


b) centre

FIGURE 56 - Typical photomicrographs of reduced pellets (6 DB).
W: wustite; Fe: metallic iron; G: glass; P: pore.



a) periphery



b) centre

FIGURE 57 - Typical photomicrographs of reduced pellets (6 DP).
W: wustite; Fe: metallic iron; G: glass; P: pore.

It was noticed that although pellets with peat moss addition have high porosity at the basicities of 0.2 and 0.8, the reducibility values are much lower compared to pellets of 1.3 basicity. In order to have a better understanding of this phenomenon, the pellets with peat moss and dolomite addition of 0.2 to 1.6 basicity were reduced for 15, 30, 45 and 60 minutes and the mineralogy of the partially reduced pellets were analysed; typical photomicrographs are shown in Figures 58-61. The following observations have been made:

- Presence of wustite with little amount of iron was observed after 15 minutes of reduction. In high basicity pellets of 1.3 and 1.6, presence of high amount of fine pores in the wustite grain was seen (see Fig. 61-a). On closer observation these pores were identified to be fine cracks developed in the grain. In low basicity pellets of 0.2 and 0.8 the pores in wustite grains were fewer in number and coarser in size (see Fig. 58). A small proportion of wustite grains had fine pores. In the reduced pellets taken out after 30 minutes of reduction formation of metallic iron near the pore was observed. The wustite grains were subdivided into numerous fine fragments due to presence of the fine pores in the high basicity pellets (Figs. 60-b & 61-b). In low basicity pellets the wustite grain was subdivided in the fewer coarse grains (Figs. 58-b & 59-b). The presence of iron was observed on the outer shell of the grain while wustite was observed in the core. Substantial amount of iron formation was observed in the high basicity pellets after 45 minutes of reduction

(Figs. 60-c & 61-c). On the other hand a good amount of unreacted wustite was still present in low basicity pellets.

From the above observations it is evident that the morphology of pore formation changes with change in basicity. It is believed that the new pores are associated with the cracks formed during hematite to magnetite transformation.

The intergranular glass phase in high basicity pellets with stand the volume expansion accompanied by the above transformation as evident from the low swelling values in these pellets (to be presented in section 6.4). The stress generated during the transformation is believed to cause formation of intragranular cracks. In low basicity pellets the volume expansion results in formation of coarser cracks and fragmentation of hematite grains.

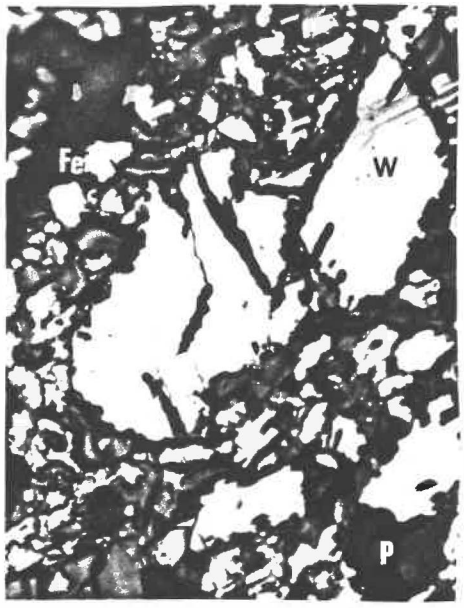
Reduction of iron oxide takes place in following stages

$$Fe_2O_3 \rightarrow Fe_3O_4 \rightarrow FeO \rightarrow Fe$$

The reduction in initial 2 steps occurs by diffusion of gaseous species. The presence of wustite in all the pellets after 15 minutes of reduction bears to the fact that rate of hematite to wustite reduction was high due to high porosity of the pellets. The reduction from wustite to metallic iron proceeds in solid state as a shell of iron forms on the outer surface of the wustite grain. Faster rate of



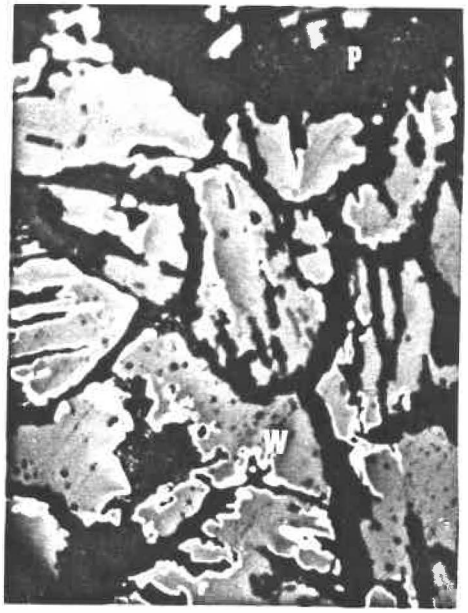
a) after 15 minutes
W: wustite
G: glass



b) after 30 minutes.
Fe: metallic iron
P : pore



c) after 45 minutes

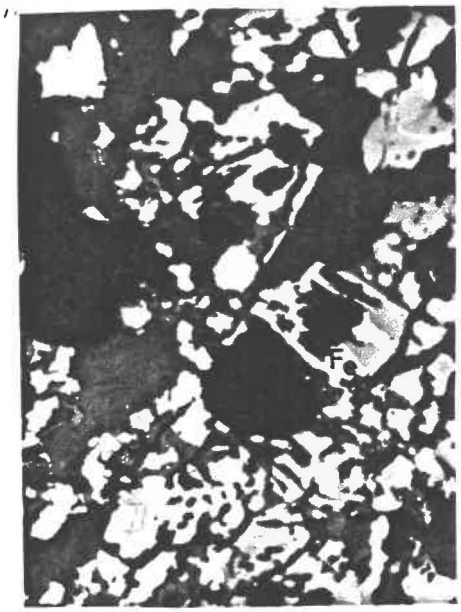


d) after 60 minutes.

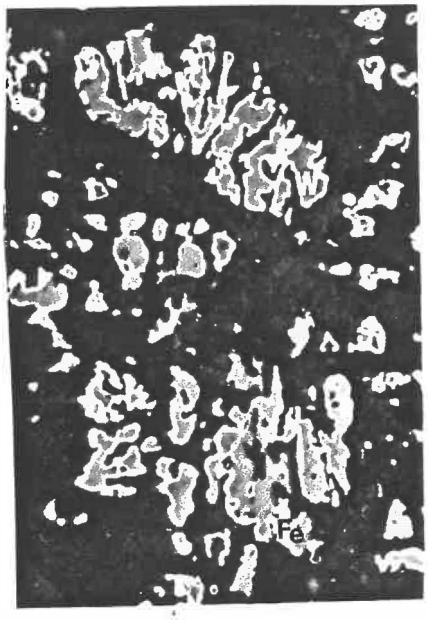
FIGURE 58 - Typical photomicrographs of reduced pellets after 15, 30, 45 and 60 minutes of reduction (pellet type 2 DP).



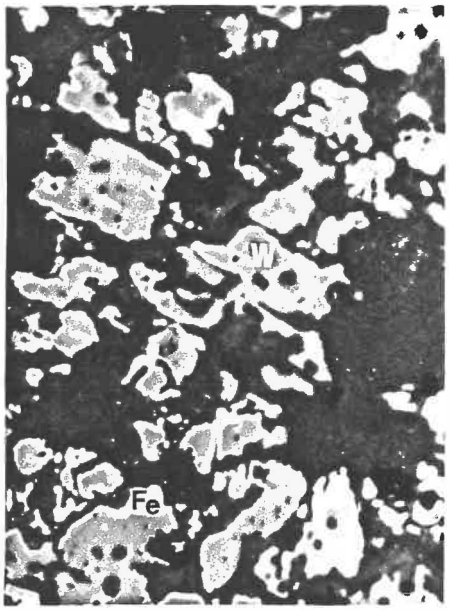
a) after 15 minutes
W: wustite
G: glass



b) after 30 minutes.
Fe: metallic iron
P : pore



c) after 45 minutes

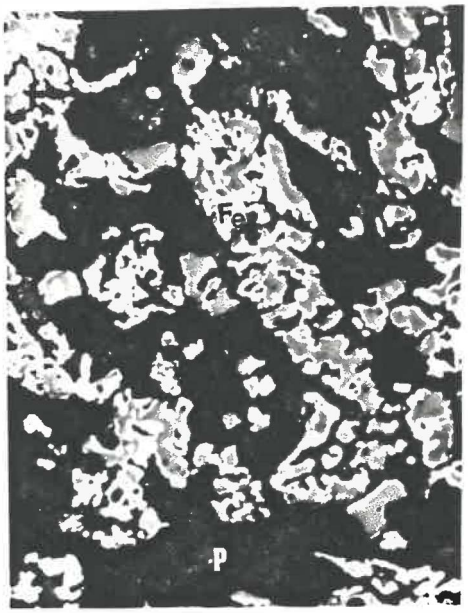


d) after 60 minutes.

FIGURE 59 - Typical photomicrographs of reduced pellets after 15, 30, 45 and 60 minutes of reduction (pellet type 3 DP).



a) after 15 minutes
W: wustite
G: glass



b) after 30 minutes.
Fe: metallic iron
P : pore

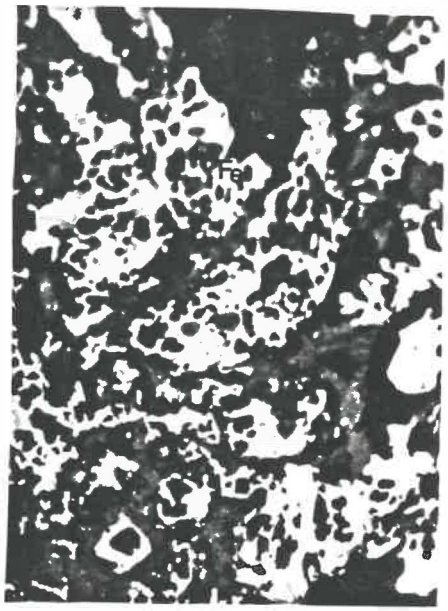


c) after 45 minutes

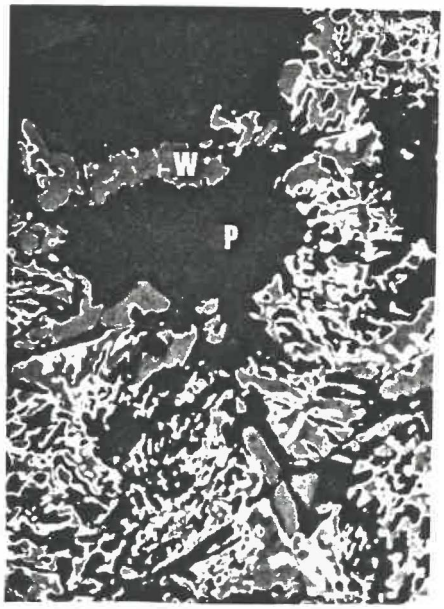
FIGURE 60 - Typical photomicrographs of reduced pellets after 15, 30, 45 and 60 minutes of reduction (pellet type 5 DP).



a) after 15 minutes
W: wustite
G: glass



b) after 30 minutes.
Fe: metallic iron
P : pore



c) after 45 minutes

FIGURE 61 - Typical photomicrographs of reduced pellets after 15, 30, 45 and 60 minutes of reduction (pellet type 6 DP).

wustite reduction in high basicity pellets was achieved due to formation of fine intragranular cracks. The reduction in the fine wustite fragment was completed faster and this was facilitated by the easier penetration of reducing gas. On the other hand as coarser fragments of wustite were formed in low basicity pellets, the reduction was slower; this has been noticed by the presence of large amount of unreacted wustite. From the above observations we conclude that apart from the initial porosity of the pellets, morphology of the pores in the reduction product may play a role in determining pellet reducibility.

From Figure 48 it is observed that the reducibility of the pellets decreases on further increase in basicity after achieving a maximum at 1.3 basicity. This decrease is attributed to the decrease in the porosity of these pellets. In Figure 62 the variation of reducibility as a function of porosity for the pellets of above 1.3 basicity is shown. The reducibility increases with increase in porosity. In pellets of 1.6 basicity the passage of reducing gas to the interior of pellet is restricted due to the decrease in porosity and the presence of intergranular slag, as a result, the reducibility is decreased. This is evident from the photomicrographs of the reduced pellet with dolomite and bentonite addition (see Figure 56). A difference in the degree of reduction at the periphery and centre of the pellet is noticed.

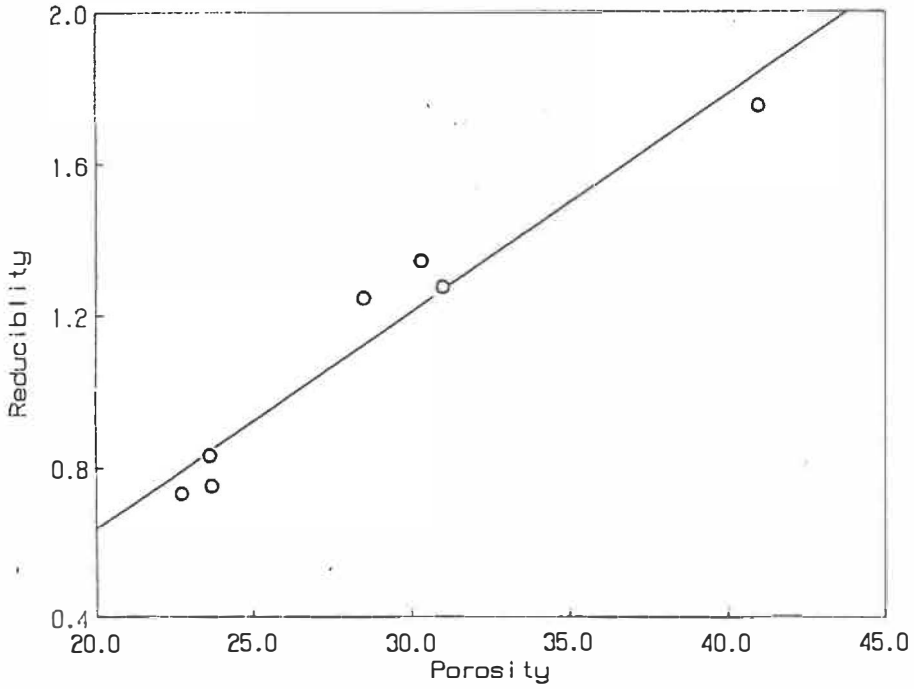


FIGURE 62 - Effect of porosity on the reducibility of the pellets above 1.3 basicity.

6.4 Swelling

The variation of swelling as a function of basicity and pellet type are given in Figure 63. It is observed that swelling is high for 0.2 and 0.8 basicity pellets, being maximum at 0.8 then decreasing at higher basicities. Addition of peat moss appears to be beneficial in decreasing swelling. Pellets with dolomite addition swell less than limestone added pellets.

Swelling is the result of structural change accompanied by the reduction of hematite to magnetite phase. Any measure which can withstand the effect of structural changes will minimise swelling. A strong bonding phase which is not affected by the reducing gas can decrease the effect of swelling. In pellets of 0.2 basicity the bonding phase

mainly consists of hematite bridges. As the bonding phase undergoes reduction the structure is severely affected and this results in high swelling. However, swelling of pellets at this basicity is slightly lower than pellets of 0.8 basicity. Lower swelling may be attributed to the presence of good amount of free silica in the pellet.

Maximum swelling was observed in the pellets of 0.8 basicity. The low basicity glass formed at this basicity appears to be brittle to withstand the stress due to transformation. The swelling decreases considerably at higher basicities. This shows that very strong bond is provided by the glass at high basicity.

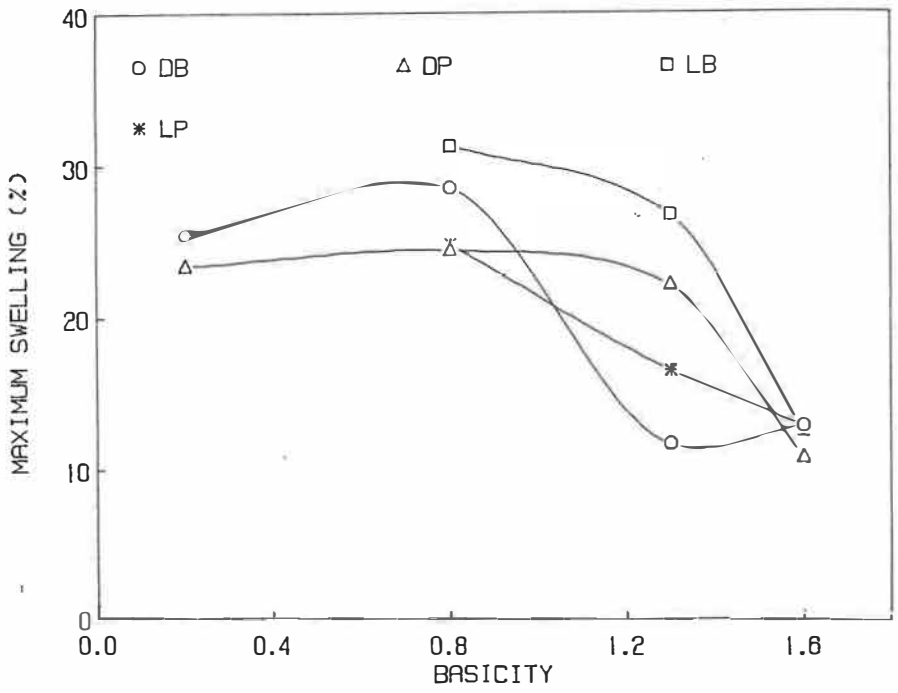


FIGURE 63 - Effect of basicity on swelling of the pellets.

The pellets with peat moss addition have lower swelling values than pellets with bentonite addition. The high porosity in the peat moss added pellets appear to have beneficial effect on swelling. It is believed that these pores minimise swelling by accommodating the stresses due to hematite reduction.

The addition of dolomite is found to be beneficial in minimising swelling particularly at basicities of 0.8 and 1.3 basicity. Zoned slag phase which was formed due to MgO addition is believed to be more effective in minimising swelling than the slag formed by addition of only CaO in the pellets fluxed with limestone.

CHAPTER 4

RESULTS: PILOT SCALE PELLETS

1. GREEN STAGE PROPERTIES

Green stage properties of the pellets such as green compression strength, dry compression strength, drop number and moisture content are shown in Table 28.

1.1 Green compression strength and drop number

From Table 28, it is seen that the pellets with peat moss addition possess green compression strength ranging between 1.3-1.5 kg/pellet and drop number of 4-5/pellet. These values are adequate as the minimum required compression strength and drop number are 1.1 kg/pellet and 4/pellet respectively [1]. However, compared to the pellets with bentonite addition, these pellets have inferior green stage properties. This is attributed to extent of bonding achieved in these pellets. Interstitial moisture is the major bonding phase in green pellets and major strength is contributed due to the capillary pressure of the moisture [10,11]. The moisture for bonding in peat moss added pellets is made available by changing the surface properties of peat moss fron hydrophobic to hydrophilic by small amount of NaOH addition. Since the degree of conversion of the peat moss surface to

hydrophilic was not fully achieved, this resulted in poorer bonding due to lesser availability of moisture.

TABLE 28 - Green pellet properties.

PELLET TYPE*	GREEN COMPRESSION STRENGTH kg/PELLET	DRY COMPRESSION STRENGTH kg/PELLET	NUMBER	MOISTURE CONTENT (%)
1 B	1.7	6.8	18	8.8
1 BP	1.5	5.7	3	9.0
1 P_2	1.4	3.0	4	9.5
2 B	1.8	6.3	15	8.8
2 BP	1.6	6.2	5	9.0
2 P_1	1.4	5.5	3	8.0
2 P_2	1.3	4.0	4	9.0
3 B	1.8	7.8	9	8.5
3 BP	1.3	4.5	3	8.5
3 P_2	1.5	3.6	4	9.5

* Pellet type designation has been described on page 38.

1.2 Dry compression strength

The pellets with peat moss addition have dry compression strength ranging between 3-4 kg/pellet. Since the desired dry compression strength in a pellet is 1.1 kg/pellet the strength can be considered to be adequate although pellets with bentonite addition have higher strength values. It is believed that bonding in the dried pel-

lets with peat moss addition is achieved through the recrystallisation of sodium hydroxide which formed a bridge between ore particles similar to the action of sodium montmorillonite in bentonite [27]. In case of bentonite added pellets, however, sodium is more uniformly dispersed in the pellet than the peat moss added pellets due to typical characteristics of sodium montmorillonite. This provides superior binding strength in the dried pellets,

2. CHEMICAL ANALYSIS OF FIRED PELLETS

The chemical analysis of the pellets is shown in Table 29. It is observed from chemical composition of the pellets that the pellets with peat moss addition have slightly higher iron content than the pellets with bentonite addition. The FeO content varied between 0.03-0.38%. The pellets contained 1.8-1.9% MgO. The pellets with peat moss addition have less amount of gangue than the pellets with bentonite addition.

3. PELLET MINERALOGY

The typical photomicrographs of the pellets are shown in Figures 64-72. The amounts of different mineralogical phases are given in Table 30 from image analyser measurement. The electron micrographs are shown in Figures 73-76 with microanalysis in Tables 31-34. The mineralogy of the pellets were identical to the mineralogy of the pellets made in the laboratory at the corresponding basicities with dolomite addition which has been discussed. Only the pellets earlier produced in the

pilot scale appeared more consolidated than the laboratory pellets. The major mineralogical phases observed were hematite, magnesioferrite and glass. The mineralogy of pellets with peat moss and bentonite addition were similar. The pellets with peat moss addition contained higher amount of pores.

TABLE 29 - Chemical composition of fired pellets.

PELLET TYPE	FeT (%)	FeO (%)	SiO_2 (%)	Al_2O_3 (%)	CaO (%)	MgO (%)
1 B	61.8	0.06	5.65	0.47	3.14	1.83
1 BP	62.8	0.15	5.05	0.38	2.70	1.91
1 P_2	62.6	0.15	5.05	0.34	2.70	1.91
2 B	61.0	0.06	5.65	0.37	4.30	1.76
2 BP	61.4	0.07	4.88	0.47	4.14	1.83
2 P_1	61.8	0.05	5.65	0.47	3.14	1.86
2 P_2	61.6	0.03	4.99	0.40	4.06	1.93
3 B	60.1	0.38	5.29	0.76	5.80	1.80
3 BP	60.6	0.18	4.67	0.72	5.70	1.90
3 P_2	60.7	0.05	5.20	0.72	5.30	1.90

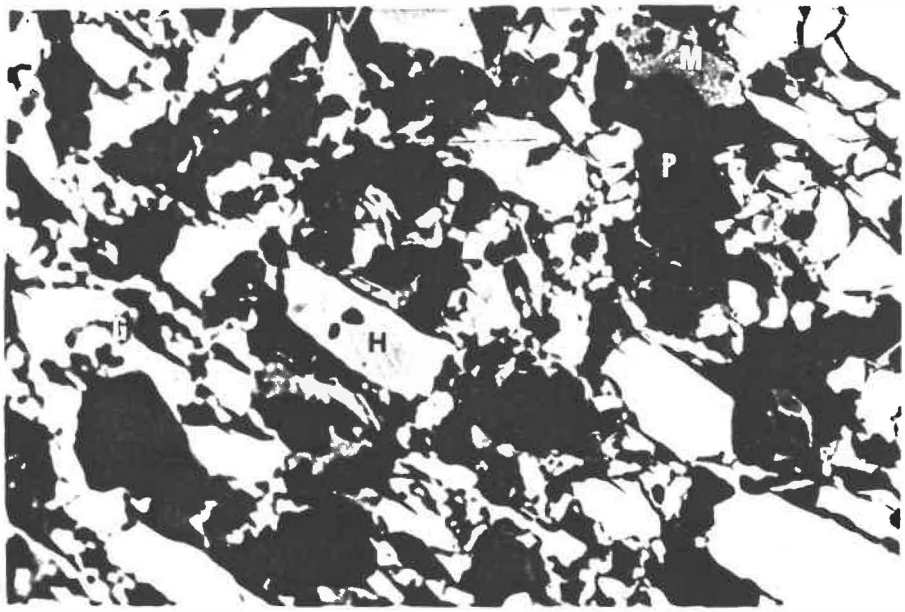


FIGURE 64 - Typical photomicrograph of the 1 B pellet.
(Basicity: 0.8, binder: bentonite).
H: hematite; M: magnesioferrite; G: glass;
S: Free silica; P: pore.

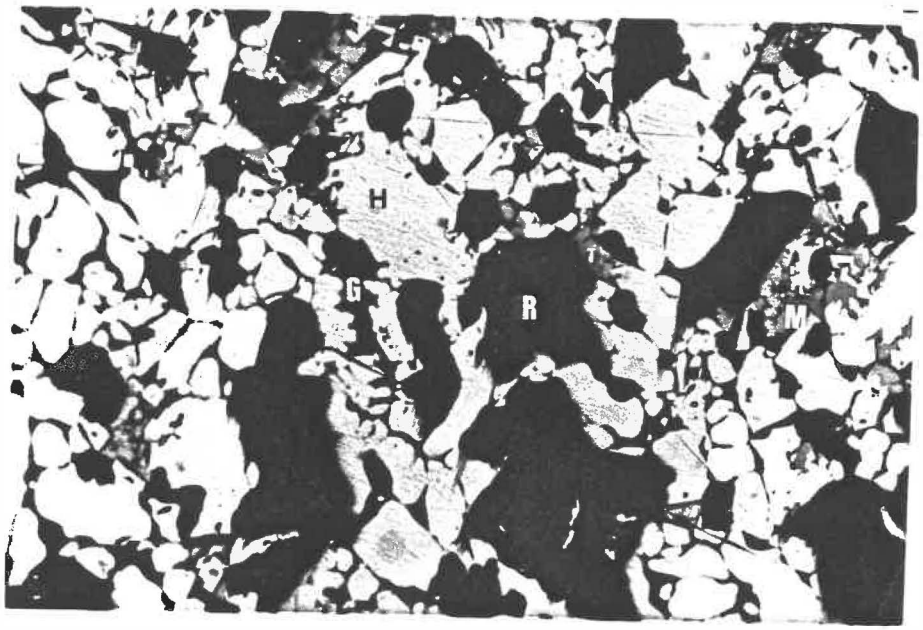


FIGURE 65 - Typical photomicrograph of the 1 BP pellet.
(Basicity: 0.8, binder: bentonite + peat moss).
H: hematite; M: magnesioferrite; G: glass;
S: Free silica; P: pore.

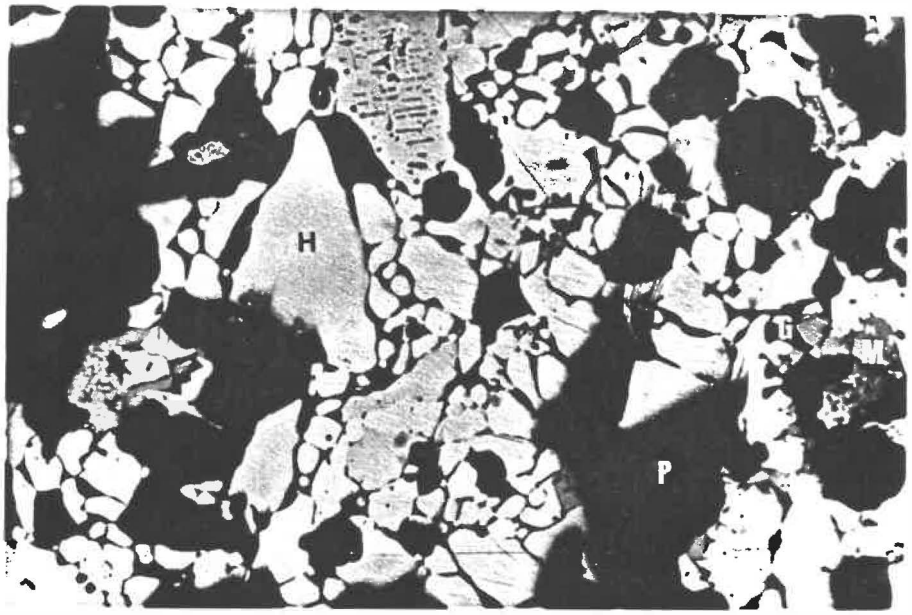


FIGURE 66 - Typical photomicrograph of the 1 P_2 pellet.
(Basicity: 0.8, binder: peat moss 3%).
H: hematite; M: magnesioferrite; G: glass;
S: Free silica; P: pore.

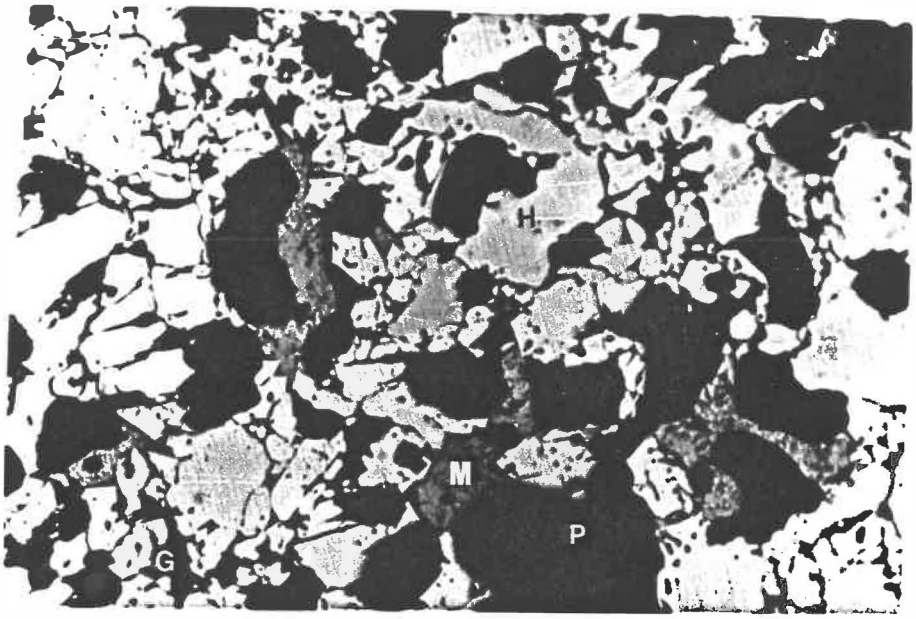


FIGURE 67 - Typical photomicrograph of the 2 B pellet.
(Basicity: 1.1, binder: bentonite).
H: hematite; M: magnesioferrite; G: glass;
S: Free silica; P: pore.

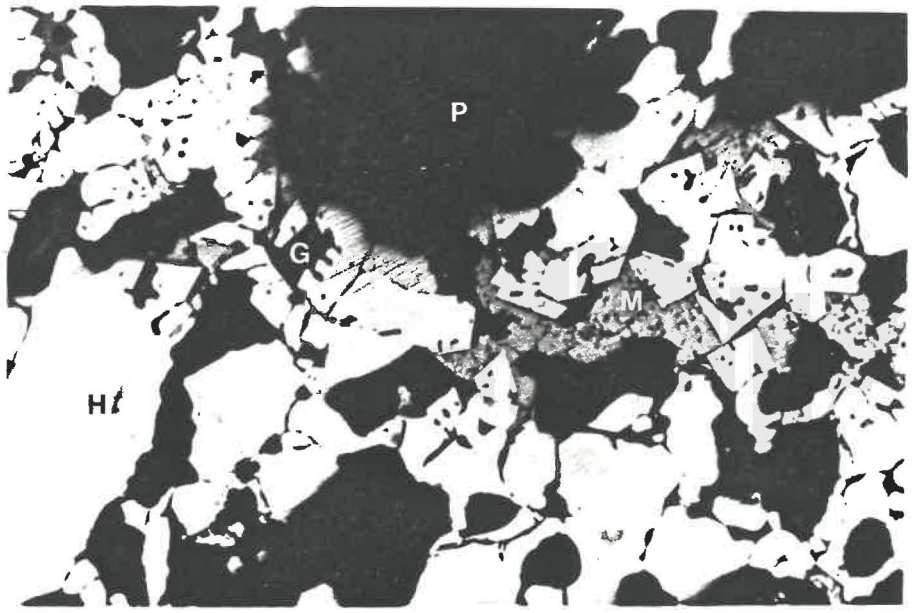


FIGURE 68 - Typical photomicrographs of the 2 BP pellet.
(Basicity: 1.1, binder: bentonite + peat moss).
H: hematite; M: magnesioferrite; G: glass;
S: Free silica; P: pore.

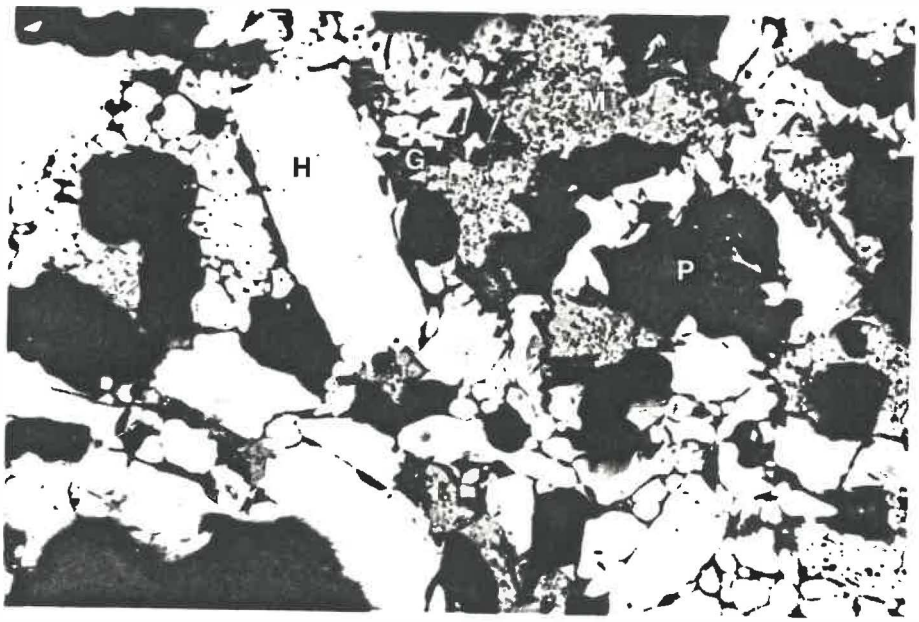


FIGURE 69 - Typical photomicrographs of the 2 P_1 pellet.
(Basicity: 1.1, binder: peat moss 1.5%).
H: hematite; M: magnesioferrite; G: glass;
S: Free silica; P: pore.

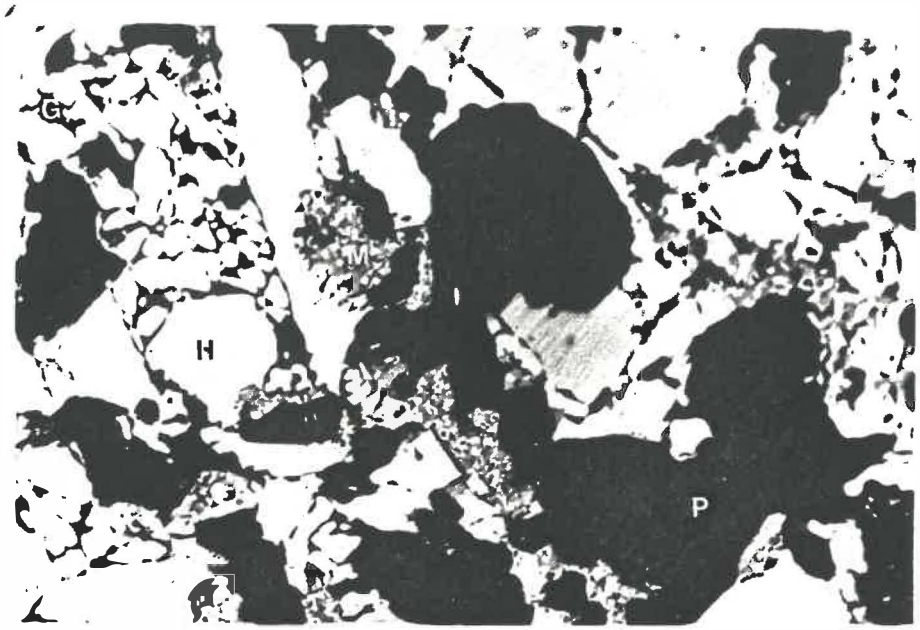


FIGURE 70 - Typical photomicrographs of the 2 P_2 pellet.
(Basicity: 1.1, binder: peat moss 3%).
H: hematite; M: magnesioferrite; G: glass;
S: Free silica; P: pore.

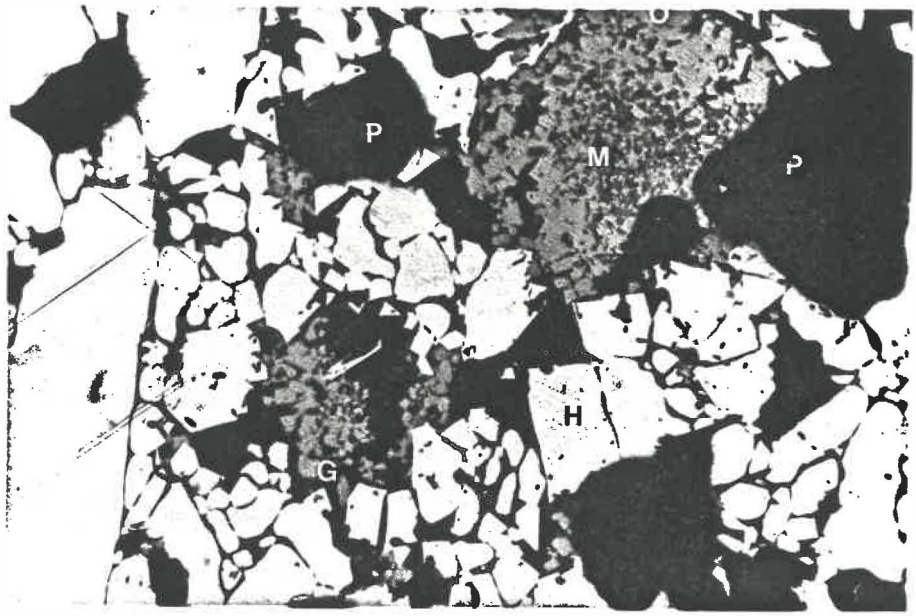


FIGURE 71 - Typical photomicrographs of the 3 B pellet.
(Basicity: 1.3, binder: bentonite).
H: hematite; M: magnesioferrite; G: glass;
S: Free silica; P: pore.

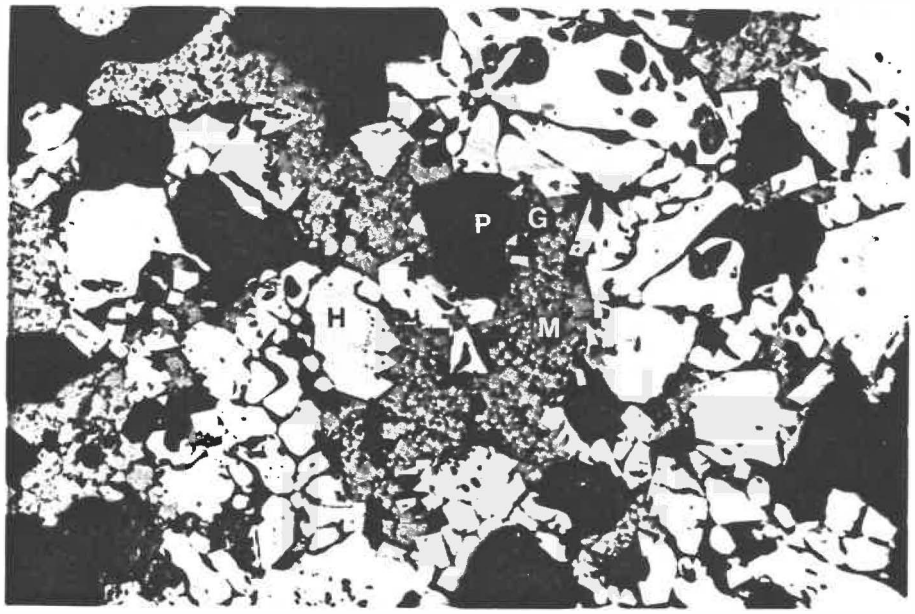


FIGURE 72 - Typical photomicrographs of the 3 P_2 pellet. (Basicity: 1.3, binder: peat moss 3%).

TABLE 30 - Percentage phase area of the mineralogical phases in pellets produced in pilot scale (measured by image analyser).

PELLET TYPE		SLAG	Ca FERRITE	MAGNETITE	HEMATITE
0.8 B	1 B	12.0	-	9.4	78.60
	1 P_2	11.20	-	7.30	81.50
1.1 B	2 B	13.0	-	12.1	74.9
	2 P_2	12.7	-	11.5	75.8
1.3 B	3 B	15.3	-	15.8	68.9
	3 P_2	13.5	-	15.0	71.5

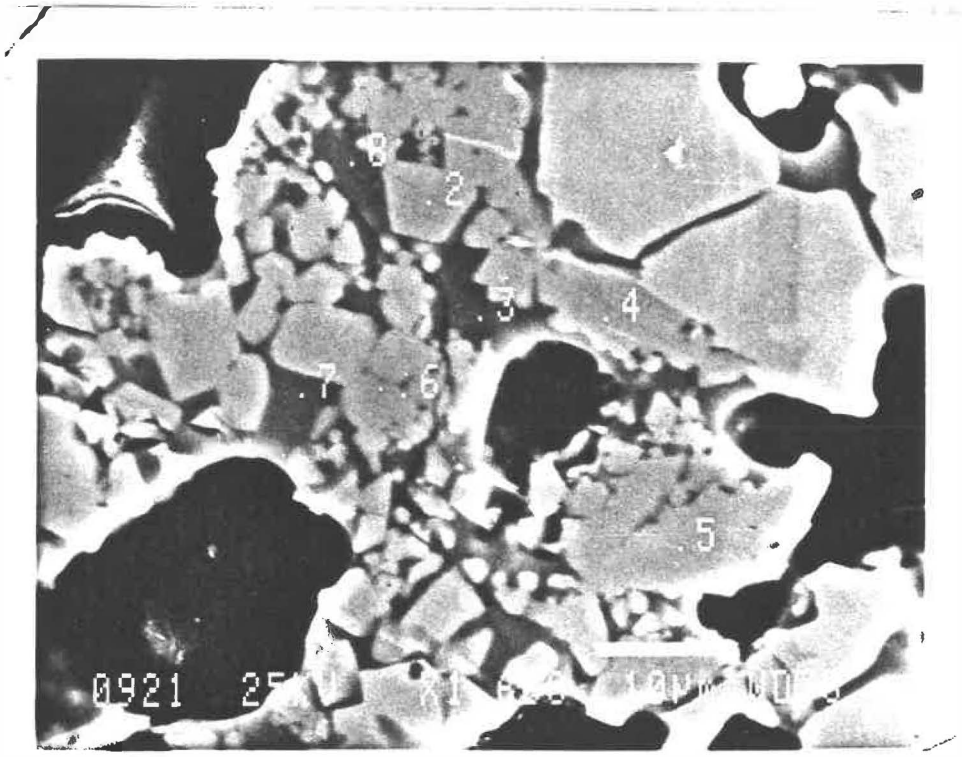


FIGURE 73 - Electron micrograph of 1 B pellet.

TABLE 31 - Microanalysis of mineralogical phases shown in Figure 73.

POINT	Fe_2O_3	SiO_2	CaO	MgO	Al_2O_3	PHASE
1	100.0	-	-	-	-	Hematite
2	94.4	0.6	0.4	4.6	-	Magnesioferrite
3	45.0	31.3	20.4	3.2	0.1	Glass
4	95.0	-	0.2	4.8	-	Magnesioferrite
5	94.5	0.5	0.4	4.7	-	Magnesioferrite
6	92.0	1.4	2.0	4.6	-	Magnesioferrite
7	49.0	27.9	19.8	2.8	0.5	Glass
8	59.4	23.0	15.3	2.3	-	Glass

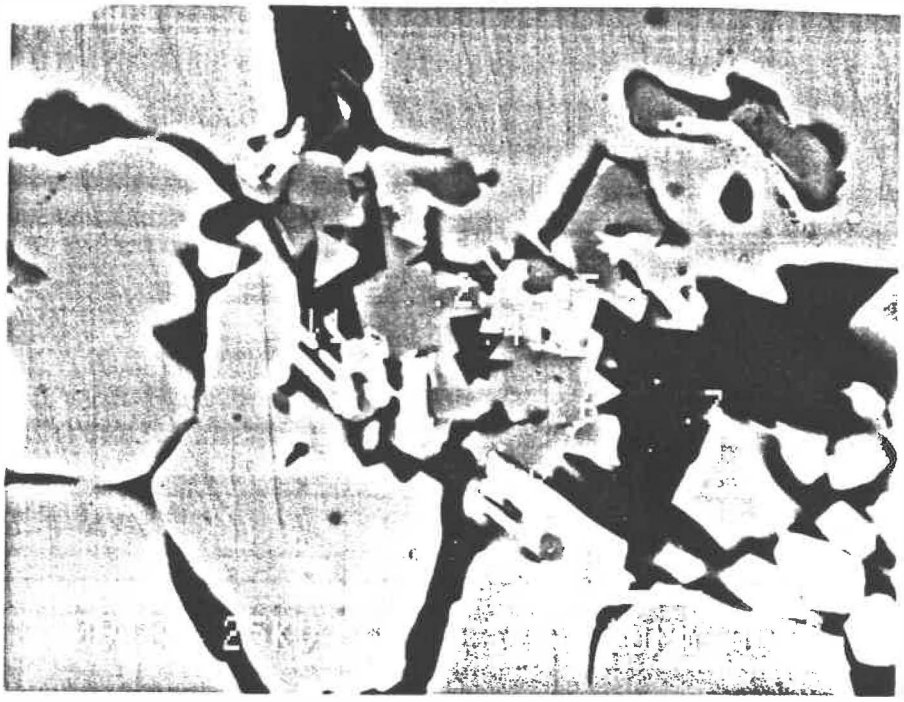


FIGURE 74 - Electron micrograph of 2 P_2 pellet.

TABLE 32 - Microanalysis of mineralogical phases shown in Figure 74.

POINT	Fe_2O_3	SiO_2	CaO	MgO	Al_2O_3	PHASE
2	91.3	0.2	1.6	6.6	0.4	Magnesioferrite
3	25.3	35.7	39.0	-	-	Glass
4	39.7	30.0	29.7	0.6	-	Glass
5	97.4	1.1	1.5	-	-	Hematite
6	91.0	0.1	2.6	6.0	0.3	Magnesioferrite
7	6.1	43.1	50.7	-	0.1	Glass

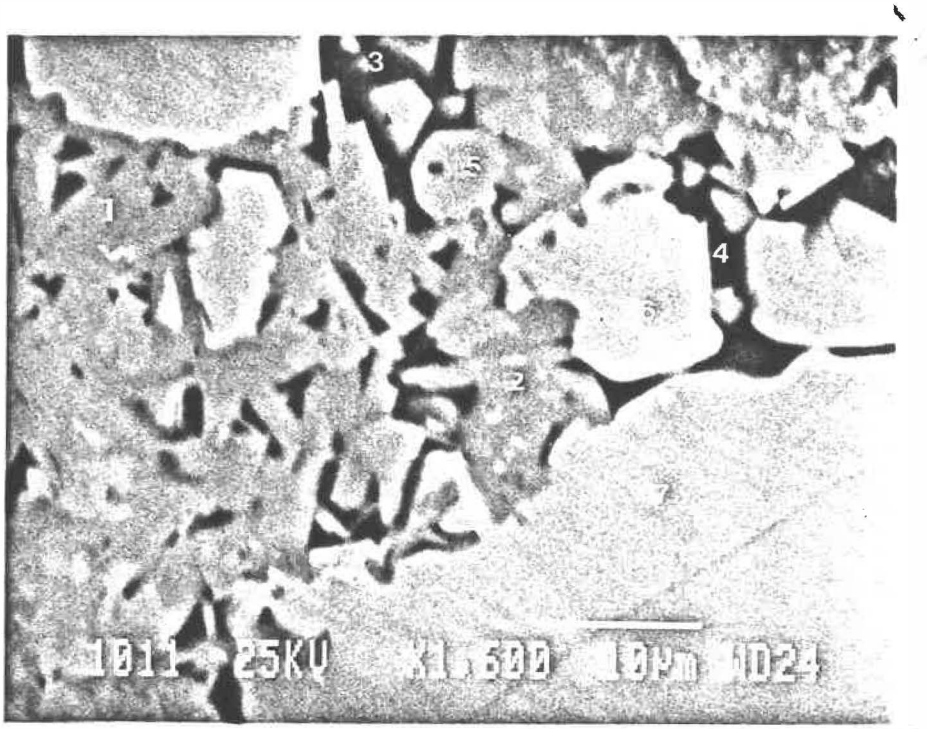


FIGURE 75 - Electron micrograph of 3 B pellet.

TABLE 33 - Microanalysis of mineralogical phases shown in Figure 75.

POINT	Fe_2O_3	SiO_2	CaO	MgO	Al_2O_3	PHASE
1	80.2	5.7	12.5	0.2	1.4	SFCA
2	80.6	5.4	12.9	0.5	0.6	SFCA
3	20.3	36.8	42.3	0.2	0.4	Glass
4	39.7	27.2	31.7	1.3	0.1	Glass
5	92.5	0.8	1.4	5.3	-	Magnesioferrite
6	99.3	-	0.7	-	-	Hematite
7	99.9	-	0.1	-	-	Hematite

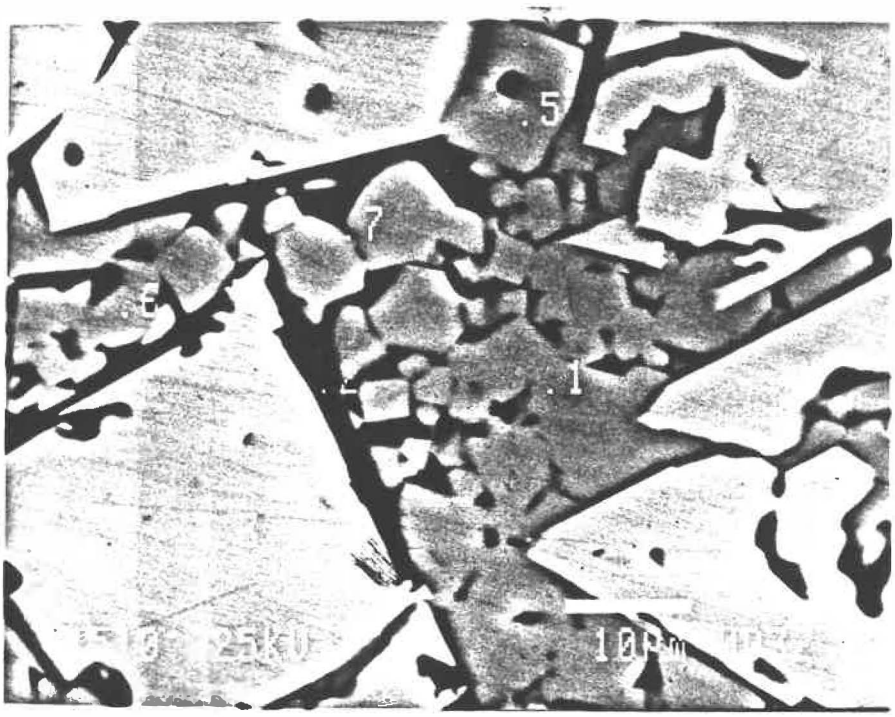


FIGURE 76 - Electron micrograph of 3 P_2 pellet.

TABLE 34 - Microanalysis of mineralogical phases shown in Figure 76.

POINT	Fe_2O_3	SiO_2	CaO	MgO	Al_2O_3	PHASE
1	95.3	-	0.9	3.8	-	Magnesioferrite
2	19.6	34.7	44.0	-	1.7	Glass
3	100.0	-	-	-	-	Hematite
4	100.0	-	-	-	-	Hematite
5	93.9	-	1.1	5.0	-	Magnesioferrite
6	91.9	0.5	1.9	5.7	-	Magnesioferrite
7	94.8	-	1.0	4.2	-	Magnesioferrite

The average chemical composition of the bonding slag phase magnesioferrite and crystalline phases are given in Tables 35, 36 and 37 respectively.

Presence of zoned glass phase was observed in the pellets similar to that observed in laboratory pellet which provided major bonding in the pellets. The proportion of pale gray phase which contained higher amount of Mg and Fe was found to decrease with increasing basicity. The amount of slag bonding was found to increase with increasing basicity due to higher amount of melt formation. This resulted in further consolidation of pellet structure as the basicity was increased from 0.8 to 1.3 which can be seen from the photomicrographs.

Presence of magnesioferrite similar to the type discussed earlier was observed. The MgO content was found to decrease with increasing basicity (see Table 36).

Hematite was the predominant phase in all the pellets. The presence of calcium ferrite was not observed until 1.3 basicity. The amount of calcium ferrite present at 1.3 basicity was very small. The chemical composition of the hematite and calcium ferrite are shown in Table 37.

TABLE 35 - Average composition of glass phase in pilot scale pellets (SEM-EDS).

BASICITY	PELLET DESIGNATION	GLASS PHASE	Fe_2O_3	SiO_2	CaO	MgO	Al_2O_3
0.8	1 B	Zoned { Pale gray	49.2	27.70	20.0	2.7	0.4
		Zoned { Dark	30.7	34.7	33.1	1.5	-
	1 P_2	Zoned { Pale gray	42.6	30.4	22.9	3.2	0.9
		Zoned { Dark	28.6	35.9	32.8	2.0	0.7
1.1	2 B	Zoned { Pale gray	40.2	26.1	30.8	1.1	1.8
		Zoned { Dark	20.6	41.5	37.9	-	-
	2 P_2	Zoned { Pale gray	36.5	31.3	29.7	1.3	1.2
		Zoned { Dark	19.6	42.3	37.9	0.2	-
1.3	3 B	Zoned { Pale gray	43.5	23.7	31.9	0.7	0.2
		Zoned { Dark	22.8	31.9	44.6	0.4	0.3
	3 P_2	Zoned { Pale gray	40.9	24.6	33.0	0.8	0.7
		Zoned { Dark	19.6	34.7	44.0	-	1.7

TABLE 36 - Average composition of magnesioferrite in pellets produced in the pilot scale.

BASICITY	PELLET DESIGNATION	Fe_2O_3	SiO_2	CaO	MgO	Al_2O_3
0.8	1 B	92.1	1.1	1.2	5.6	-
	1 P_2	90.6	1.7	1.4	6.3	-
1.1	2 P_2	92.8	0.40	0.3	6.2	0.3
1.3	3 B	91.4	3.1	0.8	4.6	0.1
	3 P_2	94.6	0.1	1.2	4.1	-

TABLE 37 - Average composition of hematite and calcium ferrite in pellets produced in pilot scale.

PHASE	MgO	SiO_2	CaO	MgO	Al_2O_3
Hematite	99.7	0.3	-	-	-
Calcium ferrite	80.8	5.7	12.6	0.4	0.5

4. POROSITY

The porosity values of the fired pellets are shown in Table 38. The value is based on the measurement of 50 randomly selected pellets of 12 ± mm diameter for each type of pellet.

The porosity of the pellets as a function of peat moss addition is shown in Figure 77. Addition of peat moss has resulted in increased porosity in the pellets as the porosity values of pellets with peat moss addition are 3-6% higher compared to pellets with bentonite addition. High amount of pores were created in the pellets due to combustion of peat moss during early period of induration. Amount of melt formed during the latter stage could not completely fill these extra pores thus leaving behind a porous structure [108]. The effect of peat moss addition in increasing the porosity is more pronounced at the basicities of 0.8 and 1.1 due to less amount of slag formation at these basicities. At 1.3 basicity the porosity of the pellet with peat moss addition decreased due to increased amount of melt formation.

TABLE 38 - Porosity of the fired pellets.

BASICITY	PELLET DESIGNATION	POROSITY (%)
0.8	1 B	28.9
	1 BP	30.5
	1 P_2	34.7
1.1	2 B	28.8
	2 BP	32.6
	2 P_1	32.25
	2 P_2	34.7
1.3	3 B	29.8
	3 BP	32.6
	3 P_2	32.7

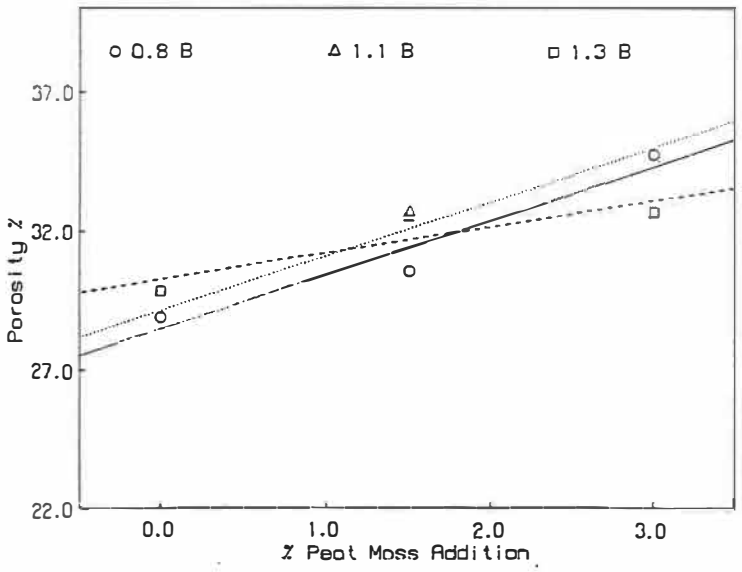


FIGURE 77 - Effect of peat moss on the porosity of the pellets.

5. COMPRESSION STRENGTH

Compression strength values of the fired pellets are given in Table 39. The effect of peat moss addition on compression strength as a function of basicity is shown in Figure 78. The pellets with peat moss addition possess adequate strength for use in the blast furnace as the compression strength of these pellets are above the acceptable strength level of 200 kg/pellet required by most industries [1]. However, these pellets are weaker than the pellets with bentonite addition. From Figure 78 it is seen that the strength of pellets with only peat moss addition increases with increase in basicity where as in case of pellets with only bentonite addition the maximum strength value is achieved at 1.1 basicity. In pellets with peat moss and bentonite addition the strength is seen to decrease with increasing basicity. In a pellet, development of compression strength is influenced by the interaction of several factors such as nature of binding phase, amount and nature of porosity, particle size and size distribution and additives etc. In the present set of pellets the porosity can be considered to be the major factor influencing the compression strength of the pellet by interacting with slag bond of the pellets. the slag phase is the major binding phase in these pellets as observed in the pellet microstructure (see Figures 64-72). As porosity decreases with increasing amount of slag phase formation the strength of the pellet improves considerably which is observed in pellets with peat moss addition. A linear correlation between porosity and compression strength is seen in Figure 79. With increasing porosity the compression strength is

found to decrease. We may, therefore, attribute the lower compression strength of peat moss added pellets to higher porosity.

TABLE 39 - Compression strength of the fired pellets.

BASICITY	PELLET DESIGNATION	COMPRESSION STRENGHT kg/PELLET
0.8	1 B	269
	1 BP	298
	1 P_2	214
1.1	2 B	338
	2 BP	274
	2 P_1	298
	2 P_2	232
1.3	3 B	304
	3 BP	254
	3 P_2	265

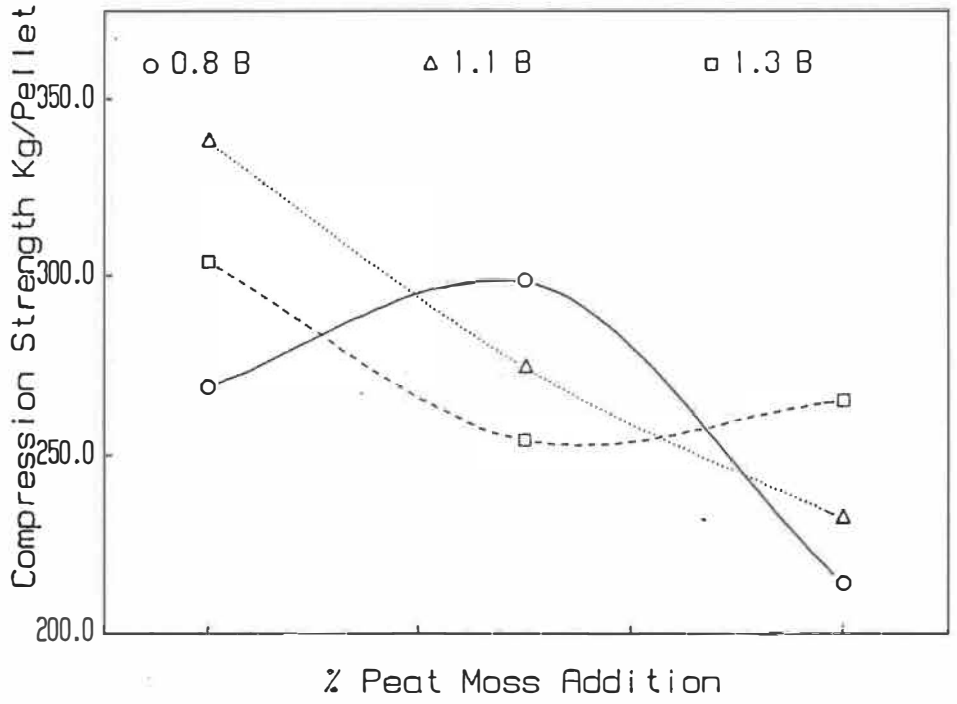


FIGURE 78 - Effect of peat moss and bentonite on the compression strength.

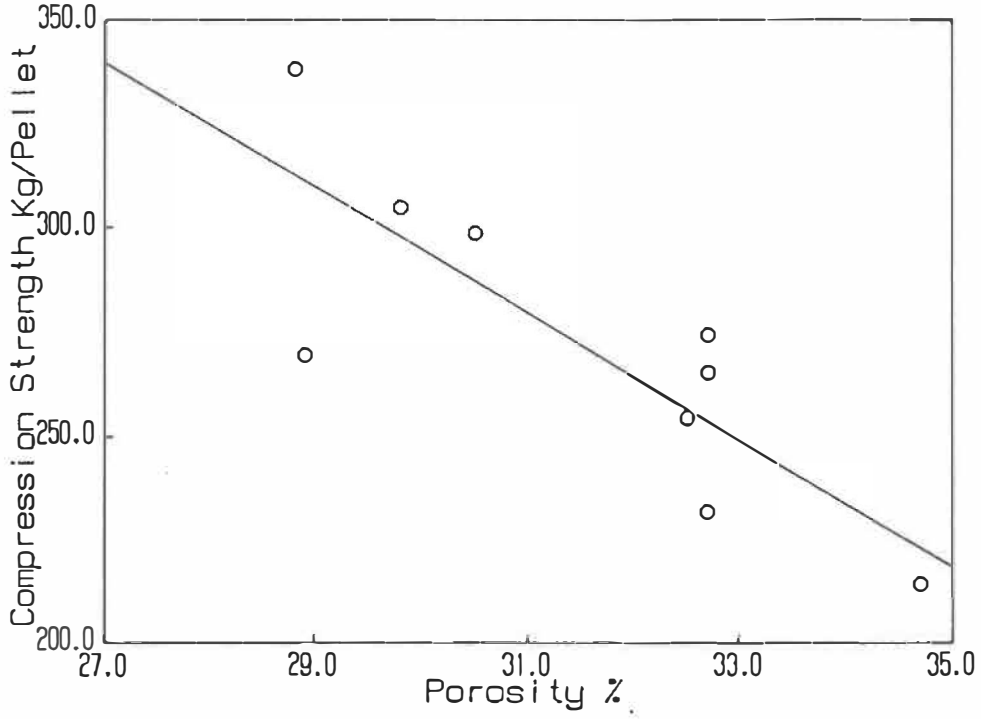


FIGURE 79 - Effect of porosity on the compression strength of the pellets.

6. TUMBLER STRENGTH

The tumbler strength "T" index of the pellets are shown in Table 40. It is observed that the tumbler strength of the pellets with peat moss addition is slightly below the industrially accepted value of 94% (1). Pellets with peat moss and bentonite addition have adequate tumbler strength. The tumbler strength is a measure of abrasion resistance of the pellets. The relationship between porosity and tumbler strength is shown in Figure 80. The tumbler strength decreases with increasing porosity. Therefore the poor abrasion resistance of the peat moss added pellets may be attributed to the high porosity of the pellets. Lower amount of peat moss addition results in high tumbler strength due to comparatively lower porosity. Increased amount of slag bonding might have some effect in improving the tumbler strength of the pellets.

7. LOW TEMPERATURE BREAK DOWN TEST (LTBF)

Low temperature break down test (LTBT) value is the measure of resistance to desintigration of the pellet after reduction at low temperature under reducing gas. The desintigration in the pellet is caused by hematite to magnetite transformation. The magnetite nuclei which nucleate at several points of the hematite grain on further growth impinge on one another and exert pressure on the hematite grain to disintigrate [114]. A strong binding phase which is not affected by the reduction atmosphere is capable of preventing disintigration.

TABLE 40 - Tumbler strength of the pellets.

BASICITY	PELLET DESIGNATION	TUMBLER STRENGTH T INDEX % + 6.3 mm
0.8	1 B	96.0
	1 BP	96.1
	1 P_2	93.0
1.1	2 B	96.9
	2 BP	95.2
	2 P_1	95.0
	2 P_2	92.6
1.3	3 B	96.5
	3 BP	94.3
	3 P_2	93.5

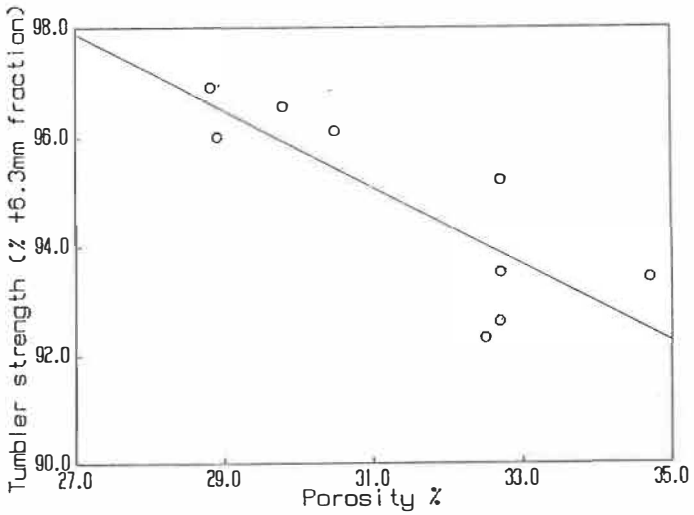


FIGURE 80 - Tumbler strength as a function of porosity.

The LTBT results are given in Table 41. The minimum acceptable values for the pellets to be used in blast furnace is 80% of + 6.3 mm fraction. All the pellets have higher LTBT values than the minimum acceptable except the pellet with bentonite addition at 1.1 basicity. Peat moss addition appears to be beneficial in improving LTBT values as the pellets with peat moss addition have higher LTBT values than bentonite added pellets. At 1.1 basicity the LTBT values of all types of pellets are low [the lowest value being that of the pellets with bentonite addition]. The LTBT value of bentonite added pellets at that basicity is 68%. This indicates that the bonding glass phase at this basicity is not capable of preventing disintigration of the pellets. Partial or full substitution of peat moss has improved the LTBT. It is believed that the cracks which occurred due to low temperature reduction were prevented from propagation by the pores resulting from peat moss addition. This improved the LTBT value of the peat moss added pellets at that basicity. At 1.3 basicity the LTBT values are high indicating the presence of a stable glass phase.

TABLE 41 - Low temperature breakdown test (LTBT) of the peat moss and bentonite added pellets.

BASICITY	PELLET DESIGNATION	L.T.B.T. % + 6.3 mm % + 6.3 mm
0.8	1 B	90.9
	1 BP	91.6
	1 P_2	94.5
1.1	2 B	68.8
	2 BP	92.0
	2 P_1	90.2
	2 P_2	86.2
1.3	3 B	94.5
	3 BP	94.4
	3 P_2	97.4

8. REDUCIBILITY

Reducibility $(dR/dt)_{40}$ values of the fired pellets are shown in Table 42. The variation of reducibility as a function of basicity index and type of binder is shown in Figure 81. For all types of pellets the reducibility is observed to increase with increase in basicity. In pellets with bentonite addition the increase in reducibility is marginal. In peat moss added pellets the increase is significantly noticeable. At higher basicities of 1.1 and 1.3 the difference between the reducibilities of peat moss and bentonite addition is very high.

The high reducibility of the pellets with peat moss addition is solely attributed to the high porosity of the pellets. As it was observed from the pellet microstructure (Figs. 70 & 72) the pellets with peat moss addition have high amount of large interconnected pores. These pores facilitate easier passage of reducing gas inside the pellet structure and enhance the rate of reduction of iron oxides. Due to the presence of pores the reduction mechanism changes to predominantly homogeneous. This is evident from the photomacrographs of the polished sections of the pellets with bentonite and peat moss addition of 1.1 basicity which were reduced up to 70% (see Fig. 82). It can be seen that more amount of metallic iron is present at the periphery than at the centre where more amount of wustite is present. This denotes topochemical mode of reaction. In pellets with peat moss addition the metallic iron is observed to be distributed in the pellet which suggests a homogeneous mode of reaction [111].

However, at lower basicity of 0.8, the high porosity does not appear to be beneficial in increasing reducibility. Low reducibility in the pellets with peat moss addition was reported. The cause of low reducibility at low basicity has been discussed in the earlier chapter and is mainly attributed to the morphology of pores in the wustite grains. This is further supported by the photomicrographs of the reduced pellets (see Figs. 83-85). It was observed that the pores formed in wustite grain of 0.8 basicity pellets are coarse and this resulted in low reducibility as unreacted wustite was seen to be pre-

sent. On the other hand fine pores were observed in the pellets of 1.1 and 1.3 basicity which enhanced wustite reduction rate.

Formation of some amount of fayalite due to the reaction of FeO with free silica might have contributed to the low reducibility of the pellets.

While increase in basicity improved the reducibility of the pellets, it is the high porosity of the pellets due to peat moss addition which is the single most important factor responsible for the high reducibility in these pellets.

TABLE 42 - Reducibility of fired pellets.

BASICITY	PELLET DESIGNATION	REDUCIBILITY $(dR/dt)_{40}$
0.8	1 B	1.01
	1 BP	0.75
	1 P_2	0.90
1.1	2 B	1.04
	2 BP	1.35
	2 P_1	1.30
	2 P_2	1.38
1.3	3 B	1.07
	3 BP	1.20
	3 P_2	1.22

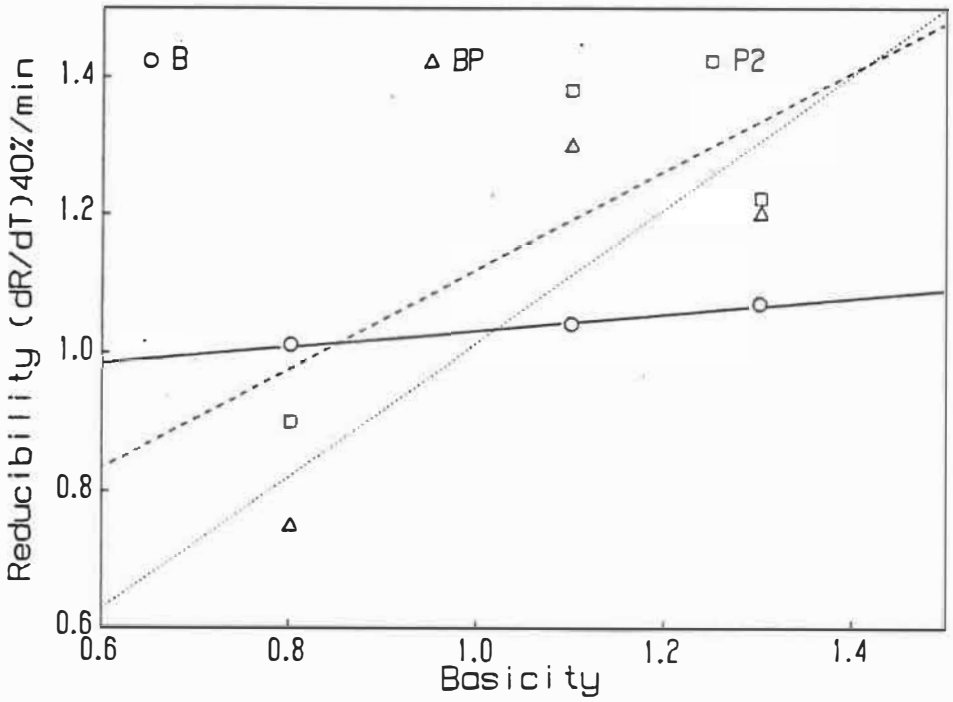
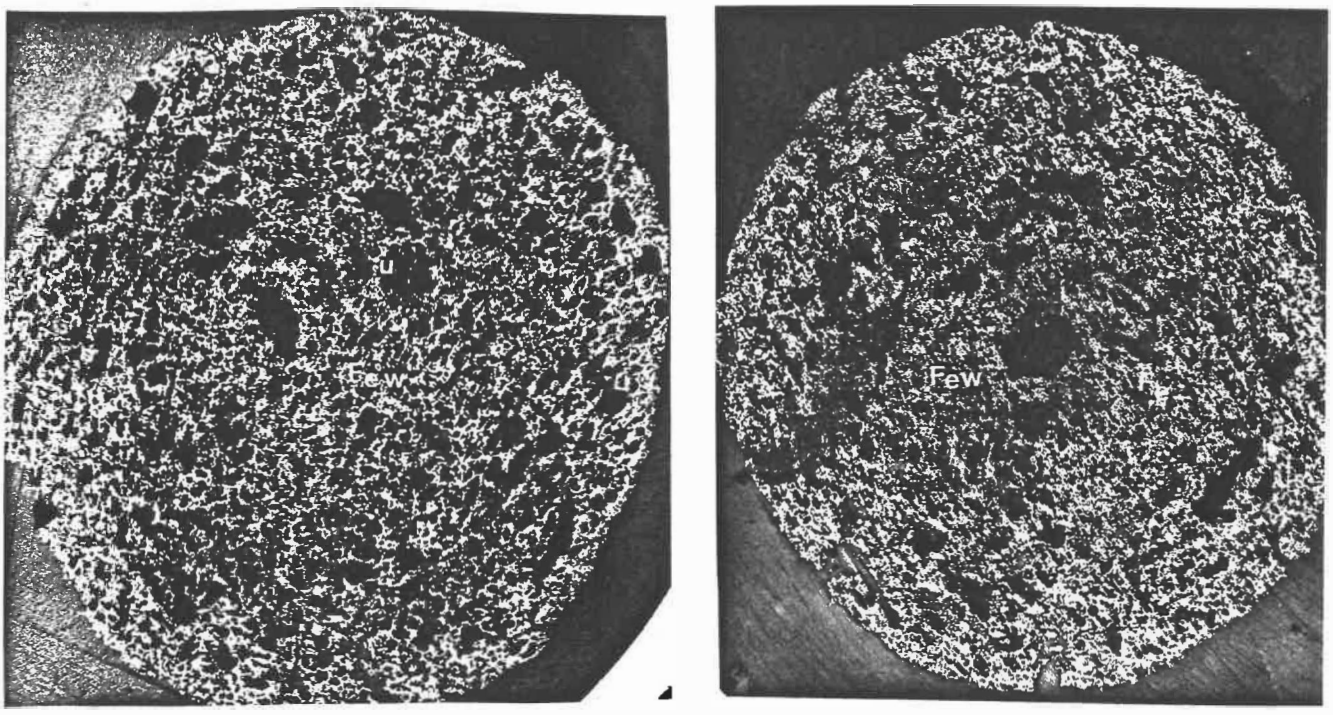


FIGURE 81 - Effect of basicity on the reducibility of the pellets.



a) x 7.5 b) x 7.5

FIGURE 82 - Polished sections of reduced bentonite - and peat moss-added pellets basicity of 1.1.
Fe : metallic iron
Few: wustite partly reduced to iron.

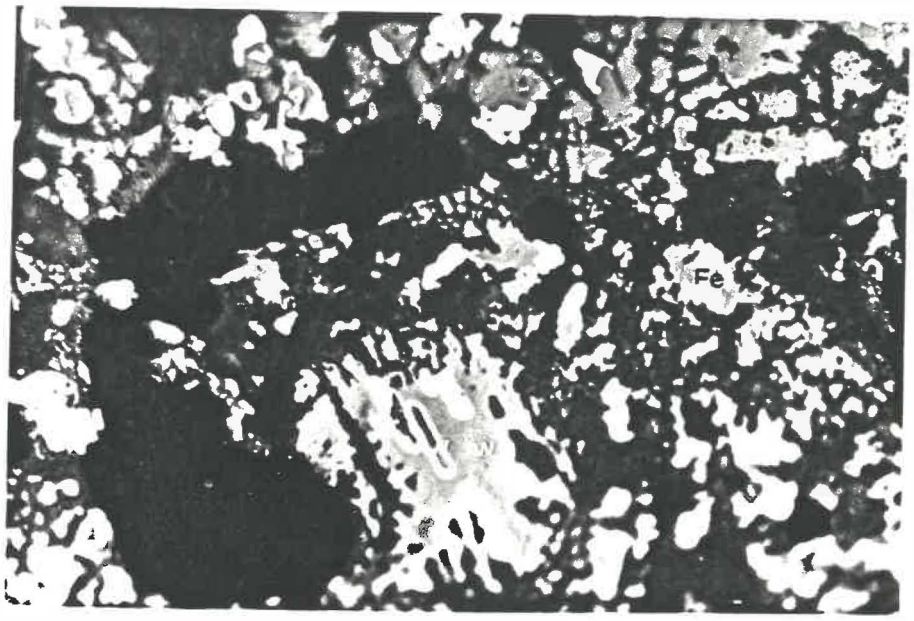


FIGURE 83 - Typical photomicrographs of reduced pellets (1 P_2).

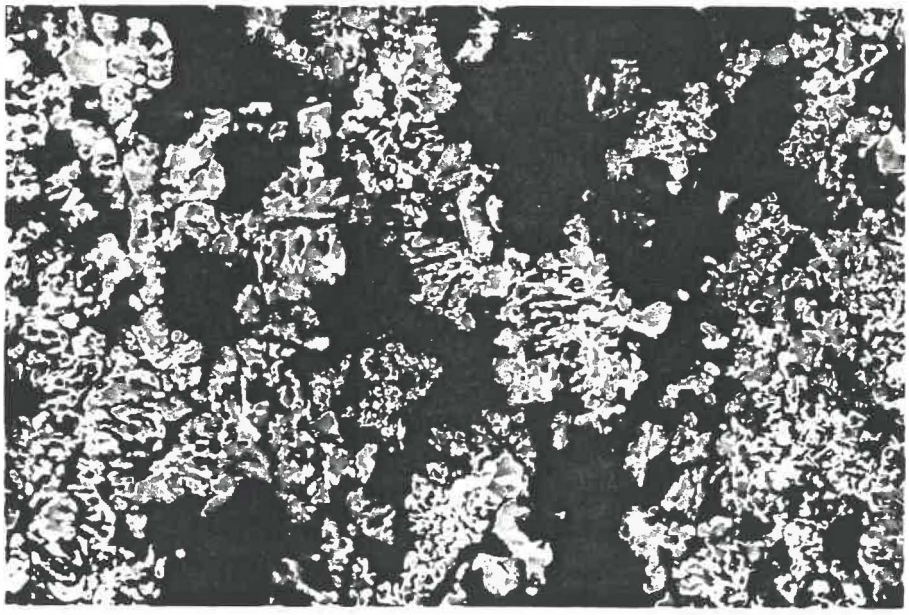


FIGURE 84 - Typical photomicrographs of reduced pellets (2 P_2).

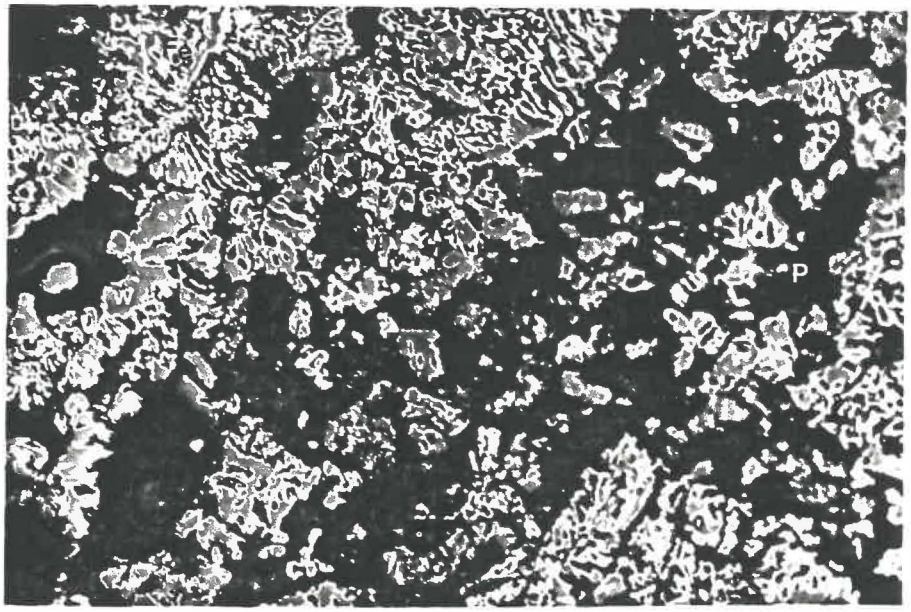


FIGURE 85 - Typical photomicrograph of reduced pellets (3 P_2).

9. SWELLING

Maximum swelling values obtained from the dilatometric method are presented in Table 43. Typical swelling curves for pellets with peat moss addition at different basicities are shown in Figure 86. The swelling starts at point A with commencement of reduction of iron oxide and reaches a maximum at point B after which a contraction is noticed. The extent of maximum swelling is observed to vary with basicity. Similar swelling curves for other types of pellets were also obtained.

The effect of basicity on the swelling behaviour of the pellets is shown in Figure 87. It is observed that the swelling is high at the 0.8 basicity and decreases with increasing basicity. The pellets with peat moss addition swell less than the pellets with bentonite addition.

High swelling in the pellets of 0.8 basicity may be attributed to the weak bonding phase formed at that basicity. The bonding phase at this basicity consists of low basicity glass which is believed to be brittle to resist the volume expansion due to hematite to magnetite transformation. The pellets were observed to have cracked after swelling. As the basicity of the pellets are increased to 1.1 and 1.3 the binding glass phase becomes stronger to resist swelling of the pellets.

Reducibility of the pellets may have influenced the swelling in the pellets. Swelling in pellets mainly occurs during hematite to magnetite reduction steps due to increase in volume. During subsequent reduction steps decrease in volume is reported. In pellets of high reducibility such as porous pellets of higher basicity all the reduc-

tion steps occur simultaneously which minimises swelling due to simultaneous occurrence of volume expansion and contraction [112]. On the other hand in the pellets of 0.8 basicity as the reducibility is low, the magnetite formation precedes subsequent reduction steps and swelling occurs before the counter balancing effect of subsequent reduction could be realised. Due to these above factors high swelling is observed in pellets of 0.8 basicity.

Peat moss addition is found to be beneficial in decreasing swelling of the pellets. High porosity due to peat moss addition is considered to be effective in minimising swelling. Apart from improving the reducibility of the pellets the porosity is believed to have accommodated the stress generated during reduction and decrease swelling.

TABLE 43 - Maximum swelling of fired pellets.

BASICITY	PELLET DESIGNATION	% MAXIMUM SWELLING
0.8	1 B	26.27
	1 BP	28.96
	1 P_2	25.86
1.1	2 B	20.94
	2 BP	15.00
	2 P_1	18.01
	2 P_2	18.02
1.3	3 B	12.41
	3 BP	11.35
	3 P_2	11.14

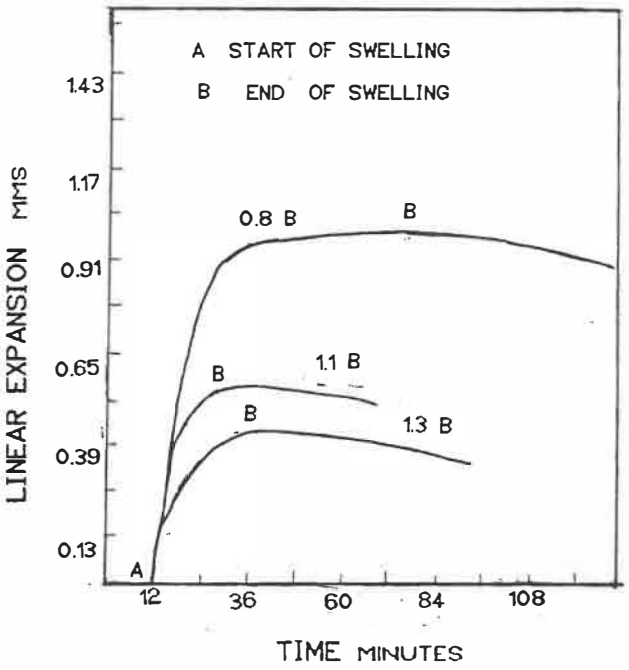


FIGURE 86 - Typical swelling curves of peatmoss added pellets at different basicities.

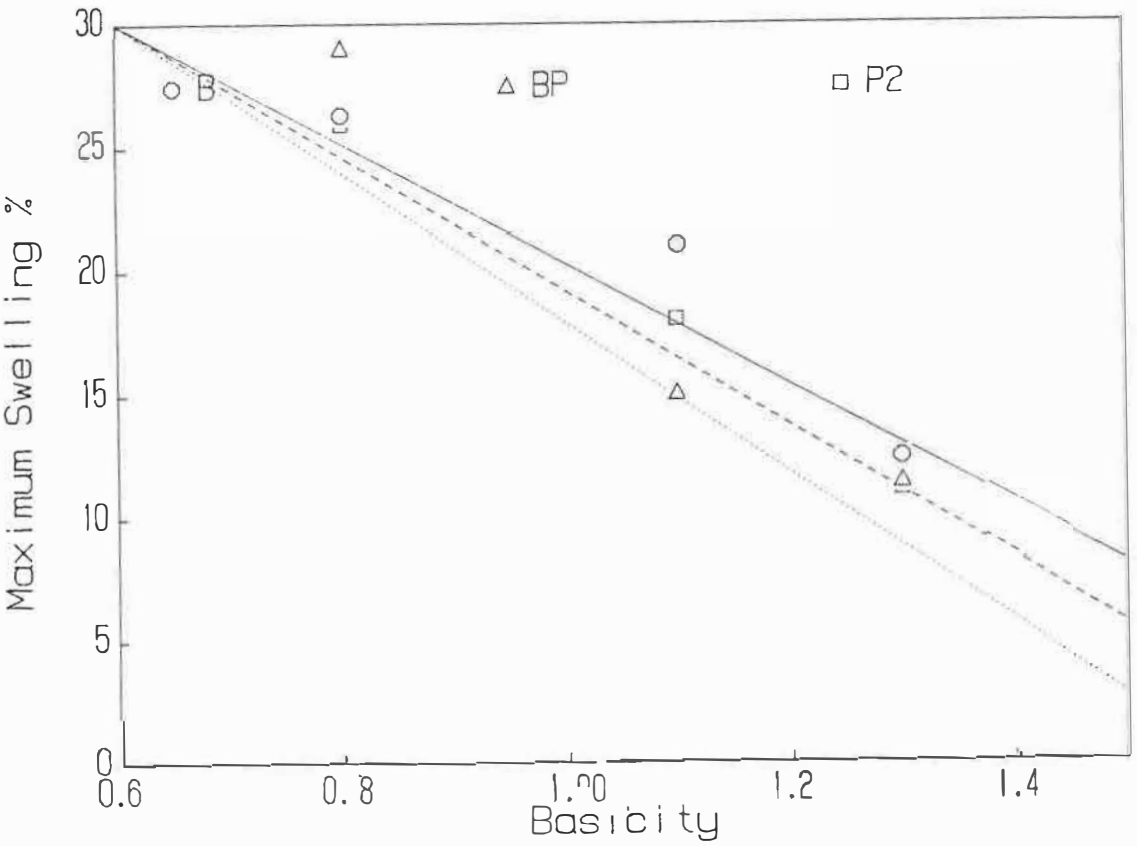


FIGURE 87 - Effect of basicity on the swelling of pellets.

CHAPTER 5

SYNTHESIS

1.1 PELLET MINERALOGY

From the mineralogical study it is observed that hematite is the predominating phase in all types of pellets. Presence of magnetite is not generally observed, although it is present in minor quantities in some types of pellets. In pellets fluxed with dolomite presence of magnesioferrite is observed which is deficient in MgO content.

The binding phase is observed to be glassy up to 1.6 basicity, the highest basicity for the present study. The type of flux is found to influence the nature of glass formation. With dolomite addition a zoned glass phase is observed in the pellet. With the increase in basicity the amount of zoned phase decreases.

The morphology of the pores is also observed to change with increasing basicity. The pores approached spherical shape and were smaller in number at 1.6 basicity. Compared to irregular pores observed at 0.2 basicity. The above observations confirm the findings of some of the previous investigators.

It was well established that various factors which affect pellet mineralogy are, additives such as binder, flux, carbonaceous materials and pellet induration cycle. The possible mineralogical

reactions which may take place during induration of the pellet have been summarised in Figure 88.

The three main phases in indurated pellets are: iron oxides, pores and slag. Since pellet firing takes place in an oxidizing atmosphere the final iron oxide phase is expected to be hematite. However, some amount of magnetite may be present depending on indurating temperature, additive, etc. Mainly three types of hematites are observed in the pellet microstructure namely primary, secondary and tertiary. The original hematite grains which do not undergo melting or chemical reaction during induration are known as primary hematite and those hematite grains which melt and recrystallise during induration are known as secondary hematite. Tertiary hematite grains are the results of reoxidation from the magnetite grains during cooling and are lamellar in nature. The magnetite observed in the pellet are secondary in nature as they are reduced from the original hematite grains.

The nature of iron oxide, slag and the configuration of pore are affected by the changes in basicity which is a function of flux addition.

An acid pellet, i.e. with no flux addition, normally consists of primary hematite, pores, a small amount of slag and unreacted gangue [5]. The pores are irregular in shape with some interconnections. Some amount of magnetite may be observed due to high firing temperature and low oxygen partial pressure during firing. Hematite does not react with

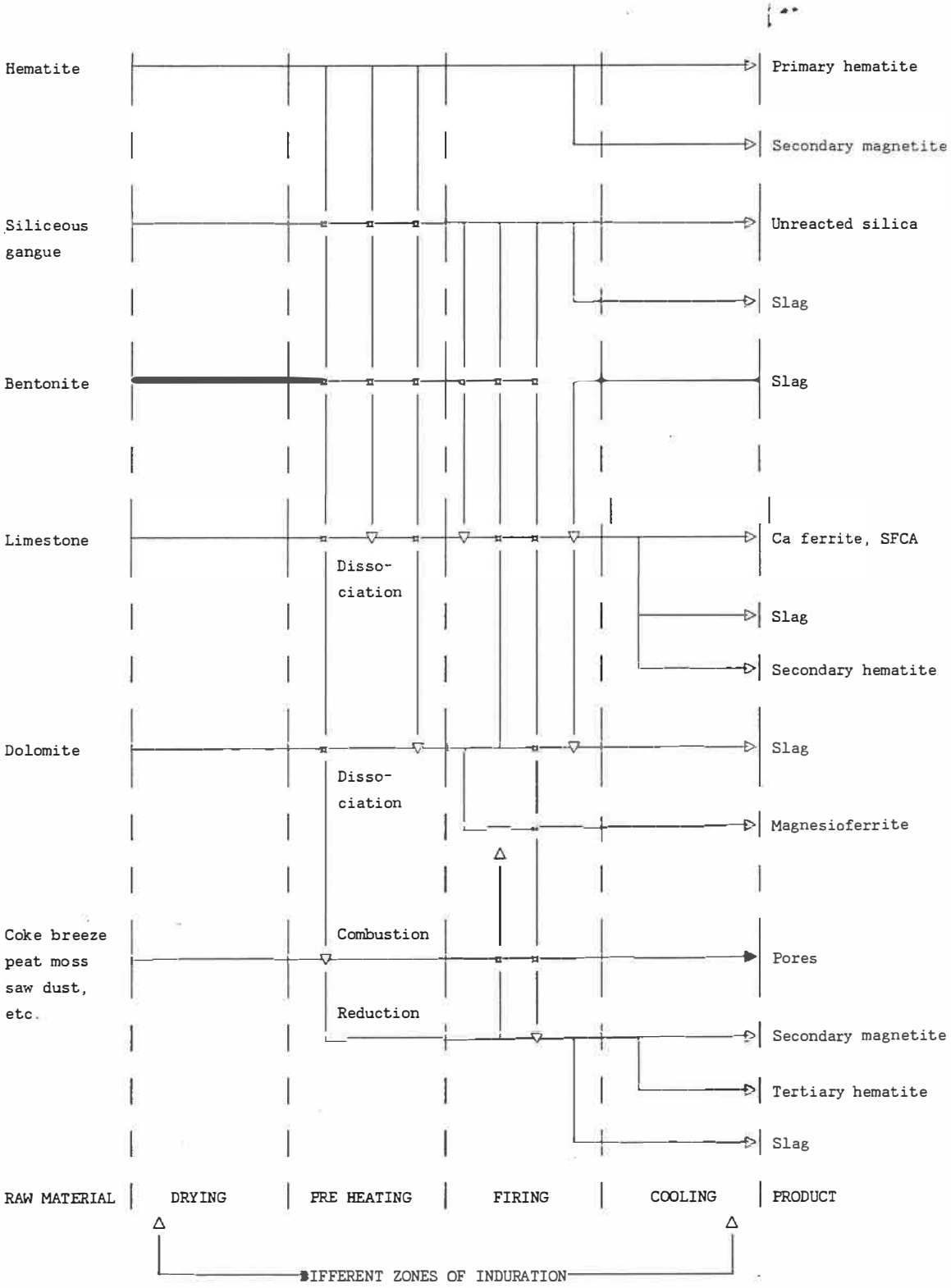


FIGURE 88 - Mineralogical reactions taking place during induration of pellet.

silica under normal indurating conditions [2, 32, 102]. However, the presence of iron silicate melt has been reported [29, 31, 48], due to reaction of ferrous oxide with silica at hematite dissociation temperature.

The formation of mineral phases in fluxed pellets begins during preheating period and continues up to cooling stage in the pellets. With CaO addition, formation of calcium ferrite takes place in the solid state in the temperature range of 800-1000°C [6, 31, 32, 34, 103, 104]. Negligible amount of calcium silicate formation takes place due to lack of direct contact between lime and silica [32]. Hamilton [6] has reported the formation of calcium silicates (gehlenite and anorthite) due to reaction of lime with meta kaolinite along with calcium ferrites at 800-1000°C in the Mount Tom Price ore pellets of Australia. These ferrites and silicates are replaced by complex silico ferrites of calcium and aluminium SFCA and pyroxene in the temperature range of 1000-1200°C [6].

With further increase in temperature the calcium ferrite begins to melt around 1200°C. The dissolution of silica takes place and the ferrite melt is replaced by a silicate melt with precipitation of iron oxide [32, 33, 102, 103, 104]. Hamilton [6] has observed the incongruent melting SFCA and pyroxene to magnetite and vitreous slag at about 1200°C and the magnetite reoxidation to hematite up to the temperature of 1350°C. The nature of melt is influenced by the amount of limestone addition, temperature and time of firing. With increase in limestone addition there is an increase in the quantity of the melt.

Dissolution of iron oxides in the melt takes place with increase in temperature.

As the pellet is cooled the solidification of slag takes place with the precipitation of iron oxide. The mineralogy of the pellet consists of primary and secondary hematite, and slag. Presence of calcium ferrite is observed in pellets above the CaO/SiO_2 ratio of 1.8 [45]. Hamilton [6] has reported these ferrites as silico ferrites of calcium and aluminium (SFCA). The nature of the slag phase is reported to be glassy at lower basicity and changes to be crystalline at higher basicities [38, 40, 42, 88]. The basicity at which the slag phase changes from glassy to crystalline is reported to be different by different investigators. While Thanning [42] has reported crystalline slag phase formation at the basicity of 0.8, Matsuno [32] has reported presence of glass phase up to 1.6 basicity. Nekrasov [38], Fraser [40] and Granse [105] have observed formation of glassy-slag phase up to 1.0 basicity. Nekrasov [38] has also observed the transformation of glassy to crystalline slag phase by changing the cooling rate. The crystalline slag phases observed were pseudo wollastonite (α-$CaSiO_3$), Wollastonite (β-$CaSiO_3$) and dicalcium silicate [40, 42].

A different mineral formation due to the presence of magnesium has been reported in dolomite fluxed pellets [2, 38, 41, 86]. A zoned silicate structure has been observed in dolomite fluxed pellets [38, 41] which has been termed as glass-ceramic structure by Nekrasov [38]. The zoned structure is formed from the common melt and the ceramic

phase contains higher iron and magnesium than the glass phase and is considered to be wollastonite [38].

Although formation of magnesioferrite in hematite concentrates is not considered favourable as it involves a change in crystal structure unlike in magnetite concentrates [73], presence of a solid solution of magnesioferrite and magnetite has been reported by Sasaki et al. [2] and Kong et al. [84]. The mechanism of formation of solid solution is related to magnetite formation. While Kong et al. [84] have suggested formation of metastable magnetite due to low oxygen potential, Sasaki et al. [2] have also suggested that MgO is responsible for dissociation of hematite to magnetite.

The morphology of pores changes with the change in basicity. In acid pellets the pores are irregular in shape and are interconnected. With increase in basicity the melt formation takes place which flows through the space between the particles and seals off the pores. Furthermore, as the melt causes shrinkage in the pellet structure the shape of the pores tend to become spherical. Thus increase in basicity results in fewer rounded pores.

The present study is in agreement with the previous findings [2, 32, 103] that hematite and quartz do not react with each other at 1300°C.

Our investigation has thrown new light on the mechanism of magnesioferrite formation in the pellets produced from hematite concentrate [113]. As discussed earlier, previous investigators [2, 84] have shown that magnesioferrite formation takes place through magnetite

formation. But how the magnetite was formed was not clear. Our thermal analysis study shows that magnetite was formed due to incongruent melting of calcium ferrite. This magnetite reacted with MgO to form magnesioferrite.

Our study has shown that as the calcium oxide content increases, less amount of iron dissolves in the glass phase.

The present study has also provided some information on the formation of silicoferrites of calcium and aluminium (SFCA). Presence of significant amount of SFCA was not observed in the pellets until 1.6 basicity. This shows that SFCA formation is a function of calcium oxide composition in the melt. With increasing basicity as the CaO content in the melt increases and less amount of iron oxide dissolves in the glass phase, more amount of SFCA forms. Decrease in the amount of SFCA in pellets with peat moss addition may be attributed to comparatively lower CaO content in these pellets.

1.2 Bonding mechanism of the pellets

In this work we have found that the bonding phases of both laboratory scale and pilot scale pellets, having similar pellet chemistry, are same. The chemical composition of the binding phases are identical. This shows that similar melts were formed during induration which was not influenced by firing cycle.

The basicity of the pellet and the nature of the flux are the two major factors which determine the nature of bonding phase in self fluxed pellets; they influence melt formation in the pellet during

induration. It was observed that with increase in basicity degree of consolidation of pellet structure and assimilation of gangue increased due to increased melt formation. Since presence of calcium oxide causes higher amount of melt formation, this is more pronounced in pellets with limestone addition than in pellets with dolomite addition. In dolomite fluxed pellets less amount of melt is formed as MgO raises the liquidus temperature of the melt. The iron oxide content in the silicate binder is found to decrease with increasing basicity as less amount of iron dissolves in the silicate with increasing calcium content. In dolomite fluxed pellets a zoned slag structure was observed due to the presence of MgO in the melt.

The type of binder has marginal effect on the nature and composition of slag bond. This shows that binders play a minor role in the localised melt formation process taking place throughout the pellet involving flux, gangue and ore particles. However, in pellets with peat moss addition, a large amount of pores are created due to combustion of peat moss at a temperature much below the formation of melt. As the amount of melt is not sufficient to fill the pores, a large number of pores are left behind. In comparison with bentonite added pellets this results in a different degree of pellet structure consolidation.

Based on the macro and microscopic observations described in chapters 3 and 4 the following overall bonding mechanisms are postulated.

Solid state bonding of the ultrafine and fine hematite particles takes place due to bridge formation and this was observed in

acid pellets (0.2 basicity). In the fluxed pellets calcium oxide dissociates from calcium carbonate around 800°C and reacts with ultrafine hematite particles to form calcium ferrites in solid state. With further increase in temperature the liquid phase appear in various localities of the pellet as calcium ferrites melt incongruently in the vicinity of 1200°C. A small amount of magnetite formation takes place. The melt begins to flow through the pore channels and comes in contact with silica and is assimilated by formation of a silicate melt in preference to ferrite melt. Other components of the gangue and flux such as Al_2O_3 and MgO also dissolve in the melt. The MgO in the melt reacts with magnetite thus forming magnesioferrite. Due to surface tension of the melt the ore particles are drawn together resulting in particle rearrangement and consolidation of pellet structure. In pellets having high porosity resulting from the combustion of carbonaceous materials the consolidation of pellet structure is achieved by high amount of melt formation. The melt also dissolves some fine hematite grains. The larger grains are attacked only at the surface. As a concentration gradient of the iron oxide exists in the melt, the iron oxide is transported in the liquid medium towards the larger grains and precipitates. This aids in agglomeration of hematite grains which is obsreved in pellets of 1.6 basicity.

During cooling of the pellets crystalline phases i.e., iron oxides, magnesioferrite, silicoferrites of calcium and aluminium precipitate out of the melt depending on pellet chemistry. The remainder

of the melt solidifies as silicate glass with heterogeneous chemical composition.

It is worthwhile to review the work of previous investigators on the bonding mechanism. Matsuno [32] observed formation of calcium ferrite at the temperature of 950-1000° due to reaction of caustic lime with hematite. The calcium ferrite melted at about 1200°C and reacted with quartz to form silicate. Bojarski et al. [34] also reported formation of calcium ferrites in the pellets below 1150°C which on increase in temperature disappeared with formation of calcium silicate. Similar observations have also been made by Kunii et al. [103], Nequist [104], Fitton and Goldring [33]. The present study is in agreement with the above observations.

1.3 Effect of peat moss on green stage properties

It was seen from the evaluation of green stage properties of the pilot scale pellets that adequate green strength can be obtained in the pellets by using peat moss as binder although these pellets are weaker than the pellets produced with bentonite addition. By comparing the present results with the results of a previous investigation in which peat moss was used as a binder for production of acid pellets [14] it is seen that the green stage properties are similar.

During pelletisation it was observed that the pellets with peat moss addition, fell into a narrower size distribution than bentonite added pellets. This is attributed to the better moisture retention capacity of the peat moss. It can be seen from the Table 28 that peat

moss added pellets have slightly higher moisture content. As the surface of peat moss is generally hydrophobic and is changed to hydrophilic by NaOH addition, most of the moisture is retained in the peat moss structure and less amount of it is available on the surface for pelletisation. This controls the growth of the pellets. Moisture retention capacity is considered to be an important property of the binder as it controls the pellet growth. Bentonite is considered to be a good binder due to its good moisture retention ability in its typical layer structure [54, 63].

This study has demonstrated that peat moss fulfills the criteria of a good binder. However, the binder properties of peat moss could be improved by improving its surface properties with optimisation of NaOH addition and particle size of peat moss. It is believed that with finer grinding more surface area will be available for NaOH treatment.

1.4 Effect of peat moss on fired pellet properties

The pellets produced in the laboratory scale possessed high porosity and compression strength which is below the acceptable level. Since these pellets were not compacted to a similar extent as would be expected in a much larger disc in a pelletising industry or pilot plant, it was not possible to obtain pellets of acceptable green stage properties. As the defects introduced during green stage were not rectified to the full extent during subsequent induration step, the fired pellets were weak and highly porous. On the other hand the results obtained from the pilot scale pellets has shown that both good green

and fired strength could be obtained in the pellet produced from a similar pellet mix.

However, from the analysis of the results of the properties of the laboratory scale pellets, it is seen that the pellet properties correlate well with the pellet chemistry, and microstructure. Therefore the present investigation on the laboratory scale pellets have provided informations on the influence of basicity, flux and binder on the pellet properties apart from the information obtained on bonding mechanism which was the primary objective of this work.

Porosity of the pellets was found to be a function of binder addition and amount of melt formation. The present study has demonstrated that the high porosity in the pellets is achieved by peat moss addition which created additional pores by burning off during induration. Dolomite addition was found to be more effective in increasing porosity than limestone. As amount of melt during induration increased with increasing flux addition at higher basicities, the porosity of the pellets decreased.

The compression strength of the pellet is influenced by several factors such as particle size, induration time and temperature, amount and distribution of the slag bond and porosity. In the pellets under study porosity appears to have major influence on the compression strength. Pores in the pellets weaken the pellet structure and the pellets have low compression strength.As the amount of pores decreases, the pellet compression strength increases. Our observation on the negative effect of porosity is in agreement with the observations made by

Elmquist [91] and Wright [106]. Therefore, lower compression strength of the peat moss added pellets can be attributed to higher porosity.

The beneficial effect of peat moss addition on the reducibility of the pellets is established from this study. High reducibility in the pellet was achieved due to high porosity. However, the high porosity is seen to be more effective in increasing reducibility at higher basicities (1.3 and 1.6). The formation of fine intragranular pores in the wustite grains were found to be the cause of high reducibility in these pellets. The pores were the sites of iron nucleation. As penetration of reducing gas was made easier through the pores, the rate of wustite reduction was faster. Although the formation of fine pores was noticed in pellets with peat moss addition after initial 15 minutes of reduction, this phenomenon also occurs in other types of pellets which is evident from the morphology of reduced iron in those pellets. Similar reducibility behaviour has also been observed in low silica pellets [110]. However, in some pellet types with low porosity presence of porous wustite was seen at the periphery whereas dense wustite was obsreved at the centre of the pellet (see Figure 56). This shows that the composition of the reducing gas may have some influence on the formation of the pores. In these pellets high concentration of the reducing gas was maintained at the periphery which resulted in fine pore formation.Due to low porosity, the passage of the gas to the interior was affected and the concentration of the reducing gas was low. On the other hand in pellets with high porosity, concentration of reducing gas was the same in all locations facilitating fine pore formation. Low

reducibility in pellets of low basicity was reported earlier by Nekrasov [38] et al., Fraser [40] and Kortmann and Burghardt [74]. They have attributed the low reducibility to formation of calcium olivine due to the reaction of wustite with the slag. They asserted that the olivine blocked the passage of reducing gas and decreased the rate of reduction. Nekrasov [38] has also reported the increase in the iron content in the slag phase of the reduced pellet. From our investigation no significant increase in the iron content of the slag phase in the reduced pellets was observed. Moreover, in the highly porous pellet under discussion the olivine formation will not have major influence on the pellet reducibility. It is our contention that low reducibility in these pellets is caused by the morphology of pore formation in the wustite grain which slows down the wustite to iron reduction. The pore morphology is influenced by several factors such as pellet basicity, porosity, etc. Our observation is in agreement with that of St-John and Hayes [107] who have noted that morphology of porous wustite and iron formation is dependent on chemical potential of the reducing gas, temperature, etc.

High reducibility in the fluxed pellets has been attributed to the presence of calcium ferrite in the pellet by Chang and Malcolm [4] and Onoda et al. [109]. Our study does not find any correlation between the presence of calcium ferrites and reducibility. It is seen that in the pellets of high reducibility a negligible quantity of calcium ferrite is present. On the other hand, good amount of calcium ferrite is present in limestone fluxed pellets at 1.6 basicity, but the reducibil-

ity is low. Our study shows that at the basicities higher than 0.8 it is the porosity of the pellets which has greater influence on the pellet reducibility than the mineralogical phases of the pellets.

Our studies have shown that peat moss addition has a beneficial effect on the swelling by increasing porosity in the pellets. It is also observed that pellets undergo high swelling in the basicity range of 0.2 to 0.8. this phenomenon has also been reported by previous investigators [40, 74, 105]. However, no satisfactory explanation has been provided by them for the high swelling at these basicity range. Kortmann [74] has attributed the high swelling to the olivine formation which destroys iron oxide bridges by dissolving them and penetrating into the weaker zones of iron oxide particles. On the other hand Fraser et al. [40] have suggested that olivine formation has the opposite effect as it provides stable bonding phase. Granse [105] and Fraser et al. [40] have suggested non topochemical mode of reduction to be the cause of high swelling which is contrary to our findings. Our observation is that the low basicity glass formed in the basicity range under consideration is too fragile to withstand structural transformation. This results in high swelling in the pellets. Our finding that non topochemical reduction of iron oxide is accompanied by low swelling is in agreement with the observations made by Panigrahy et al. [14] and Jallouli and Ajersch [112].

Although the properties of the laboratory scale and pilot scale pellets made out of the same pellet mix are not of the similar magnitude, it is seen that the factors which influence the pellet

properties are same in both cases. Our study demonstrates that superior metallurgical properties in the pellets are obtained by addition of peat moss which is attributed to the increase in the porosity of the pellets.

2. CONCLUSIONS AND RECOMMENDATIONS

The present work was undertaken with the following objectives:

1. To study the effect of type of binder and flux on the mineralogy and bonding mechanism of self fluxed pellets and,
2. To evaluate peat moss as a binder for the production of fluxed pellets.

The above objectives were achieved. We have shown that,

1. The bonding phases in self fluxed pellets produced from specular hematite consist of two silicate phases;
   a) a zoned glass phase consisting of magnesian ferrogeneous phase and a phase with no Mg and low Fe;
   b) a single glass phase containing iron, silicon, calcium and aluminium.
2. Formation of bonding phases are influenced by type of flux. A zoned silicate phase is formed due to dolomite addition. The amount of magnesian ferrugeneous phase decreases with increasing basicity.

3. Peat moss or bentonite have marginal effect on the pellet bonding mechanism.
4. The silicate phase contains high amount of iron at low basicity, with increasing basicity solubility of Fe in the glass decreases with increasing Ca content.
5. Magnesioferrite which is highly deficient in Mg is formed in pellets with dolomite addition.
6. Although presence of calcium ferrites is noticed at the basicity of 0.8 no appreciable formation takes place until the basicity of 1.6. Appreciable amounts of Ca ferrites are formed only in pellets with limestone and bentonite.
7. Melt formation during pellet induration through the addition of fluxed has a great influence on the metallurgical properties of pellets. With increased basicity up to 1.6 while there is an improvement in terms of pellet strength and swelling characteristics, well balanced metallurgical properties are obtained at the basicity of 1.3.
8. Dolomite addition is necessary to maintain a balance between various pellet properties.
9. Low reducibility in pellets of 0.8 basicity is attributed to the morphology of pore formation in wustite grains.
10. Peat moss can be successfully used as a binder for producing self fluxed pellets since it has favourable properties as a binder. With its lower cost peat moss may be regarded as a very interesting substitute for bentonite during green balling.

11. Peat moss added pellets have adequate strength properties for processing in the blast furnace.
12. Excellent metallurgical properties such as high reducibility, low swelling and good LTBT value in the pellet are obtained due to peat moss addition. This is mainly attributable to increased porosity provided by the combustion of peat moss during induration of the pellets.

2.1 Recommendations

From the present study it has been established that addition of peat moss to the pellet results in remarkable improvement in the reduction properties while retaining adequate mechanical strength in fired pellets. Moreover, adequate green stage properties can be obtained by using peat moss as binder although there pellets are inferior to green pellets with bentonite addition. However, the major advantage of peat moss addition is the superior reduction properties which will improve the performance of pellets in the blast furnace. Therefore the use of peat moss as a binder for production of self fluxed pellets is recommended.

An addition of 3% peat moss in the pellets is recommended which will provide adequate green and fired strength along with excellent reduction properties. With lower amount of peat moss addition difficulty in green balling was observed. Furthermore, it was observed that the combination of 0.5% bentonite and 1.5% peat moss addition does

not improve the green balling of the pellets. Therefore, this combination is not recommended.

Presence of MgO in the pellet is found to be beneficial to the pellet properties. MgO content in the pellet should maintained in the range of 1.8-2.0% by dolomite addition. This will ensure sufficient amount of slag formation which is the major bonding phase in self fluxed pellets. It was observed that peat moss added pellets have good compression strength at 1.3 basicity. At that basicity the pellets also have high reducibility, low swelling and low LTBT values. Therefore production of self fluxed pellets at 1.3 basicity using peat moss as binder is recommended.

The green stage properties of the peat moss added pellets could be further improved by optimising green balling conditions. More detailed study on the optimisation of green balling condition should be taken up.

The high temperature reduction behaviour of the pellets is very important for the efficient performance in the blast furnace. Because of the MgO addition and high porosity, the peat moss added self fluxed pellets are expected to have good high teperature properties. The presence of MgO will raise the liquidus temperature of the slag. Moreover, due to high porosity the pellets have high reducibility. As a result less amount of FeO will be available at high temperature which is the cause of liquid slag formation. However, assessment of high temperature properties of the pellets was beyond the scope of the present

work. Therefore it is suggested that determination of high temperature properties of these pellets should be taken up.

2.2 Claims of originality

The original contributions in this work has been:

1) Evaluation of peat moss as a binder for production of self fluxed pellets.
2) Studying the effect of peat moss on fired pellet properties.
3) Carrying out bonding mechanism studies on the Mount Wright specularite concentrates.
4) Identification of causes for low reducibility in low basicity pellets.

R E F E R E N C E S

[1] MEYER, K., "Pelletizing of Iron Ore", Springer Verlag, Berlin, 1980.

[2] SASAKI, M., NAKAZAWA, T. and KONDO, S., "Study on the Bonding Mechanism of Fired Pellets", Transactions of Iron and Steel Society of Japan, vol. 8, 1968, pp. 146-155.

[3] URICH, D.M. and HAN, T.M., A Progress Report on the Effect of Grind, Temperature and Pellet Size upon the Quantity of Specular Hematite Pellets", "Agglomeration", Ed. W.A. Knepper, Interscience Publishers, New York, 1962, pp. 669-719.

[4] CHANG, M.C. and MALCOLM, D.B., "Effect of Process Variables on Quality of Fired Pellets", Proceedings ISCTIC, Suppl. Trans. ISIJ, vol. 11, 1971, pp. 66-70.

[5] THOMAS, C.G., HAMILTON, J.D.G. and BOWLING, K.M., "Effects of Induration Conditions on the Structures and Properties of Iron Ore Pellets", Symposium on Pellets and Granules, Newcastle, October 1974, pp. 93-105.

[6] HAMILTON, J.D.G., Mechanisms of Bond Development in Hematite Ore Pellets Fluxed with Limesand", Trans. Inst. Min. Metall. (Section C), vol. 85, March 1976, pp. C30-39.

[7] BALL, D.F., FITTON, J.T., DAWSON, P.R. and GOLDRING, D.C., "Effect of Additives on the Strength of Iron Ore Pellets", Trans. Inst. Min. Metall. (Section C), vol. 83, March 1974, pp. C47-C58.

[8] TAGUCHI, K., SATO, T. and FUKIHARA, S., "Blast Furnace Performance Using Newly Developed Porous Pellets", 39th Annual Meeting of ISS-AIME Washington, 1980, Iron Making Proceedings, pp. 363-369.

[9] NISHEDA, I., UENAKA, T. and MIZUGUCHI, I., "Blast Furnace Performance Using Various New Pellets at Kakogawa Works", HF80 International Conference on the Operation of Blast Furnace, Theory and Practice, Arles, France, June 1980.

[10] RANADE, M., RICKETTE, J.A., BLATTNER, J.A. and SHUSTERICK, F.L., "A Blast Furnace Evaluation of Iron Ore Pellets Produced with an Organic Binder", Iron Making Proceedings, 1986, pp. 37-47.

[11] ROORDA, H.J., BURGHARDT, O., KORTMANN, H.A., JIPPING, M.J. and KATER, T., "Organic Binders for Iron Ore Agglomeration", Proc. of at the Eleventh International Mineral Processing Congress, Cagliary, 1975, pp. 139-180.

[12] DeSOUZA. R.P., de MENDONCA, C.F. and KATER, T., "Production of Acid Iron Ore Pellet for Direct Reduction Using an Organic Binder", Mining Engineering, October 1984, pp. 1437-1441.

[13] TREMBLAY, R., "Use of Peat Moss as a Binding Agent in the Balling of Iron Oxide Concentrates". 23rd Annual Conference on the Metallurgists, CIM, Quebec City, 1984.

[14] PANIGRAHY, S.C., RIGAUD, M., MALINSKY, I. and TREMBLAY, R., "Substitution of Bentonite with Peat Moss and its Effect on Pellets Properties", 4th International Symposium on Agglomeration, Toronto, 1985, pp. b75-82.

[15] OGBONLOWO, D.B., "Potential of Jaguar in Blast Furnace Pellet Production", Trans. Inst. Min. Metall. (Sect. C.), 96, December 1987, pp. C186-190.

[16] BALL, D.F., DARTNELL, J., DAVISON, J., GRIEVE, A. and WILD, R., Agglomeration of Iron Ores, American Elsevier Co., New York, 1970.

[17] RANISH, R.L., "Balling Drum Versus Balling Disc, an Economic Evaluation", Inst. of Briquetting and Agglomeration, Biennial Conf., 1975.

[18] LOFGREN, O., NILSSON, C.G. and ODMAN, R., Operational Experiences of Balling Circuits with Drums, Discs and Roller Seed Screens, Agglomeration 77, pp. 425-435.

[19] ENGLISH, A. and FRANS, R.D., "Developments in Pelletising", Agglomeration 77, pp. 3-23.

[20] ILMONI, P.A., CARLSSON, O. and FORSBERG, B., "Comparison of Three Pelletising Methods at LKAB", Agglomeration 81, Partikel Technologie Nurnberg, pp. B2-B22.

[21] RUMPF, H., The Strength of Granules and Agglomerates, Agglomeration (ed. W.A. Knepper), Inter Science Publishers, New York, 1962, pp. 379-418.

[22] HARDESTY, J.O., "Principles of Fertiliser Agglomeration", Chem. Engg. Progr. Symp. 60(48), 1964, pp. 46-52.

[23] NEWITT, D.M. and CONWAY-JONES, J.M., "A Contribution to the Theory and Practice of Granulation". Trans. Inst. Chem. Eng., 36, (1958), pp. 422-442.

[24] FIRTH, C.V., Agglomeration of Fine Iron Ores, Proc. AIME Blast Furnace, Coke Oven and Raw Materials, 4, 46 (1944), pp. 44-69.

[25] SASTRY, K.V.S. and FUERSTENAU, D.W., "Mechanism of Agglomerate Growth in Green Pelletising", Powder Technology, 7, 1973, pp. 97-105.

[26] WADA, M. and TSUCHIYA, O., "The Role of Hydrophile Colloid in Iron Ore Pelletisation", IXth Int. Min. Proc. Congress, Prague 1970, pp. 23-51.

[27] FUERSTENAU, D.W. and CLARK, S.W., "Interpretation of the Role of Montmorillonite in the Pelletising of Iron Ore Concentrates", Agglomeration 81, Partikel Technologie Nurnberg, pp. 133-151.

[28] WYNNYCKYZ, J.R. and FAHIDY, T.Z., Solid State Sintering in the Induration of Iron Ore Pellets, Metallurgical Trans., vol. 5, May 1974, pp. 991-1000.

[29] COOKE, S.R.B. and BAN, T.E., Microstructures in Iron Ore Pellets, Trans. Am. Inst. Min. Engrs., 193, 1952, pp. 1053-1058.

[30] NEKRASOV, Z.I. et al., Special Features of the Microstructure and Composition of the Pellets, Stal., 29, 1969, pp. 1065-70.

[31] MALYSHEVA, T.Y. and CHERNYSHEV, A.M., Comparative Study of the Mechanism of the Formation of Fluxed and Unfluxed Pellets, Stal', 1974, (5), 392-394.

[32] MATSUNO, F., Changes in Mineral Phases During the Sintering of Fe_2O_3-CaO-SiO_2 System, Trans. Iron and Steel Institute of Japan, 19, 1979, pp. 595-604.

[33] FITTON, J.T. and GOLDRING, D.C., Constitution of Iron Ore Pellets in Relation to Time and Temperature of Firing, Journal Iron and Steel Institute, 204, 1966, pp. 452-458.

[34] BOZARSKI, Z., BARSZCZ, E. and ZIELINSKI, S., Structure and Properties of Siderite Concentrate Pellets, Ibid, August 1965, pp. 452-459.

[35] KINGERY, W.D. et al., Introduction to Ceramics, Second Edition, Wiley Inter Science, New York, 1978, pp. 449-515.

[36] GERMAN, R.M., Introduction to Liquid Phase Sintering, Plenum Press, New York, 1985, pp. 5-11.

[37] BENTELL, L. and MATHISON, G., "Oxidation and Slag Forming Process in Dolomite Fluxed Pellets Based on Magnetite Concentrales, Scandinavian Journal of Metallurgy, vol. 7, 1978, pp. 230-236.

[38] NEKRASOV, Z.I., DROZDOV, G.M., SHMELEV, Y.S., BOLDENKO, M.G. and DANKO, Y.G., Nature of Slag Bond in Iron Ore Pellets, Steel in the U.S.S.R., August 1975, pp. 429-435.

[39] LU, W.K., HEGDE, V., TROFIMOV, V. and YANG, L., The "Quality" of Iron Ore Pellets, Iron Making Proceedings, 1983, pp. 258-277.

[40] FRASER, F.W., WESTENBERGER, H., BOSS, K.H. and THUMM, W., The Relationship Between Basicity and Swelling on Reduction of Iron Ore Pellets, International Journal of Mineral Processing, 2, 1975, pp. 353-365.

[41] MERLIN, A.V., ZHURAVLEV, F.M., ZIMA, S.N., DROZHILOV, L.A. and MALYSHEVA, T.Y., Influence of MgO on Fully Fluxed Pellets of High Silica Iron Ore Concentrates, Steel in the U.S.S.R., vol. 14, August 1984, pp. 361-364.

[42] THANNING, G., Reduction Strength of Super Fluxed Pellets Made from Rich Magnetite Concentrate, Iron Making and Steel Making, 1976, no 2, pp. 57-63.

[43] KANFER, V.D., BACHININA, G.A., ANDRONOV, V.N., MURAVEV, V.N. and GASPARYAN, V.E., Influence of Structure of Iron Ore Pellets on Their Strength During Reduction, Steel in the U.S.S.R., September 1977, pp. 490-493.

[44] DROZHILOV, L.A., ZHURAVLEV, F.M., MERLIN, F.M., GUBIN, G.B. and LYASHENKO, V.S., Influence of Basicity of Pellets from Iron Ore Concentrates of Different Gangue Content on Their Metallurgical Properties, Steel in the U.S.S.R., August 1975, pp. 411-413.

[45] MORIN, D.E., CAPUCCITTI, F., PICKLE, C.A., ROSS, H.V. and MEADOWCROFT, T.R., Dolomite Fluxed Pellets, ISS-AIME Iron Making Proceedings, vol. 37, 1978, pp. 69-71.

[46] YUSFIN, YU, S. and BAZILEVICH, T.N., Electron Microscope Study of Pellet Structure, Steel in the U.S.S.R., November 1971, pp. 839-841.

[47] BALL, D.F., DAWSON, P.R. and FITTON, J.T., Additives in Iron Ore Pelletising, Trans. Inst. Min. Met., Section C, 1970, pp. C189-196.

[48] TIGERSCHOLD, M., Aspects on Pelletising of Iron Ore Concentrates, Journal of Iron and Steel Institute, May 1954, pp. 13-24.

[49] EBRAHIMZADEH, MOHAMMED-REZA, Unter-suchungen Uber das pelletieren von Eisenrzen mit einem im Vergleich Zur heute Ublichen praxis groben kornanfbau unter verwendang von bindemitteln, Thesis for degree of Diplom Ingenieur Bergakademie Clausthal, FRG, 1964.

[50] RIDGION, J.M., COHEN, E. and LANG, O., The Development of a Pelletising Process for Fine Iron Ores, Journal of Iron and Steel Institute, 177, 1954, pp. 43-63.

[51] ANDERSON, A.G., "Briquetting Ores", French Patent 458,066.

[52] ANONYMOUS, Humates; Candidates for Pelletising Iron Ores, Eng. Min. J., 1968, pp. 117-118.

[53] DeVANEY, F.D., U.S. patent 2596132.

[54] SASTRY, K.V.S., NEGM, A. and KATER, T., Influence of a Cellulose Derived Binder on the Growth and Strength Behaviour of Taconite Pellets, SME Fall Meeting, Salt Lake City, Utah, 1983.

[55] GODIN, E., RIGAUD, M., PANIGRAHY, S.C. et MALINSKY, I., Étude du gonflement des boulettes d'hématite additionnées de tourbe, 23e Conférence annuelle des Métallurgistes, Québec, 1984.

[56] APPLEBY, J.E. and SHAW, G., Carbonaceous Additives in the Pelletizing Process, Agglomerate 85, pp. 49-74.

[57] Unpublished report on peat moss at University of Minnesota.

[58] CAVANAGH, R.L. and VINCZE, L.J., Investigation of Pellet Binders, Progress reports nos. 1, 2, 4, 5, 6 and 7, Ontario Research Foundation, Ontario Department of Mines, 1963-1969.

[59] APPLEBY, J.E., LEMAY, A. and MORIMOTO, W., Further Developments in Carbon Additions to the Sidbec Normines Pelletising Process, SME-AIME, Las Vegas, 1980.

[60] RICHARD, N. et JAOUICH, A., Étude de bouletage avec la tourbe, CRM, rapport préliminaire, 1977.

[61] RICHARD, N. et JAOUICH, A., Étude de bouletage avec la tourbe, CRM, rapport no 1, 1978.

[62] ST-PIERRE, R., Étude de l'effet des caractères physique et chimique de la tourbe sur le bouletage, rapport de stage T-1, CRM, avril 1979.

[63] STONE, R.L., Relation Between Zeta Potential of Bentonite and the Strength of Unfired Pellets, Trans. Society of Mining Engineers, September 1967, pp. 284-292.

[64] GARIÉPY, M., Réductibilité de boulettes d'hématite à haute teneur en silice, mémoire de M.Sc.A., École Polytechnique de Montréal, 1988.

[65] EDSTROM, J.O., The Phase $CaO \cdot 2Fe_3O_3$ in the System $CaO\text{-}Fe_2O_3$ and its Importance in Binder in Ore Pellets, Jernkont. Ann., 140, (1956), pp. 101-115.

[66] ILMONI, P.A. and UGGLA, J., Kulsintringforsok med Malmbergets A-10 Slig. Meddelande Frar Jernokonteret Tarniska Rad No 217, vol. 18 (1955), pp. 803-866.

[67] MERKLIN, K.E. and DE VANEY, F.D., Production of Self Fluxing Pellets in the Laboratory and Pilot Plant, Mining Engineering, March, 1960, pp. 46-51.

[68] KORTMANN, H.A. and BURGHARDT, O.P., Possibilities of influencing the Quality of Iron Ore Pellets as Blast Furnace Burden, Revue de Métallurgie, 1976 (9), pp. 625-636.

[69] BJORKVAAL, B. and LIMONI, P.A., Production and Use of Fluxed Pellets, Ibid, 1976 (9), pp. 583-604.

[70] SHIGAKI, I., SAWADA, N., MAEKAWA, M. and NARITA, K., Fundamental Study of Size Degradation Mechanism of Agglomerates During Reduction, Trans. I.S.I. Japan, vol. 22, 1982, pp. 838-847.

[71] EDSTROM, I.O., The Mechanism of Reduction of Iron Oxides. J. Iron Steel Inst., 1979 (1953), 289-304.

[72] MITRA, A.N., MUKHERJEE, T. and IRANI, J.J., Laboratory Investigations on the Size Degradation of Hematite Ores and Sinter in the Upper Stack Region of the Blast Furnace, Iron Making Proceedings, 1978, pp. 460-471.

[73] FRIEL, J.J. and ERICKSON, E.S.Jr., Chemistry, Microstructure and Reduction Characteristics of Dolomite Fluxed Magnetite Pellets, Metallurgical Trans. B, vol. 11B, June 1980, pp. 233-243.

[74] KORTMANN, H.A., BURGHARDT, D.P., GROVER, B.M. and KOCH, K., Effect of Lime Addition up on the Behaviour During Reduction of Iron Ore Pellets, SME-AIME Transactions, vol. 254, June 1973, pp. 184-254.

[75] TAGUCHI, K. et al., Production of Self Fluxed Pellets and Their Effect on Blast Furnace Operation at Koke Steels Nadahama Works, A.I.M.E., February 1969.

[76] SAEKI, O., TAGUCHI, K., NISHIDA, I., FUJITA, I., ONODA, M. and TUCHIYA, O., Blast Furnace Performance Using Dolomite Fluxed Pellets at Kakogawa Works, Agglomeration 77, pp. 803-815.

[77] TAGUCHI, K., AKETA, T. and MATSUMOTO, T., Production of Self Fluxing Pellets and their Performance in Blast Furnace, Revue de Métallurgie, mars 1976, pp. 247-258.

[78] BENTELL, L., CARLSSON, L. and NORRMAN, L., Development of Fluxed Pellets at LKAB, Agglomeration 81, Partikel Technologie, Nurnberg, 1981, pp. B58-B79.

[79] TSUCHIYA, O., Effect of MgO Components on the Various Metallurgical Properties, Tetsuto Hagane, vol. 66, no 13, 198, pp. 1840-1849.

[80] SUGIYAMA, T., SHIROUCHI, S., TSUCHIYA, O., ONODA, M. and FUJITA, I., Effect of Magnesia on the Properties of the Pellets at Room and Low (900°C) Temperatures. Trans. lSlJ, vol. 23, 1983, pp. 146-152.

[81] HASANEK, N. and KEDDEMAN, E., Industrial Tests at Estel Hoogovens with Olivine Additions to the Sintering and Pelletising Mixtures, Iron Making Proceedings, 1982, pp. 489-500.

[82] HEGDE, V., The Role of Basic Additives MgO and CaO during Induration and Reduction of Iron Oxide Pellets, Ph.D. Thesis, McMaster University, October 1986.

[83] BENTELL, L. and NORRMAN, L., Production and Use of LKAB Olivine Pellets, Iron Making Proceedings, 1982, pp. 501-508.

[84] KONG, L.T., YANG, L. and LU, W.K., Role of Magnesia in Iron Ore Pellets, Scandinavian Journal of Metallurgy, vol. 4, 1983, pp. 166-176.

[85] PANIGRAHY, S.C., JALLOULI, M. and RIGAUD, M., Porosity of Sinters and Pellets and its Relationship with Some of Their Properties, 43rd Iron Making Proceedings, 1984, pp. 233-240.

[86] SUGIYAMA, T. et al., High Temperature Reduction and Softening Properties with Magnesite, Trans. ISIJ, vol. 23, 1983, pp. 153-160.

[87] BENTELL, L., Means of Improving High Temperature Reducibility of the Pellets for Blast Furnace Use. Scandinavian Journal of Metallurgy.

[88] ZHURAVLEV, F.M., DROZHILOV, L.A., RIZNITSKII, I.G., MERLIN, A.V., TYKVA, P.Y. and TARANSVSKII, V.V., Technology for Producing Magnesium Containing Pellets with Basicity of 1.0 from High Silica Concentrate, Steel in the U.S.S.R., vol. 16, November 1986, pp. 517-519.

[89] MATSUNO, F., NISHIKIDA, S. and IKESAKI, H., Strength Determination of Samples of Iron Ore--5-10% CaO Systems During the Reduction at 550°C in 30% CO-N_2 Gas, Trans. ISIJ, vol. 24, 1984, pp. 275-283.

[90] SUGIYAMA, T., ONODA, M. and FUJITA, I., Improvements of High Temperature Properties of Self Fluxing Pellets by Adding Coarser Feed, Iron Making Proceedings, 1978, pp. 300-318.

[91] ELMQUIST, S.A., HUSE, J.A. and CZAKO, C.A., Assessment of the Effect of Porosity on Iron Oxide Pellet Characteristics, Iron Making Proceedings 1981, pp. 483-487.

[92] FUJITA, I. and ONODA, M., SUGIYAMA, T., SIROUCHI, S. and KOBE STEEL WORKS, U.S. patent no 4637091 1976.

[93] STEGMILLER, L., MURA, O.J.M., FRIERE, Jr. J.F. and DeSOUZA, R.P., High Porosity Pellets for Blast Furnaces, SME-AIME Fall Meeting, Honolulu, 1982.

[94] STEWART, L.G., Selection of the Pellet Burden Composition at Dofasco, Blast Furnace Symposium, Hamilton, Ontario, May 1984.

[95] JENA, B.C., Characterisation of Self Fluxed Pellets Using Peat Moss as Binder, Report prepared for Le Centre de Recherches minérales, Québec, 1986.

[96] TC/102/ISO/3271/975, Iron Ores - Determination of Tumbler Strength, International Organisation for Standardisation, 1975.

[97] TC/102/ISO/4700/1983, Iron Ore Pellets - Determination of Crushing Strength, International Organisation for Standardisation, 1983.

[98] TC/102/ISO/4696/1984, Iron Ores - Low Temperature Desintigration Test - Method Using Cold Tumbling After Static Reduction, International Organisation for Standardisation, 1984.

[99] JALLOULI, M., RIGAUD, M. and AJERSCH, F., Sintering and Swelling of Iron Oxide Pellets During Reduction, 3rd International Symposium on Agglomeration, Nurnberg, 1981, pp. B81-B103.

[100] PHILLIPS, B. and MUAN, A., Phase Equilibria in the System CaO-Iron Oxide in air and 1 atm. O_2 Pressure, Journal of American Ceramic Society, vol. 44, November 1958, pp. 445-454.

[101] LEVIN, E.M., ROBBINS, C.R. and McMURDIE, H.F., Phase Diagram for Ceramists, American Ceramic Society Inc., Columbus, Ohio, 1964, P. 49.

[102] KISSEN, D.A. and LITVINOVA, Stal in English, 1960, pp. 318...

[103] KUNII, K., NISHIDA, R. and KOIZUMI, H., On the Microstructure of the Pellets Containing Lime, Tetsu to Hagne 52, (1966), pp. 237.

[104] NYQUIST, O., Effects of Lime on the Sintering of Pure Hematite and Magnetite Concentrates, Agglomeration. Ed. W.A. Knepper, Interscience Publishers, New York, 1962, pp. 809-864.

[105] GRANSE, L., The Influence of Slag Forming Additions on the Swelling of Pellets from Very Rich Magnetite Concentrates, Proceedings ICSTIS, Suppl. Trans., ISIJ, vol. 11, 1971, pp. 45-51.

[106] WRIGHT, J.K., The Effect of Firing Conditions on the Strength of Hematite Compacts, Powder Technology, vol. 14, 1976, pp. 103-113.

[107] ST-JOHN, D.H. and HAYES, P.C., Microstructural Features Produced by Reduction of Wustite in H_2/H_2O gas mixtures, Metallurgical Transactions B, vol. 12B, March 1982, pp. 117-124.

[108] JENA, B.C., PANIGRAHY, S.C., RIGAUD, M. and LEMAY, A., A Method for Production of Fluxed Pellets Using Peat Moss as Binder, paper presented at Anual TMS-AIME meeting, New Orleans, 1986.

[109] ONODA, M., TSUCHIYA, SUGIYAMA, T. and FUJITA, I., Quality Improvements on Lime Fluxed Pellets, Iron Making Proceedings, 1983, pp. 286-298.

[110] JENA, B.C., Unpublished research.

[111] RIGAUD, M., JENA, B.C., PANIGRAHY, S.C. and PAQUET, G., A Method for Production of Highly Porous Fluxed Pellets Using Peat Moss as a Binder, ISS Transactions, vol. 9, 1988, pp. 131-138.

[112] JALLOULI, M. and AJERSCH, F., Analytical Model for the Swelling of Sintered Iron Oxide Pellets during the Hematite-Magnetite Transformation, Journal of Material Science, 1986, pp. 3528-3538.

[113] JENA, B.C., PANIGRAHY, S.C. and RIGAUD, M., Bonding Mechanism in Fluxed Pellets Using Peat Moss & Bentonite as Binder, W.O. Philbrook Memorial Symposium Proceedings, Toronto, 1988, pp. 67-76.

[114] BRILL-EDWARDS, H., DANIELL, B.L. and SAMUEL, R.L., Structural Changes Accompanying the Reduction of Polycrystalline Hematite, JISI, April 1965, pp. 361-368.

[115] SZEKELY, J., EVANS, J.W. and SOHN, H.Y., Gas Solid Reactions, Academic Press, New York, 1976, pp. 108-175.

[116] FIHEY, J.L. et AJERSCH, F., Étude théorique de la réduction gazeuse d'une boulette sphérique poreuse d'oxide, International Journal of Heat and Mass Transfer, vol. 21, 1978, pp. 1491-1498.

[117] THIELE, E.W., Relation Between Catalytic Activity and Size of Particle, Industrial and Engineering Chemistry, vol. 31, no 7, 1939, pp. 916-920.

[118] ISHIDA, M. and WEN, C.Y., Comparison of Kinetics and Diffisional Models for Solid-Gas Reactions, AIChE Journal, vol. 14, no 2, pp. 311-317.

[119] SZEKELY, J., LIN, C.I. and SOHN, H.Y., A Structural Model for Gas-Solid Reactions with a moving boundary-V; An experimental Study of the Reduction of Porous Nickel Oxide Pellets with Hydrogen, Chem. Eng. Sci., vol. 28, 1973, pp. 1975-1989.

[120] FIHEY, J.L., AJERSCH, F. and DANCY, E.A., Reduction Kinetics of Porous Pellets of Iron Titanium Oxides. Canadian Metallurgical Quarterly, vol. 18, pp. 419-434.

[121] MURAYAMA, T. and ONO, Y., Method for Determination of Parameters Included in Wen's Model, Transactions of ISIJ, vol. 26, 1986, p. B-305.

[122] BOWEN, N.L. and SCHAIRER, J.F., The System FeO-SiO_2, American Journal of Science, 5th series, 24, 1932, pp. 177-213.

[123] PHILLIPS, B. and MUAN, A., Phase Equilibria in the System CaO-Iron Oxide-SiO_2 in air, J. American Ceramic Society, vol. 42, no 9, 1959, pp. 413-423.

[124] PHILLIPS, B. and MUAN, A., Stability Relations of Calcium Ferrites, Phase Equilibria in the System $2CaO,Fe_2O_3$-FeO-Fe_2O_3 above 1135°C, Transactions of AIME, 218, 1960, 1116.

[125] HUGHES, H., ROOS, P. and GOLDRING, D.C., X-ray data on some calcium-iron-oxygen compounds, Mineralogical Magazine, vol. 36, 1967, pp. 280-291.

[126] BERGMAN, B., Solid State Reactions between CaO Powder and Fe_2O_3, Journal of American Ceramic Society, 69, (8), 1986, pp. 608-11.

[127] PHILLIPS, B. and SOMIYA, S. and MUAN, A., Melting Relations of Magnesium Oxide-Iron Oxide Mixtures in Air, Journal of American Ceramic Society, vol. 14, no 4, 1961, pp. 167-169.

[128] PALADINO, A.E., Phase Equilibria in the Ferrite Region of the System FeO-MgO-Fe_2O_3, Ibid, vol. 43, no 4, 1960, pp. 183-191.

[129] ROBERTS, H.S. and MERWIN, H.E., The System MgO-FeO-Fe_2O_3 in Air at One Atmosphere, American Journal of Science, 5th Series, vol. 21, 1931, pp. 145-57.

[130] PHILLIPS, B. and MUAN, A., Phase Equilibria in the System CaO-Iron Oxide-SiO_2 in Air, Journal of American Ceramic Society, vol. 42, no 9, 1959, pp. 413-423.

[131] OSTWALD, J., Mineralogy and Microtexture of Australian Iron Ore Sinters, BHP Technical Bulletin, vol. 25, no 1, May 1981, pp. 13-20.

[132] DAWSON, P.R., OSTWALD, J. and HAYS, K.M., Influence of Alumina on Development of Complex Calcium Ferrites in Iron Ore Sinters, Trans. Inst. Min. Metall. (Sect. C, Mineral Process. Extr. Metall.), vol. 94, June 1985, pp. C71-C78.

[133] AHSAN, S.N., MUKHERJEE, T. and WHITEMAN, J.A., Structure of Fluxed Sinter, Iron Making and Steel Making, vol. 12, no 2, 1983, pp. 55-64.

[134] JOHNSON, R.E. and MUAN, A., Phase Equilibria in the System CaO-MgO-Iron Oxide at 1500°C, J. Am. Ceram. Soc., vol. 48, 7, 1965, pp. 359-364.

[135] PRESNALL, D.C., The Join Forsterite-Diopside-Iron Oxide and its Bearing on the Crystallization of Basaltic and Ultra Mafic Magmas, Am. J. Science, vol. 264, 1966, pp. 753-809.

A P P E N D I X 1

REDUCTION KINETICS OF IRON OXIDE PELLETS

It was seen from the reducibility studies of the pellets that the reducibility is greatly influenced by the basicity, binder and flux additions. The reducibility was found to increase with the increase in basicity, reach maximum at a particular basicity and then decrease with increase in basicity. In this section the reaction mechanism of the pellet reduction is analyzed.

For analyzing the reduction mechanism of the pellet, it is pertinent to review the kinetic models which have been developed to analyze the reduction kinetics in a porous pellet. Analysis of the reaction kinetics is found to be difficult due to the absence of a sharp reaction interface. The reduction in a porous pellet is represented by the following gas-solid reaction :

$$A(gas) + B(solid) = C(gas) + D(solid) \qquad (A-1)$$

The reacting gas penetrates through the porous structure of the pellet and chemical reaction takes place on the surface of the pore walls. Depending on the relative rate of chemical reaction and diffusion through the pores of the solid oxide, the reaction could take

place in the interior of the pellet. Due to this reason, it is not possible to obtain a sharp interface between the reacted and unreacted phases. The reaction takes place in a diffuse zone whose width varies depending on the porosity of the pellet.

From the literature it is seen that two models have been developed to analyze the reduction kinetics. One of the models is developed by Szekely et al [115] which is known as "grain model". The other model is developed by Fihey and Ajersch [116]. The models have been developed with two different approaches.

According to Szekely et al [115], their model is a generalized model for gas-solid reactions. They have assumed the porous solid to be consisting of uniformly sized dense particles of a particular shape (flat plate, long cylinder or sphere). The chemical reaction takes place on the external surface of the grains (see Figure A-1). Since the grains are dense the reaction is assumed to proceed topochemically at the grain level. The differential equations for the mass balance and diffusion are derived at the grain surface on the basis of topochemical model. These equations are further modified by introduction of position coordinates and dimensionless quantities which enables these equations to be applicable at the pellet surface. By introducing a parameter σ, which they have defined as shrinking core modulus, they have tried to explain different rate controlling mechanisms.

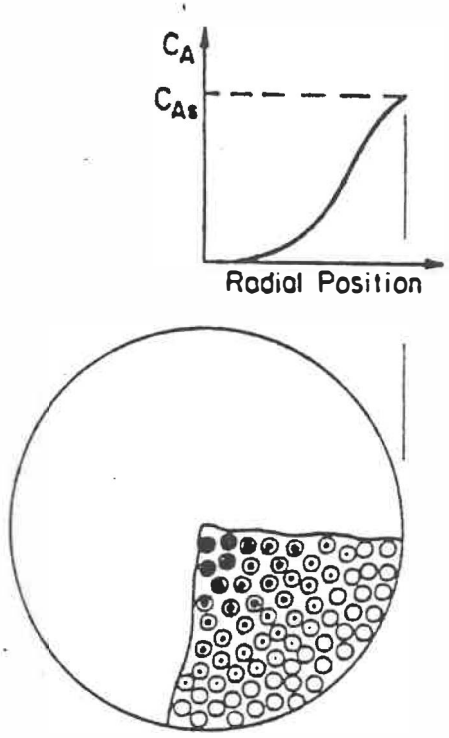


Figure A- 1. Representation of a grain model for the reaction of a porous solid with a gas [121]

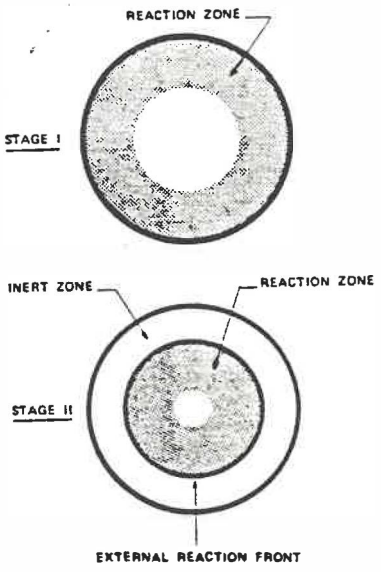


Figure A- 2. Schematic representation of the two stages of reduction of a porous pellet [122]

On the other hand Fihey and Ajersch [116] have developed the kinetic model by considering a porous spherical oxide pellet undergoing reduction by a reducing gas. They have indicated that it is not necessary to consider exact reaction position on the grain surface. It is sufficient to define the rate of reaction per unit area of the grain. They have considered the reaction to be taking place in two different stages inside the pellet (Figure A-2). In the first stage the degree of reaction is a function of the radius but the reaction is not complete on the surface of the pellet. The second stage reaction starts when the reaction on the external surface is complete. At this stage two zones in the pellet are evident. The outer zone is inert and an increase of this zone takes place at the expense of the other zone active and diminishing towards the center. They are able to present analytical solutions for the rate of progress of the reaction of a pellet for two limiting cases i.e.; purely topochemical to completely homogeneous. This has been done with the help of three parameters, the Thiele modulus $\hat{m}r_o$, the mass transfer modulus K_F and $\emptyset$, minimum time required for complete reaction.

Both the models are based on the following assumptions :

1. The reaction is isothermal.
2. No structural change takes place inside the pellet during reaction and the free surface area

remains unchanged.

3. The chemical reaction is of first order.
4. The diffusion of gas in the porous structure is under a unique concentration gradient.
5. The characteristic system parameters such as reaction rate constant, diffusion coefficient, porosity, etc. remain unchanged.

Fihey and Ajersch have assumed steady state condition for the first stage of reaction and quasi steady state condition for the second stage of the reaction by considering a moving interface between two zones of reaction. This assumption is valid because of the relatively slower movement of the interface with respect to gaseous species. Szekely et al have considered the quasi steady state approximation to be appropriate.

A brief description of the models are given below :

1. SZEKELY'S MODEL

The mass balance equation is written as :

$$D_{eff} \nabla^2 C_A - v_A = 0 \qquad \text{(A-2)}$$

$$D_{eff} \nabla^2 C_C + v_A = 0 \qquad \text{(A-3)}$$

Where

D_{eff} = effective diffusivity in the pellet

C_A, C_C= molar concentration of the reactant and product gas

v_A = local rate of consumption of gaseous reductant

$$v_A = (1 - \varepsilon)k(A_g / V_g)(A_g r_c / F_g V_g)^{F_g - 1}(C_A - C_C / K_E) \quad (A-4)$$

Where

ε = initial porosity of the pellet

k = reaction rate constant

A_g = external surface area of the grain

V_g = volume of the grain

r_c = position of the moving reaction front in the grain

F_g = shape factor

K_E =equilibrium constant

By substituting for v_A in eqn.(A-2) and introducing dimensionless variables

$$\chi = (C_A - C_C/K_E)/(C_{AS} - C_{CS}/K_E) \quad (A-5)$$

(relative concentration)

$$\zeta = A_g r_c / F_g V_g \quad \text{(shape factor)} \quad (A-6)$$

$$t^* = bk/\rho_s (A_g F_g / V_g)(C_{AS} - C_{CS}/K_E)t \qquad \text{(A-7)}$$

(dimensionless time)

$$\sigma = F_p V_p / \sqrt{(1-\varepsilon) k / D_{eff} A_g / V_g (1+1/K_E)} \qquad \text{(A-8)}$$

following equations are obtained.

$$\nabla^{*2}\chi - \sigma^2 \chi \zeta F_g^{-1} = 0 \qquad \text{(A-9)}$$

and

$$\partial\zeta / \partial t^* = -\chi \qquad \text{(A-10)}$$

where

C_{AS}, C_{CS} = molar concentration of the gaseous reactant and product in the gas stream respectively

∇^{*2} = laplacian operator with η as the position coordinate

$$\eta = A_p R / F_p V_p \qquad \text{(A-11)}$$

A_p = surface area of the pellet

R = distance from the center of symmetry of the pellet

V_p = volume of the pellet

b = stoichiometric coefficient

ρ_s = molar concentration of the solid reactant

The parameter σ is analogous to the Thiele modulus

in heterogeneous catalysis [117]. This parameter incorporates both kinetic and structural properties and is a measure of the relative magnitude of chemical reaction and diffusion. The significance of σ has been discussed by examining asymptotic behaviors. As σ approaches zero , pore diffusion offers negligible resistance to the progress of the reaction. The reactant concentration is uniform throughout the pellet and is equal to that of the bulk ($\chi = 1$). As ζ is independent of η

$$t^* = g_{F_g}(X) = 1-(1-X)^{1/F_g} \qquad (A-12)$$

As σ approaches infinity, reaction occurs mostly in a narrow zone between the unreacted core and completely reacted layer. The concentration driving force $(C_A - C_C/K_E)$ drops to nearly zero at the reaction zone. Diffusion through the product layer is the overall reaction rate controlling factor.

A generalized modulus $\hat{\sigma}$, known as shrinking core modulus is introduced at this stage which takes the shape factor of the grains and pellets into account.

$$\hat{\sigma} = \sigma/\sqrt{2F_g F_P} = V_p/A_p \sqrt{(1-\varepsilon)kF_p/2D_{eff}(A_g/F_g V_g)(1+1/K_E)} \qquad (A-13)$$

For the intermediate value of $\hat{\sigma}$, numerical solution of the differential equation has been obtained after setting up appropriate boundary conditions [119].

$$t^* = g_{F_g}(X) + \hat{\sigma}^2 p_{F_p}(X) \qquad \text{(A-14)}$$

In other words, the time required to reach a certain conversion is of the time to reach same conversion under the chemical reaction control and that under the diffusion control.

After incorporating the effect of external mass transport the equation becomes

$$t^* = g_{F_g}(X) + \hat{\sigma}^2 p_{F_p}(X) + (2X/N_{sh}) \qquad \text{(A-15)}$$

where

$$t^* = bk/\rho_s (A_g/F_g V_g) t[C_{Ao} - C_{co}/K_E] \qquad \text{(A-16)}$$

and

N_{sh} = Sherwood's number

2. FIHEY'S MODEL

As mentioned earlier, Fihey and Ajersch have considered the reaction to be proceeding in two stages. For the first stage of reaction, the mass balance and diffusion equation is written as:

$$\partial N_A/\partial r = -4\pi r^2 a k_r (1+1/k_E)(x_A - x_{AE}) \qquad (A-17)$$

$$N_A = -4\pi r^2 c D_{eff} \partial x_A/\partial r \qquad (A-18)$$

Where

N_A = molar flux of the reducing gas
r = radius of the pellet
a = free solid surface per unit volume
k_r = chemical reaction constant
K_E = equilibrium constant
c = molar concentration of the gas
x_A = molar fraction of the reacting gas
$x_{A.e}$ = equilibrium molar fraction of the reacting gas
D_{eff} = effective diffusion coefficient

From the solution of the above equations (A-17) and (A-18), expressions for the concentration profile and molar flux is obtained:

$$x_A - x_{A.e}/x_{A.s} - x_{A.e} = 1/r^* \; \mathrm{Sinh}(\hat{m} r_o r^*)/\sinh(\hat{m} r_o) \qquad (A-19)$$

$$N_A = -(x_{A.s} - x_{A.e})4\pi c r_o \times D_{eff}[\hat{mr}_o r^* \cosh(\hat{mr}_o r^*) - \sinh(\hat{mr}_o r^*)/\sinh(\hat{mr}_o r^*)] \quad (A-20)$$

Where

$x_{A.s}$ = molar fraction of reacting gas at pellet surface

r_o = radius of the pellet

r^* = reduced radius

k_r = chemical reaction constant

$$\hat{mr}_o = r_o\sqrt{[ak_r(1 + 1/K_E)/D_{eff}]} \quad (A-21)$$

(Thiele modulus)

The time t_i taken for completion of first stage of reaction is given by

$$t_1 = 6\emptyset/\hat{mr}_o[1 + (\hat{mr}_o \coth(\hat{mr}_o) - 1)/k_F \quad (A-22)$$

with

$$\emptyset = c_o r_o^2 / 6D_{eff}c(1-x_{A.e}) \quad (A-23)$$

(minimum time taken for complete reaction)

$$K_F = 1/(1/N^o_A + 1/4\pi r_o^2 k_d c)/4\pi r_o c D_{eff} \quad (A-24)$$

(mass transfer modulus)

k_d = mass transfer coefficient

Expressions for the local reduced fraction α, overall

reduction fraction F is obtained.

The overall reduction fraction F is given by

$$F = F_1 t/t_1 \qquad \text{(A-25)}$$

Where F_1 = overall reduced fraction at the end of first stage.

$$F_1 = 3(\hat{mr}_o \cosh(\hat{mr}_o) - 1)/\hat{mr}_o^2 \qquad \text{(A-26)}$$

and

t = time

F_1 is a function of Thiele modulus. For low values of $\hat{mr}_o$, $(\hat{mr}_o < 1)$, the first stage reaction predominates and for higher values of $\hat{mr}_o$, $(\hat{mr}_o > 50)$, the reaction during the first stage of reaction is negligible.

The analytical solution for the second stage of reaction is somewhat more complex. The mass balance equation leads to the expression which is considered to be the product of two functions, that is of time and of pellet radius.

$$\partial\alpha / \partial t = \psi(r^*) . \phi(t) \qquad \text{(A-27)}$$

A dimensionless radius r^* is introduced at this stage which is the ratio of interface radius and pellet radius.

The local reduced fraction α is found to be

$$\alpha = \sinh(\hat{m}r_o r^* \times r_i^* / \sinh(\hat{m}r_o r_i^*) \qquad \text{(A-28)}$$

The total time of reaction t_c is given by

$$t_c = \emptyset(1 + 2/K_F + 6/\hat{m}r_o^2) \qquad \text{(A-29)}$$

From the above it is seen that although the models were developed with two different approaches, the expression for the time of reaction consists of three similar parameters in both the models. In Szekely's model these parameters are chemical reaction control parameter, $gF_g(X)$, diffusion control parameter, $\hat{\alpha}F_g(X)$ and mass transfer parameter, $2X/N_{sh}$. The corresponding parameters in Fihey's model are $\emptyset$, the minimum time required for complete reaction, $\hat{m}r_o$, the Thiele modulus and K_F, the mass transfer modulus.

In both models the effect of mass transfer on the reaction rate has been recognized.

In cases where the effect of mass transfer is negligible, the reaction rate is mainly dependent on the diffusion control parameter. It is shown that for low values of diffusion control parameter ($\hat{\alpha} < 0.3$ and $\hat{m}r_o < 1$) the effect of diffusion is negligible therefore chemical reaction is overall reaction rate controlling. According to Fihey and

Ajersch the reaction is homogeneous and maximum conversion takes place during the first stage of the reaction. For higher values of diffusion control parameters ($\hat{\sigma} \rightarrow \infty$ and $\hat{m}r_o > 50$) diffusion is rate controlling and topochemical reaction prevails. For the intermediate values, the reaction proceeds under mixed control.

The approach made by Fihey and Ajersch is similar to the one made by Ishida and Wen [118]. However, the analytical solution obtained by Fihey and Ajersch appear to be less complex than that obtained by Ishida and Wen.

Due to the particle geometry considerations in Szekely's model the solution of the differential equations are complex. By appropriate manipulation of numerical results the effect of particle geometry is minimized and a solution is obtained.

Szekely's model was developed as a generalized model for gas solid reactions. It is based upon certain assumptions such as uniform distribution of ideally shaped grains in the pellets which is very unrealistic. As a result, the local surface area is considered to be $A_g F_g / V_g (1-\varepsilon)$ which is different from the actual surface area. Moreover, it does not account for the dependence of local rate of reaction with local extent of reaction. On the other hand Fihey's model has incorporated the equation for the local extent of reaction and obtained the solution.

Szekely et al have recognized this and have modified their model by making an alternative approach. In the modified approach they have correlated the local rate of reaction with local extent of reaction and arrived at the results similar to the ones obtained by Fihey and Ajersch.

It is also seen that by correlating the grain size factor with order of reaction, i.e., $F_g = 1/1-m$ where m = order of the reaction, the results of Fihey'model is identical to the results obtained by Szekely's model.

Szekely et al have found their model to be consistent with the experimental measurements of the rate of reduction of nickel oxide by hydrogen below a temperature at which serious structural changes occurs due to sintering [119]. Fihey and Ajersch also have found good agreement between the predicted and experimental reduction curves by using their model for iron titanium oxide reduction [120].

From the comparison of the two models we find that both models have arrived at identical relationships although they were developed with alternative approaches. Out of the two models, Fihey's model appears to be simpler and more realistic.

However, due to the difficulties encountered in determining

diffusivity etc., Fihey's model has not found wide application. Recently Murayama and Ono [117] have proposed a method for determination of these parameters from experimental data. Another limitation for use of this model for iron oxide reduction could be the assumption which says that no structural change takes place in the pellet. The iron oxide pellets are known to swell during reduction.

Fihey's model can be used qualitatively to explain reduction behavior of the present set of pellets. The reduction - time relationships as a function of basicity, flux and binder addition are shown in Figures A-3 to A-9. The time-reduction curves for all types of pellets at basicities 0 8, 1.3 and 1.6 are shown in Figures A-3, A-4, and A- 5 respectively.The reduction curves for each type of binder and flux are shown in Figures A-6 tO A-9.

It is seen from the reduction curves that each curve consists of two parts which appear to overlap at a point. The initial part of the curve may be considered to represent the first stage of reduction. The point at which both parts of the curve overlap denotes the end of first stage of reduction. The corresponding fraction of reduction is the extent of reduction which occured ouring the first stage of reduction. According to Fihey's model the fraction of reduction during first stage is a function of Thiele modulus, $\hat{m}r_o$. For low values of $\hat{m}r_o$, the first stage of reduction is predominating and a high fraction of reduction can occur during the first stage.

From Figures A-3 to A-5, it is seen that the fraction reduced during the first stage of reduction is higher for peat moss and dolomite added pellets. Since these pellets have higher porosity than other types of pellets (see Table 27, Chapter 3). This increases the effective diffusivity of the reducing gas inside the pellet. Since Thiele modulus is inversely proportional to the square root of the effective diffusivity, the Thiele modulus is considerably decreased. In physical terms, the penetration of the reducing gas inside the pellet is facilitated due to higher porosity and this increases the degree of reduction.

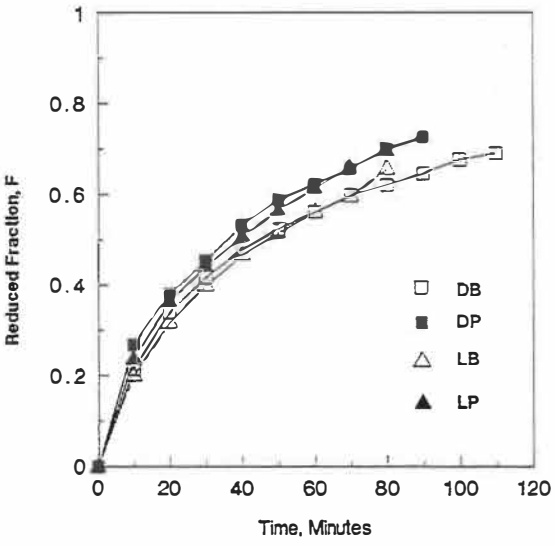


Figure A-3. Time-reduction relationships in the pellets at 0.8 basicity

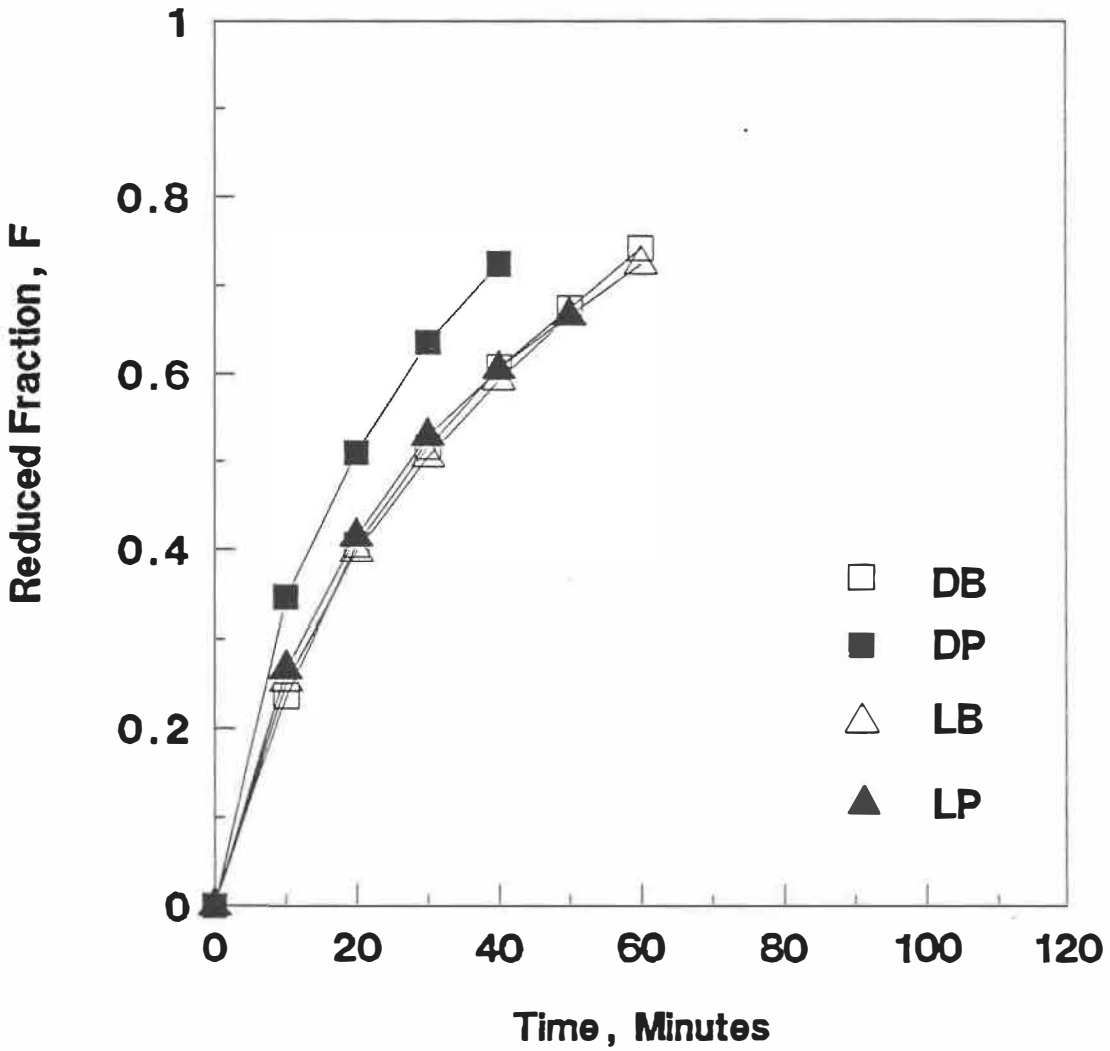


Figure A-4. Time-reduction relationships in the pellets at 1.3 basicity

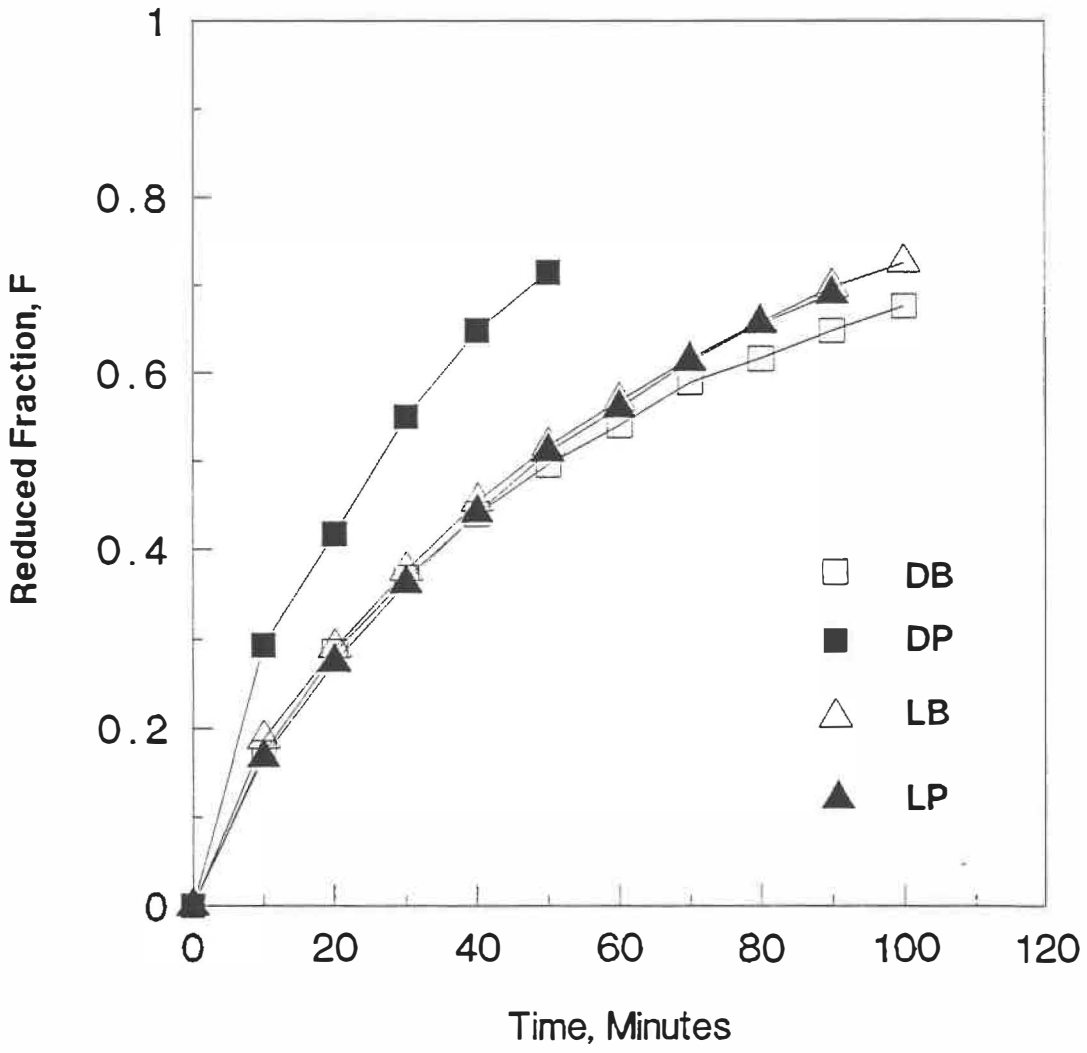


Figure A-5. Time-reduction relationships in the pellets at 1.6 basicity

In Figures A-6 to A-9, the effect of basicity on the reduction curve for each type of additive is shown. The reduction mechanism appears to be different with different types of binder and flux addition. However, it is seen that F_1, the reduction fraction during the first stage of reduction increases up to the basicity of 1.3. On further increase in basicity, the F_1 decreases. Formation of intragranular pores was observed in the microstructure of partially reduced pellets of higher basicity and the amount of pores was found to increase with basicity. This increased the effective diffusivity in the pellets of 1.3 basicity compared to the pellets of 0.8 basicity although the initial macroporosity values are comparable. The enhanced effective diffusivity values in 1.3 basicity pellets resulted in higher F_1 values. As the basicity of the pellets was increased to 1.6 the porosity decreased drastically due to higher amount of melt formation. This decreased the F_1 value. In pellets with peat moss and dolomite addition of 1.6 basicity, the pellets still have high porosity value ($\simeq$ 30%). Therefore the F_1 value for this pellet is found to be reasonably high.

It is also seen from the time-reduction curves that the reduction time to attain a certain degree of reduction varies for different types of pellets. The time taken for attaining 70% reduction is seen to be minimum for pellets of peat moss and dolomite addition at 1.3 basicity. According to Fihey's model, the total time t_c for

attaining a certain reduction fraction is a function of three parameters, Ø, $\hat{mr}_o$ and K_F . Since these parameters are depenedent on effective diffusivity, an increase in this value results in a decrease in total time t_c. As discussed earlier, peat moss and dolomite added pellets at 1.3 basicity have higher diffusivity due to effect of enhanced macro and micro porosity. Therefore these pellets took minimum time to reach 70% reduction.

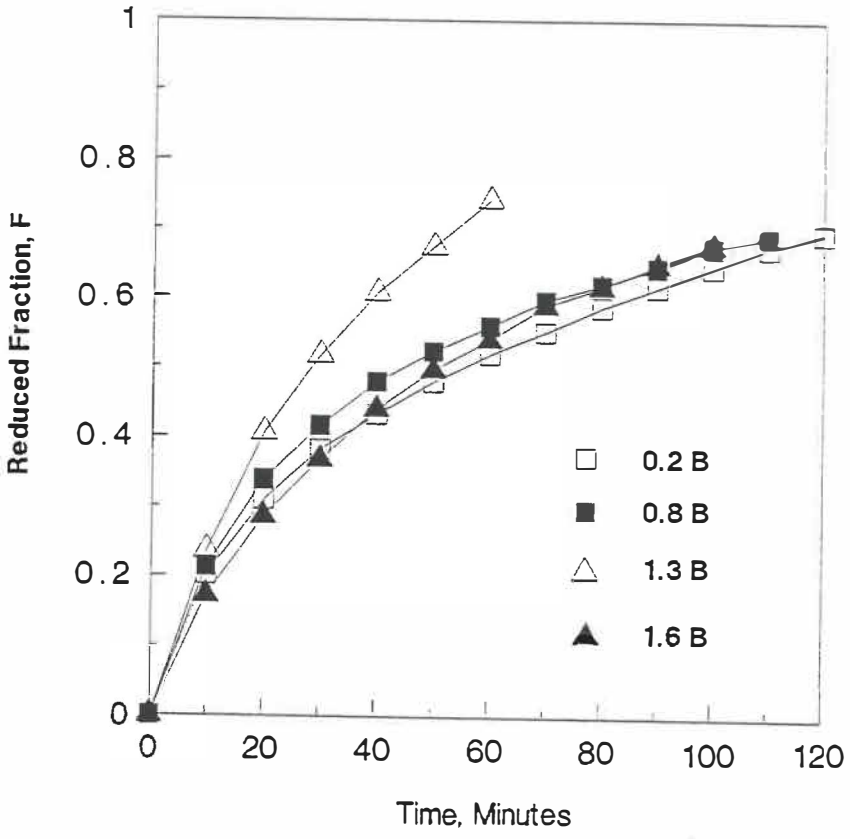


Figure A-6. Time-reduction relationships in the pellets with dolomite and bentonite addition

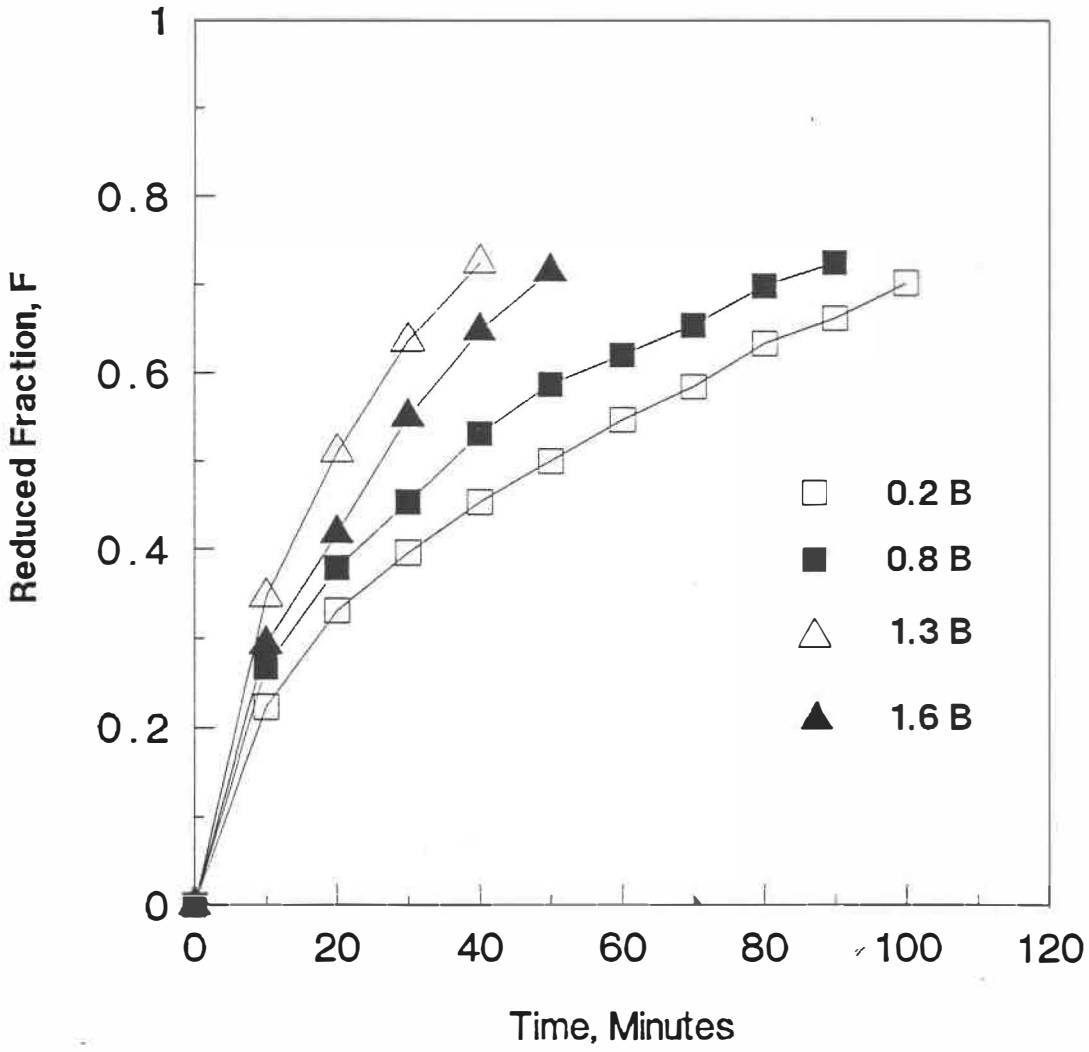


Figure A-7. Time-reduction relationships in the pellets with dolomite and peat moss addition

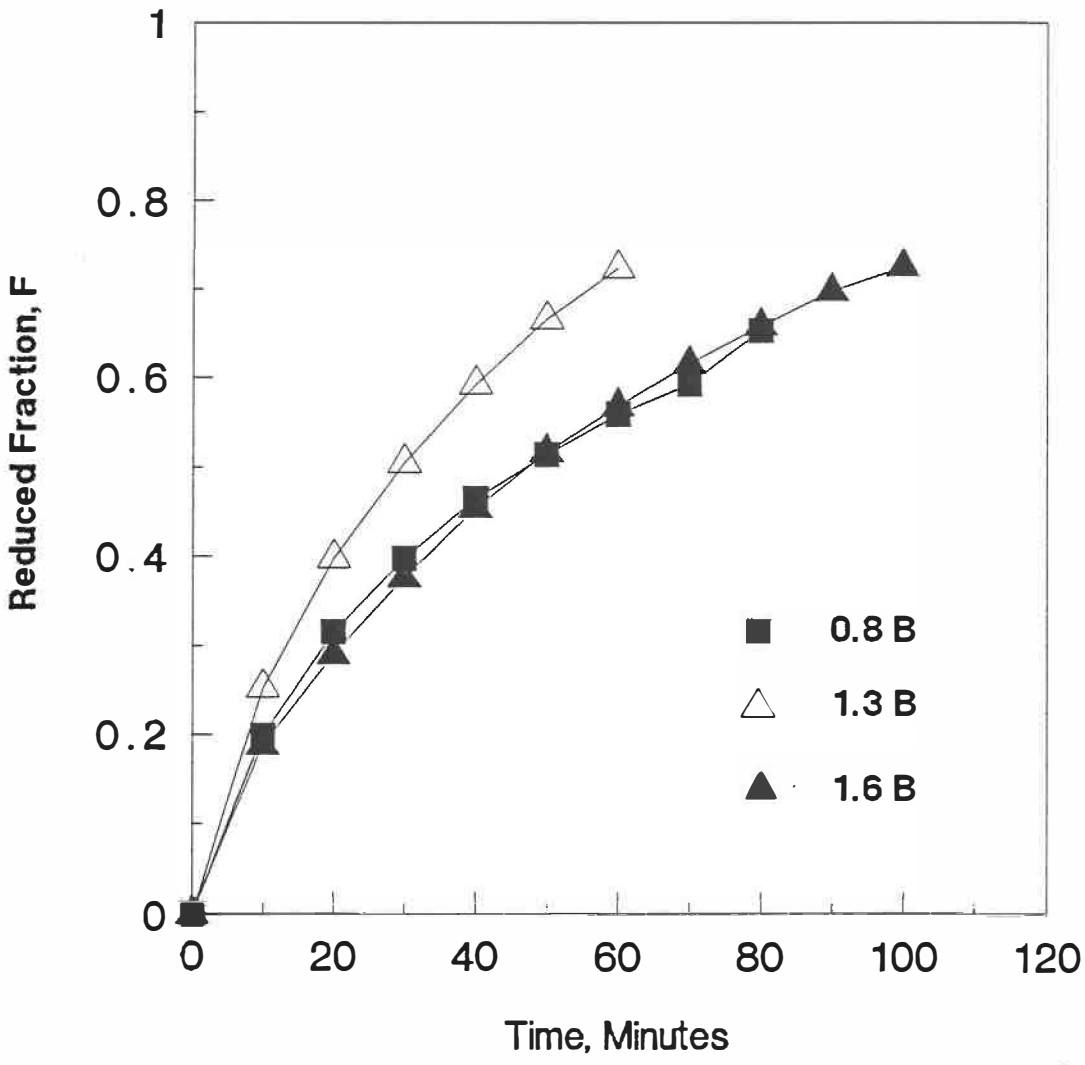


Figure A-8. Time-reduction relationships in the pellets with limestone and bentonite addition

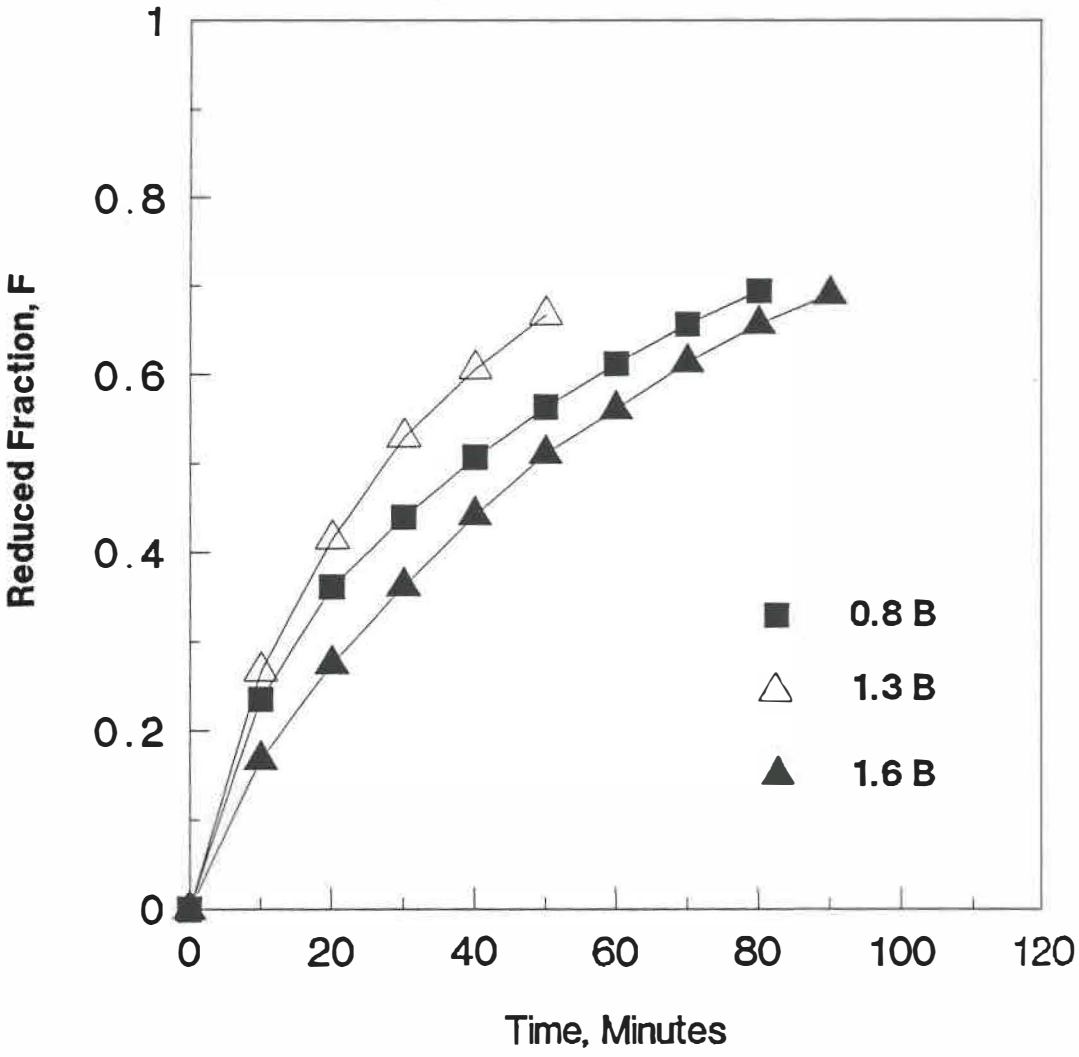


Figure A-9. Time-reduction relationships in the pellets with limestone and peat moss addition

From the above discussion we find that the reduction in the pellet proceeds under mixed control, i.e., homogeneous and topochemical. In case of high porosity pellets of high basicity the homogeneous reaction is predominating. Fihey's model could be effectively used to understand reaction mechanism.

A P P E N D I X 2

PHASE EQUILIBRIA DURING PELLET INDURATION

The major constituents in the fluxed pellets under present investigation are; iron oxides, silica, calcium oxide, magnesium oxide, and alumina. The formation of various mineralogical phases and their chemical composition was mainly dependent on the interaction of these constituents during pellet induration. In this section the formation of the mineralogical phases will be discussed in the light of phase equilibria. Due to involvement of several components the phase relationships are complex. They are further complicated due to the presence of both bivalent and trivalent iron. However, in this section the evolution of pellet morphology during pellet induration will be discussed with respect to the available pseudo binary, ternary and quaternary phase diagrams.

Among the above mentioned oxides, the contribution of Al_2O_3 may be considered to be negligible due its low concentration.

1. IRON OXIDE - SILICA SYSTEM

The $FeO - SiO_2$ and $FeO.Fe_2O_3 - SiO_2$ phase diagrams in air are

shown in Figures A-10 and A-11 respectively [122, 123]. From Figure A-10 it is seen that liquid iron silicate slag formation (fayalite) occurs at 1217 ^{o}c. The formation of fayalite requires the presence of FeO and the reduction of hematite or magnetite to FeO takes place at a very low oxygen partial pressure ($<3.5 \times 10^{-5}$ atm. at 1300 ^{o} c) [82]. Since iron ore pellets are indurated under oxidizing atmosphere, such a low oxygen partial pressure is not achieved. From Figure A-11 it is also seen that liquid formation occurs at a temperature above 1445 ^{o} c in $FeO.Fe_2O_3$ - SiO_2 system, at a temperature much higher than normal pellet induration temperature. Therefore, it is unlikely that any liquid formation takes place during pellet induration. This is evident from the presence of free silica in the pellets of low basicity pellets (0.2 and 0.8 basicity).

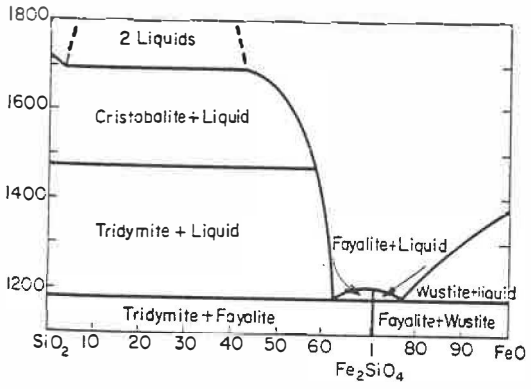


Figure A-10. The system FeO - SiO_2 in air

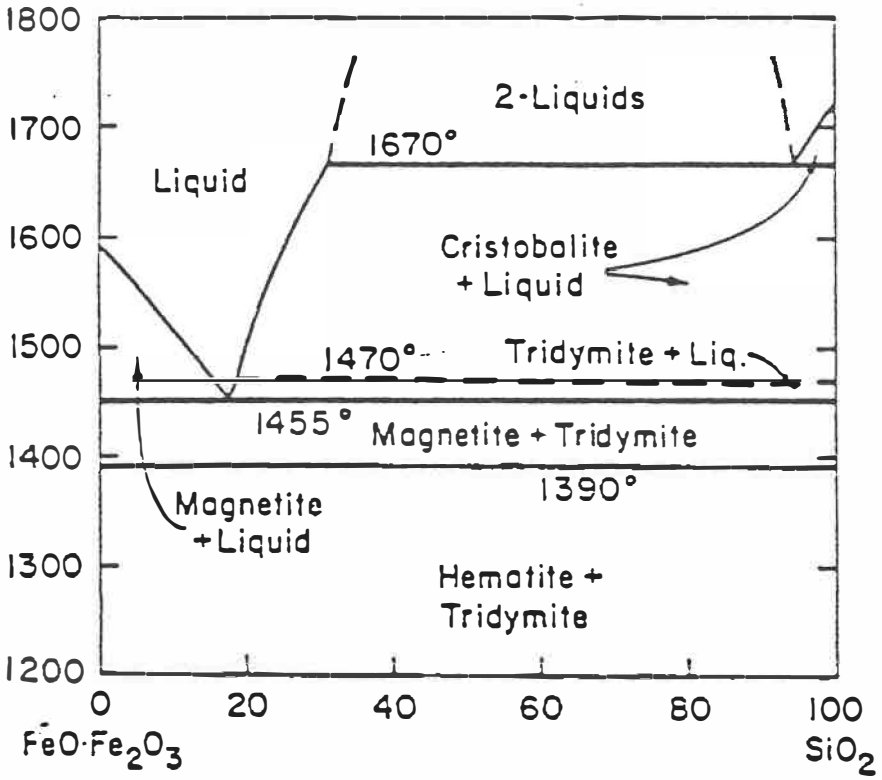


Figure A-11. The system $FeO.Fe_2O_3$ - SiO_2 in air

2. IRON OXIDES - CALCIUM OXIDE SYSTEM

formation of a number of calcium ferrites has been reported

in iron oxide - CaO system [104, 124, 125] which are ternary in nature and their formation depends on the temperature and oxygen partial pressure. The phase diagrams are shown in Figures A-12 and A-13. As shown in the CaO-Fe_2O_3 pseudo binary phase diagram (Figure 17, chapter 3), three types of calcium ferrites are formed in air; namely, CaO . $2Fe_2O_3$ (calcium diferrite), CaO . Fe_2O_3 (calcium mono-ferrite), and 2CaO . Fe_2O_3 (di-calcium ferrite) depending on the composition of calcium and iron oxide. Calcium diferrite forms in a narrow temperature range of 1155 ^{o} c to 1205 ^{o} c. Below 1155 ^{o} c it dissociates to calcium monoferrite and hematite. In a recent investigation Bergman [126] has shown the dissociation temperature of calcium diferrite to be 1125 ^{o} c. These ferrites are formed in the solid state. Calcium diferrite and calcium monoferrite melt incongruently at 1205 ^{o} c and 1216 ^{o} c respectively [100]. At the melting temperatures of these ferrites some amount of magnetite forms due to substitution of Fe^{2+} ions by Ca (see lower part of the Figure 17). As it has been discussed in Chapter 3, weight loss at the commencement of melting was observed during thermal analysis studies of the pellet mix. This confirms the formation of magnetite during melting of calcium ferrites which reoxidised during cooling. Similar observation have been reported by Hughes et al [125] and Hamilton [6]. The liquid flowed through the pore channels and dissolved silica and other oxides resulting in the formation of glassy silicates and

multi component calcium ferrites. As a result, calcium ferrite which was observed in the pellets was not binary in nature. Formation of these compounds will be discussed under multi component calcium ferrite.

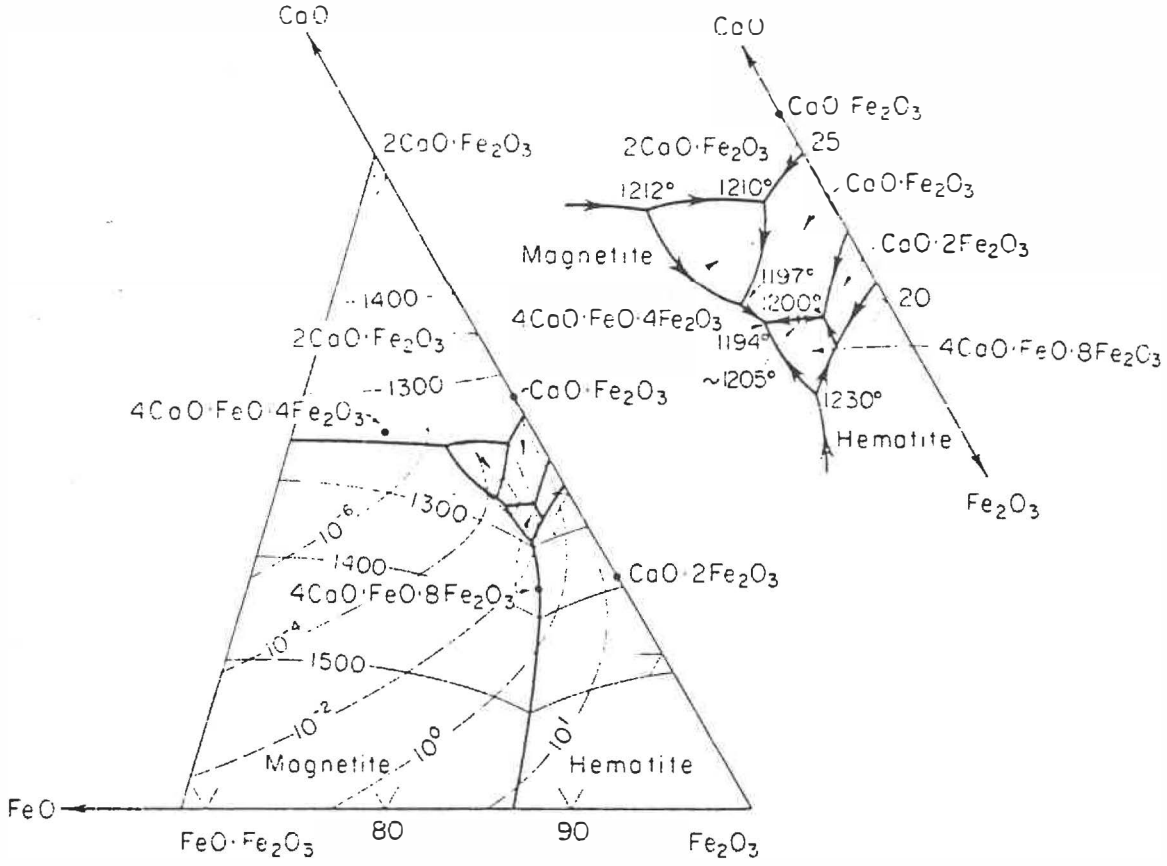
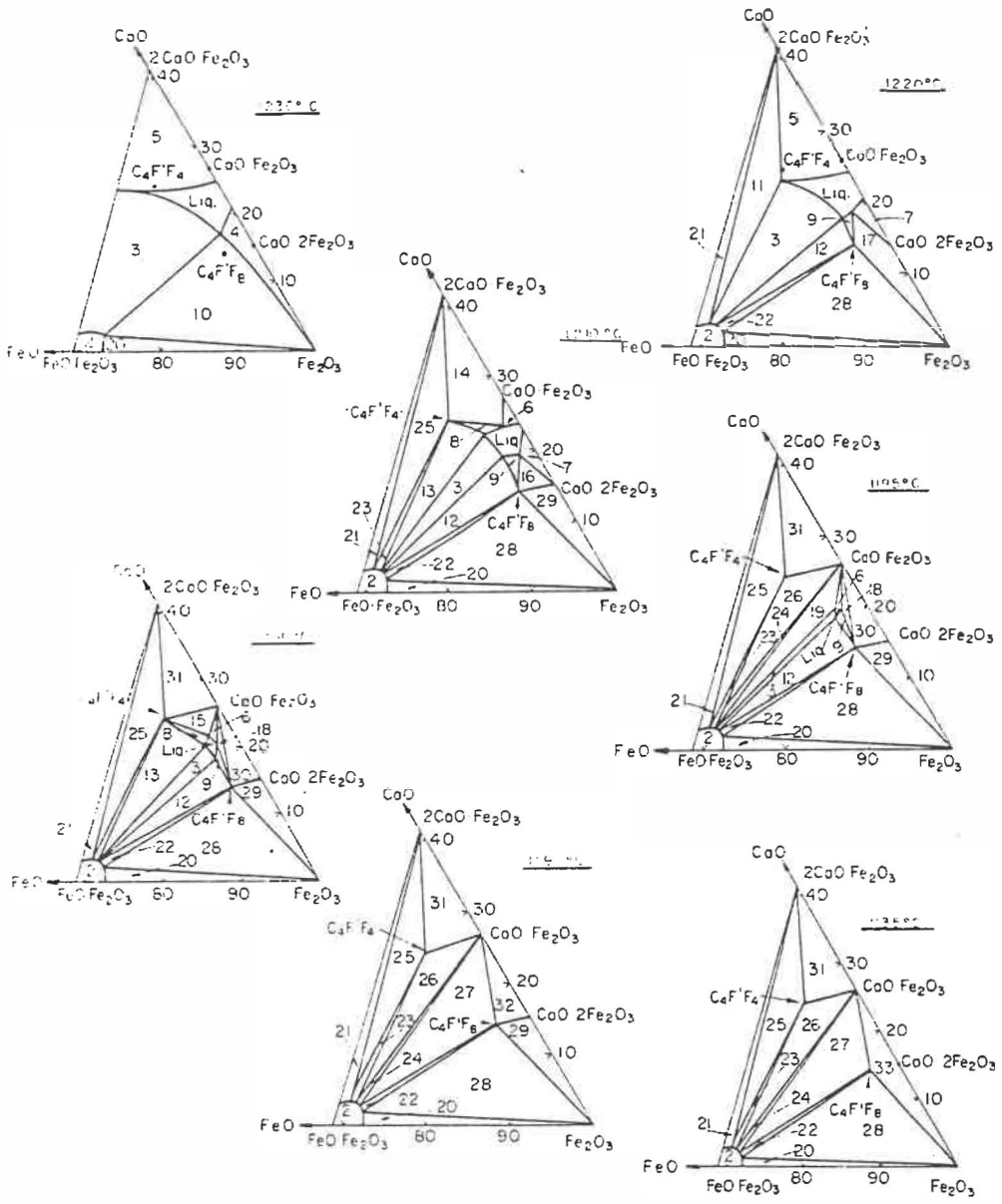


Figure A-12. System $2CaO.Fe_2O_3$- $FeO.Fe_2O_3$- Fe_2O_3



System $2CaO \cdot Fe_2O_3$-$FeO \cdot Fe_2O_3$-Fe_2O_3 showing isothermal sections between 1135° and 1230°C. 2 = Magn., 3 = Liq + Magn., 4 = Liq + Hem., 5 = Liq. + C_2F, 6 = Liq + CF, 7 = Liq + CF_2, 8 = Liq. + $C_4F'F_4$, 9 = Liq. + $C_4F'F_8$, 10 = Liq. + Magn. + Hem. + $C_4F'F_8$, 11 = Liq + Magn. + C_2F, 12 = Liq + Magn. + $C_4F'F_8$, 13 = Liq. + Magn. + $C_4F'F_8$, 14 = Liq. + CF + CF + $C_4F'F_4$, 15 = Liq. + CF + $C_4F'F_4$, 16 = Liq. + CF_2 + $C_4F'F_4$, 17 = Liq. + Hem. + CF_2 + $C_4F'F_8$, 18 = Liq. + CF + $C_4F'F_8$, 19 = Liq. + Magn. + CF, 20 = Magn. + Hem., 21 = Magn. + C_2F, 22 = Magn. + $C_4F'F_8$, 23 = Magn. + $C_4F'F_4$, 24 = Magn. + CF, 25 = Magn. + C_2F + $C_4F'F_4$, 26 = Magn. + CF + $C_4F'F_4$, 27 = Magn. + CF + $C_4F'F_8$, 28 = Magn. + Hem. + $C_4F'F_8$, 29 = Hem. + CF + $C_4F'F_8$, 30 = CF_2 + CF + $C_4F'F_4$, 31 = CF + C_2F + $C_4F'F_4$, 32 = CF + CF_2 + $C_4F'F_8$, and 33 = Hem. + CF + $C_4F'F_8$. C = CaO, F = Fe_2O_3, and F' = FeO.

Bert Phillips and Arnulf Muan, *Trans. AIME*, 218, 1117 (1960)

Figure A-13. The system $2CaO.Fe_2O_3$ - $FeO.Fe_2O_3$ - Fe_2O_3 showing isothermal sections between 1135 °C and 1230 °C

3. IRON OXIDES - MGO SYSTEM

The MgO - FeO pseudo binary system in air [127] is shown in Figure A-14 . The system contains varying amounts of Fe^{2+} and Fe^{3+} ions depending on the oxygen partial pressure and temperature. The $FeO-Fe_2O_3-MgO$ ternary system at various oxygen pressures and 1300 ^{o} c [128] is shown in Figure A-15 . The MgO containing phase in the iron oxide rich region is a spinel and its formation is reported to be due to the substitution of bivalent iron by Mg [129]. Depending on the degree of substitution by Mg, the composition of the spinel varies and is generally expressed by $(Fe_{(1-x)}Mg_x)O.Fe_2O_3$ (magnesio spinel) [84] where x is the concentration of MgO. It may be noted from the Figure A-14 that liquid formation does not take place below 1600 ^{o} c. Therefore spinel formation takes place in solid state. As the spinel is formed due to substitution of bivalent Fe by Mg, it is usually observed in pellets of magnetite concentrates. In hematite pellets the formation of spinel is attributed to the presence of magnetite either originally present in the concentrate or formed during induration. In the present set of pellets magnetite formation was due to the incongruent melting of calcium ferrites. The MgO in the pellet reacted with the magnetite to form magnesiospinel $(Fe_{(1-x)}Mg_x)O.Fe_2O_3$. During cooling the ferrous oxide was reoxidised to ferric state. As a result

the spinel which was observed in these pellets was found to be highly deficient in MgO.

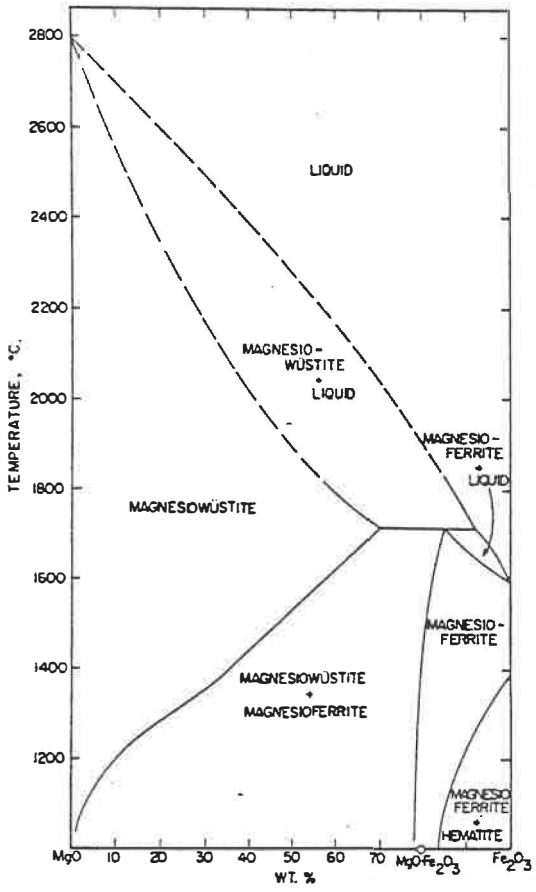


Figure A-14. The system magnesium oxide - iron oxide in air

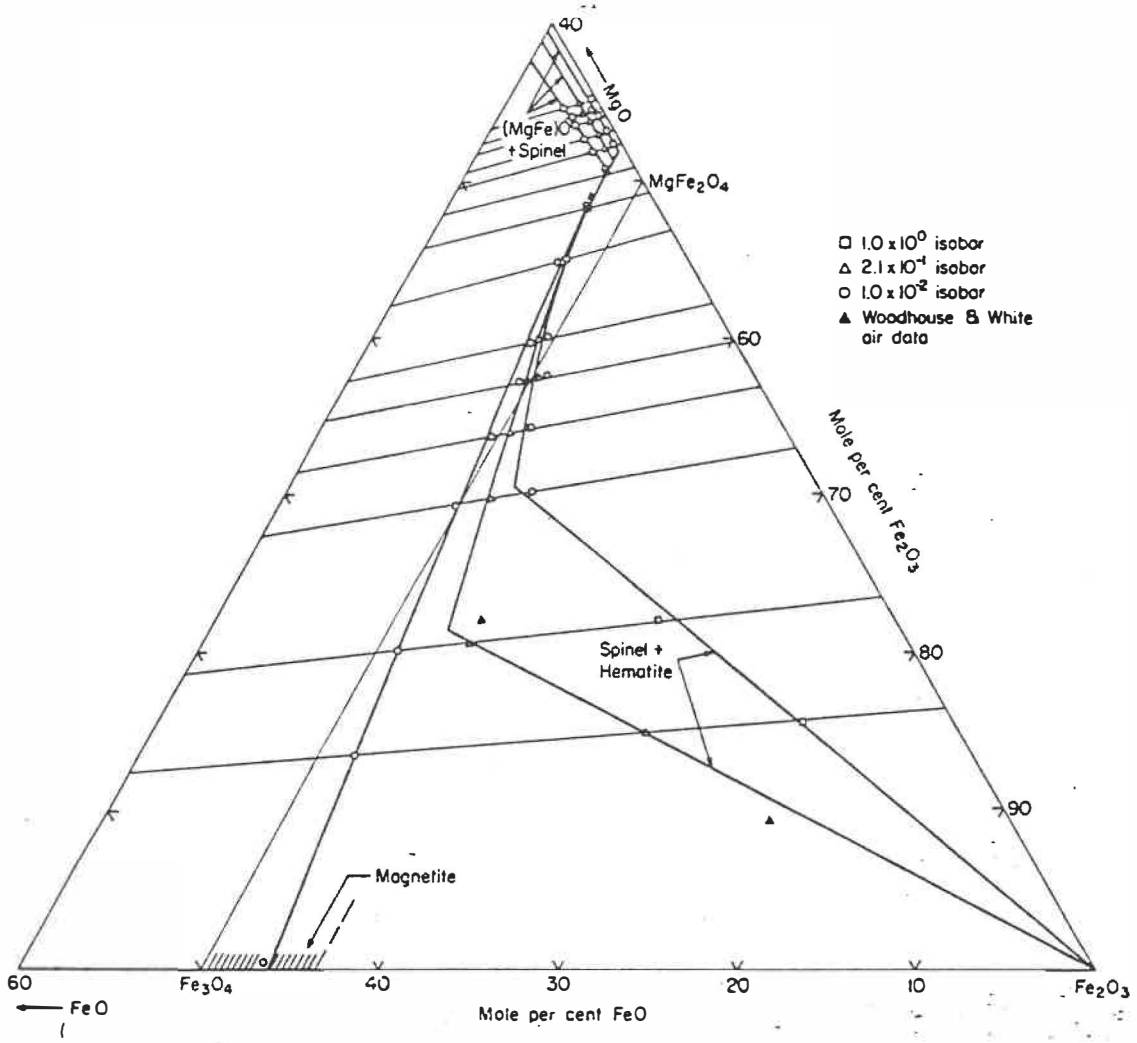


Figure A- 15. Phase equilibria relations in the system FeO-MgO-Fe_2O_3 at 1300^{o} c

4. IRON OXIDES - CAO - SIO_2 - MGO SYSTEM

The iron oxide - CaO -Si_2 pseudo ternary system in air is shown in Figure A-16 [130] . The lowest temperature at which liquid formation takes place is 1192 ^{o} c. Several phases such as silicates, ferrites are observed to exist at equilibrium around 1300 ^{o} c, i.e.; pellet induration temperature. However, at lower basicities formation of glassy silicates are reported [38, 42, 105].

In order to determine the effect of basicity on the type of silicate formation, Matsuno [32] prepared mixtures of Ca,Fe_2O_3 and SiO_2 at different compositions and heated up to 1400 ^{o} c. After keeping at that temperature for 15 minutes, the samples were quenched in water and their mineral composition and microstructures were determined. Depending on the original composition of the mixture six different groups of mineralogical phases were obtained which are shown in the Figure A-17. The composition of the present set of pellets fall in the "A" region of the Figure A-17. Glassy silicate phase was observed as the main binding phase in these pellets. This is similar to the observation made by Matsuno [32].

The presence of multi component calcium ferrite is mainly

reported in fluxed sinters which are known as silicoferrites of calcium and aluminium (SFCA) [131, 132, 133]. The composition of SFCA is reported to be similar to that of calcium diferrite with some substitution of Si and Al for Fe [132]. In the present study, the chemical composition of the calcium observed ferrites corresponded to the SFCA composition. The binary calcium ferrite which formed in solid state reacted with the silica to form silicate melt. At low concentration of CaO in the melt, solidification of glassy silicate took place. As the CaO concentration increase with increasing basicity, SFCA crystallized out of the melt.

The CaO - MgO - Fe_2O_3 ternary system at 1500 ^{o} c is shown in Figure A-18 [134]. The pseudo binary system Ca_2SiO_4 - $MgFe_2O_4$ [135] and the system $Ca_2Fe_2O_5$ - Ca_2SiO_4 - $MgFe_2O_4$ - Mg_2SiO_4 melt isotherms [101] are shown in Figures A-19 and A-20 respectively. It is noted from these Figures that the lowest temperature for liquid formation is 1300 ^{o} c which is higher than that of CaO - SiO_2 - Fe_2O_3 system (1192 ^{o} c). Due to this reason less amount of melt formation took place in dolomite fluxed pellets compared to pellets with limestone addition.

From the above discussion, we observe that morphological evolution during pellet induration is related to the phase equilibria particularly for crystalline phases.

-Fe_2O_3–SiO_2

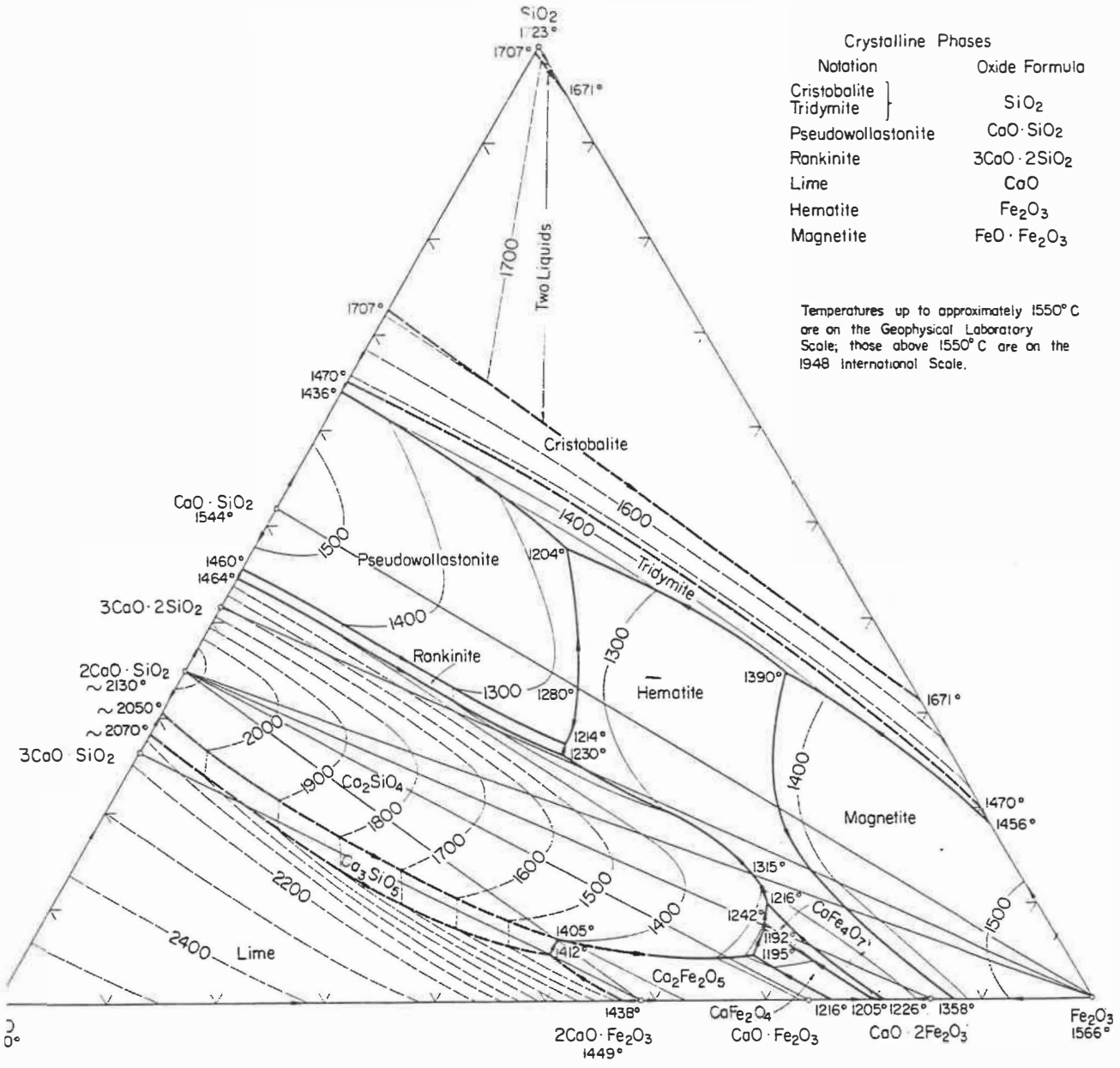
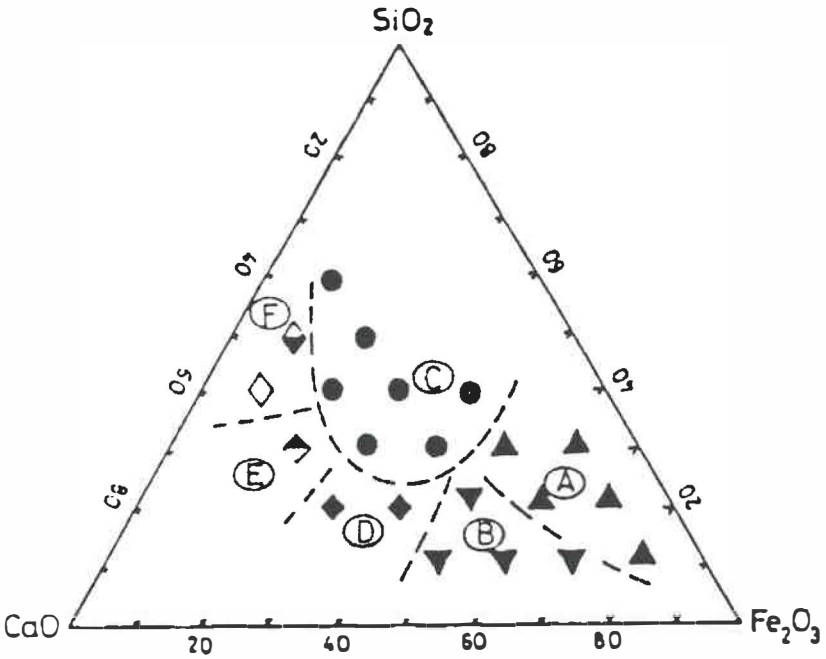


Figure A-16. System CaO - Fe_2O_3 - SiO_2 in equilibrium with air



Ⓐ: Hematite + Magnetite + Glassy slag
Ⓑ: Calcium ferrite + Magnetite + Dicalcium silicate
Ⓒ: Glassy slag
Ⓓ: Dicalcium silicate + Calcium ferrite
Ⓔ: Dicalcium silicate + Glassy slag
Ⓕ: Monocalcium silicate + Glassy slag

Figure A-17. Chemical compositions of oxide mixtures and their microstructures after heating at 1400°C for 15 min in air.

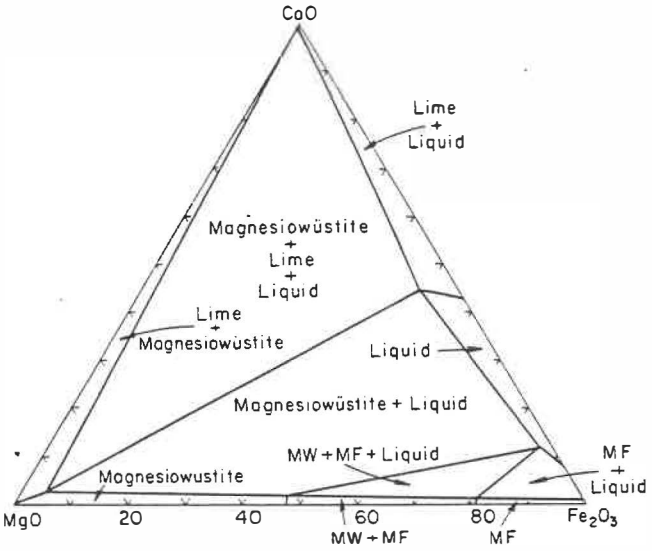


Figure A-18. System CaO - MgO - Fe_2O_3 at 1500 °C in air
(MW = magnesio wustite, MF = magnesio ferrite)

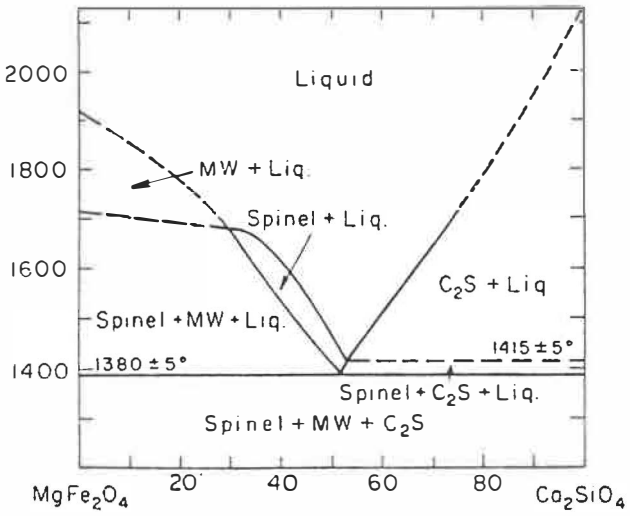


Figure A-19. Pseudo binary system Ca_2SiO_4 - $MgFe_2O_4$ in Air
(C_2S = Ca_2SiO_4 , MW = magnesio wustite

$CaO–MgO–Fe_2O_3–SiO_2$

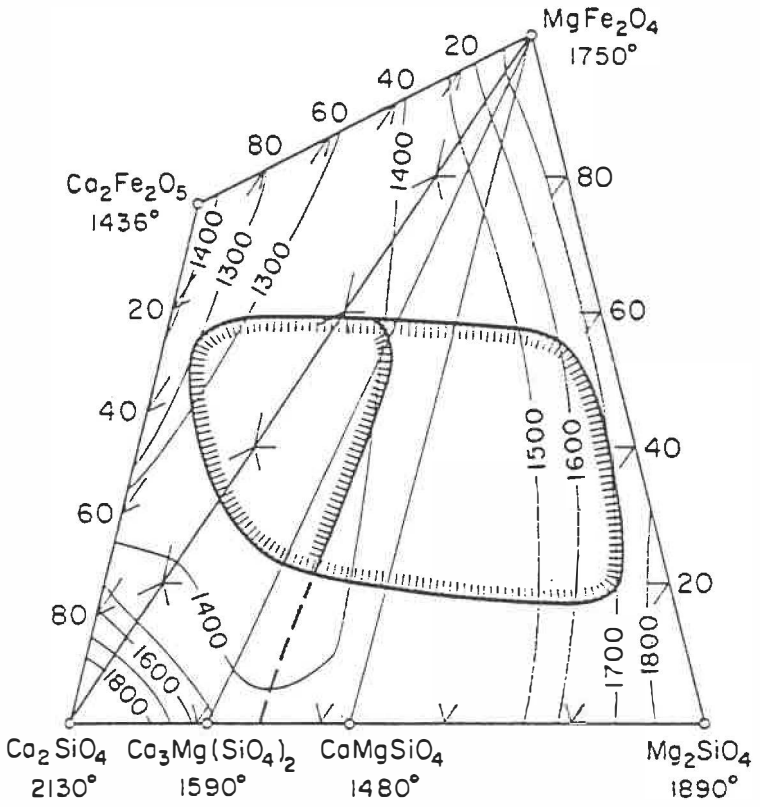


Figure A-20. System $Ca_2Fe_2O_5$ - Ca_2SiO_4 - $MgFe_2O_4$ - Mg_2SiO_4 melting isotherms

ÉCOLE POLYTECHNIQUE DE MONTRÉAL
3 9334 00291697 9